

Electronic Thesis and Dissertation Repository

---

4-20-2017 12:00 AM

## Hippocampal epigenetic changes in a mouse model of Fetal Alcohol Spectrum Disorders

Eric J. Chater-Diehl, *The University of Western Ontario*

Supervisor: Shiva M. Singh, *The University of Western Ontario*

A thesis submitted in partial fulfillment of the requirements for the Doctor of Philosophy degree in Biology

© Eric J. Chater-Diehl 2017

Follow this and additional works at: <https://ir.lib.uwo.ca/etd>



Part of the [Genomics Commons](#)

---

### Recommended Citation

Chater-Diehl, Eric J., "Hippocampal epigenetic changes in a mouse model of Fetal Alcohol Spectrum Disorders" (2017). *Electronic Thesis and Dissertation Repository*. 4479.  
<https://ir.lib.uwo.ca/etd/4479>

This Dissertation/Thesis is brought to you for free and open access by Scholarship@Western. It has been accepted for inclusion in Electronic Thesis and Dissertation Repository by an authorized administrator of Scholarship@Western. For more information, please contact [wlsadmin@uwo.ca](mailto:wlsadmin@uwo.ca).

## Abstract

Fetal alcohol spectrum disorders (FASD) refers to the neurological, developmental, and behavioural abnormalities arising from *in utero* ethanol exposure. These abnormalities included attention deficit, anxiety, and learning and memory impairment persisting into adulthood. The molecular mechanisms of such persistent behavioural changes remain unknown and are an area of intense research. In this thesis, mice were exposed to ethanol during the third trimester equivalent, the peak of synaptic development. Following this exposure, genome-wide epigenetic and gene expression and changes in the hippocampus were assessed in adult (70 day old) mice.

In the first experiment, genome-wide trimethylation of histone H3 at histone H3 lysine 4 (H3K4me3) and lysine 27 (H3K27me3) were assessed using chromatin immunoprecipitation (ChIP) microarray (ChIP-chip). Cell-cell signalling genes were enriched for changes in both methylations. It included the protocadherin (*Pcdh*) genes, which confer neuronal identity and may be important for synaptic development. Changes in methylation also occurred at imprinted genes and lipid-metabolism genes

The second experiment assessed DNA methylation using methylated DNA immunoprecipitation (MeDIP) microarray (MeDIP-chip). The screen identified genes involved in peroxisome biogenesis, which metabolize lipids and generate free-radicals. This was also true when the histone and DNA methylation changes were considered together. Combined analysis of affected genes from each experiment implicated free-radical scavenging genes. Identification of this novel interplay between epigenetic and oxidative stress genes may provide insight into diagnostic or therapeutic interventions. In general, the results support a role of epigenetic mechanisms in long-term FASD phenotypes.

Finally, the third experiment examined gene expression and miRNA microarrays identified 59 and 60 differentially expressed genes and miRNAs between ethanol-exposed and control mice. These genes primarily affect free radical scavenging genes. Differential expression of five genes in this pathway was confirmed with droplet digital PCR (ddPCR), including the transcription factor *Tcf7l2* and the apoptosis regulator *Casp3*. The affected genes also included other oxidative stress proteins, olfactory receptors, and biosynthetic enzymes that may contribute to FASD-related abnormalities.

## Keywords

Prenatal, Binge, Fetal Alcohol Spectrum Disorders (FASD), Gene expression, Epigenetics, Histone, DNA methylation, Synaptogenesis, Hippocampus

## Co-Authorship Statement

The contents of this thesis contain modified portions of published manuscripts, for which I (E.J.C.D.) was primary author. I performed, or assisted with all aspects manuscript preparation, including experimental design, sample collection and preparation, experimental execution, data analysis, and writing all alongside Dr. Shiva M. Singh.

Chapters 2 and 4 contain material from a published manuscript entitled “Alteration of gene expression, DNA methylation, and histone methylation in free radical scavenging networks in adult mouse hippocampus following fetal alcohol exposure”. This manuscript was published in *PLoS One* on May 2, 2016. It is co-authored by Benjamin I. Laufer, Christina A. Castellani, Bonnie L. Alberry, and Shiva M. Singh. E.J.C.D. raised the mice, and isolated tissue, E.J.C.D., B.I.L., C.A.C, and B.L.A. performed experiments and data analysis, E.J.C.D. and S.M.S. wrote the manuscript. This manuscript was published under an open access CC-BY 3.0 license.

Chapter 3 contains material from a published review article entitled “Changes to histone modifications following prenatal alcohol exposure: An emerging picture”. This review was published in *Alcohol* on February 4, 2017. It is coauthored by Benjamin I. Laufer and Shiva M. Singh. The content of the review was conceived by E.J.C.D., who also performed the literature review, generated images, and wrote the review. B.I.L. and S.M.S. provided creative input as well as writing and editing. This manuscript was published under a CC-BY-NC-ND 4.0 license and thus permission to reprinted images and modified text in this thesis was obtained from the publisher, which is provided in Appendix I.

## Acknowledgments

I would like to acknowledge my supervisor, Dr. Shiva Singh for his guidance and mentorship through my PhD studies. He has provided an ideal environment to foster my growth and development as a researcher. He has instilled in me a life-long interest in human epigenetics I look forward to pursuing. I would also like to acknowledge all the members of my laboratory past and present for their assistance and training. I am particularly grateful to Dr. Benjamin Laufer, Dr. Christina Castellani, Dr. Katarzyna Mantha, Bonnie Alberry, Dr. Melkaye Melka, Aniruddho Chokroborty-Hoque, and Randa Stringer for their support.

I am appreciative of my advisors Dr. Kathleen Hill and Dr. Jim Karygiannis for their guidance throughout my graduate studies. I would also like to thank David Carter from the London Regional Genomics Centre for his assistance with the expression microarrays and data analysis. I am grateful to the team at ArrayStar Inc. for their services in performing the histone and DNA methylation microarrays. I am appreciative of EpigenDx Inc. for their services in performing the sodium bisulfite pyrosequencing. I also am grateful to the animal care and veterinary services staff at Western University for their mouse care.

My family has been instrumental in my successes, especially the completion of this thesis. I am exceptionally grateful to my husband, Matthew Chater. The years of this thesis were also years of exceptional personal growth and challenge for us, including our marriage and adoption of our children. His support through my professional and personal growth have been invaluable. I am extremely grateful to my parents, Hilary Montgomery and Brian Diehl for their fervent support of my educational achievement for as long as I can remember; they made my PhD studies possible in more ways than one. I am also appreciative of my step father Richard Pumaren, my sisters, Jasmine Pumaren and Sarah Diehl, and my in-laws Ester, Paul, and Lindsay Chater for their support. I am appreciative of the personal and academic support of my friends Susan Eitutis, Carlee White, and Lauren Kolecki. Finally, I would like to thank all the faculty, administrators, and staff of the Department of Biology at the University of Western Ontario who have provided support for me over nearly a decade.

## Funding Acknowledgments

This work was supported through grants from the Natural Sciences and Engineering Research Council of Canada (NSERC) and the Canadian Institutes of Health Research (CIHR).

I also acknowledge my personal funding by NSERC through the Canada Graduate Scholarship-Masters (CGS M) and the Canada Graduate Scholarship-Doctorial (CGS D) awards as well as through by government of Ontario through the Ontario Graduate Scholarship (OGS).

# Table of Contents

Abstract.....	I
Keywords .....	II
Co-Authorship Statement.....	III
Acknowledgments.....	IV
Funding Acknowledgments.....	V
Table of Contents .....	VI
List of Tables.....	X
List of Figures .....	XI
List of Appendices .....	XIII
List of Abbreviations.....	XIV
Chapter 1. Introduction.....	1
1.1 Fetal Alcohol Spectrum Disorders (FASD).....	1
1.1.1 A Limited Definition.....	1
1.1.2 Statistics .....	2
1.1.3 Ethanol Metabolism.....	3
1.1.4 Role of Genetic Variation .....	4
1.2 Understanding FASD: Animal Models.....	5
1.2.1 Trimester Three Binge Model: Synaptogenesis.....	7
1.3 Actions of Ethanol During Trimester Three .....	8
1.3.1 Role of Hippocampus .....	9
1.4 Actions of Ethanol at the Molecular Level .....	11
1.4.1 Gene Expression Studies.....	11
1.4.2 Epigenetics.....	12
Hypothesis.....	13
Objectives.....	13
References .....	14
Chapter 2. Effects of Neonatal Ethanol Exposure on Hippocampal Histone Modification .....	23
2.1 Overview.....	23
2.2 Introduction.....	23
2.2.1 Post-translational Histone Modifications.....	23
2.2.2 Histone Methylation.....	24
2.2.3 Acquisition and Propagation of Histone Marks.....	25
2.2.4 Methods to Study Histone Modification.....	27
2.2.5 Histones and Fetal Alcohol Spectrum Disorders .....	28
2.2.6 Effect of Ethanol on Histone Modification.....	28

2.2.7	H3K4me3 and H3K27me3 Study Background.....	32
	Objectives .....	33
2.3	Materials and Methods.....	34
2.3.1	Mouse Care .....	34
2.3.2	Chromatin Immunoprecipitation Microarray (ChIP-chip).....	36
2.3.3	CTCF Motif Prediction .....	38
2.3.4	ChIP-qPCR .....	38
2.4	Results.....	40
2.4.1	Distribution of Histone Modification Changes.....	40
2.4.2	Ontology of Genes Proximal to Histone Modification Changes .....	45
2.4.3	Pathways Affected by Histone Methylation Changes .....	48
2.4.4	Genes and Pathways Affected by Both H3K4me3 and H3K27me3 Changes.....	53
2.4.5	Protocadherin-Proximal CTCF Motifs Show Altered H3K4me3 and H3K27me3.....	58
2.4.6	H3K27me3 Reduction at Snrpn/Ube3a CTCF Sites.....	58
2.5	Discussion.....	62
2.5.1	Gene Ontology Analysis Implicates Synaptic Development Genes.....	62
2.5.2	H3K4me3 Changes Affect Lipid Pathways.....	62
2.5.3	Enrichment of Protocadherin Genes for H3K4me3 & H3K27me3 Changes .....	64
2.5.4	H3K27me3 Changes Affect Imprinted Loci.....	65
2.5.5	Conclusion .....	66
2.6	References.....	68

### Chapter 3. Effects of Neonatal Ethanol Exposure on Hippocampal DNA

	Methylation.....	77
3.1	Outline.....	77
3.2	Introduction.....	77
3.2.1	DNA Cytosine Methylation .....	77
3.2.2	Regulation of DNA Methylation .....	78
3.2.3	Functions of DNA Methylation .....	79
3.2.4	DNA Methylation Analysis Methods .....	82
3.2.5	DNA Methylation and FASD .....	83
3.2.6	DNA Methylation Study Design.....	86
	Objectives .....	87
3.3	Materials and Methods.....	88
3.3.1	Mouse Care .....	88
3.3.2	MeDIP-Chip.....	88
3.3.3	8-OHdG ELISA .....	92
3.4	Results.....	94
3.4.1	Distribution of Differentially Methylated Regions.....	94
3.4.2	Ontology of Genes Proximal to DNA Methylation Changes .....	100
3.4.3	Pathways Affected by DNA Methylation Changes .....	100
3.4.4	Combined DNA & Histone Methylation Analysis .....	104
3.4.5	Combined Gene Ontology and Pathway Analyses .....	104
3.5	Discussion.....	118



3.5.1	Differential Methylation of Growth and Lysosomal Genes .....	118
3.5.2	Combined Gene Ontology and Pathway Analysis .....	119
3.5.3	Peroxisome Biogenesis Pathway .....	122
3.5.4	Pyrosequencing Confirmations .....	124
3.5.5	Conclusion .....	125
3.6	References .....	126

## Chapter 4. Effects of Neonatal Ethanol Exposure on the Hippocampal

Transcriptome .....	135
4.1 Overview .....	135
4.2 Introduction .....	135
4.2.1 Non-Protein-Coding RNAs .....	137
4.2.2 Gene Expression Changes in FASD are Gene-Specific .....	138
4.2.3 Gene Expression Changes in FASD are Pathway- and Network-Specific .....	139
4.2.4 Previous Results from the Singh Laboratory in FASD Models .....	139
4.2.5 Gene Expression Changes in the Hippocampus .....	140
Objectives .....	141
4.3 Materials and Methods .....	142
4.3.1 Mouse Care .....	142
4.3.2 DNA/RNA Isolation .....	142
4.3.3 Gene and miRNA Expression Microarray .....	142
4.3.4 Gene-Specific Confirmations .....	143
4.4 Results .....	146
4.4.1 Differentially Expressed Genes .....	146
4.4.2 Ontology of Differentially Expressed Genes .....	146
4.4.3 Pathways Affected by Differentially Expressed Genes .....	152
4.4.4 Gene-Specific Confirmations .....	152
4.4.5 Differentially Expressed MicroRNAs .....	157
4.4.6 Epigenetic Changes at Differentially Expressed Genes .....	157
4.5 Discussion .....	165
4.5.1 Olfactory Receptor Genes .....	166
4.5.2 Implication of Free Radical Scavenging Pathway .....	167
4.5.3 Low Expression Levels of Differentially Expressed Genes .....	169
4.5.4 Notable Changes in MicroRNA Expression .....	170
4.5.5 Few Co-occurring Gene Expression and Methylation Changes .....	171
4.5.6 Tcf7l2 as an FASD Candidate Gene .....	172
4.5.7 Conclusion .....	173
4.6 References .....	175

## Chapter 5. Discussion .....

5.1 Overview .....	184
5.2 Implications for Biological Processes .....	184
5.3 Free Radical Scavenging Pathway .....	185
5.4 Diagnostic and Therapeutic Potential .....	187
5.5 Limitations and Caveats .....	188
5.6 Considerations for Future Experiments .....	189

5.7 Conclusions.....	190
5.8 References.....	192
Appendices .....	194
Curriculum Vitae.....	211

## List of Tables

<b>Table 2.1</b> Allocation of mouse litters within and between microarray studies.....	35
<b>Table 2.2</b> Gene ontology (GO) analysis of genes with regions of differential H3K4me3 in their promoter.....	46
<b>Table 2.3</b> Gene ontology (GO) analysis of genes with regions of differential H3K27me3 in their promoter.....	47
<b>Table 2.4</b> Pathways identified from each software suite in the genes in proximity to H3K4me3 changes.....	49
<b>Table 2.5</b> Pathways identified from each software suite in the genes in proximity to H3K27me3 changes.....	52
<b>Table 2.6</b> Gene ontology (GO) analysis of genes with both H3K4me3 and H3K27me3 RDHMs in their promoter.....	54
<b>Table 2.7</b> Pathways identified from each software suite in the genes in proximity to both H3K4me3 and H3K27me3 changes.....	55
<b>Table 3.1</b> Characteristics of differentially methylated regions (DMRs) identified by methylated DNA immunoprecipitation microarray (MeDIP-chip).....	95
<b>Table 3.2</b> Gene ontology (GO) analysis of genes with differentially methylated regions (DMRs) in their promoter.....	101
<b>Table 3.3</b> Pathways significantly enriched with differentially methylated genes.....	102
<b>Table 3.4</b> Gene ontology (GO) analysis of genes proximal to a differential methylated region (DMR) or region of differential histone modification (RDHM).....	107
<b>Table 3.5</b> Pathways significantly enriched with genes proximal to DNA methylation or histone methylation changes.....	109
<b>Table 3.6</b> Percentage methylation of CpG cytosines in gene of interest differentially methylated regions (DMRs) as assessed by bisulfite pyrosequencing.....	115
<b>Table 4.1</b> Differentially expressed genes in response to neonatal ethanol exposure in the adult mouse hippocampus.....	148
<b>Table 4.2</b> Gene ontology (GO) analysis of differentially expressed genes.....	151
<b>Table 4.3</b> Pathways significantly enriched with differentially expressed genes.....	153
<b>Table 4.4</b> mRNA abundance from real-time PCR (qPCR) compared to droplet digital PCR (ddPCR).....	155
<b>Table 4.5</b> MicroRNAs and pre-microRNAs identified as differentially expressed from microarray analysis.....	158
<b>Table 4.6</b> MicroRNA expression changes with corresponding reciprocal changes in expression of predicted target genes.....	160
<b>Table 4.7</b> Differentially expressed genes proximal to a change in DNA methylation or histone methylation.....	163

## List of Figures

<b>Figure 2.1</b> Inhibitory actions of ethanol on one-carbon metabolism. ....	29
<b>Figure 2.2</b> Effects of the ethanol metabolism on epigenetic modifications. ....	30
<b>Figure 2.3</b> Genomic overview of regions of differential H3K4me3 and H3K27me3. ....	41
<b>Figure 2.4</b> H3K4me3 and H3K27me3 regions with differential histone methylation (RDHMs) and proximal genes. ....	42
<b>Figure 2.5</b> Distribution of regions with differential histone methylation (RDHMs) across chromosomes. ....	43
<b>Figure 2.6</b> Distribution of regions with differential histone methylation (RDHMs) across chromosomes corrected for gene density. ....	44
<b>Figure 2.7</b> Top lipid-related Ingenuity Pathway Analysis (IPA) network from H3K4me3 affected genes. ....	51
<b>Figure 2.8</b> Top Ingenuity Pathway Analysis (IPA) network for genes sharing both H3K4me3 and H3K27me3 RDHMs. ....	56
<b>Figure 2.9</b> Location of region of differential H3K4me3 & H3K27me3 containing putative CTCF binding motif in the mouse <i>Pcdhg</i> gene cluster. ....	57
<b>Figure 2.10</b> Location of region of differential H3K27me3 in mouse <i>Snrpn/Ube3a</i> locus. ...	59
<b>Figure 2.11</b> Attempted chromatin immunoprecipitation-real-time PCR confirmations of H3K27me3 RDHMs in the <i>Snrpn/Ube3a</i> locus. ....	61
<b>Figure 3.1</b> Differentially methylated regions (DMRs) identified by absolute methylation score (AMS) at increasing stringency levels. ....	96
<b>Figure 3.2</b> Differentially methylated regions (DMRs) identified by relative methylation score (RMS) at increasing stringency levels. ....	97
<b>Figure 3.3</b> Distribution of differentially methylated regions (DMRs) across chromosomes. ....	98
<b>Figure 3.4</b> Distribution of differentially methylated regions (DMRs) across chromosomes corrected for gene density. ....	99
<b>Figure 3.5</b> Top affected IPA pathway for genes proximal to a differentially methylated region (DMR). ....	103
<b>Figure 3.6</b> Top Partek pathway for genes proximal to differentially methylated regions (DMRs). ....	105
<b>Figure 3.7</b> Combined gene list characterization, genes proximal to either a DNA methylation (5mC), H3K4me3, or H3K27me3 change. ....	106
<b>Figure 3.8</b> Top affected Ingenuity Pathway Analysis (IPA) pathway for genes proximal to either a DNA methylation or histone methylation change. ....	111
<b>Figure 3.9</b> Top Partek pathway for genes proximal to either a DNA methylation or histone methylation change. ....	112
<b>Figure 3.10</b> Quantification of oxidative damage to DNA in ethanol-exposed vs. control mice. ....	114
<b>Figure 3.11</b> Confirmation of cytosine methylation changes in peroxisome genes. ....	116

<b>Figure 3.12</b> Location of differentially methylated CpG position in of <i>Acaa1</i> gene. ....	117
<b>Figure 4.1</b> Heirarchical clustering of expression patterns from indiviual mircoarrays. ....	147
<b>Figure 4.2</b> Interaction network of published interactions between differentially expressed genes .....	150
<b>Figure 4.3</b> Top IPA network for gene expression changes “Free Radical Scavenging, Gene expression, Dermatological Diseases and Conditions” .....	154
<b>Figure 4.4</b> Droplet digital PCR (ddPCR) confirmations of differential gene expression ....	156
<b>Figure 4.5</b> Distribution of implicated genes shared between experiments at $p < 0.001$ .....	161
<b>Figure 4.6</b> Distribution of implicated genes shared between experiments at $p < 0.01$ .....	162
<b>Figure 5.1</b> Potential origins of observed epigenetic and gene expression hippocampal profile in response to neonatal ethanol exposure. ....	186

## List of Appendices

<b>Appendix A</b> Animal ethical approval .....	194
<b>Appendix B</b> Ingenuity Pathway Analysis (IPA) legend .....	195
<b>Appendix C</b> Linear relationship between number of genes and number of regions of differential histone medication (RDHMs) per chromosome .....	196
<b>Appendix D</b> Affected genes in pathways identified from each software suite in proximity to H3K4me3 changes .....	197
<b>Appendix E</b> Genes bearing both H3K4me3 and H3K27me3 changes .....	200
<b>Appendix F</b> Linear relationship between number of genes and number of differentially methylated regions (DMRs) per chromosome .....	202
<b>Appendix G</b> Affected genes in pathways significantly enriched with genes proximal to differentially methylated regions (DMRs) .....	203
<b>Appendix H</b> Affected genes in pathways significantly enriched with genes proximal to differentially methylated regions (DMRs) or regions of differential histone modification (RDHMs) .....	205
<b>Appendix I</b> Journal copyright approval .....	209

## List of Abbreviations

5hmC	5-hydroxymethylcytosine
5mC	5-methylcytosine
8-OHdG	8-hydroxy-2' -deoxyguanosine
AcH3	Acetylated Histone H3
AcH4	Acetylated Histone H4
ADH	Alcohol Dehydrogenase
ALDH	Aldehyde Dehydrogenase
AMS	Absolute Methylation Score
ANOVA	Analysis of Variance
ARBD	Alcohol-Related Birth Defects
ARND	Alcohol-Related Neurodevelopmental Disorder
AUS	Animal Use Subcommittee
B6	C57BL/6J
BAC	Blood Alcohol Concentration
.CEL	Probe intensity file for Affymetrix arrays
cDNA	Complementary DNA
ChIP	Chromatin Immunoprecipitation
ChIP-chip	Chromatin Immunoprecipitation Microarray
CNS	Central Nervous System
CPD	Continuous Preference Drinking
CpG	Cytosine-Guanine Dinucleotide
CpH	Cytosine-Adenine, -Thymidine, or -Cytosine Dinucleotide
C <sub>t</sub>	Critical Cycle
$\Delta\Delta C_t$	delta delta C <sub>t</sub>
CTCF	CCCTC-binding factor
CTCFBSDB	CTCF binding site database
ddPCR	Droplet Digital PCR
DMR	Differentially Methylated Region
DNMT	DNA Methyltransferase
DSB	Double Strand Break
EDTA	Ethylenediaminetetraacetic Acid
FAE	Fetal Alcohol Effects
FAS	Fetal Alcohol Syndrome
FASD	Fetal Alcohol Spectrum Disorder
FDR	False Discovery Rate
gDNA	Genomic DNA
GEO	Gene Expression Omnibus Database
GD	Gestational Day

GO	Gene Ontology
H3K27me3	Histone H3 Lysine 27 Trimethylation
H3K4me4	Histone H3 Lysine 4 Trimethylation
HAT	Histone Acetyltransferase
IPA	Ingenuity Pathway Analysis
KEGG	Kyoto Encyclopedia of Genes and Genomes
LTP	Long-Term Potentiation
MAT	Model-Based Analysis of Tiling-Arrays
MBD	Methyl Binding Domain
MeDIP	Methylated DNA Immunoprecipitation
MeDIP-chip	MeDIP Microarray
MEDME	Modelling Experimental Data from MeDIP Enrichment
miRNA	MicroRNA
MOE	Main Olfactory Epithelium
mRNA	Messenger RNA
NPC	Neuronal Progenitor Cell
OD	Optical Density
OR	Olfactory Receptor
PND	Postnatal day
PND 4,7	Postnatal day 4 and 7 ethanol injection
PAE	Prenatal Alcohol Exposure
.PAIR	Probe intensity file for Nimblegen arrays
PCA	Principle Component Analysis
pFAS	Partial Fetal Alcohol Syndrome
POMC	Proopiomelanocortin
PPAR	Peroxisome Proliferator-Activated Receptor
PWM	Position Weight Matrices
qPCR	Real-Time PCR
RDHM	Region of Differential Histone Modification
RMS	Relative Methylation Score
ROS	Reactive Oxygen Species
SAM	S-adenosylmethionine
SDS	Sodium Dodecyl Sulfate
TSS	Transcriptional Start Site
VLCFA	Very Long Chain Fatty Acid



## Chapter 1. Introduction

### 1.1 Fetal Alcohol Spectrum Disorders (FASD)

#### 1.1.1 A Limited Definition

Fetal alcohol spectrum disorders (FASD) is a non-diagnostic umbrella term encompassing several conditions caused by prenatal alcohol exposure (PAE). It includes fetal alcohol syndrome (FAS), partial FAS (pFAS), alcohol-related neurodevelopmental disorder (ARND) and alcohol-related birth defects (ARBD) (Chudley et al., 2005). These disorders are characterized by neurological, developmental and behavioural abnormalities. Birth defects in children of alcoholic parents were first described in 1968 (Lemoine et al., 1968). The specific diagnostic criteria associated with the condition, and the term FAS were described in 1973 (Jones et al., 1973). These include four components: 1) characteristic facial dysmorphism (smooth philtrum, thin upper lip, almond shaped eyes) 2) impaired prenatal and/or postnatal growth, 3) central nervous system (CNS) or neurobehavioural disorders, 4) known exposure to alcohol (ethanol) *in utero*. The term fetal alcohol effects (FAE) was soon created to encompass individuals who presented only some FAS criteria, presumably from differing timing and dosage of ethanol (Clarren and Smith, 1978). FAE was later delineated to specific conditions: ARND and ARBD as well as segregating FAS from pFAS (Stratton et al., 1996). Each requires confirmed maternal ethanol consumption. pFAS is defined by facial dysmorphism, and one of the other FAS criteria. ARBD is defined by presence of congenital malformations. ARND is defined by presence of either CNS or behavioural abnormalities (Stratton et al., 1996).

The behavioural phenotypes associated with FASD are diverse, and highly detrimental to those affected. A behavioural phenotype is defined as “a characteristic pattern of motor, cognitive, linguistic and social observations that is consistently associated with a biological disorder” (O’Brien and Yule, 1995). Attention deficit, hyperactivity, impaired executive function, learning and memory, social skills, are observed in children with FASD (Sokol et al., 2003). Not one of these features is unique

to FASD, nor is any combination of them. Further, many of these features can be present in FASD individuals, but not be the result of PAE. This makes differentiation of FASD from other disorders very challenging. For example, FASD is often misdiagnosed as attention deficit hyperactivity disorder (ADHD) (Peadon and Elliott, 2010). ADHD also has high comorbidity with FASD adding further complexity (Rasmussen et al., 2010). FASD is distinguished primarily by known maternal ethanol exposure. Stigma and shame associated with drinking while pregnant makes these self-reported metrics unreliable (Sokol et al., 2003). PAE is believed to impact brain development creating cognitive deficits as “primary disabilities” leading to behavioral outcomes as “secondary disabilities” (Streissguth et al., 2004).

While the definitions of the FASD component disorders allow for phenotypic classification, they do not provide any mechanistic or etiological insight. It is unknown what dosage or developmental timing of ethanol exposure lead to which FASD conditions. It is clear that the behavioural aberrations are caused by ethanol, but the intervening molecular and cellular mechanisms are unclear. As such, the central questions in FASD research concern characterizing molecular and cellular changes.

### 1.1.2 Statistics

FASD is the most common cause of developmental disability in the Western world (May et al., 2009). The general estimate of FAS prevalence across Canada is approximately 1 per 1000 live births while the estimate for FASD is 10 per 1000 live births (Public Health Agency of Canada., 2003). Incidence rates vary greatly, and are highly community-specific. Certain First Nations communities for example are at substantially elevated risk. FASD prevalence in an isolated First Nations community in British Columbia was estimated at 190 per 1000 live births (Robinson et al., 1987). The incidence of FAS in northeastern Manitoba was estimated at 7.2 per 1000 live births (Williams et al., 1999). A study of another Manitoba First Nations community estimated an incidence of FAS and pFAS of 55-101 per 1000 live births (Square, 1997).

Despite societal efforts to raise awareness about the risks, many women still consume alcohol during pregnancy. Approximately 14% of women among the general Canadian population (McCourt and Public Health Agency of Canada., 2005) and as high

as 50% and 60% in isolated northern communities consume alcohol regularly while pregnant (Dow-Clarke et al., 1994; Muckle et al., 2011). In a study of drinking patterns in Inuit women in Quebec, more 19% of women who drank during pregnancy engaged in binge drinking, defined as drinking bringing the blood alcohol concentration (BAC) to 0.08 grams percent or above (Fortin et al., 2015).

The cost of FASD in Canada in 2013 was conservatively estimated to be between \$1.3 billion and \$2.3 billion (Popova et al., 2015). The largest contributing factor was the cost of productivity losses due to disability and premature mortality, accounting for 42% of the total cost. Second at 30% was the cost of corrections, including all interactions with the criminal justice system. Indeed, FASD individuals are at substantially elevated risk involvement with the criminal justice system (Fast et al., 1999). Third was the cost of health care at 10% (Popova et al., 2015). The authors of these studies point out that these estimates include only individuals diagnosed with FASD conditions, and as such undiagnosed or misdiagnosed individuals may be driving the costs much higher.

### 1.1.3 Ethanol Metabolism

In adults, ethanol is metabolised in the liver by alcohol dehydrogenase (ADH) to acetaldehyde which is converted to acetate by aldehyde dehydrogenase (ALDH). The mitochondrial form of ADH (ADH2) is responsible for most acetaldehyde oxidation in the body (Licinio and Wong, 2002). The equilibrium constant of ADH actually strongly favors reduction of acetaldehyde to ethanol. ALDH however irreversible converts acetaldehyde to acetate, which is what drives ethanol oxidation (Bosron and Li, 1987). This also means that acetaldehyde is normally found at very low levels, which is important since it exerts many of the detrimental effects commonly attributed to ethanol (Tong et al., 2011). Ethanol can also be metabolized to acetaldehyde by catalase found in peroxisomes and CYP2E1 found in microsomes (Haorah et al., 2008). ADH is not expressed in sufficient levels in fetal liver to break down ethanol. CYP2E1 and other cytochromes metabolize ethanol at much slower rates (Hines and McCarver, 2002). These enzymes produce oxygen free radicals as part of their enzymatic action which are believed to contribute to ethanol teratogenicity (Haorah et al., 2008). Further, this means that ethanol remains present in the fetus much longer than the maternal bloodstream.

ALDH2 is produced by fetal liver, but not until late in gestation in mice (Sanchis and Guerri, 1986). This means that acetaldehyde is not readily metabolized; due to its instability this leads to free radical formation and cellular damage (Tong et al., 2011). Since ethanol can cross the blood brain barrier, these effects all occur in the developing fetal brain (Muralidharan et al., 2013).

#### 1.1.4 Role of Genetic Variation

The diversity of phenotypic outcomes from similar ethanol exposures suggests that genetic factors may modulate the teratogenic effects of ethanol. Siblings of children with FAS have a higher risk of FAS, 170 per 1000 live births among older sibs and 771 per 1000 live births in younger sibs (Abel, 1988). Monozygotic twins have a higher concordance rate for FAS diagnosis than dizygotic twins (Streissguth and Dehaene, 1993). Several studies have examined the role of polymorphisms in ethanol metabolism enzymes. ADH2 has several non-synonymous, common polymorphisms that alter the rate of ethanol oxidation. ADH2\*3 has two amino acid changes (Arg47 and Cys369) leading to a greatly increased ethanol turnover rate, 80 times other variants (Licinio and Wong, 2002). The ADH2\*3 allele was shown to have a protective effect when the mother had at least one copy (Jacobson et al., 2006). When present in the fetus, ADH2\*3 was associated with reduced risk of low birth weight (Arfsten et al., 2004). Another variant with increased enzyme kinetics, ADH2\*2, was associated with decreased FAS presence (Viljoen et al., 2001). Genetic variation also appears to play a role in the drinking behaviour of pregnant women. ADH2\*2 was associated with reduced alcohol consumption during pregnancy (Zuccolo et al., 2009). ALDH polymorphisms are known to be important in alcohol preference in risk for alcoholism in adults (Quertemont, 2004); however, no studies have implicated these variants in FASD risk. Variants of CYP2E1 have also not been assessed in FASD and very little in alcoholism risk either. While genetic factors play a role in risk, the mechanisms of FASD etiology encompass many more molecular pathways.

## 1.2 Understanding FASD: Animal Models

It is difficult to assess the action of ethanol on a cellular level in humans. As such, animal models of PAE have been developed to gain insight into the molecular actions of ethanol. There are several key advantages to animal models. First, all animal models provide access to all tissues at many timepoints. In FASD, access to brain tissue of ethanol exposed fetuses during development is key (Patten et al., 2014). Further, given the clear importance of genetic background, use of genetically inbred strains allows researchers to control for genetic effects (Nestler and Hyman, 2010). Animal models usually have sequenced genomes with genetic tools available to characterize genomic and transcriptional changes. Many animals have well documented behavioural tests to assess changes in disease-relevant behaviours. Animal models also allow for replication using many animals to increase statistical power. Specific to FASD, the developmental timing and dosage of ethanol can be precisely controlled.

The most logical choice for a model of FASD would seem to be non-human primates. Primates are close evolutionary relatives of humans, have similar gestational development, and have complex social behaviours which could be assessed for ethanol responsiveness (Patten et al., 2014). In practice, there have been very few studies of FASD done in primates. Primates have very long gestational times compared to other model organisms, and are also much longer lived, making experiments time consuming (Schneider et al., 2011). Ethical approval can also be challenging, and the number of animals raised is usually quite low, limiting statistical power. Experiments in these models report growth restriction as well as various behavioural aberrations including learning and memory deficits and tactile aversion (Clarren and Astley, 1992; Clarren et al., 1992; Schneider et al., 2001, 2008).

Rodents are the most popular model organism in FASD research, with rats and mice being the most common. Rats and mice have a short gestation period (21 days), large litters, and complex behaviour with a battery of tests available. Mice are the most common animal model of human disease in general, due to ease of care, ease of genetic manipulation, and similarity to human development and physiology (Patten et al., 2014). Rats are larger, generally allowing easier study of physiology compared to mice and more tissue for molecular analyses. Rats also have more sophisticated behaviour than mice,

with more behavioural tests available. Both are used in genetic, biochemical, physiological, and behavioural studies of FASD. In mice, the C57BL/6J (B6) inbred laboratory strain has become the most common. B6 mice have a long history of use in ethanol research, in part because they voluntarily consume more ethanol solution than all other strains (Rodgers, 1966). In response to ethanol during development, they have a high amount of fetal malformations compared to other strains (Boehm et al., 1997).

Some research has taken place in guinea pigs. Guinea pigs have an advantage over other rodent models of FASD: their gestation is much more similar to humans. All three trimester equivalents of brain development occur *in utero* for guinea pigs, whereas in mice and rats the third trimester equivalent brain development occurs postnatally (Dobbing and Sands, 1979; Dringenberg et al., 2001). Drawbacks of guinea pigs include longer gestation time (three times that of mice and rats), smaller litter size, and non-exploratory behavioural tendencies that make behavioural tests difficult (Dringenberg et al., 2001). PAE models in other model organisms have been developed, including *Caenorhabditis elegans* (Davis et al., 2008), *Drosophila* (McClure et al., 2011), *Xenopus laevis* (Nakatsuji, 1983), zebrafish (Marrs et al., 2010), chickens (Smith, 2008), and sheep (Cudd et al., 2001) (for review see Patten et al., 2014). The diverse strengths of these models allow for examinations of FASD etiology at various biological levels.

The creation of specific FASD models must balance dosage and timing of ethanol exposure. Dosage/duration of ethanol exposure is key, as it determines which developmental processes are affected. CNS development begins at gestational day (GD) 7 in mice, equivalent to the first trimester in humans (Rice and Barone, 2010). Neurulation initiates CNS formation, after which neurons proliferate, migrate outward, and differentiate into mature neurons during trimester two (Rice and Barone, 2010). After differentiation, neurons undergo synaptogenesis and maturation in trimester three. Ethanol will disrupt each of these processes if it is administered at that time. The dosage of ethanol is related to the timing; usually either moderate over a longer time (mimicking human BAC levels) or high and episodic to maximize effects. ethanol exposure time point: early gestation, late gestation, or post-natal (in mice and rats). Ethanol exposure at these various timepoints has markedly different molecular and behavioral outcomes (Kleiber et al., 2014; Mantha, Kleiber, & Singh, 2013; Miller, 2006; Patten, Fontaine, &

Christie, 2014; Wozniak et al., 2004). In addition to dosage and timing, the vehicle of exposure is also variable. The primary methods used are gavage, injection, consumption (drinking or food), and inhalation (Kelly et al., 2009). Finally, the endpoint will determine what type of effects are studied: acute vs. long-term. Along these various dimensions, FASD rodent models are created and adjusted quite often; however, several specific models have been consistently employed. The Singh laboratory has developed and employed the continuous preference drinking model, trimester 1- and 2- equivalent injections, and postnatal trimester three-equivalent injections (Mantha et al., 2013).

### 1.2.1 Trimester Three Binge Model: Synaptogenesis

Post-natal day (PND) 7 is a particularly important developmental timepoint in mice. It is the peak of a rapid brain growth period termed “the brain growth spurt” and synaptogenesis (Dobbing and Sands, 1979). Synaptogenesis refers to the establishment and maturation of synaptic connections in the brain (Rice and Barone, 2000). In humans, it peaks near birth, and but continues at low levels into adulthood (Dobbing and Sands, 1979; Rice and Barone, 2000). In mice and rats, it occurs in the first two postnatal weeks. Exposure of mice to a high dose of ethanol at this time can be considered a model of binge drinking behaviour in humans. However, PND 7 binge model has been refined to cause BAC levels peaking at 500 mg/dl, which is would induce unconsciousness in humans (Ikonomidou et al., 2000). Injection of ethanol twice on PND 7 spaced 2 hours apart has a maximal effect on maintaining BAC: over 200 mg/dl for 15 hours (Ikonomidou et al., 2000). As such, this model is viewed as a tool clearly delineate the effects of a high dose of ethanol at this key timepoint, and not necessarily accurately model FASD in humans. Other laboratories have shown that injection of ethanol on PND 7 causes widespread apoptotic neurodegeneration in the hippocampus and prefrontal cortex and learning and memory impairment (Goodlett and Johnson, 1997; Ikonomidou et al., 2000; Olney et al., 2002; Zimmerberg et al., 1991). The Singh laboratory has introduced a model wherein pups are exposed to ethanol on PND 4 and 7. PND 4,7 exposure is intended to affect both the initiation and peak of synaptogenesis.

PND 4,7 mice demonstrate consistent FASD-relevant phenotypes. These mice show delayed development, hyperactivity, and impaired learning and memory. PND 4,7

mice are generally morphologically normal, but show delayed developmental milestones (Mantha et al., 2013). These mice show reduced time exploring an open field, which is associated with increased anxiety-related behaviours (Carola et al., 2002; Kleiber et al., 2013). They also display increased home cage activity, indicating hyperactivity (Mantha et al., 2013). PND 4,7 mice have particularly strong impairment on the Barnes maze memory task. The Barnes maze is a circular table with one escape hole and many block holes around its periphery (Barnes, 1979). A mouse is placed on the board in given four attempts per day for one week to find the exit hole. Mice eventually learn the location of the hole based on spatial cues; latency to the target hole decreases over the week. PND 4,7 mice show highly reduced latency to the target hole across multiple testing days compared to controls. Further, the greater statistical differences were identified than that of trimesters one, two, or binge models indicating particularly strong impairment (Mantha et al., 2013). Further, after one week, the mice were tested again to assess memory, and were delayed in finding the target hole compared to controls (Mantha et al., 2013). The PND 4,7 model thus provides an effective system to model FASD learning and memory impairment in mice, and should provide utility in studying molecular changes underlying such aberrations.

### 1.3 Actions of Ethanol During Trimester Three

Exposure of mice and rats to ethanol during the first postnatal week is associated with dramatic changes in brain structure and function. Synaptogenesis is the formation and maturation of synapses. Synapses are small gaps that function as junctions between neurons. They facilitate neuron-to-neuron communication via neurotransmitters (Cohen-Cory, 2002). Synapses permit and regulate neuronal communication throughout the brain, and thus are critical in regulation of nearly all brain processes (Cohen-Cory, 2002). During synaptogenesis, many more synaptic connections than are ultimately needed are formed initially. Necessary connections are reinforced while unnecessary connections are removed in a process known as synaptic pruning (D'Amelio et al., 2012). Similarly, unnecessary neurons are removed during this time through apoptosis (programmed cell death). Selection of these neurons is regulated by synaptic NMDA and GABA<sub>A</sub> receptors (Olney, 2004). NMDA receptor activation promotes neuronal survival while GABA<sub>A</sub>



receptors promote apoptosis. Ethanol acts as both an NMDA antagonist and GABA<sub>A</sub> agonist, triggering widespread neuronal apoptosis during the synaptogenesis period (D'Amelio et al., 2012; Ikonomidou et al., 2000; Olney et al., 2002). This process occurs in nearly all brain regions, but is particularly prevalent in the hippocampus, prefrontal cortex, and cerebellum (Ikonomidou et al., 2000; Olney et al., 2002; Wozniak et al., 2004). Loss of neurons in these key brain regions is believed to account, in part, for the behavioural phenotypes associated with FASD.

In addition to apoptosis, ethanol causes neurodegeneration via activating the immune response in the brain. The immune system of the brain utilizes microglia: macrophage cells that respond to and remove damaged neurons by phagocytosis. Surveillance microglia are important for guiding neuronal development by regulating glutamatergic receptors and maturation and synaptic transmission (Dheen et al., 2007). Upon receiving environmental cues, these surveying microglia can transition to an activated state, characterized by production of pro-inflammatory factors and reactive oxygen species (ROS). These lead to neuronal death during development (Dheen et al., 2007). Ethanol triggers microglia activation, resulting in neuron death during the first postnatal week in mice (Drew and Kane, 2014). Ethanol also triggers ROS production as a result of its metabolism, further precipitating microglia activation and neuronal death (Brocardo et al., 2011). In addition, ethanol causes a loss of microglia, reducing their ability to carry out their maintenance functions later in life (Dheen et al., 2007).

### 1.3.1 Role of Hippocampus

#### 1.3.1.1 Structure and Function

The hippocampal complex refers to the hippocampus proper and dentate gyrus. The hippocampal formation includes the hippocampal complex, subiculum, presubiculum, parasubiculum, and entorhinal cortex (Canto et al., 2008; Schultz and Engelhardt, 2014). Its structure is conserved across mammals, and has analogous regions in other vertebrates (Insausti, 1993). The hippocampus proper is divided into the CA1, CA2, and CA3 regions. The hippocampus is similar to other cortical regions in that it has large, pyramid-shaped projection neurons and smaller interneurons (Schultz and Engelhardt, 2014). It is unique in the brain due to the largely unidirectional passage of

information through intra hippocampal circuits, highly distributed three-dimensional organization of connections, and organization of neurons into layers (Amaral et al., 2007; Schultz and Engelhardt, 2014). The hippocampus receives highly processed sensory information from numerous other regions. Information travels from the entorhinal cortex up through the subiculum into the hippocampus proper then out through the dentate gyrus. The predominate hippocampal cell type is glutamatergic excitatory pyramidal neurons. These neurons differ in morphology and transcriptional profiles through the hippocampus, which is what differentiates the CA1, CA2, and CA3 regions (Schultz and Engelhardt, 2014). The dentate gyrus contains dentate granule neurons which project out of the hippocampus (Amaral et al., 2007). Granule neurons and pyramidal neurons are highly laminated into distinct layers (Andersen et al., 1971). Hippocampal structure is very similar between rodents and humans, but there are subtle differences. The hippocampus occupies a much larger relative proportion of the mouse brain (Insausti, 1993). Hippocampus neurogenesis begins on GD15.5 in mice, and is one of two brain regions that continues neurogenesis into adulthood (Insausti, 1993). At PND 7, the hippocampus is undergoing neurogenesis and synaptogenesis, making it exceptionally vulnerable to ethanol exposure.

The hippocampus plays a major role in the formation of new memories and visual/spatial memory. In mice and humans, damage to the hippocampus results in profound difficulties forming new memories (Cho et al., 1999; Morris et al., 1982; Squire, 2009) and difficulties with spatial, but not other learning (Cho et al., 1999; Olton et al., 1978). The unique neuronal architecture of the hippocampus is believed to play a major role in processing of sensory information to form new memories. Long-term potentiation (LTP) is a mechanism believed to mediate memory formation in the hippocampus. LTP refers to an increase in strength of a synaptic connection following neuronal activation, lasting for hours or days (Bliss and Lomo, 1973; Lynch, 2004). By changing synaptic strength, neuronal pathways are believed to store information (i.e. memories) (Lynch, 2004). The precise mechanisms by which this occurs remain an area of intense research. LTP is known to be accomplished in part by changes in neuronal gene expression. Chemical or genetic impairment of LTP results in impaired learning and memory in mice (Muñoz et al., 2016; Subbanna and Basavarajappa, 2014)

### 1.3.1.2 Vulnerability to Ethanol

The hippocampus is particularly vulnerable to the effects of ethanol exposure during development. Ethanol-induced neuronal apoptosis during synaptogenesis occurs at relatively high levels in the hippocampus (Ikonomidou, 2000). Mice exposed to ethanol in the first postnatal week display reductions in neuronal number (Gil-Mohapel et al., 2010), adult neurogenesis (Bonthius and West, 1991; Gil-Mohapel et al., 2010) synaptic efficacy (Bellinger et al., 1999), and dendritic spine density (Abel et al., 1983) in adolescence and into adulthood. Mice exposed to ethanol on PND 7 also show spatial learning and memory impairment, similar to mice with hippocampal lesions (Cho et al., 1999; Mantha et al., 2013). Children with FAS show similar spatial deficits (Hamilton et al., 2003; Uecker and Nadel, 1996, 1998), even though differences in hippocampal structure are inconsistent (Spadoni et al., 2007). Data on non-hippocampal memory such as object and verbal memory are inconsistent between studies (Mattson et al., 1996; Smith and Milner, 1989; Uecker and Nadel, 1998).

## 1.4 Actions of Ethanol at the Molecular Level

### 1.4.1 Gene Expression Studies

Many of the changes ethanol exerts on the brain may occur via changes in gene expression. Gene expression changes are involved in ethanol-induced neuronal apoptosis. The genes *Bax* and *Casp3* are required for apoptosis, which are upregulated by ethanol (Nowoslawski et al., 2005). Blockage of upregulation of these genes prevents ethanol-induced neurotoxicity and behavioural changes (Sadrian et al., 2012). Exposure of embryos to ethanol early in gestation results in dysregulation of cell proliferation, differentiation, and apoptosis related genes (Hard et al., 2005). Ethanol can also cause changes in transcription in immune response and inflammation genes, which can be blocked by drugs that alter gene expression (Drew et al., 2015). PAE mice with induced inflammation show distinct expression profiles in the hippocampus, failing to activate genes and regulators involved in the immune response (Lussier et al., 2015).

Previous work in our laboratory has examined gene expression changes in four mouse models of FASD. In the PND 4,7 mice, within two hours of exposure, there was

dysregulation of apoptosis, lipid metabolism, and neurogenesis genes (Kleiber et al., 2014b). In adult mice, genes involved in glutamate signalling, neurological diseases, and cell-cell signalling were differentially expressed (Mantha et al., 2013). For a complete introduction to gene expression, FASD, and previous results see Chapter 2. The mechanisms which maintain gene expression changes into adulthood in these mice remain unknown; however, epigenetic mechanisms are a strong candidate.

### 1.4.2 Epigenetics

Modern epigenetics is typically defined as a heritable change in chromosome conformation without a change in DNA sequence (Berger et al., 2009). Various chemical modifications to chromatin structure can promote the condensation or relaxation of its structure, leading to repression or activation of gene expression, respectively. Covalent modifications of histone proteins and methylation of DNA cytosine residues are the two most studied mechanisms. For a complete introduction to histone modification and DNA methylation, see Chapters 3 and 4 respectively. There are dozens of histone modifications which are associated with open or closed chromatin at various genomic locations (Barski et al., 2007). DNA methylation is associated with chromatin condensation and stable repression of gene expression (Medvedeva et al., 2014). Both modification types are stable through cell division, allowing long-term control over gene expression. There is complex cross-talk between histone modification and DNA methylation which cooperate to coordinate complex transcriptional responses (Cedar and Bergman, 2009; Schultz et al., 2002). Despite their longevity, epigenetic marks are also reversible, and highly sensitive to environmental perturbation, including by ethanol exposure (Rosenfeld, 2010). Ethanol may act through epigenetic mechanisms to affect gene expression changes. Indeed, histone modification and DNA methylation are sensitive to ethanol (Chapters 3, 4; Kleiber et al., 2014a; Liu et al., 2009; Shukla et al., 2008). Despite interest in epigenetics in FASD, few studies have examined multiple epigenetic marks simultaneously. Given the coordination of DNA methylation and histone modification, examining both may provide broader insights into the effects of ethanol.

## Hypothesis

*Neonatal ethanol exposure promotes epigenetic and gene expression changes in the hippocampus in a mouse model of FASD.*

## Objectives

1. To assess all mouse genes and their promoters in adult mouse hippocampus exposed to ethanol on postnatal days 4 & 7 and identify changes in:
  - a. two histone modifications, H3K4me3 and H3K27me3, using chromatin immunoprecipitation (ChIP) coupled to the Roche NimbleGen MM9 Meth 2.1M CpG plus Promoter array.
  - b. DNA cytosine methylation using methylated DNA immunoprecipitation (MeDIP) coupled to the Roche NimbleGen MM9 Meth 2.1M CpG plus Promoter array.
  - c. gene and miRNA expression and using the Affymetrix GeneChip<sup>®</sup> Mouse Gene 1.0 ST array and Affymetrix miRNA 2.0 array, respectively.
2. To characterize genes and pathways affected by epigenetic and gene expression changes.
3. To confirm changes at specific genes using:
  - a. ChIP-real-time PCR (ChIP-qPCR) for histone modification changes.
  - b. sodium bisulfite pyrosequencing for DNA methylation changes.
  - c. qPCR and droplet digital PCR (ddPCR) for gene expression changes.

## Thesis Organization:

The results of this thesis are organized into three chapters. Chapter 2 describes histone modification changes in response to early ethanol exposure. Chapter 3 describes DNA methylation changes as well as their relationship to histone medication changes from Chapter 2. Chapter 4 describes gene expression changes and their relationship to results from Chapters 2 and 3.

## References

- Abel, E.L. (1988). Fetal alcohol syndrome in families. *Neurotoxicol. Teratol.* *10*, 1–2.
- Abel, E.L., Jacobson, S., and Sherwin, B.T. (1983). In utero alcohol exposure: functional and structural brain damage. *Neurobehav. Toxicol. Teratol.* *5*, 363–366.
- Amaral, D.G., Scharfman, H.E., and Lavenex, P. (2007). The dentate gyrus: fundamental neuroanatomical organization (dentate gyrus for dummies). *Prog. Brain Res.* *163*, 3–22.
- Andersen, P., Bliss, T. V, and Skrede, K.K. (1971). Lamellar organization of hippocampal pathways. *Exp. Brain Res.* *13*, 222–238.
- Arfsten, D.P., Silbergeld, E.K., and Loffredo, C.A. (2004). Fetal *ADH2\*3*, Maternal Alcohol Consumption, and Fetal Growth. *Int. J. Toxicol.* *23*, 47–54.
- Barnes, C.A. (1979). Memory deficits associated with senescence: a neurophysiological and behavioral study in the rat. *J. Comp. Physiol. Psychol.* *93*, 74–104.
- Barski, A., Cuddapah, S., Cui, K., Roh, T.-Y., Schones, D.E., Wang, Z., Wei, G., Chepelev, I., and Zhao, K. (2007). High-resolution profiling of histone methylations in the human genome. *Cell* *129*, 823–837.
- Bellinger, F.P., Bedi, K.S., Wilson, P., and Wilce, P.A. (1999). Ethanol exposure during the third trimester equivalent results in long-lasting decreased synaptic efficacy but not plasticity in the CA1 region of the rat hippocampus. *Synapse* *31*, 51–58.
- Berger, S.L., Kouzarides, T., Shiekhatar, R., and Shilatifard, A. (2009). An operational definition of epigenetics. *Genes Dev.* *23*, 781–783.
- Bingol, N., Schuster, C., Fuchs, M., Iosub, S., Turner, G., Stone, R.K., and Gromisch, D.S. (1987). The Influence of Socioeconomic Factors on the Occurrence of Fetal Alcohol Syndrome. *Adv. Alcohol Subst. Abuse* *6*, 105–118.
- Bliss, T. V, and Lomo, T. (1973). Long-lasting potentiation of synaptic transmission in the dentate area of the anaesthetized rabbit following stimulation of the perforant path. *J. Physiol.* *232*, 331–356.
- Boehm, S.L., Lundahl, K.R., Caldwell, J., and Gilliam, D.M. (1997). Ethanol teratogenesis in the C57BL/6J, DBA/2J, and A/J inbred mouse strains. *Alcohol* *14*, 389–395.
- Bonthius, D.J., and West, J.R. (1991). Permanent Neuronal Deficits in Rats Exposed to Alcohol during the Brain Growth Spurt. *Teratology* *44*, 147–163.
- Bosron, W.F., and Li, T.K. (1987). Catalytic properties of human liver alcohol dehydrogenase isoenzymes. *Enzyme* *37*, 19–28.

- Brocardo, P.S., Gil-Mohapel, J., and Christie, B.R. (2011). The role of oxidative stress in fetal alcohol spectrum disorders. *Brain Res. Rev.* 67, 209–225.
- Canto, C.B., Wouterlood, F.G., and Witter, M.P. (2008). What does the anatomical organization of the entorhinal cortex tell us? *Neural Plast.* 2008, 381243.
- Carola, V., D'Olimpio, F., Brunamonti, E., Mangia, F., and Renzi, P. (2002). Evaluation of the elevated plus-maze and open-field tests for the assessment of anxiety-related behaviour in inbred mice. *Behav. Brain Res.* 134, 49–57.
- Cedar, H., and Bergman, Y. (2009). Linking DNA methylation and histone modification: patterns and paradigms. *Nat. Rev.* 10, 295–304.
- Cho, Y.H., Friedman, E., and Silva, A.J. (1999). Ibotenate lesions of the hippocampus impair spatial learning but not contextual fear conditioning in mice. *Behav. Brain Res.* 98, 77–87.
- Chudley, A.E., Conry, J., Cook, J.L., Looock, C., Rosales, T., LeBlanc, N., and Disorder, P.H.A. of C.N.A.C. on F.A.S. (2005). Fetal alcohol spectrum disorder: Canadian guidelines for diagnosis. *CMAJ* 172, S1–S21.
- Clarren, S.K., and Astley, S.J. (1992). Pregnancy outcomes after weekly oral administration of ethanol during gestation in the pig-tailed Macaque: Comparing early gestational exposure to full gestational exposure. *Teratology* 45, 1–9.
- Clarren, S.K., and Smith, D.W. (1978). The fetal alcohol syndrome. *Lamp* 35, 4–7.
- Clarren, S.K., Astley, S.J., Gunderson, V.M., and Spellman, D. (1992). Cognitive and behavioral deficits in nonhuman primates associated with very early embryonic binge exposures to ethanol. *J. Pediatr.* 121, 789–796.
- Cohen-Cory, S. (2002). The developing synapse: construction and modulation of synaptic structures and circuits. *Science* 298, 770–776.
- Cudd, T.A., Chen, W.J., Parnell, S.E., and West, J.R. (2001). Third trimester binge ethanol exposure results in fetal hypercapnea and acidemia but not hypoxemia in pregnant sheep. *Alcohol. Clin. Exp. Res.* 25, 269–276.
- D'Amelio, M., Sheng, M., and Ceconi, F. (2012). Caspase-3 in the central nervous system: beyond apoptosis. *Trends Neurosci.* 35, 700–709.
- Davis, J.R., Li, Y., and Rankin, C.H. (2008). Effects of Developmental Exposure to Ethanol on *Caenorhabditis elegans*. *Alcohol. Clin. Exp. Res.* 32, 853–867.
- Dheen, S.T., Kaur, C., and Ling, E.-A. (2007). Microglial activation and its implications in the brain diseases. *Curr. Med. Chem.* 14, 1189–1197.
- Dobbing, J., and Sands, J. (1979). Comparative aspects of the brain growth spurt. Early

Hum. Dev. 3, 79–83.

- Dow-Clarke, R.A., MacCalder, L., and Hessel, P.A. (1994). Health behaviours of pregnant women in Fort McMurray, Alberta. *Can. J. Public Health* 85, 33–36.
- Drew, P.D., and Kane, C.J.M. (2014). Fetal Alcohol Spectrum Disorders and Neuroimmune Changes. *Int. Rev. Neurobiol.* 118, 41.
- Drew, P.D., Johnson, J.W., Douglas, J.C., Phelan, K.D., and Kane, C.J.M. (2015). Pioglitazone blocks ethanol induction of microglial activation and immune responses in the hippocampus, cerebellum, and cerebral cortex in a mouse model of fetal alcohol spectrum disorders. *Alcohol. Clin. Exp. Res.* 39, 445–454.
- Dringenberg, H.C., Richardson, D.P., Brien, J.F., and Reynolds, J.N. (2001). Spatial learning in the guinea pig: cued versus non-cued learning, sex differences, and comparison with rats. *Behav. Brain Res.* 124, 97–101.
- Fast, D.K., Conry, J., and Loock, C. a (1999). Identifying fetal alcohol syndrome among youth in the criminal justice system. *J. Dev. Behav. Pediatr.* 20, 370–372.
- Fortin, M., Muckle, G., Anassour-Laouan-Sidi, E., Jacobson, S.W., Jacobson, J.L., and Bélanger, R.E. (2015). Trajectories of Alcohol Use and Binge Drinking Among Pregnant Inuit Women. *Alcohol Alcohol.*
- Gil-Mohapel, J., Boehme, F., Kainer, L., and Christie, B.R. (2010). Hippocampal cell loss and neurogenesis after fetal alcohol exposure: Insights from different rodent models. *Brain Res. Rev.* 64, 283–303.
- Goodlett, C.R., and Johnson, T.B. (1997). Neonatal Binge Ethanol Exposure Using Intubation: Timing and Dose Effects on Place Learning. *Neurotoxicol. Teratol.* 19, 435–446.
- Hamilton, D.A., Koditwakku, P., Sutherland, R.J., and Savage, D.D. (2003). Children with Fetal Alcohol Syndrome are impaired at place learning but not cued-navigation in a virtual Morris water task. *Behav. Brain Res.* 143, 85–94.
- Haorah, J., Ramirez, S.H., Floreani, N., Gorantla, S., Morsey, B., and Persidsky, Y. (2008). Mechanism of alcohol-induced oxidative stress and neuronal injury. *Free Radic. Biol. Med.* 45, 1542–1550.
- Hard, M.L., Abdolell, M., Robinson, B.H., and Koren, G. (2005). Gene-expression analysis after alcohol exposure in the developing mouse. *J. Lab. Clin. Med.* 145, 47–54.
- Hines, R.N., and McCarver, D.G. (2002). The Ontogeny of Human Drug-Metabolizing Enzymes: Phase I Oxidative Enzymes. *J. Pharmacol. Exp. Ther.* 300.
- Ikonomidou, C. (2000). Ethanol-Induced Apoptotic Neurodegeneration and Fetal Alcohol



Syndrome. *Science* (80-. ). 287, 1056–1060.

- Ikonomidou, C., Bittigau, P., Ishimaru, M.J., Wozniak, D.F., Koch, C., Genz, K., Price, M.T., Stefovská, V., Horster, F., Tenkova, T., et al. (2000). Ethanol-induced apoptotic neurodegeneration and fetal alcohol syndrome. *Science* 287, 1056–1060.
- Insausti, R. (1993). Comparative anatomy of the entorhinal cortex and hippocampus in mammals. *Hippocampus* 3 *Spec No*, 19–26.
- Jacobson, S.W., Carr, L.G., Croxford, J., Sokol, R.J., Li, T.-K., and Jacobson, J.L. (2006). Protective Effects of the Alcohol Dehydrogenase-ADH1B Allele in Children Exposed to Alcohol During Pregnancy. *J. Pediatr.* 148, 30–37.
- Jones, K., Smith, D., Liu, Y., Goodlett, C.R., Liang, T., McClintick, J.N., Edenberg, H.J., Li, L., Jones, K., Smith, D., et al. (1973). Recognition of the fetal alcohol syndrome in early infancy. *Lancet* 302, 999–1001.
- Kelly, S.J., Goodlett, C.R., and Hannigan, J.H. (2009). Animal models of fetal alcohol spectrum disorders: impact of the social environment. *Dev. Disabil. Res. Rev.* 15, 200–208.
- Kleiber, M.L., Mantha, K., Stringer, R.L., and Singh, S.M. (2013). Neurodevelopmental alcohol exposure elicits long-term changes to gene expression that alter distinct molecular pathways dependent on timing of exposure. *J. Neurodev. Disord.* 5, 6.
- Kleiber, M.L., Diehl, E.J., Laufer, B.I., Mantha, K., Chokroborty-Hoque, A., Alberry, B., and Singh, S.M. (2014a). Long-term genomic and epigenomic dysregulation as a consequence of prenatal alcohol exposure: a model for fetal alcohol spectrum disorders. *Front. Genet.* 5, 161.
- Kleiber, M.L., Laufer, B.I., Stringer, R.L., and Singh, S.M. (2014b). Third trimester-equivalent ethanol exposure is characterized by an acute cellular stress response and an ontogenetic disruption of genes critical for synaptic establishment and function in mice. *Dev. Neurosci.* 36, 499–519.
- Lemoine, P., Harousseau, H., Borteyru, J., and Menuet, J. (1968). Les enfants de parents alcooliques - anomalies observées: à propos de 127 cas. *Ouest Med.*
- Licinio, J., and Wong, M.-L. (2002). *Pharmacogenomics: The Search for Individualized Therapies* (Weinheim, FRG: Wiley-VCH Verlag GmbH & Co. KGaA).
- Liu, Y., Balaraman, Y., Wang, G., Nephew, K.P., and Zhou, F.C. (2009). Alcohol exposure alters DNA methylation profiles in mouse embryos at early neurulation. *Epigenetics* 4, 500–511.
- Lussier, A.A., Stepien, K.A., Neumann, S.M., Pavlidis, P., Kobor, M.S., and Weinberg, J. (2015). Prenatal alcohol exposure alters steady-state and activated gene

- expression in the adult rat brain. *Alcohol. Clin. Exp. Res.* 39, 251–261.
- Lynch, M.A. (2004). Long-term potentiation and memory. *Physiol. Rev.* 84, 87–136.
- Mantha, K., Kleiber, M., and Singh, S. (2013). Neurodevelopmental Timing of Ethanol Exposure May Contribute to Observed Heterogeneity of Behavioral Deficits in a Mouse Model of Fetal Alcohol Spectrum Disorder (FASD). *Behav. Brain Sci.* 3, 85–99.
- Marrs, J.A., Clendenon, S.G., Ratcliffe, D.R., Fielding, S.M., Liu, Q., and Bosron, W.F. (2010). Zebrafish fetal alcohol syndrome model: effects of ethanol are rescued by retinoic acid supplement. *Alcohol* 44, 707–715.
- Mattson, S.N., Riley, E.P., Delis, D.C., Stern, C., and Jones, K.L. (1996). Verbal learning and memory in children with fetal alcohol syndrome. *Alcohol. Clin. Exp. Res.* 20, 810–816.
- May, P.A., Gossage, J.P., Kalberg, W.O., Robinson, L.K., Buckley, D., Manning, M., and Hoyme, H.E. (2009). Prevalence and epidemiologic characteristics of FASD from various research methods with an emphasis on recent in-school studies. *Dev. Disabil. Res. Rev.* 15, 176–192.
- McClure, K.D., French, R.L., and Heberlein, U. (2011). A *Drosophila* model for fetal alcohol syndrome disorders: role for the insulin pathway. *Dis. Model. Mech.* 4, 335–346.
- McCourt, C., and Public Health Agency of Canada. (2005). Make every mother and child count : report on maternal and child health in Canada (Public Health Agency of Canada=Agence de santé publique du Canada).
- Medvedeva, Y.A., Khamis, A.M., Kulakovskiy, I. V, Ba-Alawi, W., Bhuyan, M.S.I., Kawaji, H., Lassmann, T., Harbers, M., Forrest, A.R.R., Bajic, V.B., et al. (2014). Effects of cytosine methylation on transcription factor binding sites. *BMC Genomics* 15, 119.
- Miller, M.W. (2006). Effect of prenatal exposure to ethanol on glutamate and GABA immunoreactivity in macaque somatosensory and motor cortices: critical timing of exposure. *Neuroscience* 138, 97–107.
- Morris, R.G., Garrud, P., Rawlins, J.N., and O’Keefe, J. (1982). Place navigation impaired in rats with hippocampal lesions. *Nature* 297, 681–683.
- Muckle, G., Laflamme, D., Gagnon, J., Boucher, O., Jacobson, J.L., and Jacobson, S.W. (2011). Alcohol, smoking, and drug use among Inuit women of childbearing age during pregnancy and the risk to children. *Alcohol. Clin. Exp. Res.* 35, 1081–1091.
- Muñoz, P., Estay, C., Díaz, P., Elgueta, C., Ardiles, Á.O., Lizana, P.A., Ardiles, &#xc1,

- O., Ivaro, and Lizana, P.A. (2016). Inhibition of DNA Methylation Impairs Synaptic Plasticity during an Early Time Window in Rats. *Neural Plast.* 2016, 1–13.
- Muralidharan, P., Sarmah, S., Zhou, F.C., and Marrs, J.A. (2013). Fetal Alcohol Spectrum Disorder (FASD) Associated Neural Defects: Complex Mechanisms and Potential Therapeutic Targets. *Brain Sci.* 3, 964–991.
- Nakatsuji, N. (1983). Craniofacial malformation in *Xenopus laevis* tadpoles caused by the exposure of early embryos to ethanol. *Teratology* 28, 299–305.
- Nestler, E.J., and Hyman, S.E. (2010). Animal models of neuropsychiatric disorders. *Nat. Neurosci.* 13, 1161–1169.
- Nowoslawski, L., Klocke, B.J., and Roth, K. a (2005). Molecular regulation of acute ethanol-induced neuron apoptosis. *J. Neuropathol. Exp. Neurol.* 64, 490–497.
- O'Brien, G., and Yule, W. (1995). Behavioural phenotypes: Clinics in developmental medicine No. 138 (London: Mac Keith Press).
- Olney, J.W. (2004). Fetal alcohol syndrome at the cellular level. *Addict. Biol.* 9, 137–49; discussion 151.
- Olney, J.W., Tenkova, T., Dikranian, K., Qin, Y.Q., Labruyere, J., and Ikonomidou, C. (2002). Ethanol-induced apoptotic neurodegeneration in the developing C57BL/6 mouse brain. *Brain Res.* 133, 115–126.
- Olton, D.S., Walker, J.A., and Gage, F.H. (1978). Hippocampal connections and spatial discrimination. *Brain Res.* 139, 295–308.
- Patten, A.R., Fontaine, C.J., and Christie, B.R. (2014). A comparison of the different animal models of fetal alcohol spectrum disorders and their use in studying complex behaviors. *Front. Pediatr.* 2, 93.
- Peadon, E., and Elliott, E.J. (2010). Distinguishing between attention-deficit hyperactivity and fetal alcohol spectrum disorders in children: clinical guidelines. *Neuropsychiatr. Dis. Treat.* 6, 509–515.
- Popova, S., Lange, S., Burd, L., and Rehm, J. (2015). The Burden and Economic Impact of Fetal Alcohol Spectrum Disorder in Canada. *Cent. Addict. Ment. Heal.*
- Public Health Agency of Canada. (2003). Fetal alcohol spectrum disorder (FASD) : a framework for action. (Health Canada).
- Quertemont, E. (2004). Genetic polymorphism in ethanol metabolism: acetaldehyde contribution to alcohol abuse and alcoholism. *Mol. Psychiatry* 9, 570–581.
- Rasmussen, C., Benz, J., Pei, J., Andrew, G., Schuller, G., Abele-Webster, L., Alton, C.,

- and Lord, L. (2010). The impact of an ADHD co-morbidity on the diagnosis of FASD. *Can. J. Clin. Pharmacol.* *17*, e165-76.
- Rice, D., and Barone, S. (2000). Critical periods of vulnerability for the developing nervous system: evidence from humans and animal models. *Environ. Health Perspect.* *108 Suppl*, 511–533.
- Rice, D., and Barone, S. (2010). Critical Periods of Vulnerability for the Developing Nervous System : Evidence from Humans and Animal Models. *Environ. Heal.* *108*, 511–533.
- Robinson, G.C., Conry, J.L., and Conry, R.F. (1987). Clinical profile and prevalence of fetal alcohol syndrome in an isolated community in British Columbia. *CMAJ* *137*, 203–207.
- Rodgers, D. (1966). Factors Underlying Differences in Alcohol Preference Among Inbred Strains of Mice initiated in collaboration with McClearn. *Psychosom Med* *28*, 498–513.
- Rosenfeld, C.S. (2010). Animal models to study environmental epigenetics. *Biol. Reprod.* *82*, 473–488.
- Sadrian, B., Subbanna, S., Wilson, D.A., Basavarajappa, B.S., and Saito, M. (2012). Lithium prevents long-term neural and behavioral pathology induced by early alcohol exposure. *Neuroscience* *206*, 122–135.
- Sanchis, R., and Guerri, C. (1986). Alcohol-metabolizing enzymes in placenta and fetal liver: effect of chronic ethanol intake. *Alcohol. Clin. Exp. Res.* *10*, 39–44.
- Schneider, M.L., Moore, C.F., and Kraemer, G.W. (2001). Moderate alcohol during pregnancy: learning and behavior in adolescent rhesus monkeys. *Alcohol. Clin. Exp. Res.* *25*, 1383–1392.
- Schneider, M.L., Moore, C.F., Gajewski, L.L., Larson, J.A., Roberts, A.D., Converse, A.K., and DeJesus, O.T. (2008). Sensory Processing Disorder in a Primate Model: Evidence From a Longitudinal Study of Prenatal Alcohol and Prenatal Stress Effects. *Child Dev.* *79*, 100–113.
- Schneider, M.L., Moore, C.F., and Adkins, M.M. (2011). The Effects of Prenatal Alcohol Exposure on Behavior: Rodent and Primate Studies. *Neuropsychol. Rev.* *21*, 186–203.
- Schultz, C., and Engelhardt, M. (2014). Anatomy of the Hippocampal Formation. In *Frontiers of Neurology and Neuroscience*, pp. 6–17.
- Schultz, D.C., Ayyanathan, K., Negorev, D., Maul, G.G., and Rauscher, F.J. (2002). SETDB1: a novel KAP-1-associated histone H3, lysine 9-specific methyltransferase that contributes to HP1-mediated silencing of euchromatic

- genes by KRAB zinc-finger proteins. *Genes Dev.* *16*, 919–932.
- Shukla, S.D., Velazquez, J., French, S.W., Lu, S.C., Ticku, M.K., and Zakhari, S. (2008). Emerging role of epigenetics in the actions of alcohol. *Alcohol. Clin. Exp. Res.* *32*, 1525–1534.
- Smith, S.M. (2008). The Avian Embryo in Fetal Alcohol Research. In *Methods in Molecular Biology* (Clifton, N.J.), pp. 75–84.
- Smith, M.L., and Milner, B. (1989). Right hippocampal impairment in the recall of spatial location: encoding deficit or rapid forgetting? *Neuropsychologia* *27*, 71–81.
- Sokol, R.J., Delaney-Black, V., and Nordstrom, B. (2003). Fetal alcohol spectrum disorder. *JAMA* *290*, 2996–2999.
- Sood, B., Delaney-Black, V., Covington, C., Nordstrom-Klee, B., Ager, J., Templin, T., Janisse, J., Martier, S., and Sokol, R.J. (2001). Prenatal alcohol exposure and childhood behavior at age 6 to 7 years: I. dose-response effect. *Pediatrics* *108*, E34.
- Spadoni, A.D., McGee, C.L., Fryer, S.L., and Riley, E.P. (2007). Neuroimaging and fetal alcohol spectrum disorders. *Neurosci. Biobehav. Rev.* *31*, 239–245.
- Square, D. (1997). Fetal alcohol syndrome epidemic on Manitoba reserve. *CMAJ* *157*, 59–60.
- Squire, L.R. (2009). The legacy of patient H.M. for neuroscience. *Neuron* *61*, 6–9.
- Stratton, K., Howe, C., and Battaglia, F. (1996). *Fetal Alcohol Syndrome. Diagnosis, Epidemiology, Prevention, and Treatment.* (Washington, D.C.: National Academies Press).
- Streissguth, A.P., and Dehaene, P. (1993). Fetal alcohol syndrome in twins of alcoholic mothers: Concordance of diagnosis and IQ. *Am. J. Med. Genet.* *47*, 857–861.
- Streissguth, A.P., Bookstein, F.L., Barr, H.M., Sampson, P.D., O'Malley, K., and Young, J.K. (2004). Risk factors for adverse life outcomes in fetal alcohol syndrome and fetal alcohol effects. *J. Dev. Behav. Pediatr.* *25*, 228–238.
- Subbanna, S., and Basavarajappa, B.S. (2014). Pre-administration of G9a/GLP inhibitor during synaptogenesis prevents postnatal ethanol-induced LTP deficits and neurobehavioral abnormalities in adult mice. *Exp. Neurol.* *261*, 34–43.
- Tong, M., Longato, L., Nguyen, Q.-G., Chen, W.C., Spaisman, A., and de la Monte, S.M. (2011). Acetaldehyde-Mediated Neurotoxicity: Relevance to Fetal Alcohol Spectrum Disorders. *Oxid. Med. Cell. Longev.* *2011*, 1–13.

- Uecker, A., and Nadel, L. (1996). Spatial locations gone awry: object and spatial memory deficits in children with fetal alcohol syndrome. *Neuropsychologia* 34, 209–223.
- Uecker, A., and Nadel, L. (1998). Spatial But Not Object Memory Impairments in Children with Fetal Alcohol Syndrome. *Am. J. Ment. Retard.* 103, 12.
- Viljoen, D.L., Carr, L.G., Foroud, T.M., Brooke, L., Ramsay, M., and Li, T.K. (2001). Alcohol dehydrogenase-2\*2 allele is associated with decreased prevalence of fetal alcohol syndrome in the mixed-ancestry population of the Western Cape Province, South Africa. *Alcohol. Clin. Exp. Res.* 25, 1719–1722.
- Williams, R.J., Odaibo, F.S., and McGee, J.M. (1999). Incidence of fetal alcohol syndrome in northeastern Manitoba. *Can. J. Public Health* 90, 192–194.
- Wozniak, D.F., Hartman, R.E., Boyle, M.P., Vogt, S.K., Brooks, A.R., Tenkova, T., Young, C.L., Olney, J.W., and Muglia, L.J. (2004). Apoptotic neuro degeneration induced by ethanol in neonatal mice is associated with profound learning/memory deficits in juveniles followed by progressive functional recovery in adults RID C-5767-2008. *Neurobiol. Dis.* 17, 403–414.
- Zimmerberg, B., Sukel, H.L., and Stekler, J.D. (1991). Spatial learning of adult rats with fetal alcohol exposure: deficits are sex-dependent. *Behav. Brain Res.* 42, 49–56.
- Zuccolo, L., Fitz-Simon, N., Gray, R., Ring, S.M., Sayal, K., Smith, G.D., and Lewis, S.J. (2009). A non-synonymous variant in ADH1B is strongly associated with prenatal alcohol use in a European sample of pregnant women. *Hum. Mol. Genet.* 18, 4457–4466.

## Chapter 2.

# Effects of Neonatal Ethanol Exposure on Hippocampal Histone Modification

### 2.1 Overview

Histone modifications have not been well researched in FASD. In this chapter, histone H3 lysine 4 trimethylation (H3K4me3) and H3 lysine 27 trimethylation (H3K27me3) were assessed using ChIP-chip in the hippocampus of 70 day-old mice exposed to ethanol as neonates. The results identified regions of differential histone methylation (RDHMs) and genes proximal to them. These genes were used in pathway analysis to identify impacted biological processes. The top pathway for the genes having both methylation changes was protocadherin-guided synaptic development. There was an RDHM in the protocadherin gamma gene cluster which contains a putative CTCF motif. There were also putative CTCF motifs in two regions of differential H3K27me3 methylation the imprinted *Snrpn/Ube3a* region. Finally, there was a substantial occurrence of lipid metabolism pathways in H3K4me3 affected genes suggesting a novel interaction of lipid metabolism and epigenetics. These results are the first assessment of genome-wide changes in histone modification in FASD.

### 2.2 Introduction

#### 2.2.1 Post-translational Histone Modifications

The role of histone modifications in transcription was inferred following the crystal structure of the nucleosome (Luger et al., 1997). The crystal structure showed that the highly basic N-terminal tails of the histones extend from the nucleosome. The authors postulated modification to these tails that could alter the intra-histone interactions and interaction of the octamer with the DNA. Indeed, it is now clear that histone modifications affect nucleosome stability via several mechanisms. To view the role of such histone modifications in cellular events was formally described in the histone code hypothesis (Turner, 1993). The hypothesis postulates that each histone modification codes for a specific chromatin conformation. The different modifications would then

form a combinatorial pattern which could heritably affect gene expression (Turner, 2000). In recent years the rigidity of the histone code hypothesis has been relaxed. Some view histone modifications as more of a “language” (Oliver and Denu, 2011). The same modifications can have different meanings in the context of nearby modifications, and are not strictly associated with any chromatin state. There are also multiple modifications on the same histone tail creating combinatorial complexity which is difficult to assay and evaluate. As such, correlation mapping of each modification on its own is problematic for grasping the full complexity of chromatin.

At least twelve histone modifications have been reported to over 60 different amino acid residues. These include methylation of lysines and arginines, phosphorylation of serine and threonine, acetylation of lysine, ubiquitylation, sumoylation, ADP-ribosylation, propionylation, butyrylation and crotonylation as well as arginine citrullination, proline isomerization, and N-terminal formylation (Kouzarides, 2007). The tails of histone H3 and H4 undergo the most modifications. While all the histone tails are required for higher order chromatin structure (Allan et al., 1982), the H3 and H4 tails are individually sufficient for nucleosome oligomerization (Gordon et al., 2005). This indicates that while the tails work cooperatively, there is a greater contribution of H3 and H4 to chromatin structure. Because histones and especially histone modification vary greatly between species, this section will focus on mammalian histones only. The nomenclature used here is “histone-residue-modification-number” (if applicable), where modifications are shortened from acetylation to ac, methylation to me, and phosphorylation to ph, for example histone H3 lysine 4 trimethylation is H3K4me3.

### 2.2.2 Histone Methylation

Histone methylation occurs at lysine and arginine residues on histone tails. Like acetylation, lysine methylation predominantly occurs on histone H3 and to a lesser degree on H4. An additional layer of complexity exists for lysine methylation, as the  $\epsilon$ -amino group of lysine residues can be mono-, di-, or tri-methylated. Different methylation states of the same lysine residue can show unique genomic localization and carry out differing functional roles. Since histone methylation does not affect the nucleosome charge, it must carry out its effects on chromatin structure indirectly via effector proteins (Taverna et al.,



2007; Voigt and Reinberg, 2011). Many domains recognize histone lysine methylation including chromo, PHD, tudor, WD40, and MBT domains among others (Yun et al., 2011). Further, histone H3 lysine 4 tri-methylation (H3K4me3) enhances transcription via recruitment of the PHD domain-containing TAF3 subunit of the TFIID complex (Lauberth et al., 2013). TFIID is the first protein to bind to chromatin during RNA polymerase II pre-initiation complex formation (Dymlacht et al., 1991). Many of these domains are present in multi-protein complexes that can bind and modify other marks.

Specific histone methylations are linked to nearly every chromatin state and are very consistent between mammalian cell types (Barski et al., 2007; Zhou et al., 2011b). Two in particular—H3K4me3 and H3K27me3—are commonly assessed in the context of gene expression. H3K4me3 is often concomitant with transcription at transcriptional initiation sites (Santos-Rosa et al., 2002; Schneider et al., 2004). H3K4me3 is often viewed as the on/off switch of transcription (Dong et al., 2012). However, the true roles of chromatin marks are clearly much more complex as transcription can occur in the absence of H3K4me3 (Hödl and Basler, 2012). Further, H3K4me3 can mark poised genes together with H3K27me3 termed bivalent domains (Bernstein et al., 2006). These domains are believed to keep developmental genes poised for rapid activation while maintaining repression (Voigt, Tee, & Reinberg, 2013). In somatic cells, H3K27 methylations, are linked with facultatively and constitutively repressed genes (Barski et al., 2007). H3K27me3 is linked more tightly with repressed TSSs, while the mono- and di-methylated forms are more dispersed (Barski et al., 2007). H3K9 methylations are also linked with repressed transcription; H3K9me3 is deposited over large genomic regions facilitating heterochromatin formation (Lehnertz et al., 2003; Soufi et al., 2012). Given this background, H3K4me3 and H3K27me3 were chosen for this study as they have the clearest known relationship with gene expression, and therefore are more likely to represent relevant changes.

### 2.2.3 Acquisition and Propagation of Histone Marks

Histone marks like most other epigenetic marks are mutable and responsive to the environment. Indeed, many studies have linked changes in gene expression in response to various stimuli to changes in DNA methylation and histone modification at promoters

(Rosenfeld, 2010). Studies such as these provide evidence that histone processes may mediate gene-environment interactions. However, with any change in epigenetic marks, it is not easy to distinguish between correlation and causation. Irrespective of their function, histone modifications often reflect the structure of chromatin and it remains an active area of research.

For a histone modification to be passed on, it must be passed through cell division. It appears that some modifications can be passed on and are epigenetic in the classical sense, while others are not. As the DNA replication fork propagates producing two nascent DNA strands, the parental histones are displaced and are evenly distributed to the daughter strands (Alabert and Groth, 2012; Annunziato, 2005; Margueron and Reinberg, 2010; Probst et al., 2009). Parental H3/H4 dimers tend to stay together as tetramers, H2A/H2B are loaded as dimers (Jackson, 1988; Xu et al., 2010). New and parental tetramers are evenly distributed on average. Importantly, this means that the simplest conceptual model for histone modification propagation—copying of histone modifications within the same nucleosome—is not possible for H3 and H4 as both copies of each are either parental or new. The parental histones retain their post-translational marks (Alabert et al., 2015); the mechanism by which the modifications are copied onto new histones remains unclear. There are currently two models which apply to different modifications. For most histone modifications, new histones acquire modifications to become identical to the old ones. Before the next cell cycle, within 2-24 hours, the modifications are written on the new histones until they become identical to the parental histones (Alabert et al., 2015). Therefore, histone modification writing is not tightly coupled to replication, and oscillates with the cell cycle.

The buffer model proposed by (Huang et al., 2013) applies to the repressive heterochromatin marks H3K27me and H3K9me. The buffer model protects constitutively silent genes from being activated by varying repressive mark levels after DNA replication. In general, repressive marks are found across large regions and function by recruiting effector proteins that shape the region to become inaccessible (Boyer et al., 2006). As such, exact replication of each histone modification after cell division is not necessary for gene repression. Huang et al. (2013) propose relatively few nucleosomes (20-30%) must bear repressive modifications to repress transcriptional activity.

Therefore, the system functions as a buffer, wherein the levels of repressive marks never drop below the critical threshold and remain non-permissive to transcription. This model is supported by experimental evidence, which shows that the repressive H3K27me3 and H3K9me3 methylations are slowly written on new histones after replication. Further, even old histones acquired more H3K27me3 and H3K9me3 to reach pre-mitosis levels after replication (Alabert et al., 2015).

## 2.2.4 Methods to Study Histone Modification

Nearly all technologies to assess histone modification rely on chromatin immunoprecipitation. First devised in the 1970s, chromatin Immunoprecipitation (ChIP) relies on a specific antibody to pull down a protein of interest and its interacting genomic DNA (Jackson, 1978). In the case of histone analyses, the antibody is specific to a histone modification of interest. After the DNA is isolated and purified, it can be assessed using a number of approaches. Techniques including PCR (ChIP-qPCR), microarray (ChIP-chip), and sequencing (ChIP-seq) are the most popular (Collas, 2010). In each case, the data are output in “peaks” of DNA enrichment (Wilbanks and Facciotti, 2010).

ChIP-seq and ChIP-chip are the most common methods used to assess whole-genome changes in histone modification, while ChIP-qPCR is popular for assessing specific loci. ChIP-chip has the advantage of utilizing the diversity of commercially available microarrays, allowing researchers control over experimental scale. In contrast, ChIP-seq examines the entire genome with greater resolution, and reduced signal-to-noise ratio allowing identification of more subtle binding events (Massie and Mills, 2012). ChIP-chip is more economical than ChIP-seq; however as sequencing technologies advance, the price differential is becoming less dramatic. Microarrays are limited in resolution compared to sequencing (Park, 2009). This is important for identifying protein binding sites, but is less crucial for identifying histone modification domains. Pinpointing individual histone binding sites is difficult with microarrays however.

### 2.2.5 Histones and Fetal Alcohol Spectrum Disorders

Ethanol has long been known to be an epigenetic disruptor. Garro et al., (1991) found for the first time that fetuses exposed to ethanol had inhibited DNA methyltransferase 1 (DNMT1) activity. Further, this inhibition was attributed to the first metabolite of ethanol, acetaldehyde (Garro et al., 1991). Since this study, ethanol has been found to impact methylation pathways in other direct and indirect ways (**Figure 2.1**). Ethanol inhibits folate absorption in both the intestine and kidney in part by downregulating the expression of its transporter reduced folate carrier 1 (RFC1) (Hamid and Kaur, 2005, 2007a). Reduced folate absorption impairs pyrimidine synthesis and therefore DNA synthesis (**Figure 2.1**). Further, acetaldehyde inhibits methionine synthase which converts homocysteine to methionine. (Halsted et al., 2002). These actions reduce the availability of s-adenosylmethionine (SAM) which is the primary substrate of methyltransferases and source of methyl groups.

Ethanol also induces oxidative stress as a primary effect and through its metabolism which can alter methylation pathways. Conversion of ethanol to acetaldehyde and acetate produces reactive oxygen species (ROS) directly via CYP2E1 and via increased NADH levels (**Figure 2.2**). Ethanol-induced mitochondrial damage produces additional ROS (Hoek et al., 2002). Increased ROS has numerous damaging effects on macromolecules including DNA. Specifically, the hydroxyl radical causes mutations including base substitutions, deletions, single and DSBs (Hoek et al., 2002). Single stranded DNA can signal *de novo* DNMTs causing hyper-methylation of these regions (Christman et al., 1995). With respect to methylation enzymes, under oxidative conditions, homocysteine is converted to the ROS scavenging glutathione, depleting SAM and reducing methylation (**Figure 2.2**; Kerksick and Willoughby, 2005). Ethanol also impacts acetylation pathways. The metabolism of ethanol produces acetaldehyde followed by acetate then acetyl-CoA. Acetyl-CoA is the substrate HATs use as an acetyl group source (**Figure 2.2**).

### 2.2.6 Effect of Ethanol on Histone Modification

The first studies on histone modification and alcohol were focused on the effects of ethanol directly on liver cells. They provided several key insights into how histone

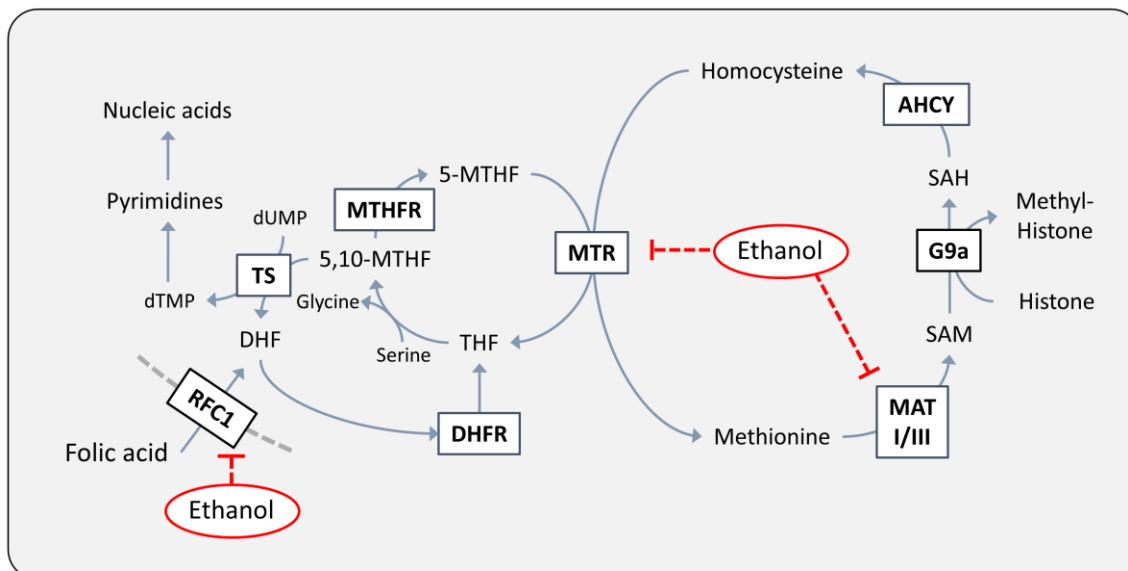


**Figure 2.1 Inhibitory actions of ethanol on one-carbon metabolism.**

Dotted lines indicate indirect inhibitory actions. Ethanol indirectly inhibits the folate cycle (left) by its first metabolite acetaldehyde inhibiting MTR (Kenyon et al., 1998) and by blocking folate uptake via RFC1 by downregulating its expression (Hamid and Kaur, 2007b). Ethanol induced oxidative stress (**Figure 2.2**) irreversibly inactivates MAT I and III in the liver (Seitz and Stickel, 2007). AHCY: adenosylhomocysteinase; DHF: dihydrofolate; DHFR: dihydrofolate reductase; dTMP: deoxythymidine monophosphate; dUMP: deoxyuridine monophosphate; G9a: also known as EHMT2: euchromatic histone-lysine N-methyltransferase 2; MAT: methionine adenosyl transferase; 5-MTHF: 5-methyltetrahydrofolate; 5,10-MTHF: 5,10-methylenetetrahydrofolate; MTHFR: methylenetetrahydrofolate reductase; MTR: methionine synthase; RFC1: reduced folate carrier 1; SAH: S-adenosylhomocysteine; SAM: S-adenosylmethionine; THF: tetrahydrofolate; TS: thymidylate synthase. Reprinted from Chater-Diehl et al., (2017) with permission from Elsevier (**Appendix I**).

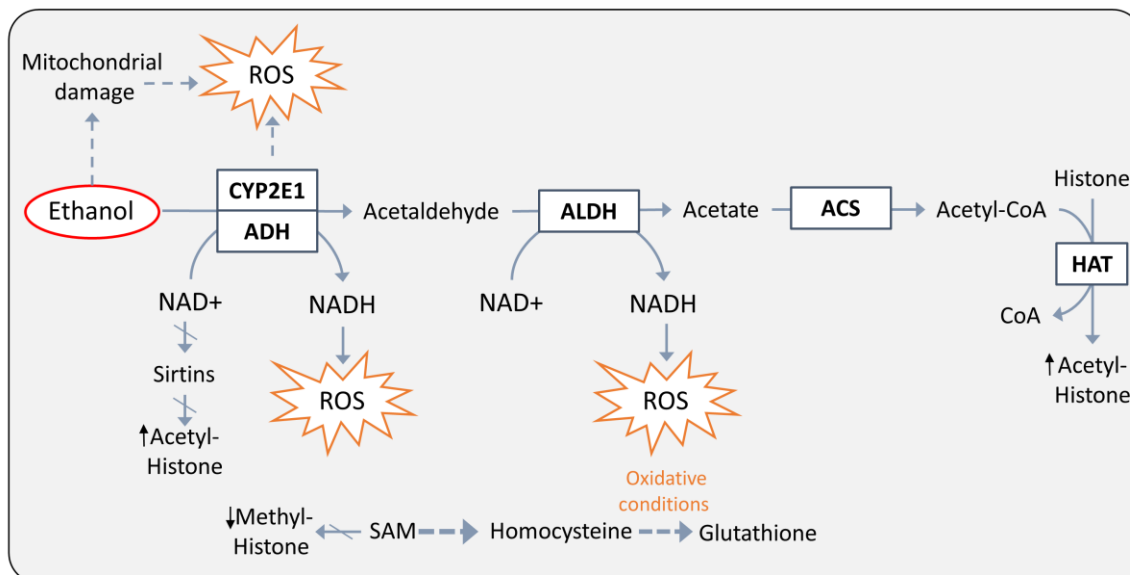


**Figure 2.2 Effects of the ethanol metabolism on epigenetic modifications.**

Slashed lines indicate reduction/impairment of that step. Dashed lines indicate simplified mechanism. Ethanol is metabolized to acetaldehyde, the acetate, both of which produce NADH which led to increased ROS production. Ethanol also induces mitochondrial damage which leads to further ROS production (Hoek et al., 2002). Oxidative conditions drive production of glutathione, deleting SAM and therefore reducing methyl-donors for histone (and other) methylation. Increased acetyl-CoA as a result of ethanol metabolism drives histone (and other protein) acetylation. Depletion of NAD<sup>+</sup> by ethanol metabolism reduces the activity of NAD<sup>+</sup>-dependent sirtins, which prevents histone de-acetylation. Metabolism of ethanol to acetaldehyde by CYP2E1 is simplified, not shown is intermediate production of gem-diol and water, which convert to acetaldehyde and an oxygen radical (shown as ROS above). Conversion of homocysteine to glutathione is greatly simplified. Conversion of SAM to homocysteine is simplified (**Figure 2.1**). ACS: acetyl-CoA synthetase; ADH: alcohol dehydrogenases; ALDH: aldehyde dehydrogenase; CYP2E1: cytochrome P450 2E1; HAT: histone acetyltransferase; ROS: reactive oxygen species; SAM: S-adenosylmethionine. Reprinted from Chater-Diehl et al., (2017) with permission from Elsevier (**Appendix I**).

modifications respond to ethanol. These studies found that H3K9ac (and not other lysine acetylations) was increased in a time- and dose-dependent manner in (Kim and Shukla, 2005; Park et al., 2003). In 2007, Pal-Bhadra et al. examined H3K9me2 and H3K4me2 in cultured hepatocytes. There were site-specific histone modification changes correlated with gene expression changes in response to ethanol (Pal-Bhadra et al., 2007). H3K9me2 reduction and H3K4me2 increase occurred in the upregulated genes. In the downregulated genes, H3K9me2 increased with little H3K4me2 (Pal-Bhadra et al., 2007). This study showed that changes in histone modification can be correlated with changes in gene expression, implying that they do have functional relevance.

Since these early studies, 15 publications have examined histone modifications specifically in response to fetal ethanol exposure (Chater-Diehl et al., 2017). The first study of histone modifications in the brain in FASD used inhalation exposure of rat pups to ethanol from P2-12 (Guo et al., 2011). This study found reduced acetylated histone H3 (AcH3) and H4 (AcH4) in cerebellum. In two studies, C57BL/6J mice were exposed to ethanol using a PND 7 dual injection model. Expression and activity of the HMT G9a mRNA, protein expression, and protein activity were increased after ethanol exposure in both hippocampus and neocortex (Subbanna et al., 2013, 2014). G9a catalyzes H3K27me2 (facilitating conversion to H3K27me3) and is involved in early synaptic remodeling (Schaefer et al., 2009; Shinkai and Tachibana, 2011; Tachibana, 2002). PND 7 ethanol exposure was associated with increased H3K9me2 and H3K27me2 as well as apoptotic neurodegeneration. Treatment with the G9a inhibitor Bix prior to ethanol exposure prevented these effects (Subbanna et al., 2014; Subbanna et al., 2013).

Two papers from Rajesh Miranda and Michael Golding's group have examined the effects of gestational ethanol exposure on H3K4me3 and H3K27me3 changes at specific genes in the brain. Using neurospheres from fetal mice cultured in ethanol, the investigators found that *Hox* and other gene promoters had reduced H3K4me3 (Veazey, Carnahan, Muller, Miranda, & Golding, 2013). This study also used ChIP-qPCR of repetitive transposable element sequences—up to 45% of the human genome—as a proxy for genome-wide H3K4me3 and H3K27me3 changes (Slotkin and Martienssen, 2007). There was significant reduction of H3K27me3 for all investigated transposon types. There was also a trend toward reduction in H3K4me3 though it was non-significant

(Veazey et al., 2013). In a follow-up study, these authors examined how histone modification at specific genes changed following recovery from ethanol, and compared these changes to an *in vivo* mouse model. In general, after 3 days of ethanol exposure there were modest H3K4me3 changes, more pronounced H3K27me3 H3K9ac changes and large-scale H3K9me2 changes (Veazey et al., 2015). After a four day recovery period, the closed-chromatin marks (H3K27me3 and H3K9me2) became greatly enriched (Veazey et al., 2015). In an *in vivo* model, the histone modification profile of malformed ethanol-exposed pups correlated with the cell culture data: there was a reduction of H3K27me3 at more than half of the candidates, an enrichment of H3K9ac at some, and a dramatic increase in H3K9me2 at most (Veazey et al., 2015). The robust closed-chromatin mark changes are interesting as H3K9 and H3K27 methylations are stable and heritable through development likely replicating through the buffer model, acting as true epigenetic marks of repressed chromatin (Chater-Diehl et al., 2017; Huang et al., 2013). They are thus are very strong candidates for the transmission of a lasting ethanol-induced signature (Veazey et al., 2015).

These studies have investigated several histone methylations globally and at specific genes very soon after ethanol exposure. Only two previous studies from the same group have examined histone modifications in adult rats in response to PAE. After exposure to ethanol from GD 7-21, the rats matured to PND 60-80 when cells from POMC cells in the hypothalamus were collected. There were reduced numbers of H3K4me2,3-positive POMC cells, increased H3K9me2-positive POMC cells, and a reduced H3K9ac-positive POMC (Bekdash et al., 2013; Govorko et al., 2012). To date, no other study has examined specific genome-wide changes in histone modifications in response to fetal ethanol, and very few have explored changes in adult mice.

### 2.2.7 H3K4me3 and H3K27me3 Study Background

In this chapter, H3K4me3 and H3K27me3 are assessed for changes across all promoters in the PND 70 mouse hippocampus in the PND 4,7 treatment model. Regions of differential histone modification (RDHMs) were identified for H3K4me3 and H3K27me3 as were genes proximal to these regions. Gene ontology and pathway analysis were used to identify the functional categories of these genes and the potential



biological impact of their differential methylation. Both the pathway analysis and previous work from our laboratory focused the analysis of this chapter on CCCTC-binding factor (CTCF) and imprinted loci.

CTCF is a highly conserved, ubiquitous protein involved in diverse processes such as transcriptional regulation and organization of chromatin architecture. CTCF creates three dimensional chromatin domains in which it promotes specific regulatory interactions that positively or negatively affect transcription (Ong and Corces, 2014). CTCF creates DNA loops at the *Pcdha* and *Pcdhg* genes, likely to bring isoform promoters into contact with enhancers and transcriptional machinery (Golan-Mashiach et al., 2012). The interactions of CTCF are dependent on specific patterns of DNA methylation within its binding motifs (Golan-Mashiach et al., 2012; Wang et al., 2012). In this chapter, CTCF binding motifs in RDHMs are identified and characterized.

CTCF is critical for regulating genomic imprinting. Genomic imprinting refers to the expression of genes in a parent-of-origin-specific manner (Bartolomei and Tilghman, 1997). The regulation of gene expression is accomplished with methylation and repression of one parental copy of the locus (the imprinted allele) while the other is demethylated and expressed (Morgan et al., 2005). These patterns are established early in development and are critical for normal cellular function, with aberrations leading to a host of genetic disorders (Butler, 2009). CTCF has numerous functions at imprinting loci, including binding to methylated DNA and preventing enhancer-promoter interactions and repressing gene expression (Holwerda and de Laat, 2013). In this chapter, the relationship between histone methylation, CTCF, and imprinted loci are explored in the context of FASD.

## Objectives

1. To assess all mouse genes and their promoters in adult mouse hippocampus exposed to ethanol on postnatal days 4 & 7 and identify changes in H3K4me3 and H3K27me3
2. To identify genes and pathways proximal to changes in H3K4me3, H3K27me3, and both.
3. To confirm specific changes with ChIP-qPCR

## 2.3 Materials and Methods

### 2.3.1 Mouse Care

Protocols were approved by the Animal Use Subcommittee (AUS) at the University of Western Ontario, London, Ontario, Canada (**Appendix A**). C57BL/6J (B6) mice were originally obtained from Jackson Laboratories (Bar Harbor, MA) and a population was subsequently maintained at the Animal Care Facility at the University of Western Ontario. Mice were housed in standard shoe-box sized cages and given access to water and food (Lab-Diet<sup>®</sup> 5P00 ProLab<sup>®</sup> RMH 3000 (St. Louis, MO)) *ad libitum*. Environmental conditions were maintained at a temperature range of 19-22°C, a humidity range of 40%-60% and a 14/10-hour light/dark cycle. 25 female mice age 12-18 weeks were separated into individual cages and mated with males of approximately the same age. The male was removed once the female was visibly pregnant. The day of birth was PND zero.

Sex and weight-matched littermate pups were divided into two groups: ethanol-treated and saline control. Pups were given two subcutaneous dorsal injections at 9 am and 11 am on both PND 4 and PND 7 using 30 gauge BD PrecisionGlide™ needles. Ethanol-treated mice were injected with 2.5 g/kg of ethanol in 0.15 M NaCl (Ikonomidou, 2000). This protocol produces blood alcohol concentrations above the toxic threshold of 200 mg/dl for over eight hours (Wozniak et al., 2004). Control mice were injected with 0.15 M saline. Pups were weaned on PND 21 and housed in cages of two to four same-sex littermates. Male mice were used for all subsequent analyses (n=18). Mice were sacrificed on PND 70 via carbon dioxide asphyxiation followed by cervical dislocation. The hippocampus was dissected out (Spijker, 2011), snap-frozen in liquid nitrogen, and stored at -80°C. Mice were divided among gene expression, DNA methylation, and histone modification experiments (**Table 2.1**). Treatment groups (control vs. ethanol-exposed) always contained littermates for each microarray comparison. Mice from the same litter were not repeated in the same microarray experiment. The same litters were represented in each microarray experiment.

**Table 2.1 Allocation of mouse litters within and between microarray studies<sup>†</sup>.**

<b>Histone methylation</b>					
<b>Array 1</b>		<b>Array 2</b>		<b>Array 3</b>	
E5.2	C5.4	E10.4	C10.6	E11.3	C11.4
E12.5	C12.1	E16.5	C16.4	E17.3	C17.4
E19.1	C19.2	E19.5	C19.6	E20.5	C20.6
<b>Gene/miRNA expression and <i>DNA methylation</i></b>					
<b>Array 1</b>		<b>Array 2</b>		<b>Array 3</b>	
<i>E5.1</i>	<i>C5.3</i>	<i>E10.3</i>	<i>C10.5</i>	<i>E11.1</i>	<i>C11.2</i>
E12.4	C12.2	E16.3	C16.2	E17.1	C17.2
E19.4	C19.4	E19.7	C19.8	E20.3	C20.4

<sup>†</sup>Each alphanumeric code refers to a single mouse. The first letter refers to ethanol-exposed (E) or control (C); the number after the letter refers to the litter number; the number after the period refers to the individual mouse. Each for each individual array, the three samples were pooled together. Mice used for the DNA methylation microarray experiment are in italics, which were not pooled with any other samples.

## 2.3.2 Chromatin Immunoprecipitation Microarray (ChIP-chip)

### 2.3.2.1 Chromatin Immunoprecipitation

Hippocampal tissue samples were thawed on ice then treated with 1% formaldehyde for five minutes and sonicated with the truChIP™ Tissue Prep Kit for SDS Chromatin Shearing (Covaris) and the Covaris® S2 Sonicator (Woburn, MA, USA) according to the manufacturer's protocol. The EpiQuik™ Tissue Chromatin Immunoprecipitation Kit (Epigentek) was used to perform ChIP. After sonication, samples were divided and immunoprecipitated with ChIP-grade polyclonal antibodies anti-H3K4me3 (Epigentek cat # A-4033) and anti-H3K27me3 (Millipore cat #07-499). Two microarray experiments were performed, one for each methylation state using the same chromatin sample from the same mice for each. Immunoprecipitated samples were sent to ArrayStar Inc. (Rockville, MD, USA). ArrayStar performed whole-genome amplification, target preparation DNA labelling, array hybridization, scanning, and data summarization.

### 2.3.2.2 Whole Genome Amplification (WGA) and DNA Labelling

The enriched DNA was amplified using a WGA kit from Sigma-Aldrich (the GenomePlex® Complete Whole Genome Amplification (WGA2) kit). The amplified DNA samples were then purified with QIAquick PCR purification kit (Qiagen). The NimbleGen Dual-Color DNA Labeling Kit was used according to the manufacturer's NimbleGen ChIP-on-chip protocol (Nimblegen Systems, Inc., Madison, WI, USA). One µg of DNA from each sample was incubated for 10 min at 98°C with 1 OD of Cy5-9mer primer (IP sample) or Cy3-9mer primer (input sample). Then, 100 pmol of deoxynucleoside triphosphates and 100U of the Klenow fragment (New England Biolabs, USA) was added and incubated at 37°C for 2 hours. The reaction was stopped by adding 0.1 volume of 0.5 M EDTA. The labelled DNA was purified by isopropanol/ethanol precipitation.

### 2.3.2.3 Microarray Hybridization

Microarrays were hybridized at 42°C for four hours with 4µg of Cy3/5 labelled DNA in Nimblegen hybridization buffer/ hybridization component A in a hybridization

chamber (Nimblegen Systems, Inc., Madison, WI, USA). Washing was performed after hybridization using the Nimblegen Wash Buffer kit (Nimblegen Systems, Inc., Madison, WI, USA). For array hybridization, Roche NimbleGen's Mouse ChIP-chip 2.1M Deluxe Promoter Array was used. Samples were pooled in triplicate and hybridized to three arrays for each treatment; i.e. 9 ethanol-treated mice on three arrays were compared to 9 litter-matched controls on three arrays. Scanning was performed with the Axon GenePix 4000B microarray scanner. Raw data were extracted as pair files by NimbleScan software. The files were uploaded to GEO (Series record GSE61488).

#### 2.3.2.4 Microarray analysis

The .pair files were analyzed utilizing the tiling workflow provided in Partek Genomics Suite<sup>®</sup> version 6.6 (St. Louis, Missouri, USA). Nimblegen .pair files (representing the 635 nm and 532 nm scans) for each sample were normalized using the default methods of normalization in the tiling workflow in Partek. The default method includes adjustments for probe sequence, background correction, quantile normalization, and Log (base 2) transformation. In addition, to ensure quality, Principal Components Analysis (PCA) was performed. Files were annotated against the mm9 mouse genome build and enriched regions were detected using a one-way ANOVA to compare enrichment between the ethanol-exposed and control groups: three ethanol-exposed mouse arrays contrasted to the three matched control mouse arrays. The enriched regions settings were set at a minimum  $p$ -value of 0.01 and the number of probes to call a region was set at a minimum of five. The Model-based Analysis of Tiling-arrays (MAT) algorithm was used to detect enriched regions [64]. The MAT algorithm is designed to detect enriched regions in tiling ChIP-chip experiments, and provides a score for the degree of enrichment between experimental samples or groups of samples. A list of regions with MAT scores and corresponding  $p$ -values was the output. These regions with differential histone methylation (RDHMs) were scored to overlap with RefSeq (2014-01-03 version) genes when they were present in the gene body or within 5000 bp upstream or 3000 bp downstream of the transcriptional start site. The list of gene names overlapping RDHMs with a MAT  $p$ -value < 0.001 were generated. A false discovery rate

(FDR)  $q$ -value  $< 0.05$  was used to assess multiple testing error. No RDHMs passed this threshold.

The list of gene names from Partek were submitted as text files to Ingenuity Pathway Analysis (Ingenuity Systems Inc, CA, USA), Partek Pathway (Fishers Exact Test), and Enrichr to determine overrepresented genes using gene ontology (GO) analysis. A cut-off of  $p < 0.05$  was used to determine significant pathways for all software programs.

### 2.3.3 CTCF Motif Prediction

To determine putative CTCF sites in the identified RDHMs, the online CTCFBS database was used (Zentner and Henikoff, 2013). RDHM sequences were extracted from the UCSC genome browser. Five additional nucleotides were extracted at the 5' and 3' ends of the RDHM to capture for CTCF sequences that may only partially overlap in the RDHM. The sequences were submitted to CTCFBS's prediction tool. The position weight matrices (PWM) score associated with each predicted CTCF site was used to identify significant predictions; a cut-off of PWM  $> 3$  was used to identify matches as recommended by the CTCFBSDB creators.

### 2.3.4 ChIP-qPCR

ChIP was performed on independent biological samples. Mice were treated with ethanol or saline and hippocampus was isolated as described above. Five ethanol-exposed and five control mice were generated. ChIP was performed against H3K27me3 as described above. Input DNA was compared against H3K27me3 enrichment and normal mouse IgG (background control) enrichment using SYBR green-based real time PCR. qPCR was performed using SsoAdvanced™ Universal SYBR® Green Supermix (BioRad) according the manufacture's protocol on the CFX Connect™ Real-Time PCR Detection System (BioRad). Primer sequences were as follows: *Snrpn* forward TCCACATCCTTGTCAGCATC, reverse TCAAAAATTCAGGTGACAGCA; *Snord 1* forward AGATTGCTTTTGGCCATCC, reverse GCCTGAGAACTTTTCACCAGA; *Snord 3* forward CCACCTTGTCATGAGATTGC, reverse GAGATCAAAGCAGGGATGGA; *Ipw* forward CCACCTTGTCATGAGATTGC reverse GAGATCAAAGCAGGGATGGA;

*PCDHb5/a9* forward TTTTCCCAAGTGGCAGAGAC, reverse  
AACTCTGTCTCCCTTGAAGTGC. The efficiency of each primer pair was calculated using a standard curve. The *Pcdhb5/a9* primers did not fall within the acceptable 90-110% efficiency and were not pursued further. After amplification, the raw  $C_t$  values were corrected based on reaction efficiency. Enrichment was calculated as % enrichment =  $100\% \times \text{efficiency}^{(\text{input } C_t - \text{K3K27me3 } C_t)}$  and reported as average percent H3K27me3 enrichment  $\pm$  standard error. Significant differences were assessed using a Paired Samples t-Test.

## 2.4 Results

### 2.4.1 Distribution of Histone Modification Changes

To define significant regions of differential histone modification (RDHMs), a Model-based Analysis of Tiling-arrays (MAT) score  $p$ -value cut-off of  $p < 0.001$  was used. At this significance level, there were 625 unique H3K4me3 RDHMs and 165 unique H3K27me3 RDHMs (**Figure 2.3**). For H3K4me3, 29% (181) of RDHMs had a negative MAT score indicating increased methylation (**Figure 2.4**); for H3K27me3, 16% (26) of RDHMs had a negative MAT score (**Figure 2.4**). Thirteen regions had a change in both H3K4me3 and H3K27me3.

The RDHMs were unevenly distributed across chromosomes (**Figure 2.5**). For H3K4me3, chromosomes 7 and 11 had the most RDHMs. Most chromosomes mirrored the positive MAT/negative MAT ratio of the genome overall i.e. they had more RDHMs with more negative MAT scores than positive; however, chromosomes 11-15 did not. Each of these had more positive MAT RDHMs, with chromosome 14 having all positive MAT RDHMs (**Figure 2.5**). For H3K27me3, chromosomes 2, 7, and 11 had the most RDHMs (**Figure 2.5**). Most chromosomes displayed the same positive MAT/negative MAT ratio of the genome overall. i.e. they had more RDHMs with more positive MAT scores than negative. An exception was chromosome 18 which had much more negative than positive (**Figure 2.5**).

Since the experiment employed a promoter microarray, chromosomes with more genes were interrogated more often. The RDHMs per chromosome were therefore corrected based on gene density (**Figure 2.6**). Chromosomes 7 and 11 are very gene-dense, and as such their enrichment was somewhat normalized. Nevertheless, chromosome 11 along with 15 and 18 had the most H3K4me3 RDHMs per gene. Chromosome 15 also had the most H3K27me3 RDHMs per gene (**Figure 2.6**). Chromosome 3 and the X chromosome were depleted of RDHMs of both methylations. A linear regression of the number of genes per chromosome vs. the number of RDHMs found  $R^2$  values of 0.51 for H3K4me3 and 0.30 for H3K27me3 (**Appendix C**). These values indicate a modest correlation between these two variables, suggesting other factors account for a substantial portion of the variation in RDHM distribution.



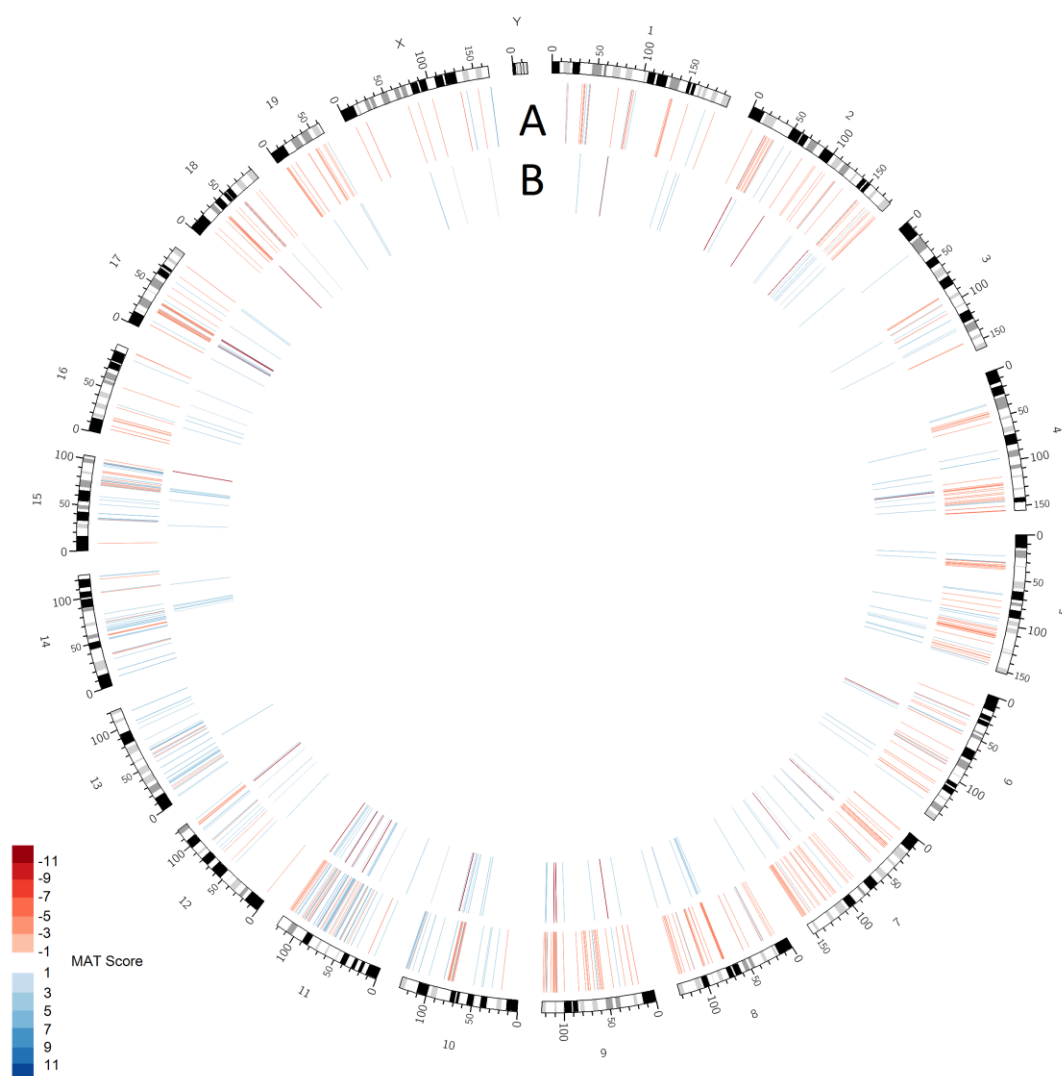


**Figure 2.3 Genomic overview of regions of differential H3K4me3 and H3K27me3.**

Negative MAT score (red) indicates increased methylation, positive (blue) indicates decreased methylation. Track A shows H3K4me3 regions of differential histone modification (RDHMs)  $p < 0.001$ ; track B shows H3K27me3 RDHMs  $p < 0.001$ .

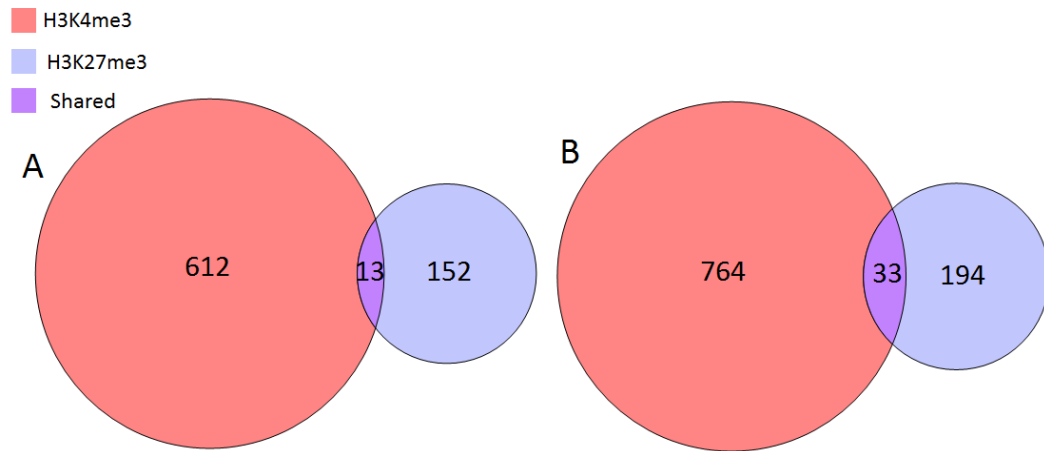


**Figure 2.4 H3K4me3 and H3K27me3 regions with differential histone methylation (RDHMs) and proximal genes.**

Venn diagrams show numbers of unique A) RDHMs and B) genes identified at MAT score  $p$ -value cut-off of  $p < 0.001$  (two-way ANOVA).

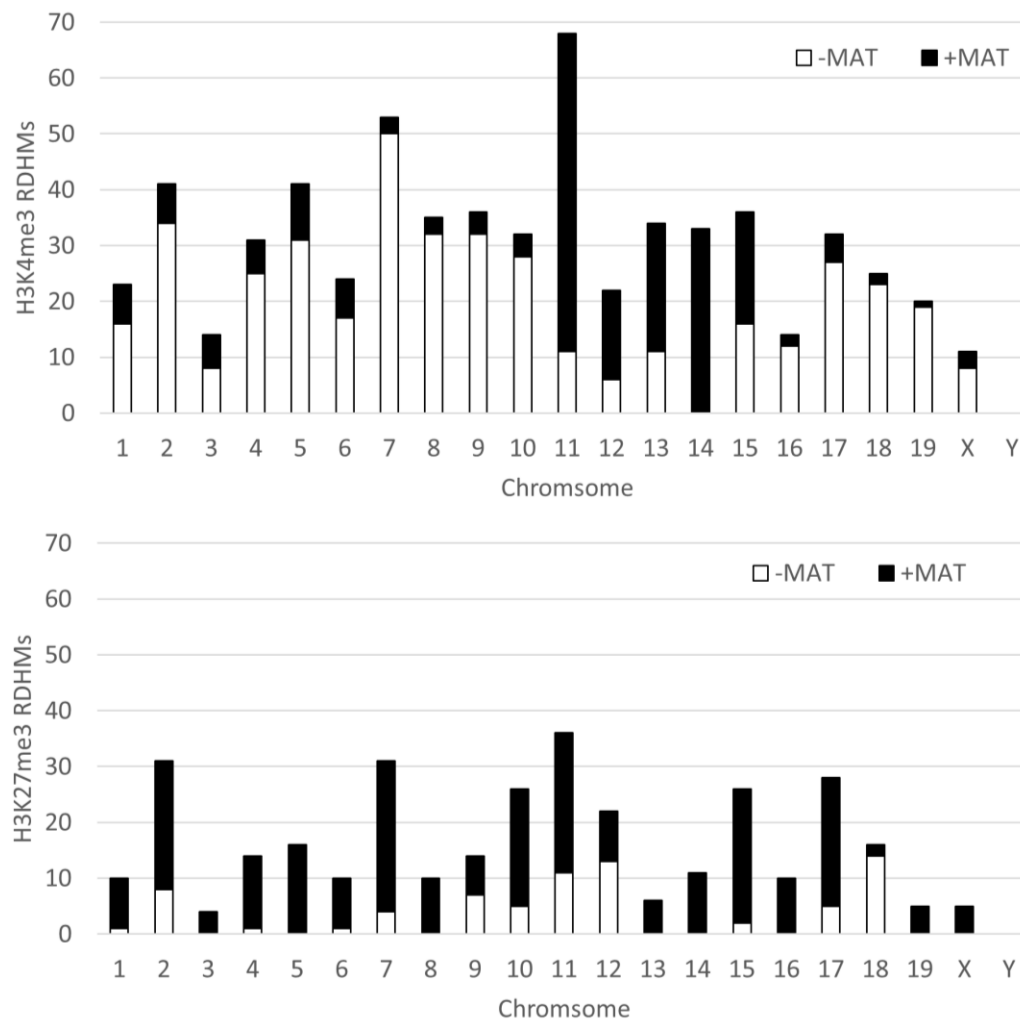


**Figure 2.5 Distribution of regions with differential histone methylation (RDHMs) across chromosomes.**

Bars show the number of RDHMs present on each chromosome at MAT  $p < 0.001$ . Black denotes RDHMs with a positive MAT score indicating depleted methylation, while white denotes RDHMs with a negative MAT score indicating enriched methylation.

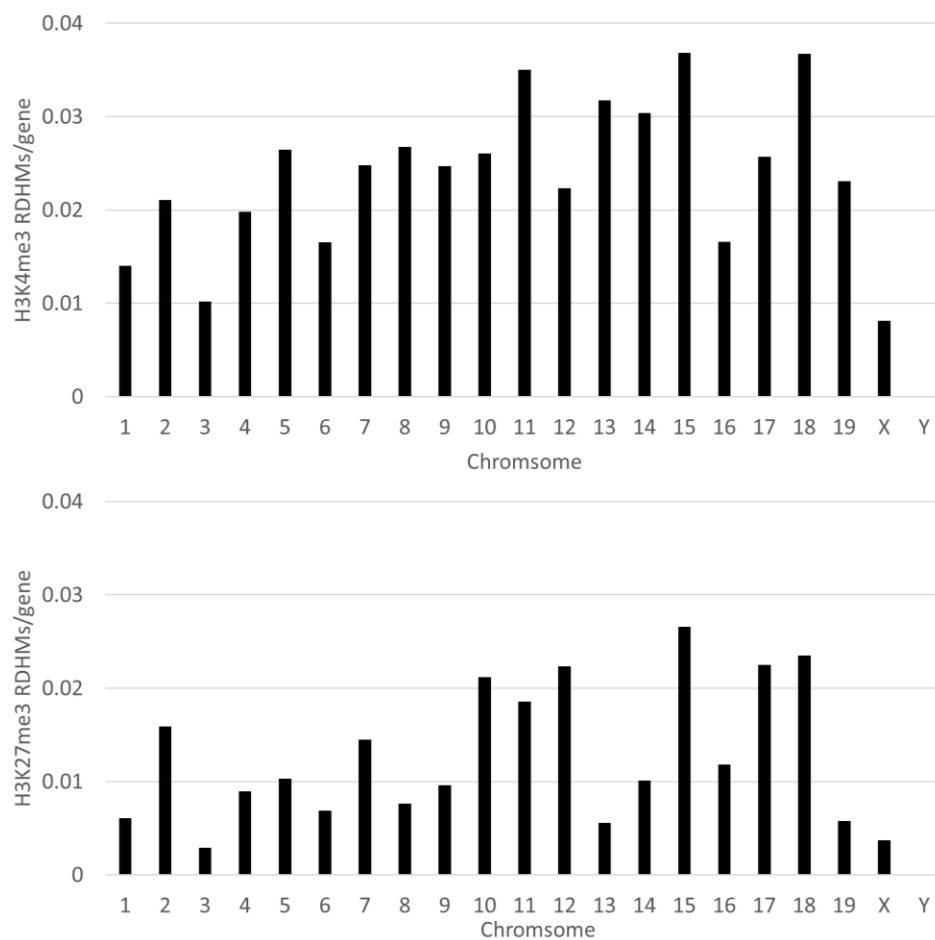


**Figure 2.6 Distribution of regions with differential histone methylation (RDHMs) across chromosomes corrected for gene density.**

The number of RDHMs on each chromosome was divided by the total number of genes (from build mm10) on each chromosome.

## 2.4.2 Ontology of Genes Proximal to Histone Modification Changes

A list of genes potentially affected by RDHMs was next assembled. Genes were included in the list if their promoter (defined as -5000 to 0 bp relative to the transcriptional start site), or gene body contained at least one RDHM. For H3K4me3, 61% of RDHMs lay in gene promoters while 39% lay in gene bodies (including introns). For H3K27me3, 68% of RDHMs lay in gene promoters, while 32% lay in gene bodies. There were 797 genes proximal to H3K4me3 RDHMs, 227 genes proximal to H3K27me3 RDHMs, and 33 genes proximal to both (**Figure 2.4**).

To identify genetic systems affected by H3K4me3 changes in the PND 4,7 FASD model, gene ontology (GO) analysis was performed. The list of 797 genes proximal to a H3K4me3 RDHM was used for GO analysis using Enrichr (Chen et al., 2013) (**Table 2.2**). Enricher determined biological processes, cellular components, molecular functions overrepresented in the gene list. The top affected biological processes for this gene set was “Cell-cell adhesion via plasma-membrane adhesion molecules”. The penultimate affected biological process was also related to cell-cell adhesion (**Table 2.2**). Three of the top ten biological processes were also related to the nervous system, and two were related to kinase signaling (**Table 2.2**). The top affected cellular component was “Ionotropic glutamate receptor complex”, with five other entries related to neurons, three of which were synapse-specific (**Table 2.2**). Other components included cytosolic and cytoskeleton proteins. The top affected molecular function was “Calcium ion binding”. Nine of the top ten entries were related to substrate binding, including phosphoprotein, phosphorylated amino acid, Ras GTPase, Rab GTPase binding. The other was “Receptor signaling complex scaffold activity” (**Table 2.2**). In summary, the GO analysis implicates synaptic, cell adhesion, and signal transduction genes as affected by H3K4me3 changes.

The list of 227 genes proximal to a H3K27me3 RDHM was used for GO analysis using Enrichr (Chen et al., 2013) (**Table 2.3**). Similar to the H3K4me3 genes, the top affected biological process was “Homophilic cell adhesion via plasma membrane adhesion molecules”, and the second and third processes were also cell-cell

**Table 2.2 Gene ontology (GO) analysis of genes with regions of differential H3K4me3 in their promoter<sup>†</sup>.**

<b>GO biological process</b>	
<b>GO term</b>	<b><i>p</i>-value</b>
Cell-cell adhesion via plasma-membrane adhesion molecules (GO:0098742)	1.49E-09
Cell-cell adhesion (GO:0098609)	1.66E-09
Nervous system development (GO:0007399)	0.003
Negative regulation of growth (GO:0045926)	0.0033
Regulation of neuron differentiation (GO:0045664)	0.0036
Sympathetic nervous system development (GO:0048485)	0.0042
Regulation of stress-activated MAPK cascade (GO:0032872)	0.0042
Cellular response to organonitrogen compound (GO:0071417)	0.0043
Regulation of stress-activated protein kinase signaling cascade (GO:0070302)	0.0044
<b>GO cellular component</b>	
Ionotropic glutamate receptor complex (GO:0008328)	0.002
Spectrin-associated cytoskeleton (GO:0014731)	0.0045
Synaptic membrane (GO:0097060)	0.0056
Postsynaptic membrane (GO:0045211)	0.0078
Transcription factor complex (GO:0005667)	0.011
Cell body (GO:0044297)	0.012
Neuronal cell body (GO:0043025)	0.023
Axon (GO:0030424)	0.023
Cytosol (GO:0005829)	0.027
Synapse part (GO:0044456)	0.028
<b>GO molecular function</b>	
Calcium ion binding (GO:0005509)	0.00012
Phosphoprotein binding (GO:0051219)	0.00091
Receptor signaling complex scaffold activity (GO:0030159)	0.007
Protein phosphorylated amino acid binding (GO:0045309)	0.0081
Vinculin binding (GO:0017166)	0.011
Ras GTPase binding (GO:0017016)	0.011
SH3 domain binding (GO:0017124)	0.013
Rab GTPase binding (GO:0017137)	0.013
Gamma-catenin binding (GO:0045295)	0.013
GTPase binding (GO:0051020)	0.015

<sup>†</sup>The top ten GO terms are shown where the number of entries exceeds ten. GO identification numbers are shown for each term. *p*-values for each entry are shown (Fisher's exact test).

**Table 2.3 Gene ontology (GO) analysis of genes with regions of differential H3K27me3 in their promoter<sup>†</sup>.**

<b>GO biological process</b>	
<b>GO term</b>	<b><i>p</i>-value</b>
Homophilic cell adhesion via plasma membrane adhesion molecules (GO:0007156)	9.48E-10
Cell-cell adhesion via plasma-membrane adhesion molecules (GO:0098742)	2.52E-08
Cell-cell adhesion (GO:0098609)	2.67E-08
Mammary gland development (GO:0030879)	6.15E-05
Neuron fate specification (GO:0048665)	0.0015
Proximal/distal pattern formation (GO:0009954)	0.0018
Negative regulation of cell aging (GO:0090344)	0.0056
Insulin-like growth factor receptor signaling pathway (GO:0048009)	0.0084
Fibril organization (GO:0097435)	0.0084
Mitochondrial calcium ion homeostasis (GO:0051560)	0.0095
<b>GO cellular component</b>	
Microfibril (GO:0001527)	0.0032
Fibril (GO:0043205)	0.006
Intermediate filament cytoskeleton (GO:0045111)	0.011
Integral component of mitochondrial membrane (GO:0032592)	0.038
Golgi apparatus (GO:0005794)	0.043
<b>GO molecular function</b>	
Calcium ion binding (GO:0005509)	0.00011
Pre-mRNA binding (GO:0036002)	0.0071
Ankyrin binding (GO:0030506)	0.016
Extracellular matrix structural constituent (GO:0005201)	0.023
Core promoter sequence-specific DNA binding (GO:0001046)	0.025
Galactosyltransferase activity (GO:0008378)	0.038
Oxygen binding (GO:0019825)	0.044

<sup>†</sup>Top 10 GO processes are shown where number of entries exceeds 10. GO identification numbers are shown for each term. *p*-values for each entry are shown (Fisher's exact test).

adhesion related (**Table 2.3**). FASD-relevant biological processes include “Neuron fate specification” and “Insulin-like growth factor receptor signaling pathway”. The top two affected cellular components were “Microfibril” and “Fibril” with several other structural components implicated (**Table 2.3**). The affected biological functions did not show any trends, several binding activities were implicated including “Calcium ion binding”, “pre-mRNA binding”, and “Oxygen binding” (**Table 2.3**).

### 2.4.3 Pathways Affected by Histone Methylation Changes

The set of enriched H3K4me3 genes was also submitted to three separate pathway suites: Ingenuity Pathway Analysis (IPA), Partek Pathway, and Enrichr. The most common process identified by each software suite was fatty acid metabolism, with 10 pathways identified across the three software platforms (**Table 2.4**). The top lipid-related IPA network identified was “Endocrine System Development and Function, Lipid Metabolism, Small Molecule Biochemistry” (**Figure 2.7**). IPA canonical pathways identified include “Fatty acid  $\beta$ -oxidation”, “Sphingomyelin metabolism”, and “Fatty acid metabolism” (**Table 2.4**). Partek pathway and Enrichr also identified “Sphingolipid metabolism”. The individual genes present in the H3K4me3 list driving the identification of these pathways include  $\beta$ -oxidation enzymes (*Acsl4*, *Acsl6*), lipases (*Pnpla2*, *Lipe*), sialidases (*Neu1*, *Neu2*), sphingomyelinases (*Smpd4*, *Smpd3*), pre-angiotensinogens (*Agt*) and oxidoreductases (*Ecsit*). Importantly, there is little redundancy in the genes identified between these pathways, indicating diversity of affected lipid genes that cannot be captured by one software alone. Other pathways identified include cell morphology, development, and survival IPA networks, and cancer signaling pathways identified by both IPA and Partek pathway (**Table 2.4**).

Unlike H3K4me3, the alterations in H3K27me3 methylation following ethanol exposure appear to affect relatively few networks (**Table 2.5**). Predominantly, they affect processes such as endocrine system development and function, molecular transport and protein synthesis. The canonical pathways identified by IPA are enriched for biosynthetic processes including eumelanin, myo-inositol, and proline biosynthesis. Partek pathway analysis also identified two pathways, “Tyrosine metabolism” and



**Table 2.4 Pathways identified from each software suite in the genes in proximity to H3K4me3 changes<sup>†</sup>.**

<b>Pathway name</b>	<b><i>p</i>-value</b>
<b>IPA network/pathway</b>	
Carbohydrate Metabolism, Molecular Transport, Small Molecule Biochemistry	10E-63
Hematological System Development and Function, Tissue Morphology, Cell Death and Survival	10E-49
Humoral Immune Response, Protein Synthesis, Cellular Function and Maintenance	10E-31
Endocrine System Disorders, Gastrointestinal Disease, Immunological Disease	10E-25
Endocrine System Development and Function, Lipid Metabolism, Small Molecule Biochemistry	10E-24
Cellular Development, Cellular Growth and Proliferation, Cancer	10E-24
Cell Morphology, Connective Tissue Development and Function, Cellular Development	10E-23
Energy Production, Lipid Metabolism, Small Molecule Biochemistry	10E-22
Endocrine System Development and Function, Carbohydrate Metabolism, Molecular Transport	10E-20
Cellular Growth and Proliferation, Cell Morphology, Cellular Assembly and Organization	10E-20
Embryonic Development, Organismal Development, Gene Expression	10E-18
Cellular Movement, Immune Cell Trafficking, Hematological System Development and Function	10E-17
Lipid Metabolism, Molecular Transport, Small Molecule Biochemistry	10E-14
<b>IPA canonical</b>	
Regulation of cellular mechanics by calpain protease	0.0039
Fatty acid $\beta$ -oxidation	0.0044
Amyotrophic lateral sclerosis signaling	0.0088
Bladder cancer signaling	0.013
Thyroid cancer signaling	0.014
Giloma invasiveness signaling	0.016
Non-small cell lung cancer signalling	0.029
Sphingomyelin metabolism	0.032
Estrogen biosynthesis	0.035
Spliceosomal cycle	0.038
FGF signaling	0.040
TREM1 signaling	0.045
FAK signaling	0.048
<b>Partek Pathway</b>	
Pathways in cancer	0.034
Fatty acid metabolism	0.035
Sphingolipid metabolism	0.040

<b>Enrichr KEGG</b>	
MAPK Signaling pathway	0.041
Sphingolipid metabolism	0.046

†*p*-values provided for each pathway are shown (Fishers exact test). Lists of genes present in each pathway are found in **Appendix D**.

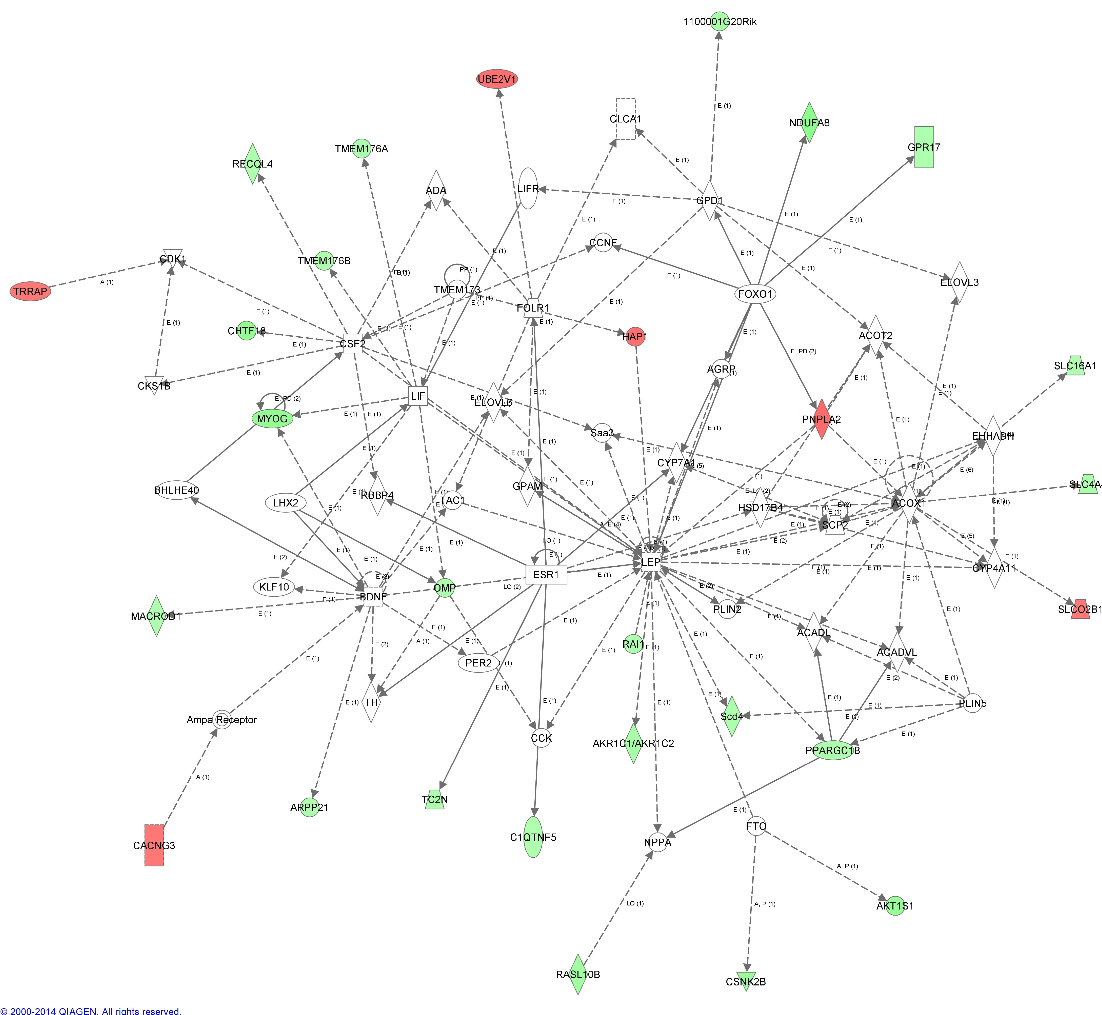


**Figure 2.7 Top lipid-related Ingenuity Pathway Analysis (IPA) network from H3K4me3 affected genes.**

The pathway is termed “Energy production, lipid metabolism, small molecule biochemistry”. Nodes in red indicate increased H3K4me3 while nodes in green indicate decreased H3K3me3 in ethanol exposed mice. Score determined in IPA was 23 corresponding to  $p=10E-23$  (right-tailed Fisher’s Exact Test). See **Appendix B** for symbol legend.

**Table 2.5 Pathways identified from each software suite in the genes in proximity to H3K27me3 changes<sup>†</sup>.**

Pathway name	Genes in pathway and list	p-value
<b>IPA network/pathway</b>		
Endocrine System Development and Function, Molecular Transport, Protein Synthesis	<i>Myadml2, Nphs1, Igf1, Kif5a, Ublcp1, Appl2, Mfap4, App, Tinagl1, Rbm39, Lingo1, Zbtb20, Abcg2, Tmem40, Slc39a14, Tsc2, Sh2b2, Sult1e1, Mif, Ccdc109b, Plec, Smad1, Retnlb, Eif5b, Dnm1, Itm2b, Pou3f1, Sox9</i>	10E-39
Cancer, Skeletal and Muscular Disorders, Tissue Morphology	<i>Hoxd9, Hoxd10, Hoxb9, Cst12, Bcl6b, Hoxb3, Hoxc10, Grik3, Lhx5, Epha3, Disp2, Rgs19, Mb, Rpl10a, Rasa2, Phf1, Cd300e, Ccl6, B3gnt3, Scnn1b, Muc4, Tmbim1, S1pr2</i>	10E-30
Cellular Function and Maintenance, Inflammatory Response, Hematological System Development	<i>Mir195, Mir497b, Mir376c, H2-DMA, Tbx4, Mir196a-2, Mir375, Pycr1, Rassf1, Tusc2, Calb2, Icosl, Atp2b3, Fzr1, Gtf2h4, Apol6, Nthl1, Psg28, Slc8a1, Cabin1, Zfhx3, Lrch1</i>	10E-28
Organismal Survival, Gene Expression, Endocrine System Development and Function	<i>Hoxa7, Mir337, Mir543, Mir667, Sall3, Asap1, Prdx4, Csnk1a1, Naf1, Dnajc6, Prh1, Rhof, Snrk, Dmrt2, Casz1, Macf1, Astn2, Dnal4, Ap1b1, Matk, Flii, Ctnnd2</i>	10E-28
<b>IPA canonical</b>		
Eumelanin Biosynthesis	<i>Mif</i>	0.037
Myo-inositol Biosynthesis	<i>Impa1</i>	0.037
Proline Biosynthesis I	<i>Pycr1</i>	0.037
<b>Partek Pathway</b>		
Tyrosine Metabolism	<i>Mettl2, Mif</i>	0.031
Aldosterone-regulated sodium reabsorption	<i>Igf1, Scnn1b</i>	0.036
<b>Enrichr KEGG</b>		
MTOR signalling pathway	<i>Igf1, Tsc2, Eif5b, Ulk4</i>	0.033

<sup>†</sup>p-values for each pathway are shown (Fisher's exact test).

“Aldosterone-regulated sodium reabsorption” while Enrichr KEGG identified only “MTOR signaling” (**Table 2.5**).

#### 2.4.4 Genes and Pathways Affected by Both H3K4me3 and H3K27me3 Changes

Genes affected by changes in both H3K4me3 and H3K27me3 following alcohol exposure were next examined. This list constituted 33 genes ( $p < 0.001$ ; **Appendix E**). Six of these regions had reciprocal changes in H3K4me3 and H3K27me3, meaning the changes were in opposite directions. Similar to both of the individual H3K4me3 and H3K27me3 gene lists, there was enrichment of cell-cell adhesion ontologies, representing the top three biological processes (**Table 2.6**). Implicated cellular components included many dendrite and synapse-related categories such as “Dendrite cytoplasm”, “Cell projection cytoplasm” and “Presynaptic membrane” (**Table 2.6**). The top molecular function was “Calcium ion binding”, with “Oxidoreductase activity” and “Glutamate receptor” also implicated (**Table 2.6**).

Many of the Partek and IPA canonical pathways identified included very few genes, often only one (**Table 2.7**). However, the top IPA network contained 12 genes, termed “Cell-to-cell signaling and interaction, cellular assembly and organization, nervous system development and function” (**Figure 2.8**). This pathway represents the proteins that interact to organize synaptic networks during brain development. This gene network contains at least five “hub genes” *MYC*, *TP53*, *TNF*, *Rad21* and *CTCF* which are transcription factors. Of special interest to these results is the CTCF (CCCTC-binding factor) gene involved in the regulation of protocadherins. CTCF is a master transcriptional regulator involved in establishing and maintaining specific chromatin environments (Ong and Corces, 2014). Fourteen of the 33 genes in the shared H3K4me3/H3K27me3 list were *Pcdh* genes (**Appendix C**). There are 11 RDHMs that affect these 14 *Pcdh* genes, five of these have changes in both H3K4me3 and H3K27. One particular RDHM overlaps with all 14 affected genes (**Figure 2.9**). Confirmation this RDHM with ChIP-qPCR was attempted; however, suitably efficient primers could not be designed to target the region. All RDHMs had a negative MAT score, indicating increased trimethylation in these regions at both H3K4me3 and H3K27me3.

**Table 2.6 Gene ontology (GO) analysis of genes with both H3K4me3 and H3K27me3 RDHMs in their promoter.**

<b>GO biological process</b>	
<b>GO term</b>	<b><i>p</i>-value</b>
Homophilic cell adhesion via plasma membrane adhesion molecules (GO:0007156)	1.80E-20
Cell-cell adhesion via plasma-membrane adhesion molecules (GO:0098742)	6.60E-19
Cell-cell adhesion (GO:0098609)	7.04E-19
Regulation of mitochondrial membrane potential (GO:0051881)	0.0013
Regulation of membrane potential (GO:0042391)	0.0088
Proline biosynthetic process (GO:0006561)	0.014
Positive regulation of mitochondrial fission (GO:0090141)	0.016
Positive regulation of protein homooligomerization (GO:0032464)	0.016
Negative regulation of interleukin-17 production (GO:0032700)	0.018
Killing of cells in other organism involved in symbiotic interaction (GO:0051883)	0.018
<b>GO cellular component</b>	
Dendrite cytoplasm (GO:0032839)	0.013
Cell projection cytoplasm (GO:0032838)	0.013
Terminal bouton (GO:0043195)	0.036
Presynaptic membrane (GO:0042734)	0.040
Perikaryon (GO:0043204)	0.044
Intermediate filament cytoskeleton (GO:0045111)	0.050
Ionotropic glutamate receptor complex (GO:0008328)	0.044
<b>GO molecular function</b>	
Calcium ion binding (GO:0005509)	5.95E-12
Extracellular-glutamate-gated ion channel activity (GO:0005234)	0.031
FMN binding (GO:0010181)	0.026
Ionotropic glutamate receptor activity (GO:0004970)	0.032
Oxidoreductase activity, acting on NAD(P)H, heme protein as acceptor (GO:0016653)	0.021
Oxidoreductase activity, acting on the CH-NH group of donors, NAD or NADP as acceptor (GO:0016646)	0.032
Glutamate receptor activity (GO:0008066)	0.045
Oxidoreductase activity, acting on the CH-NH group of donors (GO:0016645)	0.047

**Table 2.7 Pathways identified from each software suite in the genes in proximity to both H3K4me3 and H3K27me3 changes.**

Pathway name	Genes in pathway and list	p-value
<b>IPA</b>		
Cell-To-Cell Signaling and Interaction, Cellular Assembly and Organization, Nervous System Development and Function	<i>Fbxl16, Flii, Pebp4, Hoxa7, Pycr1, Pcdhga4, Pcdhgb5, Pcdhga7, Pcdhgb2, Pcdhga9, Pcdhgb1, Rassf1</i>	10E-23
Cell Death and Survival, Cancer, Infectious Disease	<i>Tusc2</i>	0.013
Immunological Disease, Infectious Disease, Cell Morphology	<i>H2-DMa</i>	0.04
<b>IPA canonical</b>		
Proline biosynthesis I	<i>Pycr1</i>	0.02
<b>Partek</b>		
Asthma	<i>Rassf, Pycr1, H2-DMa</i>	0.017
Intestinal immune network for IgA production	<i>Rassf</i>	0.030
Bladder cancer	<i>Rassf1</i>	0.031
Inflammatory bowel disease (IBD)	<i>Rassf1</i>	0.032
Arginine and proline metabolism	<i>Pycr1</i>	0.033
Staphylococcus aureus infection	<i>Rassf1</i>	0.033
Graft-versus-host disease	<i>Rassf1</i>	0.033
Allograft rejection	<i>Rassf1</i>	0.034
Type I diabetes mellitus	<i>Pycr1</i>	0.039
Autoimmune thyroid disease	<i>H2-DMa</i>	0.039
Non-small cell lung cancer	<i>Rassf1</i>	0.039
Biosynthesis of amino acids	<i>Pycr1</i>	0.041
<b>KEGG</b>		
Bladder cancer	<i>Rassf1</i>	0.018
Arginine and proline metabolism	<i>Pycr1</i>	0.021
Non-small cell lung cancer	<i>Rassf1</i>	0.025
Biosynthesis of amino acids	<i>Pycr1</i>	0.031
Glutamatergic synapse	<i>Rassf1</i>	0.048

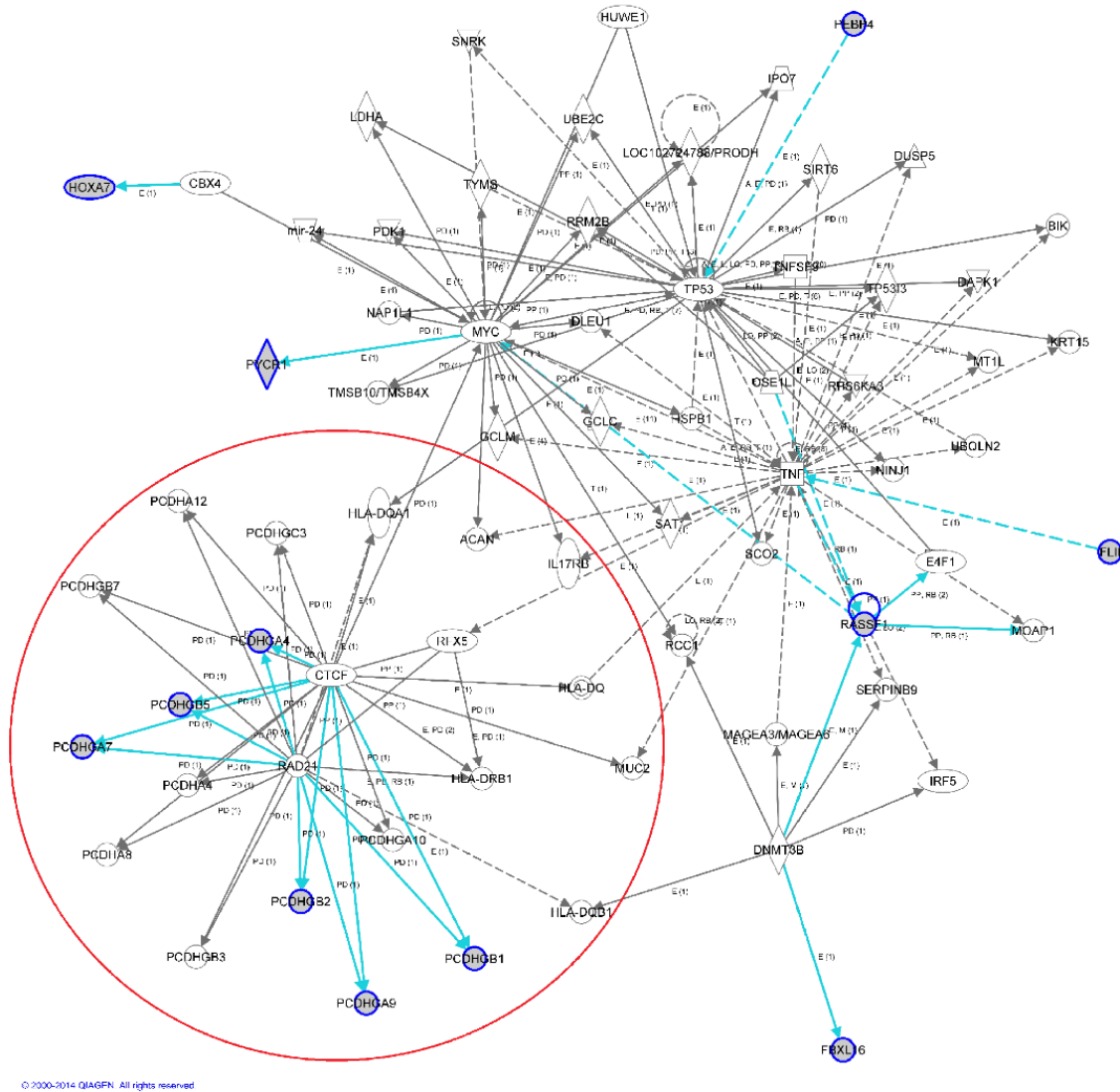


**Figure 2.8 Top Ingenuity Pathway Analysis (IPA) network for genes sharing both H3K4me3 and H3K27me3 RDHMs.**

The pathway is termed “Cell-To-Cell Signaling and Interaction, Cellular Assembly and Organization, Nervous System Development and Function”. Nodes outlined in blue represent proteins whose genes bear both H3K4me3 and H3K27me3 changes; functional relationships with these proteins are highlighted in light blue. Red circle highlights CTCF regulation of *Pcdh* genes. IPA pathway score 23 corresponding to  $p=10E-23$  (right-tailed Fisher Exact Test). See **Appendix B** for symbol legend.



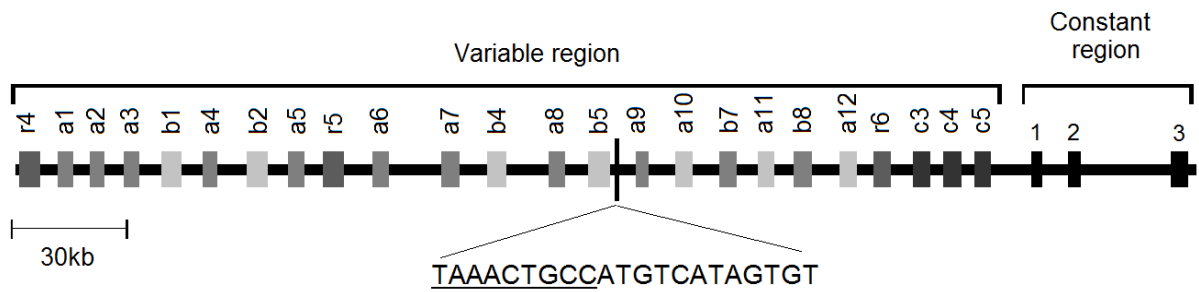


**Figure 2.9 Location of region of differential H3K4me3 & H3K27me3 containing putative CTCF binding motif in the mouse *Pcdhg* gene cluster.**

Total expanded DNA sequence shows the DMR, while the underlined region shows the putative CTCF binding motif. This DMR was enriched for H3K4me3 and H3K27me3 in ethanol-exposed mice (H3K4me3 MAT score = -11.2,  $p= 9.36E-5$ .; H3K27me3 MAT score = -14.1,  $p= 4.8E-4$ , CTCF position weight matrices score = 3.31)

#### 2.4.5 Protocadherin-Proximal CTCF Motifs Show Altered H3K4me3 and H3K27me3

Due to the implication of *Pcdh* genes and CTCF in the shared H3K4me3/H3K27me3 gene list, CTCF motif analysis was performed on the RDHM sequences using the CTCF prediction tool on the CTCFBS database 2.0. There were 150 out of 625 (24%) H3K4me3 RDHMs which contained a putative CTCF binding motif. For the H3K27me3 RDHMs, 46 out of 166 (28%) contained a putative CTCF binding motif. Further, CTCF was identified as a top upstream regulator for both the H3K4me3 and H3K27me3 genes by IPA and Enrichr, respectively.

The 11 specific RDHMs affecting the *Pcdh* genes were assessed for putative CTCF sites. One of the RDHMs contained a putative CTCF site (H3K4me3 MAT score = -11.2,  $p=9.36E-5$ ; H3K27me3 MAT score = -14.1,  $p=4.8E-4$ , CTCF PWM score = 3.31). This RDHM overlapped with the gene bodies of all 14 *Pcdh* genes identified, and is situated just after the first exon of *Pcdhgb5* (**Figure 2.9**). The TAAACTGCC sequence contained within the 20 bp RDHM is a predicted M2 CTCF binding motif (Schmidt et al., 2012). This particular sequence at this position is somewhat conserved in rat, and absent in humans.

#### 2.4.6 H3K27me3 Reduction at *Snrpn/Ube3a* CTCF Sites

CTCF also controls the expression of many imprinted genes. Given our laboratory's previous findings regarding CTCF binding sites in the *Snrpn/Ube3a* imprinted region (Laufer et al., 2013), histone methylation changes in potential CTCF binding motifs in this region were assessed. There were five RDHMs in the *Snrpn/Ube3a* region, two of which had significant predicted CTCF binding motifs (**Figure 2.10**). One was a reduction of H3K27me3 in ethanol-treated mice 2.5 kb upstream of the *Snrpn* transcriptional start site (H3K27me3 MAT score=1.5,  $p=0.001$ , CTCF position weight matrices score=3.23). The other was a reduction in H3K27me3 1.2 kb upstream of the *Snord116* first transcriptional start site (H3K27me3 MAT score=3.1,  $p=0.0004$ , CTCF PWM score=7.6). These CTCF motifs were in the correct orientation with respect to their gene promoters. One is a predicted M2 motif upstream of the *Snrpn* gene, the other is a

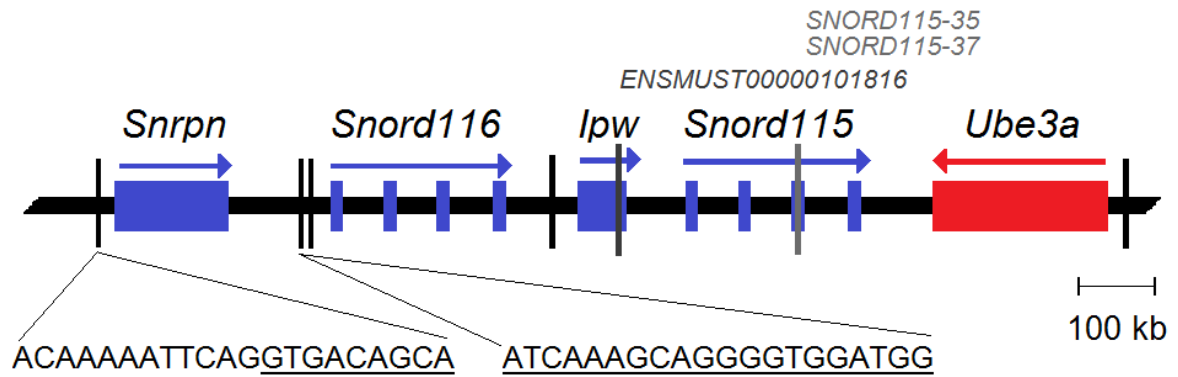


**Figure 2.10** Location of region of differential H3K27me3 in mouse *Snrpn/Ube3a* locus.

RDHMs are shown as vertical black lines. RDHMs containing a putative CTCF binding site are expanded to sequence view, with the CTCF motif underlined. The RDHM upstream of *Snrpn* was depleted of H3K27me3 in ethanol-exposed mice (MAT score = 1.5,  $p = 0.002$ , CTCF position weight matrices score = 3.23). The RDHM upstream of *Snord116* was also depleted of H3K27me3 in ethanol-exposed mice (MAT score = 3.1,  $p = 0.0004$ , CTCF position weight matrices score = 7.6).

predicted LM7 motif (Xie et al., 2007) upstream of the *Snord116* promoter. There were no H3K4me3 changes in the region.

Confirmation of all the RDHMs in Figure 2.10 were attempted with ChIP-qPCR (**Figure 2.11**). The *Snrpn* RDHM showed  $2.55 \pm 0.69$  fold H3K27me3 enrichment in ethanol-exposed mice vs.  $2.88 \pm 1.13$  in control mice ( $p=0.42$ , Paired Samples t-Test). The more 5' region upstream of *Snord116* showed  $3.18 \pm 1.26$  fold H3K27me3 enrichment in ethanol-exposed mice vs  $3.90 \pm 0.85$  in control mice ( $p=0.34$ , Paired Samples t-Test). The region more proximal to *Snord116* showed  $3.03 \pm 0.92$  fold H3K27me3 enrichment in ethanol-exposed mice vs.  $4.18 \pm 1.93$  in control mice ( $p=0.32$ , Paired Samples t-Test). The RDHM upstream of *IPW* showed  $2.53 \pm 0.35$  fold H3K27me3 enrichment in ethanol-exposed mice vs.  $4.30 \pm 0.22$  in control mice ( $p=0.26$ , Paired Samples t-test). Primers could not be designed to target the RDHM upstream of *Ube3a*.

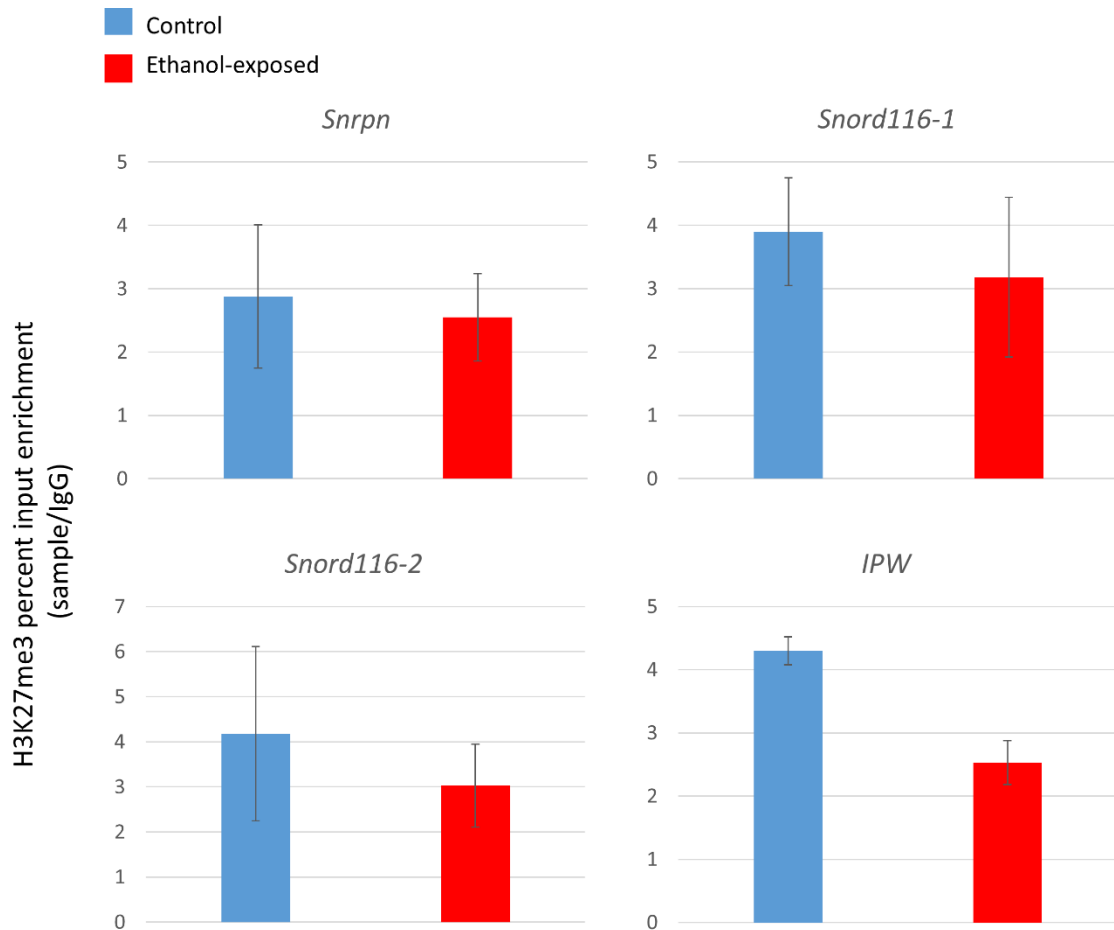


**Figure 2.11 Attempted chromatin immunoprecipitation-real-time PCR confirmations of H3K27me3 RDHMs in the *Snrpn/Ube3a* locus.**

ChIP against each region was performed in independent biological samples (n=5 ethanol, n=5 control) i.e. different mice than the ChIP-chip array. Enrichment for each sample was assessed using qPCR and compared to its IgG control using  $\% \text{ enrichment} = 100\% \times \text{efficiency}^{(\text{input } C_t - \text{H3K27me3 } C_t)}$ . Data shown are average percent H3K27me3 enrichment  $\pm$  standard error. Significance was assessed using a Paired Samples t-Test; no region was significantly enriched between ethanol and control groups.

## 2.5 Discussion

### 2.5.1 Gene Ontology Analysis Implicates Synaptic Development Genes

GO analysis of each of the H3K4me3, H3K27me3, and shared H3K4me3/H3K27me3 gene lists implicate synaptic development genes. The H3K4me3 gene list was enriched for cell-cell adhesion genes, nervous system development genes, and synaptic genes (**Table 2.2**). Similarly, GO analysis of the H3K27me3 gene list showed enrichment of cell-cell adhesion genes, and neuron development genes (**Table 2.3**). In the shared gene list, the top three GO biological processes were cell-cell adhesion related (**Table 2.6**). The top implicated cellular components included many dendrite and synapse-related categories.

Taken together, the GO analyses of each gene list suggest that nervous system development and cell-cell adhesion genes are disproportionately proximal to H3K4me3 and H3K27me3 changes in this model. The development of synapses during the neonatal period in mice is guided by communication via cell-cell adhesion molecules, including protocadherins (Cohen-Cory, 2002); the presence of these genes in each list likely drive the implication of synaptic GO categories (Discussed in section 2.5.3 below). Disruption of synaptogenesis by ethanol can lead to improper synapse formation, interfering with synaptic transmission, potentiation, and plasticity in adulthood (Mameli et al., 2005; Olney et al., 2002; Puglia and Valenzuela, 2010). Dysregulation in the expression of cell-cell communication and synaptic development GO categories at PND 70 was reported previously in our laboratory in this model (Kleiber et al., 2013). In this previous work and this thesis, these alterations to synaptic development genes persist long after exposure to ethanol. Such changes may represent the presence of a different pool of cells in the brain following PND 4,7 ethanol-induced apoptosis, differential expression/methylation of genes in remaining cell, or a combination of both (Kleiber et al., 2014). In any case, these changes may represent a residual footprint of ethanol exposure.

### 2.5.2 H3K4me3 Changes Affect Lipid Pathways

The most striking feature of the pathways affected in the H3K4me3 genes is the abundance of lipid metabolism pathways (**Table 2.4**). There were 10 pathways involving

lipids identified across the three software platforms. Figure 2.7 shows the top lipid-related pathway. The hub of this network is leptin, a peptide hormone that is the master regulator of hunger and adipocyte function. Failure of leptin to cross the blood-brain implicates leptin in neurological disorders such as Alzheimer's (Lee, 2011). Other important hub genes are the  $\beta$ -oxidation enzymes ACOX1 and BDNF, implicated in a host of neurodevelopmental and processes and pathologies. There were several individual genes identified as having proximal H3K4me3 driving lipid pathway identification. These include the genes encoding the  $\beta$ -oxidation enzymes *Acs14* and *Acs16*, lipases *Pnpla2* and *Lipe*, sialidases *Neu1* and *Neu2*, sphingomyelinases *Smpd4* and *Smpd3*, pre-angiotensinogen *Agt* and oxidoreductase *Ecsit* (**Table 2.4**). *Acs16* was upregulated in an embryonic model of FASD (Zhou et al., 2011a). *Pnpla2* expression was reduced in adult mice exposed to fetal ethanol (Christensen et al., 2015).

Alteration of lipid metabolism is a feature of FASD. Prenatal ethanol exposure causes changes in cholesterol in the adult mouse brain (Barcelo-Coblijn et al., 2013). Prenatal ethanol exposure also causes changes to the entire phospholipid profile in the hippocampus (Wen and Kim, 2004). Neonatal ethanol exposure during the third trimester equivalent is characterized by widespread apoptosis involving Bax and caspase-3 activation.  $\beta$ -oxidation of fatty acids also produces reactive oxygen species (ROS). The ACOX enzyme (present in the top network shown in **Figure 2.7**) catalyzes the first step of  $\beta$ -oxidation in the brain and is a major source of ROS (Trompier et al., 2014). Fetal alcohol exposure causes lipid peroxidation in the brain after ethanol exposure which can persist to adulthood (Brocardo et al., 2016; Petkov et al., 1992; Smith et al., 2005). Supplementation with omega-3 fatty acids can prevent oxidative damage and hippocampal synaptic changes caused by prenatal ethanol exposure (Patten et al., 2013a, 2013b). This thesis is the first report of an interaction of histone modification and lipid metabolism in ethanol-exposed hippocampus, the region implicated in learning and memory deficits.

### 2.5.3 Enrichment of Protocadherin Genes for H3K4me3 & H3K27me3 Changes

The simultaneous changes in H3K4me3 and H3K27me3 are proximal to genes in the network “Cell-to-cell signaling and interaction, cellular assembly and organization, nervous system development and function” (**Figure 2.8**). This is the gene network responsible for shaping cell-to-cell communication in the brain—synaptogenesis—during development. The peak of synaptogenesis occurs on PND 7 in mice (Dobbing and Sands, 1979). Several RDHM-proximal genes in the top pathway were protocadherin (*Pcdh*) genes which are crucial for synaptogenesis. *Pcdh* genes are clusters of related genes that are believed to be responsible for establishing specific connections between neurons in vertebrate brain development by generating single-neuron diversity (Thu et al., 2014). *The Pcdhg* genes are necessary for neurite self-avoidance (Lefebvre et al., 2012). PCDH proteins allow neurons to determine if they are self-synapsing, or synapsing with another neuron. Neurites can then use this diversity to form the complex web of synaptic connections during trimester three. Most *Pcdh* genes are organized into three genomic clusters which are conserved across species. The *Pcdha*, *Pcdhb* and *Pcdhg* gene clusters are located in tandem on human chromosome 5, and mouse chromosome 18. *Pcdha* and *Pcdhg* have alternative first exons and are regulated by complex hierarchical chromatin looping (Tasic et al., 2002; Wang et al., 2002). This leads to proteins with differing extracellular domains, and constant cytoplasmic domains generating neuronal individuality and guiding synaptic interactions.

The *Pcdh* genes are regulated in part by CCCTC-binding factor (CTCF). CTCF creates three dimensional chromatin domains, and promotes specific regulatory interactions that positively or negatively affect transcription (Ong and Corces, 2014). The relationship of CTCF with histone modification is complex, and differs based on the genomic context. Little is known about the relationship between H3K4me3 and CTCF. H3K27me3 is enriched at CTCF binding sites, and may play a functional role in its binding at some loci (Handoko et al., 2011). CTCF can also recruit the PRC2 complex which trimethylates H3K27me3 (Li et al., 2012). CTCF acts as an insulator to the repressive H3K27me3 mark and thereby promotes gene expression. Loss of CTCF can thus lead to inappropriate gene silencing at such loci (Witcher and Emerson, 2009). All of



the H3K4me3 and H3K27me3 RDHMs in the *Pcdh* loci identified here were increases in methylation (**Appendix E**). These gains of H3K27me3 may be correlated with enhanced CTCF binding, disrupting regulation of the region. Increased histone methylation and enhanced CTCF binding in response to early ethanol exposure is consistent with DNA methylation data.

Two recent studies—one from our laboratory—associate increased DNA methylation at *Pcdh* loci with FASD in humans. Laufer et al., (2015) found that there was increased DNA methylation in the *Pcdhg* cluster in children with FAS. A similar study design with a larger sample size found again increases in DNA methylation in the *Pcdhb* and *Pcdhg* cluster in children with FASD (Portales-Casamar et al., 2016). These two studies point to *Pcdh* loci as candidate epigenetic biomarkers of FASD. Together with the data presented in this thesis, a clear picture emerges suggesting protocadherin genes as strong candidates for FASD etiology.

#### 2.5.4 H3K27me3 Changes Affect Imprinted Loci

Previous work from our laboratory implicated DNA methylation changes at CTCF sites in imprinted loci. Therefore, such sites were assessed for histone methylation changes. The *Snrpn-Ube3a* locus expresses a neuron-specific polycistronic transcript that includes two clusters of snoRNAs (Le Meur et al., 2005). The function of this transcript is not clear; however its timing and dosage are critical, with alterations leading to neurodevelopmental disorders (Leung et al., 2009). There were putative CTCF sites at two of five H3K27me3 RDHMs in the *Snrpn/Ube3a* imprinted region. One site was upstream of *Snrpn* and the other is upstream of *Snord116* (**Figure 2.10**). A reduction of methylation in H3K27me3 at CTCF sites could have a number of explanations. It is likely that the H3K27me3 change itself was a result of altered one-carbon metabolism by ethanol, which would then affect CTCF binding. It is also possible that ethanol-induced changes in CTCF binding occurred, which precipitated H3K27me3 reduction, but a mechanism for this is not clear. As described in the previous section, H3K27me3 may be involved in the formation of CTCF DNA loops. Therefore, the reduction of H3K27me3 at CTCF motifs found at the *Snrpn/Ube3a* locus here may correlate with reduced CTCF binding and a loss of looping and gene expression. It is known that a loss of CTCF at

imprinted loci is associated with loss of insulator function, and thus deregulation of imprinted genes (Kanduri et al., 2002; Szabo et al., 2004).

Confirmation of each of the RDHMs in the region was attempted (**Figure 2.11**). The differences in enrichment between the ethanol-exposed and control groups were not statistically significant. Each of the regions did trend toward the expected difference, that is a decrease in H3K27me3 enrichment in ethanol-exposed mice. It is possible that increased sample size would bring these regions toward significance. It should also be noted that these confirmation ChIP-qPCR experiments were done in independent biological samples, i.e. different mice than the ChIP-Chip assessment. Replication between biological groups can be a challenge in ethanol research due to the heterogeneous nature of the effects of ethanol.

The results of this section are supported by previous work from our laboratory which found several ethanol-induced DNA methylation changes at imprinted regions including CTCF sites. There was an increase in DNA methylation at CTCF sites in the imprinting control region (ICR) of *H19* and *Igf2* (*H19/Igf2*) in response to fetal ethanol exposure (Laufer et al., 2013). Others have also found changes in this particular CTCF site in FASD including differential DNA methylation in FASD placental tissue (Haycock, 2009) and in sperm of alcohol-consuming fathers (Knezovich and Ramsay, 2012). At the *Snrpn/Ube3a* locus specifically, our laboratory has shown increased expression of ncRNA in FASD individuals (Laufer et al., 2015). Other research has found methylation changes in the *Ube3a* gene in a model of FASD (Liu et al., 2009).

### 2.5.5 Conclusion

In this chapter, genes and pathways affected by histone methylation changes in response to early ethanol exposure are described. Lipid metabolism genes were predominantly proximal to H3K4me3 changes, which is consistent with results from the gene expression and DNA methylation chapters of this thesis. A putative CTCF motif in one of the *Pcdhg* promoters was found to have increased levels of H3K4me3 and H3K27me3. Confirmation of this change by ChIP-qPCR was attempted; however, efficient primers could not be designed for the region. Alteration of the epigenetic state of this motif could affect the regulation of the entire region given that loss of CTCF is associated

with reduced *Pcdh* expression dendritic arborisation (Hirayama et al., 2012). The methylation changes may be remnants of earlier dysregulation, perhaps from the synaptogenesis period. This observation may relate to learning and memory deficits in FASD since these processes are dependent on synaptic structure and plasticity in the hippocampus (Bliss and Collingridge, 1993; Whitlock et al., 2006). Indeed, our laboratory has previously shown that this mouse model has impaired learning and memory into adulthood (Mantha et al., 2014) and that many CTCF sites show altered DNA methylation in whole-brain tissue (Laufer et al., 2013). The potential for epigenetic deregulation of *Pcdh* genes to underlie this phenotype is also evident in changes in gene expression and DNA methylation (Laufer et al., 2013). Such long lasting effects are viewed as stable; they may account for cellular changes underling learning and memory deficits in FASD. Finally, reduction in H3K27me3 across the *Snrpn/Ube3A* locus was identified. These changes were not confirmed, but trended towards a reduction. Again, this loss of methylation may represent footprint of earlier ethanol exposure.

The results of this section represent a timepoint in a small portion of the hippocampal epigenome in response to ethanol. Based on the known effects of ethanol on lipid metabolism, oxidative stress, methylation pathways, etc. hypotheses can be generated regarding the origins of these histone methylation changes. The results of this chapter suggest that altered one-carbon metabolism affects H3K4me3 and H3K27me3 soon after ethanol exposure which are maintained to PND 70. Further work characterizing the histone methylation of the identified regions and their expression is needed at earlier timepoints.

### **Footnote**

A modified version of this chapter has been published (Chater-Diehl et al., 2017).

## 2.6 References

- Alabert, C., and Groth, A. (2012). Chromatin replication and epigenome maintenance. *Nat. Rev. Mol. Cell Biol.* *13*, 153–167.
- Alabert, C., Barth, T.K., Reverón-Gómez, N., Sidoli, S., Schmidt, A., Jensen, O.N., Imhof, A., and Groth, A. (2015). Two distinct modes for propagation of histone PTMs across the cell cycle. *Genes Dev.* *29*, 585–590.
- Allan, J., Harborne, N., Rau, D.C., and Gould, H. (1982). Participation of core histone “tails” in the stabilization of the chromatin solenoid. *J. Cell Biol.* *93*, 285–297.
- Allfrey, V.G., Faulkner, R., and Mirsky, A.E. (1964). Acetylation and Methylation of Histones and their Possible Role in the Regulation of Rna Synthesis. *Proc. Natl. Acad. Sci. U. S. A.* *51*, 786–794.
- Annunziato, A.T. (2005). Split decision: what happens to nucleosomes during DNA replication? *J. Biol. Chem.* *280*, 12065–12068.
- Barcelo-Coblijn, G., Wold, L.E., Ren, J., and Murphy, E.J. (2013). Prenatal ethanol exposure increases brain cholesterol content in adult rats. *Lipids* *48*, 1059–1068.
- Barski, A., Cuddapah, S., Cui, K., Roh, T.-Y., Schones, D.E., Wang, Z., Wei, G., Chepelev, I., and Zhao, K. (2007). High-resolution profiling of histone methylations in the human genome. *Cell* *129*, 823–837.
- Bartolomei, M.S., and Tilghman, S.M. (1997). Genomic imprinting in mammals. *Annu. Rev. Genet.* *31*, 493–525.
- Bekdash, R.A., Zhang, C., and Sarkar, D.K. (2013). Gestational Choline Supplementation Normalized Fetal Alcohol-Induced Alterations in Histone Modifications, DNA Methylation, and Proopiomelanocortin (POMC) Gene Expression in beta-Endorphin-Producing POMC Neurons of the Hypothalamus. *Alcohol. Clin. Exp. Res.*
- Bernstein, B.E., Mikkelsen, T.S., Xie, X., Kamal, M., Huebert, D.J., Cuff, J., Fry, B., Meissner, A., Wernig, M., Plath, K., et al. (2006). A bivalent chromatin structure marks key developmental genes in embryonic stem cells. *Cell* *125*, 315–326.
- Bliss, T. V., and Collingridge, G.L. (1993). A synaptic model of memory: long-term potentiation in the hippocampus. *Nature* *361*, 31–39.
- Boyer, L.A., Plath, K., Zeitlinger, J., Brambrink, T., Medeiros, L.A., Lee, T.I., Levine, S.S., Wernig, M., Tajonar, A., Ray, M.K., et al. (2006). Polycomb complexes repress developmental regulators in murine embryonic stem cells. *Nature* *441*, 349–353.
- Brocardo, P.S., Gil-Mohapel, J., Wortman, R., Noonan, A., McGinnis, E., Patten, A.R.,

- and Christie, B.R. (2016). The Effects of Ethanol Exposure During Distinct Periods of Brain Development on Oxidative Stress in the Adult Rat Brain. *Alcohol. Clin. Exp. Res.*
- Butler, M.G. (2009). Genomic imprinting disorders in humans: a mini-review. *J. Assist. Reprod. Genet.* *26*, 477–486.
- Chater-Diehl, E.J., Laufer, B.I., and Singh, S.M. (2017). Changes to histone modifications following prenatal alcohol exposure: An emerging picture. *Alcohol.*
- Chen, E.Y., Tan, C.M., Kou, Y., Duan, Q., Wang, Z., Meirelles, G. V., Clark, N.R., and Ma'ayan, A. (2013). Enrichr: interactive and collaborative HTML5 gene list enrichment analysis tool. *BMC Bioinformatics* *14*, 128.
- Christensen, K.E., Mikael, L.G., Leung, K.-Y., Lévesque, N., Deng, L., Wu, Q., Malysheva, O. V, Best, A., Caudill, M.A., Greene, N.D.E., et al. (2015). High folic acid consumption leads to pseudo-MTHFR deficiency, altered lipid metabolism, and liver injury in mice. *Am. J. Clin. Nutr.* *101*, 646–658.
- Christman, J.K., Sheikhnejad, G., Marasco, C.J., and Sufrin, J.R. (1995). 5-Methyl-2'-deoxycytidine in single-stranded DNA can act in cis to signal de novo DNA methylation. *Proc. Natl. Acad. Sci. U. S. A.* *92*, 7347–7351.
- Cohen-Cory, S. (2002). The developing synapse: construction and modulation of synaptic structures and circuits. *Science* *298*, 770–776.
- Collas, P. (2010). The current state of chromatin immunoprecipitation. *Mol. Biotechnol.* *45*, 87–100.
- Dobbing, J., and Sands, J. (1979). Comparative aspects of the brain growth spurt. *Early Hum. Dev.* *3*, 79–83.
- Dong, X., Greven, M.C., Kundaje, A., Djebali, S., Brown, J.B., Cheng, C., Gingeras, T.R., Gerstein, M., Guigó, R., Birney, E., et al. (2012). Modeling gene expression using chromatin features in various cellular contexts. *Genome Biol.* *13*, R53.
- Dynlacht, B.D., Hoey, T., and Tjian, R. (1991). Isolation of coactivators associated with the TATA-binding protein that mediate transcriptional activation. *Cell* *66*, 563–576.
- Garro, A.J., McBeth, D.L., Lima, V., and Lieber, C.S. (1991). Ethanol consumption inhibits fetal DNA methylation in mice: implications for the fetal alcohol syndrome. *Alcohol. Clin. Exp. Res.* *15*, 395–398.
- Golan-Mashiach, M., Grunspan, M., Emmanuel, R., Gibbs-Bar, L., Dikstein, R., and Shapiro, E. (2012). Identification of CTCF as a master regulator of the clustered protocadherin genes. *Nucleic Acids Res.* *40*, 3378–3391.

- Gordon, F., Luger, K., and Hansen, J.C. (2005). The core histone N-terminal tail domains function independently and additively during salt-dependent oligomerization of nucleosomal arrays. *J. Biol. Chem.* *280*, 33701–33706.
- Govorko, D., Bekdash, R.A., Zhang, C., and Sarkar, D.K. (2012). Male germline transmits fetal alcohol adverse effect on hypothalamic proopiomelanocortin gene across generations. *Biol. Psychiatry* *72*, 378–388.
- Guo, W., Crossey, E.L., Zhang, L., Zucca, S., George, O.L., Valenzuela, C.F., and Zhao, X. (2011). Alcohol exposure decreases CREB binding protein expression and histone acetylation in the developing cerebellum. *PLoS One* *6*, e19351.
- Halsted, C.H., Villanueva, J.A., Devlin, A.M., Niemela, O., Parkkila, S., Garrow, T.A., Wallock, L.M., Shigenaga, M.K., Melnyk, S., and James, S.J. (2002). Folate deficiency disturbs hepatic methionine metabolism and promotes liver injury in the ethanol-fed micropig. *Proc. Natl. Acad. Sci. U. S. A.* *99*, 10072–10077.
- Hamid, A., and Kaur, J. (2005). Kinetic characteristics of folate binding to rat renal brush border membrane in chronic alcoholism. *Mol. Cell. Biochem.* *280*, 219–225.
- Hamid, A., and Kaur, J. (2007a). Long-term alcohol ingestion alters the folate-binding kinetics in intestinal brush border membrane in experimental alcoholism. *Alcohol* *41*, 441–446.
- Hamid, A., and Kaur, J. (2007b). Decreased Expression of Transporters Reduces Folate Uptake across Renal Absorptive Surfaces in Experimental Alcoholism. *J. Membr. Biol.* *220*, 69–77.
- Handoko, L., Xu, H., Li, G., Ngan, C.Y., Chew, E., Schnapp, M., Lee, C.W., Ye, C., Ping, J.L., Mulawadi, F., et al. (2011). CTCF-mediated functional chromatin interactome in pluripotent cells. *Nat. Genet.* *43*, 630–638.
- Haycock, P.C. (2009). Fetal alcohol spectrum disorders: the epigenetic perspective. *Biol. Reprod.* *81*, 607–617.
- Hirayama, T., Tarusawa, E., Yoshimura, Y., Galjart, N., and Yagi, T. (2012). CTCF is required for neural development and stochastic expression of clustered Pcdh genes in neurons. *Cell Rep.* *2*, 345–357.
- Hödl, M., and Basler, K. (2012). Transcription in the absence of histone H3.2 and H3K4 methylation. *Curr. Biol.* *22*, 2253–2257.
- Hoek, J.B., Cahill, A., and Pastorino, J.G. (2002). Alcohol and mitochondria: a dysfunctional relationship. *Gastroenterology* *122*, 2049–2063.
- Holwerda, S.J.B., and de Laat, W. (2013). CTCF: the protein, the binding partners, the binding sites and their chromatin loops. *Philos. Trans. R. Soc. Lond. B. Biol. Sci.* *368*, 20120369.

- Huang, C., Xu, M., and Zhu, B. (2013). Epigenetic inheritance mediated by histone lysine methylation: maintaining transcriptional states without the precise restoration of marks? *Philos. Trans. R. Soc. Lond. B. Biol. Sci.* 368, 20110332.
- Ikonomidou, C., Bittigau, P., Ishimaru, M.J., Wozniak, D.F., Koch, C., Genz, K., Price, M.T., Stefovská, V., Horster, F., Tenkova, T., et al. (2000). Ethanol-induced apoptotic neurodegeneration and fetal alcohol syndrome. *Science* 287, 1056–1060.
- Jackson, V. (1978). Studies on histone organization in the nucleosome using formaldehyde as a reversible cross-linking agent. *Cell* 15, 945–954.
- Jackson, V. (1988). Deposition of newly synthesized histones: hybrid nucleosomes are not tandemly arranged on daughter DNA strands. *Biochemistry* 27, 2109–2120.
- Kanduri, M., Kanduri, C., Mariano, P., Vostrov, A.A., Quitschke, W., Lobanenkova, V., and Ohlsson, R. (2002). Multiple nucleosome positioning sites regulate the CTCF-mediated insulator function of the H19 imprinting control region. *Mol. Cell. Biol.* 22, 3339–3344.
- Kenyon, S.H., Nicolaou, A., and Gibbons, W.A. (1998). The effect of ethanol and its metabolites upon methionine synthase activity in vitro. *Alcohol* 15, 305–309.
- Kerksick, C., and Willoughby, D. (2005). The antioxidant role of glutathione and N-acetyl-cysteine supplements and exercise-induced oxidative stress. *J. Int. Soc. Sports Nutr.* 2, 38–44.
- Kim, J.-S., and Shukla, S.D. (2005). Histone h3 modifications in rat hepatic stellate cells by ethanol. *Alcohol* 40, 367–372.
- Kleiber, M.L., Mantha, K., Stringer, R.L., and Singh, S.M. (2013). Neurodevelopmental alcohol exposure elicits long-term changes to gene expression that alter distinct molecular pathways dependent on timing of exposure. *J. Neurodev. Disord.* 5, 6.
- Kleiber, M.L., Diehl, E.J., Laufer, B.I., Mantha, K., Chokroborty-Hoque, A., Alberry, B., and Singh, S.M. (2014). Long-term genomic and epigenomic dysregulation as a consequence of prenatal alcohol exposure: a model for fetal alcohol spectrum disorders. *Front. Genet.* 5, 161.
- Knezovich, J.G., and Ramsay, M. (2012). The effect of preconception paternal alcohol exposure on epigenetic remodeling of the h19 and rasgrf1 imprinting control regions in mouse offspring. *Front. Genet.* 3, 10.
- Kouzarides, T. (2007). Chromatin modifications and their function. *Cell* 128, 693–705.
- Lauberth, S.M., Nakayama, T., Wu, X., Ferris, A.L., Tang, Z., Hughes, S.H., and Roeder, R.G. (2013). H3K4me3 interactions with TAF3 regulate preinitiation complex assembly and selective gene activation. *Cell* 152, 1021–1036.

- Laufer, B.I., Mantha, K., Kleiber, M.L., Diehl, E.J., Addison, S.M., and Singh, S.M. (2013). Long-lasting alterations to DNA methylation and ncRNAs could underlie the effects of fetal alcohol exposure in mice. *Dis. Model. Mech.* 6, 977–992.
- Laufer, B.I., Kapalanga, J., Castellani, C.A., Diehl, E.J., Yan, L., and Singh, S.M. (2015). Associative DNA methylation changes in children with prenatal alcohol exposure. *Epigenomics* 1–16.
- Lee, E.B. (2011). Obesity, leptin, and Alzheimer's disease. *Ann. N. Y. Acad. Sci.* 1243, 15–29.
- Lefebvre, J.L., Kostadinov, D., Chen, W. V, Maniatis, T., and Sanes, J.R. (2012). Protocadherins mediate dendritic self-avoidance in the mammalian nervous system. *Nature* 488, 517–521.
- Lehnertz, B., Ueda, Y., Derijck, A.A., Braunschweig, U., Perez-Burgos, L., Kubicek, S., Chen, T., Li, E., Jenuwein, T., and Peters, A.H. (2003). Suv39h-mediated histone H3 lysine 9 methylation directs DNA methylation to major satellite repeats at pericentric heterochromatin. *Curr. Biol.* 13, 1192–1200.
- Leung, K.N., Vallero, R.O., DuBose, A.J., Resnick, J.L., and LaSalle, J.M. (2009). Imprinting regulates mammalian snoRNA-encoding chromatin decondensation and neuronal nucleolar size. *Hum. Mol. Genet.* 18, 4227–4238.
- Li, G., Ruan, X., Auerbach, R.K., Sandhu, K.S., Zheng, M., Wang, P., Poh, H.M., Goh, Y., Lim, J., Zhang, J., et al. (2012). Extensive Promoter-Centered Chromatin Interactions Provide a Topological Basis for Transcription Regulation. *Cell* 148, 84–98.
- Liu, Y., Balaraman, Y., Wang, G., Nephew, K.P., and Zhou, F.C. (2009). Alcohol exposure alters DNA methylation profiles in mouse embryos at early neurulation. *Epigenetics* 4, 500–511.
- Luger, K., Mader, A.W., Richmond, R.K., Sargent, D.F., and Richmond, T.J. (1997). Crystal structure of the nucleosome core particle at 2.8 Å resolution. *Nature* 389, 251–260.
- Mameli, M., Zamudio, P.A., Carta, M., and Valenzuela, C.F. (2005). Developmentally regulated actions of alcohol on hippocampal glutamatergic transmission. *J. Neurosci.* 25, 8027–8036.
- Mantha, K., Laufer, B.I., and Singh, S.M. (2014). Molecular changes during neurodevelopment following second-trimester binge ethanol exposure in a mouse model of fetal alcohol spectrum disorder: from immediate effects to long-term adaptation. *Dev. Neurosci.* 36, 29–43.
- Margueron, R., and Reinberg, D. (2010). Chromatin structure and the inheritance of epigenetic information. *Nat. Rev. Genet.* 11, 285–296.



- Massie, C.E., and Mills, I.G. (2012). Mapping protein-DNA interactions using ChIP-sequencing. *Methods Mol. Biol.* *809*, 157–173.
- Le Meur, E., Watrin, F., Landers, M., Sturny, R., Lalande, M., and Muscatelli, F. (2005). Dynamic developmental regulation of the large non-coding RNA associated with the mouse 7C imprinted chromosomal region. *Dev. Biol.* *286*, 587–600.
- Morgan, H.D., Santos, F., Green, K., Dean, W., and Reik, W. (2005). Epigenetic reprogramming in mammals. *Hum. Mol. Genet.* *14 Spec No*, R47-58.
- Oliver, S.S., and Denu, J.M. (2011). Dynamic interplay between histone H3 modifications and protein interpreters: emerging evidence for a “histone language”. *Chembiochem* *12*, 299–307.
- Olney, J.W., Tenkova, T., Dikranian, K., Qin, Y.Q., Labruyere, J., and Ikonomidou, C. (2002). Ethanol-induced apoptotic neurodegeneration in the developing C57BL/6 mouse brain. *Brain Res. Brain Res.* *133*, 115–126.
- Ong, C.T., and Corces, V.G. (2014). CTCF: an architectural protein bridging genome topology and function. *Nat. Rev.* *15*, 234–246.
- Pal-Bhadra, M., Bhadra, U., Jackson, D.E., Mamatha, L., Park, P.-H., and Shukla, S.D. (2007). Distinct methylation patterns in histone H3 at Lys-4 and Lys-9 correlate with up- & down-regulation of genes by ethanol in hepatocytes. *Life Sci.* *81*, 979–987.
- Park, P.J. (2009). ChIP-seq: advantages and challenges of a maturing technology. *Nat. Rev.* *10*, 669–680.
- Park, P.-H., Miller, R., and Shukla, S.D. (2003). Acetylation of histone H3 at lysine 9 by ethanol in rat hepatocytes. *Biochem. Biophys. Res. Commun.* *306*, 501–504.
- Patten, A.R., Brocardo, P.S., and Christie, B.R. (2013a). Omega-3 supplementation can restore glutathione levels and prevent oxidative damage caused by prenatal ethanol exposure. *J. Nutr. Biochem.* *24*, 760–769.
- Patten, A.R., Sickmann, H.M., Dyer, R.A., Innis, S.M., and Christie, B.R. (2013b). Omega-3 fatty acids can reverse the long-term deficits in hippocampal synaptic plasticity caused by prenatal ethanol exposure. *Neurosci. Lett.* *551*, 7–11.
- Petkov, V. V., Stoianovski, D., Petkov, V.D., and Vyglanova, I. (1992). Lipid peroxidation changes in the brain in fetal alcohol syndrome. *Biull. Eksp. Biol. Med.* *113*, 500–502.
- Portales-Casamar, E., Lussier, A.A., Jones, M.J., MacIsaac, J.L., Edgar, R.D., Mah, S.M., Barhdadi, A., Provost, S., Lemieux-Perreault, L.-P., Cynader, M.S., et al. (2016). DNA methylation signature of human fetal alcohol spectrum disorder. *Epigenetics Chromatin* *9*, 25.

- Probst, A. V, Dunleavy, E., and Almouzni, G. (2009). Epigenetic inheritance during the cell cycle. *Nat. Rev. Mol. Cell Biol.* *10*, 192–206.
- Puglia, M.P., and Valenzuela, C.F. (2010). Ethanol Acutely Inhibits Ionotropic Glutamate Receptor-Mediated Responses and Long-Term Potentiation in the Developing CA1 Hippocampus. *Alcohol. Clin. Exp. Res.* *34*, 594–606.
- Rosenfeld, C.S. (2010). Animal models to study environmental epigenetics. *Biol. Reprod.* *82*, 473–488.
- Santos-Rosa, H., Schneider, R., Bannister, A.J., Sherriff, J., Bernstein, B.E., Emre, N.C., Schreiber, S.L., Mellor, J., and Kouzarides, T. (2002). Active genes are trimethylated at K4 of histone H3. *Nature* *419*, 407–411.
- Schaefer, A., Sampath, S.C., Intrator, A., Min, A., Gertler, T.S., Surmeier, D.J., Tarakhovsky, A., and Greengard, P. (2009). Control of cognition and adaptive behavior by the GLP/G9a epigenetic suppressor complex. *Neuron* *64*, 678–691.
- Schmidt, D., Schwalie, P.C., Wilson, M.D., Ballester, B., Gonçalves, Â., Kutter, C., Brown, G.D., Marshall, A., Flicek, P., and Odom, D.T. (2012). Waves of Retrotransposon Expansion Remodel Genome Organization and CTCF Binding in Multiple Mammalian Lineages. *Cell* *148*, 335–348.
- Schneider, R., Bannister, A.J., Myers, F.A., Thorne, A.W., Crane-Robinson, C., and Kouzarides, T. (2004). Histone H3 lysine 4 methylation patterns in higher eukaryotic genes. *Nat. Cell Biol.* *6*, 73–77.
- Seitz, H.K., and Stickel, F. (2007). Molecular mechanisms of alcohol-mediated carcinogenesis. *Nat. Rev. Cancer* *7*, 599–612.
- Shinkai, Y., and Tachibana, M. (2011). H3K9 methyltransferase G9a and the related molecule GLP. *Genes Dev.* *25*, 781–788.
- Slotkin, R.K., and Martienssen, R. (2007). Transposable elements and the epigenetic regulation of the genome. *Nat. Rev. Genet.* *8*, 272–285.
- Smith, A.M., Zeve, D.R., Grisel, J.J., and Chen, W.J. (2005). Neonatal alcohol exposure increases malondialdehyde (MDA) and glutathione (GSH) levels in the developing cerebellum. *Brain Res. Brain Res.* *160*, 231–238.
- Soufi, A., Donahue, G., and Zaret, K.S. (2012). Facilitators and impediments of the pluripotency reprogramming factors' initial engagement with the genome. *Cell* *151*, 994–1004.
- Spijker, S. (2011). Dissection of Rodent Brain Regions. *NeuroMethods* *57*, 13–26.
- Subbanna, S., Shivakumar, M., Umapathy, N.S., Saito, M., Mohan, P.S., Kumar, A., Nixon, R.A., Verin, A.D., Psychoyos, D., and Basavarajappa, B.S. (2013). G9a-

mediated histone methylation regulates ethanol-induced neurodegeneration in the neonatal mouse brain. *Neurobiol. Dis.* *54*, 475–485.

- Subbanna, S., Nagre, N.N., Shivakumar, M., Umapathy, N.S., Psychoyos, D., and Basavarajappa, B.S. (2014). Ethanol induced acetylation of histone at G9a exon1 and G9a-mediated histone H3 dimethylation leads to neurodegeneration in neonatal mice. *Neuroscience* *258*, 422–432.
- Szabo, P.E., Tang, S.H., Silva, F.J., Tsark, W.M., and Mann, J.R. (2004). Role of CTCF binding sites in the *Igf2/H19* imprinting control region. *Mol. Cell. Biol.* *24*, 4791–4800.
- Tachibana, M. (2002). G9a histone methyltransferase plays a dominant role in euchromatic histone H3 lysine 9 methylation and is essential for early embryogenesis. *Genes Dev.* *16*, 1779–1791.
- Tasic, B., Nabholz, C.E., Baldwin, K.K., Kim, Y., Rueckert, E.H., Ribich, S.A., Cramer, P., Wu, Q., Axel, R., and Maniatis, T. (2002). Promoter choice determines splice site selection in protocadherin alpha and gamma pre-mRNA splicing. *Mol. Cell* *10*, 21–33.
- Taverna, S.D., Li, H., Ruthenburg, A.J., Allis, C.D., and Patel, D.J. (2007). How chromatin-binding modules interpret histone modifications: lessons from professional pocket pickers. *Nat. Struct. Mol. Biol.* *14*, 1025–1040.
- Thu, C.A., Chen, W. V, Rubinstein, R., Chevee, M., Wolcott, H.N., Felsovalyi, K.O., Tapia, J.C., Shapiro, L., Honig, B., and Maniatis, T. (2014). Single-Cell Identity Generated by Combinatorial Homophilic Interactions between alpha, beta, and gamma Protocadherins. *Cell* *158*, 1045–1059.
- Trompier, D., Vejux, A., Zarrouk, A., Gondcaille, C., Geillon, F., Nury, T., Savary, S., and Lizard, G. (2014). Brain peroxisomes. *Biochimie* *98*, 102–110.
- Turner, B.M. (1993). Decoding the nucleosome. *Cell* *75*, 5–8.
- Turner, B.M. (2000). Histone acetylation and an epigenetic code. *Bioessays* *22*, 836–845.
- Veazey, K.J., Carnahan, M.N., Muller, D., Miranda, R.C., and Golding, M.C. (2013). Alcohol-induced epigenetic alterations to developmentally crucial genes regulating neural stemness and differentiation. *Alcohol. Clin. Exp. Res.* *37*, 1111–1122.
- Veazey, K.J., Parnell, S.E., Miranda, R.C., and Golding, M.C. (2015). Dose-dependent alcohol-induced alterations in chromatin structure persist beyond the window of exposure and correlate with fetal alcohol syndrome birth defects. *Epigenetics Chromatin* *8*, 39.
- Voigt, P., and Reinberg, D. (2011). Histone tails: ideal motifs for probing epigenetics

- through chemical biology approaches. *Chembiochem* 12, 236–252.
- Voigt, P., Tee, W.W., and Reinberg, D. (2013). A double take on bivalent promoters. *Genes Dev.* 27, 1318–1338.
- Wang, H., Maurano, M.T., Qu, H., Varley, K.E., Gertz, J., Pauli, F., Lee, K., Canfield, T., Weaver, M., Sandstrom, R., et al. (2012). Widespread plasticity in CTCF occupancy linked to DNA methylation. *Genome Res.* 22, 1680–1688.
- Wang, X., Su, H., and Bradley, A. (2002). Molecular mechanisms governing Pcdh-gamma gene expression: evidence for a multiple promoter and cis-alternative splicing model. *Genes Dev.* 16, 1890–1905.
- Wen, Z., and Kim, H.Y. (2004). Alterations in hippocampal phospholipid profile by prenatal exposure to ethanol. *J. Neurochem.* 89, 1368–1377.
- Whitlock, J.R., Heynen, A.J., Shuler, M.G., and Bear, M.F. (2006). Learning induces long-term potentiation in the hippocampus. *Science* 313, 1093–1097.
- Wilbanks, E.G., and Facciotti, M.T. (2010). Evaluation of algorithm performance in ChIP-seq peak detection. *PLoS One* 5, e11471.
- Witcher, M., and Emerson, B.M. (2009). Epigenetic silencing of the p16(INK4a) tumor suppressor is associated with loss of CTCF binding and a chromatin boundary. *Mol. Cell* 34, 271–284.
- Xie, X., Mikkelsen, T.S., Gnirke, A., Lindblad-Toh, K., Kellis, M., and Lander, E.S. (2007). Systematic discovery of regulatory motifs in conserved regions of the human genome, including thousands of CTCF insulator sites. *Proc. Natl. Acad. Sci. U. S. A.* 104, 7145–7150.
- Xu, M., Long, C., Chen, X., Huang, C., Chen, S., and Zhu, B. (2010). Partitioning of histone H3-H4 tetramers during DNA replication-dependent chromatin assembly. *Science* 328, 94–98.
- Yun, M., Wu, J., Workman, J.L., and Li, B. (2011). Readers of histone modifications. *Cell Res.* 21, 564–578.
- Zentner, G.E., and Henikoff, S. (2013). Regulation of nucleosome dynamics by histone modifications. *Nat. Struct. Mol. Biol.* 20, 259–266.
- Zhou, F.C., Zhao, Q., Liu, Y., Goodlett, C.R., Liang, T., McClintick, J.N., Edenberg, H.J., Li, L., Jones, K., Smith, D., et al. (2011a). Alteration of gene expression by alcohol exposure at early neurulation. *BMC Genomics* 12, 124.
- Zhou, V.W., Goren, A., and Bernstein, B.E. (2011b). Charting histone modifications and the functional organization of mammalian genomes. *Nat. Rev. Genet.* 12, 7–18.

## Chapter 3.

# Effects of Neonatal Ethanol Exposure on Hippocampal DNA Methylation

### 3.1 Outline

Ethanol impairs one-carbon metabolic pathways from which methyl groups are derived. Ethanol-induced changes in gene expression may lead to altered brain function and behaviour. Previous work has implicated DNA methylation changes in models of FASD, but none have examined long-term changes in the hippocampus. In this chapter, hundreds of changes in DNA methylation were identified using methylated DNA immunoprecipitation microarray in PND 70 mice exposed to ethanol as neonates. Changes occurred in genes related to lysosomes, peroxisomes, and cell structure. Differential methylation in the peroxisome gene *Acaa1* was confirmed with sodium bisulfite pyrosequencing. Also in this chapter, the DNA methylation results and histone modification results are analyzed together. The combined analysis strengthened the implication of peroxisome genes, and also implicated novel processes not found in individual analyses including cardiovascular pathways and notch signalling. These data suggest a novel interplay between oxidative stress and epigenetic methylation in the ethanol exposed hippocampus.

### 3.2 Introduction

#### 3.2.1 DNA Cytosine Methylation

Methylation of cytosine nucleotides in DNA is a well characterized modification regulating chromatin structure and gene expression through development. 5-methylcytosine (5mC) was first described in 1948, with its chemical makeup inferred from its chromatography separation pattern from cytosine (Hotchkiss, 1948). It was several decades until the function of 5mC (often referred to as simply DNA methylation) was determined. Studies in the late 70's and early 80's found that DNA methylation was involved with local gene expression at developmental genes and regulating cell differentiation (Compere and Palmiter, 1981; Holliday and Pugh, 1975). After intensive

investigation, it has become clear that DNA methylation is principally a negative regulator of gene expression in mammals. DNA methylation in gene promoters is associated local gene repression and is stable over cellular differentiation once established (Medvedeva et al., 2014).

Cytosine methylation occurs predominately at CpG dinucleotides in mammals, which are almost always methylated (Deaton and Bird, 2011). 5mC has a high mutagenic potential, as it is easily deaminated to thymine (Coulondre et al., 1978). As such, CpG sites are evolutionarily constrained, and are depleted through the most eukaryotic genomes (Bird, 1980). However, there are concentrations of CpG sites often found within gene promoters which can be heavily demethylated called CpG islands (Bird et al., 1985). CpG islands are routinely defined as a region at least 200 bp long with greater than 50% GC content, and an observed-to-expected CpG ratio greater than 60% (Gardiner-Garden and Frommer, 1987). Methylation of CpG islands is associated with the repression of nearby (both up- and down-stream) genes (Deaton and Bird, 2011).

### 3.2.2 Regulation of DNA Methylation

DNA methylation patterns are established by complex protein interactions which catalyze methylation at the appropriate time and genomic location. *De novo* CpG methylation is established by the DNMT3A and DNMT3B enzymes which can methylate unmodified CpG sites (Okano et al., 1998). CpG sites are a simple genetic palindrome, the same 5' to 3' sequence on each strand. This structure is exploited by the maintenance DNA methyltransferase DNMT1 to maintain DNA methylation after cell division. The hemi-methylated CpG site in each daughter cell is recognized by DNMT1, which then catalyzes the addition of a methyl group to the unmethylated strand. In this way, methylation information is preserved through cell division. DNMT3A and DNMT3B are highly active during embryonic development, during which time they establish patterns which direct stem cell differentiation and ultimately provide somatic cell identity (Seisenberger et al., 2012). DNA methylation is erased during gamete production (Messerschmidt et al., 2014). During gametogenesis, there is an initial wave of demethylation, followed by another after fertilization (Geiman and Muegge, 2009; Smith and Meissner, 2013). This active demethylation is believed to be achieved by recently

discovered DNA demethylases called TET proteins (Kohli and Zhang, 2013). *De novo* methyltransferases and TET proteins are highly active during embryogenesis and early development, but are then inactive in most adult tissues (Okano et al., 1999). DNMT1 remains active at low levels (Ratnam et al., 2002). In conjunction with DNA methylation data, this suggest that DNA methylation is stable in most somatic tissues.

Once DNA methylation patterns are established, they must be translated into signals to direct chromatin-based processes such as transcription. DNA methylation can achieve repressive effects on transcription and promote condensed chromatin by either promoting negative factor binding or blocking positive factor binding. There are several classes of proteins that fill the former role. The MBD, SRA, Kaiso and Kaiso-like protein domains are the major groups that bind to methyl-CpG sites (Defossez and Stancheva, 2011). These domains are components of proteins which form large multi-protein complexes containing other domains that affect chromatin structure and/or transcription. For example, the H3K9 methylase SETDB1 contains an MBD domain suggesting that DNA methylation can drive the deposition of H3K9me (Schultz et al., 2002). H3K9me directs chromatin condensation, prohibiting gene expression (Audergon et al., 2015). Similarly, histone deacetylation is observed at 5mC-containing promoters, suggesting DNA methylation carries out gene repression in part through blocking open-chromatin marks (Cedar and Bergman, 2009). There are many such examples suggesting complex crosstalk between DNA methylation and other chromatin modifications. The presence of DNA methylation in specific DNA motifs may also occlude the binding of positive transcription factors, repressing transcription (Spruijt and Vermeulen, 2014). Initially, this was imagined to be the primary mechanism by which DNA methylation modulated gene expression. Recent data suggest that it is rare however, restricted to specific examples at particular genes (Medvedeva et al., 2014).

### 3.2.3 Functions of DNA Methylation

#### 3.2.3.1 Unique Role in the Adult Brain

DNA methylation is relatively stable once established, supported by the downregulation of *de novo* DNA methyltransferases in most adult tissues. In the brain however, this pattern does not hold true. *De novo* DNMTs are expressed in post-mitotic

neurons in the mammalian brain (Feng et al., 2005; Goto et al., 1994). Pharmacological inhibition or deletion of DNMT3A and DNMT3B in the hippocampus results in impaired synaptic plasticity and long-term potentiation (LTP) (Muñoz et al., 2016). These processes are key to many brain functions including learning and memory. Specific studies indicate that methylation is increased at some genes and decreased at others in response to neuronal activation (Lubin et al., 2008; Miller and Sweatt, 2007; Miller et al., 2010). This suggests that the blockage of DNMT3A and DNMT3B in neurons impairs synaptic plasticity via disrupting the balance between the memory activating and repressing genes (Zovkic et al., 2013).

The DNA demethylating TET enzymes are believed to play an important role in maintaining a 5mC balance in the brain. The TET enzymes produce several intermediate modifications of cytosine during demethylation: 5-hydroxymethylcytosine, 5-formylcytosine, and 5-carboxylcytosine (Ito et al., 2011). 5-hydroxymethylcytosine (5hmC) is enriched in the brain, specifically at genes involved in synaptic function (Khare et al., 2012). Whether it is functioning as a unique epigenetic mark or is simply a step in demethylation remains unclear. Some researchers hypothesize that 5hmC blocks repressive 5mC-binding proteins and thus promotes transcription (Branco et al., 2011). Some believe that during evolution the mammalian brain co-opted epigenetic mechanisms which evolved to govern development, and tweaked them to accomplish complex neurological functions.

Non-CpG cytosine methylation is also enriched in the brain. CpH (H=A, C, or T) methylation is enriched in regions of low CpG density, reduced at protein binding sites, and is negatively correlated with gene expression (Guo et al., 2014). CpH methylation can be recognized by the same reader proteins as CpG methylation, such as the MBD-containing MeCP2 implying that it may also repress gene expression (Guo et al., 2014). CpH methylation is established by *de novo* methyltransferases in mature neurons, suggesting it is involved in higher neuronal functions (Guo et al., 2014). More research is needed to understand the role of this methylation subtype.



### 3.2.3.2 Control of Gene Expression

CpGs islands are one of the organizational paradigms by which DNA methylation regulates gene expression. CpG islands are a vertebrate-specific phenomenon where in CpG sites are concentrated near a gene or genes. They are at least 200 bp long, but 1000 bp on average. Approximately 70% of genes are associated with a CpG island, (Illingworth et al., 2010; Saxonov et al., 2006). CpG islands are sites of transcriptional initiation, with about half localized over TSSs (Macleod et al., 1998). Interestingly, many CpG islands are not associated with known gene TSSs; however, many such sites have proved to be previously unknown genes (Macleod et al., 1998). Indeed, many CpG islands not associated with genes have been shown to overlap with non-coding RNA TSSs (Guttman et al., 2009). H3K4me3 is a hallmark of CpG islands and is necessary but not sufficient for transcription to occur, as it is present even at inactive genes (Guenther et al., 2007). CpG density alone correlates with H3K4me3 levels (Thomson et al., 2010). Methylated CpG islands are associated with local gene repression; however, DNA methylation often occurs after repression via histone modifications (Okamoto and Heard, 2009). Therefore, methylation of CpG islands may act to stably lock genes in a repressed state. Examples from specific genes show that methylation of non-CpG-island promoters cause similar changes to histones and repress gene expression (Han et al., 2011).

DNA methylation at enhancers is more complex. Enhancers tend to be CpG poor, and incompletely methylated (Jones, 2012). Since TET proteins are also present at enhancers during embryonic development, active DNA demethylation in may occur at these loci (Lu et al., 2014). Indeed, whole-genome 5hmC analyses have shown that TET-mediated demethylation occurs mainly at enhancers during development (Lu et al., 2014) and is also prevalent in the adult brain (Tognini et al., 2015). Current research in this field is testing the hypothesis that DNA demethylation and 5hmC at enhancers controls gene expression in response to neuronal stimulation, long-term potentiation, and learning (Tognini et al., 2015).

### 3.2.3.3 Genomic Imprinting

A key function of DNA methylation is regulating genomic imprinting. Genomic imprinting refers to the expression of genes in a parent-of-origin-specific manner (Smith

and Meissner, 2013). Depending on the locus, the maternal or paternal allele can be imprinted. The imprinted allele is methylated and not expressed, while the other is unmethylated and expressed. Often, differential methylation occurs at imprinting control regions (ICRs) which direct the expression of several proximal imprinted genes (Bartolomei and Tilghman, 1997). These patterns are established during germline development and are maintained through epigenomic reprogramming that occurs during fertilization (Bartolomei and Tilghman, 1997). Only a small number of genes are imprinted; the total number is estimated to be a few hundred in mice and humans (Ishida and Moore, 2013). Imprinting is specific to eutherian mammals, and has evolved independently in flowering plants (Scott and Spielman, 2006). Mutations and other molecular aberrations at imprinted loci cause many genetic diseases in humans (Butler, 2009). The non-disease functions of genomic imprinting are not clear. It seems disadvantageous to only express one copy of any gene in a diploid organism. The most widely accepted theory of imprinting function is the kinship theory (Moore and Haig, 1991). It postulates that the paternal expressed genes promote maximal fetal growth, with no regard for maternal health. The maternal expressed genes promote optimal fetal growth, balanced with maternal health (Moore and Haig, 1991). DNA methylation is a key mechanism by which this parent-of-origin expression is achieved.

### 3.2.4 DNA Methylation Analysis Methods

There are many methods to assess DNA methylation, and most fall into two categories: enrichment-based or bisulfite-based. Enrichment-based techniques rely on a protein to pull down methylated genomic DNA. The methylated DNA can then be characterized by gene-specific methods such as qPCR, or genome-wide methods such as microarrays and sequencing. Global analysis methods are also possible, in which the amount of DNA enrichment between samples is simply compared. Global methods are inexpensive and quick, but provide no genomic location information. Methylated DNA immunoprecipitation (MeDIP) and MBD capture are specific enrichment methods. MeDIP uses an antibody against 5mC (Jacinto et al., 2008), while MBD capture uses beads coated with MBD to pull down 5mC. MBD capture is more sensitive to regions

with high CpG density while MeDIP is more sensitive to regions with low CpG density (Nair et al., 2011).

Bisulfite-based techniques use sodium bisulfite to chemically modify all unmethylated cytosines to uracils. Following PCR amplification, these uracils are read as thymines, but the methylated cytosines remain cytosines. The converted DNA can then be sequenced using any region-specific or whole-genome technology. Comparison to the reference genome can thus identify C-to-T transitions as unmethylated sites. Microarrays which are specific to the converted and uncovered sequences are also used (Li and Tollefsbol, 2011). Enrichment approaches have the advantage of not damaging DNA as bisulfite does. Further, 5hmC is also insensitive to bisulfite conversion, meaning bisulfite sequencing is unable to distinguish 5mC from 5hmC. The resolution of bisulfite is much greater than enrichment techniques, allowing identification of single-base methylation differences (Li and Tollefsbol, 2011). Enrichment techniques also greatly reduce the total DNA sample amount, requiring a whole-genome application step that can introduce biases against CpG regions (Robinson et al., 2010). Whole-genome bisulfite sequencing is also very expensive, and often provides more information than the experiment necessitates. Enrichment of CpG dense regions using enzymatic digestion at CCGG sites reduces the total DNA to be sequenced dramatically, reducing cost per sample by 10 times (Gu et al., 2011). The diversity of methods available allows researchers to tailor the technique to their experimental question.

### 3.2.5 DNA Methylation and FASD

DNA methylation is believed to be a key component of numerous disease etiologies, including FASD. Aberration of DNA methylation is associated with many human diseases. In particular, diseases involving errors in cellular differentiation such as cancers often involve altered DNA methylation (Robertson and Wolffe, 2000). Imprinting disorders are also caused by genetic or epigenetic changes at imprinting loci. Repeat expansion disorders involve DNA methylation, as the expanded region is often methylated leading to silencing (Robertson and Wolffe, 2000). Given the important role of DNA methylation in neurological function, it is unsurprising that numerous neurodevelopmental and neurodegenerative disorders are associated with changes in

DNA methylation (Lu et al., 2013). Identifying a causative role for DNA methylation in these disorders is very difficult compared with growth disorders. Nevertheless, DNA methylation at disease-relevant genes is associated with dozens of human neurological disorders (Lu et al., 2013). As the interest in DNA methylation in neurological disorders increased through the 1990s, research was initiated into the role of DNA methylation in FASD.

DNA methylation was suspected to be particularly relevant in FASD due to the molecular actions of ethanol. DNA methyltransferases rely on one-carbon metabolic pathways to transfer a methyl group onto cytosine. Briefly, DNMTs transfer the methyl group from the methyl donor SAM. The first metabolite ethanol, acetaldehyde, exerts several inhibitory effects on SAM availability. Acetaldehyde prevents the uptake of folate, a precursor of SAM (Hamid and Kaur, 2007). Acetaldehyde also directly inhibits methionine adenosyl transferase and methionine synthase which produce SAM and its precursor methionine respectively (Kenyon et al., 1998; Seitz and Stickel, 2007). Much of this information emerged from studies of adult alcohol-induced liver disease, which has since been associated with changes in DNA methylation (Shukla et al., 2008). These effects have also been observed in *in vivo* FASD models. Garro et al. (1991) provided the first implication of DNA methylation in FASD. Exposure of mouse fetuses to ethanol from GD9-11 resulted in DNA hypomethylation. Nuclei from ethanol-exposed fetuses had lower levels of DNMT activity even when exposed to excess SAM, suggesting irreversible enzyme activation (Garro et al., 1991). Furthermore, DNA methylation provides a molecular mechanism for gene-by-environment interactions: environmental changes can potentially affect gene expression via DNA methylation which is dependent on environmental sources of carbon (Baccarelli and Bollati, 2009). Combined with emerging studies on the importance of DNA methylation in neurological disease, these data provided the theoretical basis for exploration of the role of 5mC in FASD.

DNA methylation has become a popular research area in FASD. Interestingly, histone modifications were initially more studied in FASD through the late 1990's and early 2000s. At this time this thesis was undertaken in 2011, there had been only three studies of DNA methylation in FASD models. The first was the aforementioned study by Garro et al. (1991) which found global DNA hypomethylation in mouse fetuses following

acute exposure to a high dose of ethanol from GD 9-11. Haycock and Ramsay (2009) assessed the *H19* imprinted domain using bisulfite sequencing of mouse embryos exposed to ethanol during preimplantation (GD 1.5-2.5). When assessed at GD 10.5, the authors found no DNA methylation changes in the embryos (Haycock and Ramsay, 2009). There was a reduction in methylation at the paternal alleles in ethanol-exposed placentae. The third study was the most comprehensive, and has driven much of the interest in the role of DNA methylation in FASD. Using whole-embryo culture, Liu et al. (2009) investigated the effects of ethanol exposure on DNA methylation and gene expression during neurulation. Using MeDIP-chip, the authors compared DNA methylation in embryos that developed or did not develop neural tube deficits in response to ethanol exposure. There was a 10-fold increase in the number of genes with increased methylation on chromosomes 7, 10, and X (Liu et al., 2009). DNA methylation changes were enriched in imprinted genes and olfactory genes, with notable examples of developmental and chromatin-regulating genes (Liu et al., 2009). There were 84 genes differentially expressed and differentially methylated. The results from these studies provide evidence that ethanol may exert its neurotoxic effects at least in part through epigenetic changes in gene expression.

Since the initiation of this thesis, there have been numerous other studies investigating DNA methylation following various exposure paradigms in various tissues. Rat pups exposed to ethanol from PND 2-10 showed global hypomethylation in the hippocampus and prefrontal cortex (Otero et al., 2012). In another study, the promoter of *Pomc* (a gene involved in neuronal control of stress and metabolism) showed reduced methylation at PND 60 following GD 7-21 ethanol exposure. *Pomc* expression was also reduced (Govorko et al., 2012). Interestingly, this effect was passed to the F2 and F3 male offspring of ethanol exposed mice. This study provided the first evidence that ethanol-induced epigenetic changes could be passed transgenerationally. In another study, mice exposed to ethanol from GD 7-16 showed altered 5mC and 5hmC levels in hippocampus at PND 7 which were correlated with delayed hippocampal development (Chen et al., 2013). Other studies have attempted to understand the mechanisms of ethanol-induced DNA methylation changes. Blockage of the apoptosis-inducing factor Caspase 3 prevented ethanol-induced reduction in DNMT1 and DNMT3A proteins and

DNA methylation in the hippocampus. This suggests that DNA methylation changes occur downstream of apoptosis in response to ethanol.

Our laboratory has also assessed DNA methylation in other models of FASD. Using the CPD model, we found that adult mice show genome-wide changes in DNA methylation in the whole-brain. These changes were enriched at imprinted genes and genes regulated by CTCF (Laufer et al., 2013). When these data were compared to human children with FAS, we found that both the mouse brain and human buccal cells had enrichment of DNA methylation changes at protocadherins, glutamatergic synapses, and hippo signaling genes (Laufer et al., 2015). Another group also found decreased methylation at protocadherins genes in children with FASD, suggesting this may serve as a biomarker for FASD (Portales-Casamar et al., 2016).

### 3.2.6 DNA Methylation Study Design

Previous studies have not assessed genome-wide DNA methylation changes in adult mice exposed to ethanol during development. Studies have focused on the hippocampus, but most have examined short-term responses to ethanol exposure (Chen et al., 2013; Liu et al., 2009; Otero et al., 2012). The effects of DNA methylation in the adult brain have only been assessed by one other group, which only investigated a single gene (Govorko et al., 2012). Given that FASD is associated with lifelong changes in behaviour (Among and Women, 2010) our laboratory has focused on studying molecular changes in the young adult brain. In terms of tissue of interest, our laboratory and others have focused on the hippocampus. As reviewed in Chapter 1, the hippocampus is highly vulnerable to ethanol-induced neurotoxicity (Gil-Mohapel et al., 2010), and is the brain region associated with spatial learning and memory which are disrupted in FASD (Among and Women, 2010). DNA methylation also plays a dynamic role in learning in the hippocampus. For these reasons, the experiments of this thesis were designed to assess DNA methylation in the hippocampus of adult mice exposed to ethanol during PND4-7. Given the nature of the experimental question, MeDIP-chip was selected with confirmations by a completely different technology, bisulfite pyrosequencing. MeDIP was coupled to a promoter microarray to restrict analysis to only regions relevant to gene

expression, and reduce costs. Given the crosstalk between DNA methylation and histone modifications, the genes and pathways affected by both were also considered.

## Objectives

1. To assess all mouse genes and their promoters in PND 70 mouse hippocampus exposed to ethanol on postnatal days 4 & 7 and identify changes in DNA methylation.
2. To identify genes proximal to changes in DNA methylation, and pathways affected.
3. To confirm specific changes with ChIP-qPCR.

## 3.3 Materials and Methods

### 3.3.1 Mouse Care

For full mouse care protocol, see Chapter 2, section 2.3.1. In brief, all protocols were approved by the Animal Use Subcommittee (AUS) at the University of Western Ontario, London, Ontario, Canada. The day of birth was termed post-natal day (PND) zero. Sex and weight-matched littermate pups were divided into two groups: ethanol-treated and saline control mice. Pups were given two subcutaneous dorsal injections on both PND 4 and PND 7. Ethanol-treated mice were injected with 2.5 g/kg of ethanol in 0.15 M NaCl (Ikonomidou et al., 2000). Control mice were injected with 0.15 M saline only. Male mice were used for all subsequent analyses (n=18). Mice were sacrificed on PD 70 via carbon dioxide asphyxiation. The hippocampus was dissected out (Spijker, 2011), snap-frozen in liquid nitrogen, and stored at -80°C for no longer than 30 days until formaldehyde fixation. The mice used in this chapter were the same used for the RNA analysis in Chapter 2 (**Table 2.1**) The experimental design of this Chapter differs, in that three individual mice were used for three separate microarrays per treatment group, i.e. three biological replicates were not pooled together as in Chapter 2. The biological sample used for each microarray in this section was used on one of the microarrays from Chapter 2 (**Table 2.1**).

### 3.3.2 MeDIP-Chip

#### 3.3.2.1 Genomic DNA Fragmentation

Genomic DNA (gDNA) was quantified and quality assessed by NanoDrop ND-1000. Genomic DNA of each sample was sonicated to ~200 – 1000 bp with a Bioruptor sonicator (Diagenode) on “Low” mode for 10 cycles of 30 seconds “ON” & 30 seconds “OFF”. The gDNA and each sheared DNA were analyzed with agarose gel electrophoresis.

#### 3.3.2.2 Methyl-Cytosine Immunoprecipitation

1 µg of sonicated genomic DNA was used for immunoprecipitation using a mouse monoclonal anti-5-mC antibody (Diagenode). For this, DNA was heat-denatured at 94°C



for 10 min, rapidly cooled on ice, and immunoprecipitated with 1  $\mu$ L primary antibody overnight at 4°C with rocking agitation in 400  $\mu$ L immunoprecipitation buffer (0.5% BSA in PBS). To recover the immunoprecipitated DNA fragments, 200  $\mu$ L of anti-mouse IgG magnetic beads was added and incubated for an additional 2 hours at 4°C with agitation. After immunoprecipitation, five immunoprecipitation washes were performed with ice-cold immunoprecipitation buffer. Washed beads were resuspended in TE buffer with 0.25% SDS and 0.25 mg/mL proteinase K for 2 hours at 65°C and then allowed to cool down to room temperature. MeDIP DNA were purified using Qiagen MinElute columns (Qiagen).

### 3.3.2.3 Whole Genome Amplification (WGA)

The MeDIP-enriched DNA was amplified using a WGA kit from Sigma-Aldrich (GenomePlex<sup>®</sup> Complete Whole Genome Amplification (WGA2) kit) following the manufacturer's protocol. The amplified DNA samples were then purified with QIAquick PCR purification kit (Qiagen) following the manufacture's protocol.

### 3.3.2.4 Real-time PCR Assessment of Fold-Enrichment

The purpose of the qPCR experiment is to verify that the MeDIP DNA has been enriched for methylated fragments and depleted for unmethylated fragments (Butcher and Beck, 2010). This experiment was performed by ArrayStar Inc. The primers for specifically methylated regions (the positive control, *Tsh2b* promoter) and unmethylated regions (the negative control, *Gapdh* promoter) were used to assess the enrichment level of these two regions in both input (sonicated DNA) and MeDIP-enriched DNA (Butcher and Beck, 2010). All six samples showed expected enrichment. An enrichment value for two samples could not be calculated due to complete lack of amplification in the IgG negative control. All samples can be considered quantitatively above the background signal (noise) for both. The PCR primer sequences were: *Tsh2b* 101 bp  
 F:5'CTCTCCTTGCGGCATCTCT3' R:5'GCGGTAAAGGGTGCTACTATT3'. *Gapdh*  
 161 bp F:5'GCCCTTGAGCTAGGACTGGATAA3'  
 R:5'CCTGGCACTGCACAAGAAGATG3'.

### 3.3.2.5 DNA Labelling and Array Hybridization

The purified DNA was quantified using a NanoDrop ND-1000. For DNA labelling, the NimbleGen Dual-Color DNA Labeling Kit was used according to the manufacturer's guideline detailed in the NimbleGen MeDIP-chip protocol (NimbleGen Systems, Inc., Madison, WI, USA). 1  $\mu$ g DNA of each sample was incubated for 10 min at 98°C with 1 OD of Cy5-9mer primer (IP sample) or Cy3-9mer primer (Input sample). Then, 100 pmol of deoxynucleoside triphosphates and 100U of the Klenow fragment (New England Biolabs, USA) were added and the mix incubated at 37°C for 2 hours. The reaction was stopped by adding 0.1 volume of 0.5 M EDTA, and the labeled DNA was purified by isopropanol / ethanol precipitation. Microarrays were hybridized at 42°C during 16 to 20h with Cy3/5 labelled DNA in NimbleGen hybridization buffer/ hybridization component A in a hybridization chamber (Hybridization System - NimbleGen Systems, Inc., Madison, WI, USA). Following hybridization, washing was performed using the NimbleGen Wash Buffer kit (NimbleGen Systems, Inc., Madison, WI, USA). For array hybridization, Roche NimbleGen's MM9 Meth 2.1M CpG plus Promoter array was used.

### 3.3.2.6 Data Extraction and Normalization

Raw data were extracted as pair files by NimbleScan software. ArrayStar performed Median-centering, quantile normalization, and linear smoothing by Bioconductor packages Ringo, limma, and MEDME. After normalization, a normalized log<sub>2</sub>-ratio data (\*\_ratio.gff file) was created for each sample. From the normalized log<sub>2</sub>-ratio data, a sliding-window peak-finding algorithm provided by NimbleScan v2.5 (Roche-NimbleGen) was applied to find the enriched peaks with specified parameters (sliding window width: 750 bp; mini probes per peak: 2; *p*-value minimum cut-off: 2; maximum spacing between nearby probes within peak: 500 bp). Raw and normalized data files were uploaded to GEO.

### 3.3.2.7 MEDME Analysis

To accurately quantify CpG methylation levels, MEDME (modeling experimental data with MeDIP enrichment) was used to improve the evaluation and interpretation of

MeDIP derived DNA methylation estimates. MEDME relies on generating a fully methylated gDNA sample for comparison. To generate the fully methylated profiles, DNA from each sample was pooled and treated with CpG methyltransferase (M.SssI, NEB) to add methyl-groups to all cytosine residues within CpG di-nucleotides, in order to obtain fully methylated genomic DNA. Raw data for fully methylated sample and test samples were median-centered and quantile normalized using Bioconductor packages Ringo and limma. Then MEDME was performed to calculate probe AMS and RMS. In the fully methylated DNA MeDIP experimental dataset, the weighted count of methylated CpG di-nucleotides in the 1 kb window centered at each probe is calculable by genomic CpG in the window, as every CpG is expected to be methylated.

The MEDME protocol utilizes the absolute methylation score (AMS) as the indicator of DNA methylation, which is decided by the weighted count of methylated CpG di-nucleotides in a 1 kb window centered at each probe. The AMS is verified to be a more accurate and sensitive indicator of DNA methylation than log-Ratio. The MEDME method also provides a relative methylation score (RMS) that normalizes AMS with respect to the total number of CpGs represented by CpGw. Differentially methylated probes between ethanol-exposed and control groups were identified using AMS by Paired Samples t-Test. And probes with  $p$ -value $<0.05$  and ABS (AMS\_dif) $>8$  were selected and used to find AMS DMRs. The RMS is more useful when comparing regions with different CpG densities. Since this study is only comparing the same region across samples, AMS was used in characterization and analysis. After probe AMS and RMS were obtained from analyzing the MeDIP-chip data by MEDME, a further analysis of identification of DMRs (differentially methylated regions) was performed to identify significantly differentially methylated regions. An FDR  $q$ -value  $< 0.05$  was used to determine multiple testing error; no DMRs survived this threshold.

### 3.3.2.8 Sodium Bisulfite Pyrosequencing

The same DNA samples used for MeDIP-chip were used for sodium bisulfite pyrosequencing (n=3 control and n=3 ethanol). EpigenDx Inc. performed pyrosequencing on the PSQ96 HS System (Qiagen) following the manufacturer's instructions, using custom assays and a gradient of controls with known methylation levels. This

allowed for the quantification of the absolute percent methylation (Lim et al., 2014) of each CpG at specific loci using QCpG software (Qiagen). The absolute percent methylation at each assayed cytosine was averaged among ethanol-exposed (n=3) and control (n=3) samples and compared using a Paired Samples t-Test. The custom primers assayed CpGs at the following positions (mm10): *Acaa1*: chr9:119342321, chr9:119342332, chr9:119342352, chr9:119342366, chr9:119342378, chr9:119342386; *Pxmp1*: 110285970, chr5110285964, chr5110285959, chr5110285948, chr5110285944, chr5110285940, chr5110285908, chr5110285878; *Pex6*: chr17:46706646, chr17:46706654, chr17:46706661, chr17:46706672, chr17:46706678, chr17:46706691, chr17:46706698, chr17:46706715; *Mafg*: chr11:120625270, chr11:120625264, chr11:120625261, chr11:120625225, chr11:120625205, chr11:120625131; *Tcf7l2*: chr19:55745017, chr19:55745023.

### 3.3.3 8-OHdG ELISA

To assess oxidative damage to hippocampal DNA in PND 70 mice, 8-hydroxy-2'-deoxyguanosine (8-OHdG) levels were assessed. The Colorimetric EpiQuik 8-OHdG DNA Damage Quantification Direct Kit (Epigentek) was used according to the manufacturer's protocol. The same DNA samples from the six ethanol-exposed and six control mice used for MeDIP-chip were used (Chapter 2, **Table 2.1**). Florescence levels were quantified by the Epoch 2 Microplate Spectrophotometer (BioTek). A standard curve was generated from provided 8-OHdG standards. Individual 8-OHdG values for each sample were calculated using **Equation 1**. Once 8-OHdG (ng) was calculated, technical replicates for each sample (3) were averaged, then compared to input DNA levels to obtain the percentage of 8-OHdG for each sample.

$$8 - OHdG (ng) = \frac{Sample\ OD - NC\ OD}{slope}$$

**Equation 1. Quantity of 8-OHdG.**

OD refers to optical density determined by the instrument, NC refers to negative control, slope refers to the slope of the line obtained by plotting OD vs. 8-OHdG concentration for each standard.

## 3.4 Results

### 3.4.1 Distribution of Differentially Methylated Regions

MeDIP-chip identified thousands of differentially methylated regions (DMRs) across the mouse genome in response to ethanol exposure. DMRs are genomic regions containing several differentially methylated cytosines. Two algorithms were used to generate DMRs, absolute methylation score (AMS) and relative methylation score (RMS). AMS is derived by the weighted count of methylated CpG di-nucleotides in a 1 kb window centered at each probe. RMS is simply the AMS score that normalized with respect to the total number of CpGs in the region. Each algorithm produced different DMRs, though there was overlap (**Table 3.1**). The AMS produced mostly DMRs with increased methylation in response to ethanol, the RMS DMRs were nearly equally increases and decreases. These trends in direction of methylation change remained constant as the significance level of the AMS was increased (**Figure 3.1; Figure 3.2**). There were more AMS DMRs than RMS DMRs. AMS identified changes in CpG islands, while RMS did not, likely due the high CpG density of the regions. RMS is intended to compare the relative methylation of different regions within the same sample. Since this experiment only compared the same genomic regions between different samples, AMS score alone was used for the remainder of the analysis.

The AMS DMRs were distributed relatively evenly across the genome (**Figure 3.3**). Chromosomes 7 and 11 had the most DMRs, while 18 and 19 and Y had the fewest, with none on the Y chromosome. All chromosomes showed a similar distribution of increased and decreased AMS scores: each had more increases than decreases indicating hypermethylation (**Figure 3.3**). Since the experiment employed a promoter microarray, chromosomes with more genes were interrogated more often. The DMRs per chromosome were therefore corrected based on gene density (**Figure 3.4**). Despite being relatively gene dense, chromosome 11 had the highest number of DMRs per gene. Chromosome 6 had the lowest DMRs per gene, but the distribution was relatively even across chromosomes. Indeed, a linear regression of number of genes vs. number of DMRs found an  $R^2$  value of 0.86 indicating a strong correlation (**Appendix C**). Thus, most of the variation in DMRs across chromosomes is attributed the number of genes on the chromosome.

**Table 3.1 Characteristics of differentially methylated regions (DMRs) identified by methylated DNA immunoprecipitation microarray (MeDIP-chip)<sup>†</sup>.**

Location	<i>p</i> -value cut off	Number of DMRs (% increased methylation)		Number of Identical DMRs
		AMS	RMS	
Promoter	<i>p</i> <0.05	10599 (82.2%)	7738 (55%)	3773 (43.6%↑↑, 8.4%↓↓, 47.8% differ)
Promoter	<i>p</i> <0.01	4640 (82.3%)	2766 (52%)	582 (48.6%↑↑, 10.1%↓↓, 46.4 differ)
Promoter	<i>p</i> <0.001	733 (83.3%)	435 (47%)	18 (27.7%↑↑, 5.6%↓↓, 66.7% differ)
CpG island	<i>p</i> <0.05	1112 (91.7%)	0	N/A
CpG island	<i>p</i> <0.01	549 (93.2%)	0	N/A
CpG island	<i>p</i> <0.001	100 (92%)	0	N/A
miRNA promoter	<i>p</i> <0.05	292 (66.1%)	238 (47.9%)	3 (66.6%↑↑, 33.3%↓↓)
miRNA promoter	<i>p</i> <0.01	126 (65.1%)	63 (52.3%)	0
miRNA promoter	<i>p</i> <0.001	16 (87.5%)	3 (66.6%)	0

<sup>†</sup>Lists of DMRs for each genomic location (as identified by Array-star analysis) were generated for three *p*-values. The number of DMRs in these lists for both absolute methylation score (AMS) and relative methylation score (RMS) algorithms are shown. The number of identical DMRs, i.e. those having are the same start and end points, is shown. The agreement of the direction of methylation change (up “↑” or down “↓”) for the identical DMRs is shown.

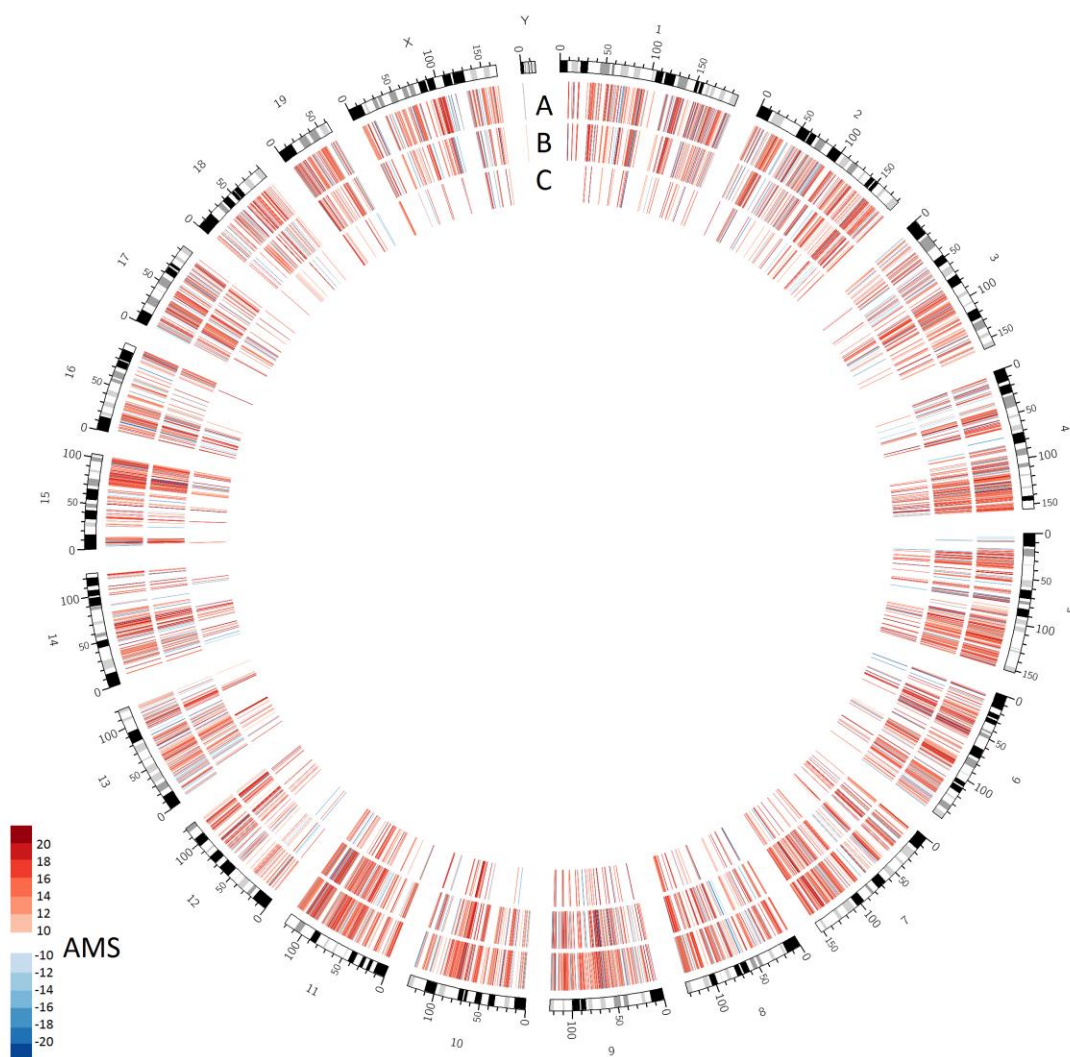


**Figure 3.1 Differentially methylated regions (DMRs) identified by absolute methylation score (AMS) at increasing stringency levels.**

Track A shows genomic locations of DMRs with AMS  $p$ -value < 0.05; Track B shows genomic locations of DMRs with AMS  $p$ -value < 0.01; Track C shows genomic locations of DMRs with AMS  $p$ -value < 0.001. Colours denote the direction and magnitude of the AMS score of each DMR.



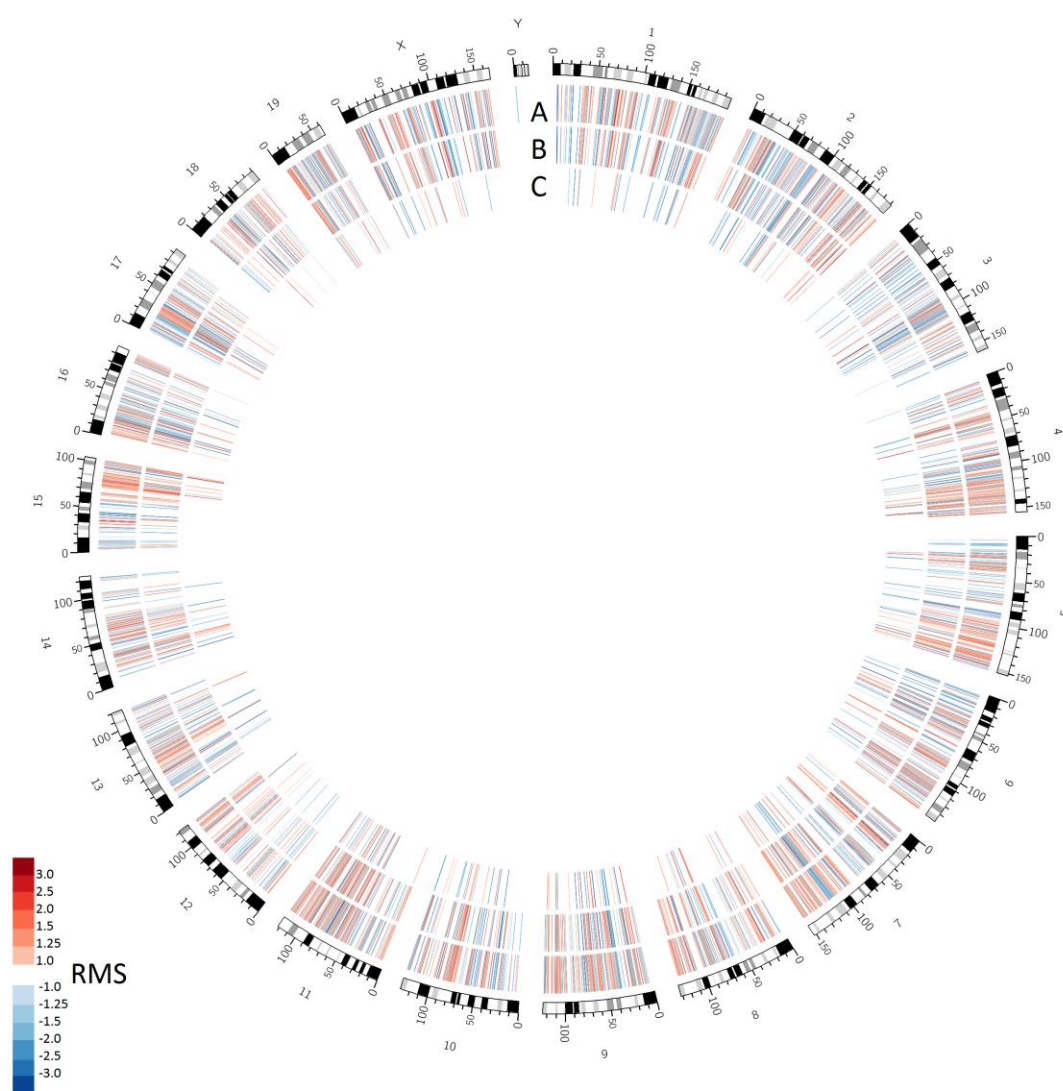


**Figure 3.2 Differentially methylated regions (DMRs) identified by relative methylation score (RMS) at increasing stringency levels.**

Track A shows genomic locations of DMRs with RMS  $p$ -value < 0.05; Track B shows genomic locations of DMRs with RMS  $p$ -value < 0.01; Track C shows genomic locations of DMRs with RMS  $p$ -value < 0.001. Colours denote the direction and magnitude of the RMS score of each DMR.

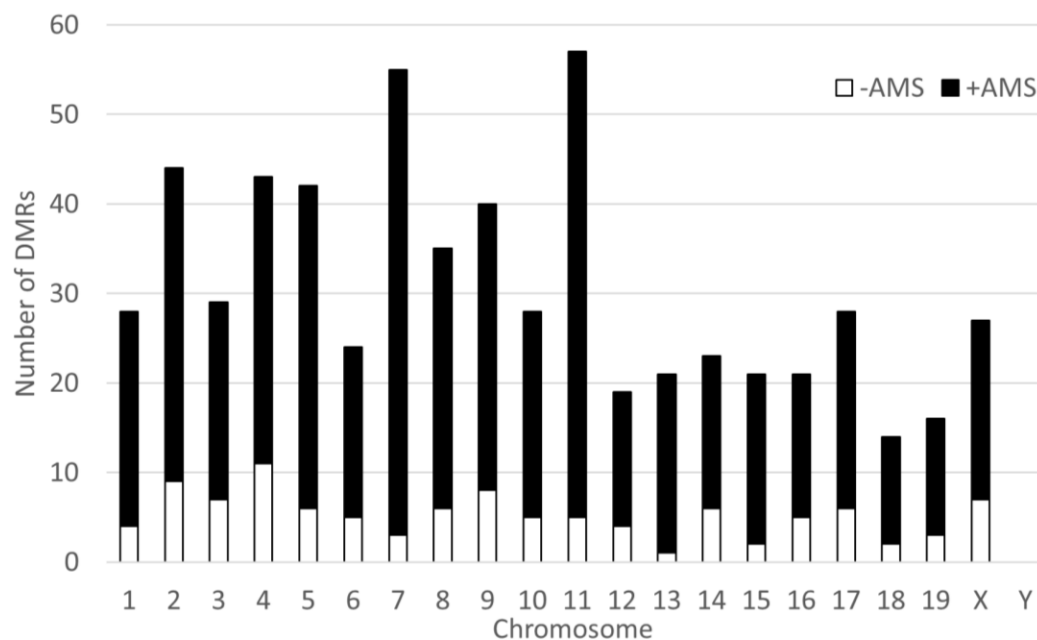


**Figure 3.3 Distribution of differentially methylated regions (DMRs) across chromosomes.**

Bars show the number of DMRs present on each chromosome at an AMS  $p < 0.001$ . Black denotes positive AMS score, indicating increased methylation, while white denotes negative AMS score indicating reduced methylation.

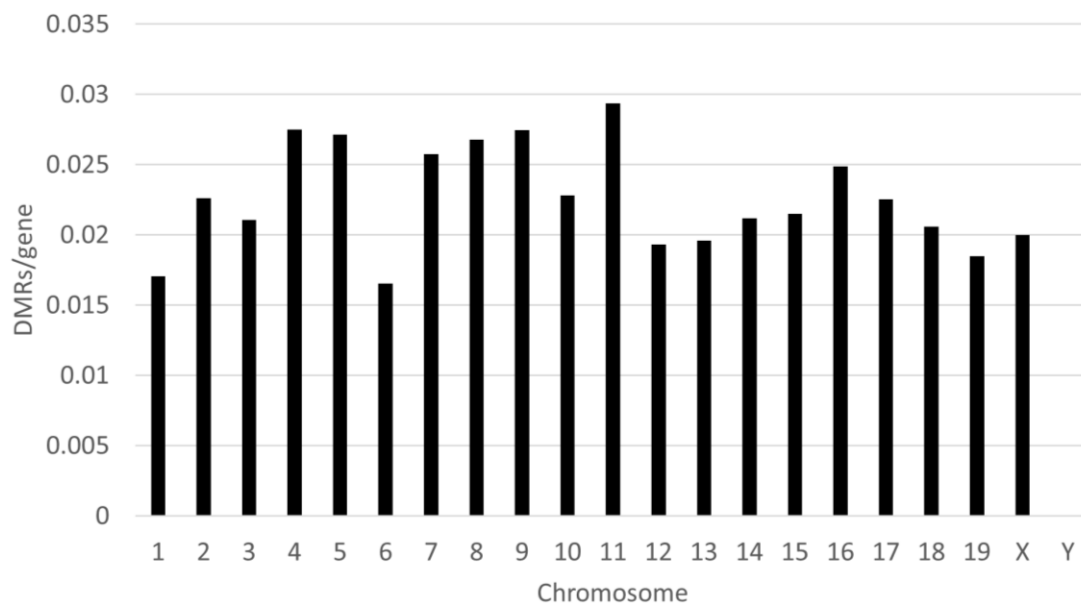


**Figure 3.4 Distribution of differentially methylated regions (DMRs) across chromosomes corrected for gene density.**

The number of DMRs on each chromosome was divided by the total number of genes (from build mm10) on each chromosome.

### 3.4.2 Ontology of Genes Proximal to DNA Methylation Changes

To identify genetic systems affected by DNA methylation changes in the PND 4,7 FASD model, gene ontology (GO) analysis was performed. A list of 689 genes in proximity to the 733 DMRs (AMS  $p < 0.001$ ) was generated for gene ontology and pathway analysis. The DMR was required to lay within 5000 bp upstream of the transcriptional start site of the gene, or the gene body. Genes were also implicated if a DMR occurred in a CpG island known to correlate with expression of the gene. These genes were submitted to gene ontology software. The top two affected biological processes were related to myeloid cell differentiation (**Table 3.2**). Several other processes were related to cell growth and development. Three of the top ten biological processes were related to hormone response (**Table 3.2**). Also notable were “Negative regulation of lipid biosynthetic process” and “Regulation of neuron projection development”. The top ten cellular components were all related to cellular structure or membrane components (**Table 3.2**). The top affected component was “Basement membrane” with various other membranes and components implicated (**Table 3.2**). The top three affected molecular functions were hormone, estrogen, and growth factor binding (**Table 3.2**). Other receptors were implicated including neuropeptide, nuclear hormone, and tumor necrosis factor, and notch binding.

### 3.4.3 Pathways Affected by DNA Methylation Changes

The list of 689 genes proximal to DMRs was also submitted to three separate pathway suites: Ingenuity Pathway Analysis (IPA), Partek Pathway, and Enrichr (**Table 3.3**). The top IPA pathway was “Cellular Movement, Cell Death and Survival, Cellular Development” (**Figure 3.5**). In total five pathways were identified by IPA, each related to cell growth and development, or cell death (**Table 3.3**). Partek pathway identified five pathways, the top being “Hematopoietic cell lineage”. Enrichr identified two pathways, which were the same as two identified by Partek pathway: “Peroxisome” and “Lysosome”. Due to “Peroxisome” being identified by both software suites, and

**Table 3.2 Gene ontology (GO) analysis of genes with differentially methylated regions (DMRs) in their promoter<sup>†</sup>.**

<b>GO term</b>	<b><i>p</i>-value</b>
<b>GO biological processes</b>	
Myeloid leukocyte differentiation (GO:0002573)	0.0004
Myeloid cell differentiation (GO:0030099)	0.0004
Cellular response to thyroid hormone stimulus (GO:0097067)	0.0008
Positive regulation of cell fate commitment (GO:0010455)	0.0013
Negative regulation of lipid biosynthetic process (GO:0051055)	0.0017
Granulocyte differentiation (GO:0030851)	0.0020
Response to thyroid hormone (GO:0097066)	0.0020
Positive regulation of developmental growth (GO:0048639)	0.0022
Cellular response to hormone stimulus (GO:0032870)	0.0026
Regulation of neuron projection development (GO:0010975)	0.0027
<b>GO cellular component</b>	
Basement membrane (GO:0005604)	0.0002
Extracellular matrix part (GO:0044420)	0.0008
Anchored component of membrane (GO:0031225)	0.0027
Extrinsic component of cytoplasmic side of plasma membrane (GO:0031234)	0.011
Extracellular matrix (GO:0031012)	0.011
Ruffle (GO:0001726)	0.021
Cortical cytoskeleton (GO:0030863)	0.022
Extrinsic component of plasma membrane (GO:0019897)	0.025
Cell surface (GO:0009986)	0.027
Exosome (RNase complex) (GO:0000178)	0.028
<b>GO molecular function</b>	
Hormone receptor binding (GO:0051427)	0.0020
Estrogen receptor binding (GO:0030331)	0.0027
Growth factor activity (GO:0008083)	0.0060
Glycosaminoglycan binding (GO:0005539)	0.0076
S100 protein binding (GO:0044548)	0.0074
Neuropeptide receptor binding (GO:0071855)	0.011
Sequence-specific DNA binding RNA polymerase II transcription factor activity (GO:0000981)	0.013
Nuclear hormone receptor binding (GO:0035257)	0.013
Tumor necrosis factor receptor superfamily binding (GO:0032813)	0.013
Notch binding (GO:0005112)	0.015

<sup>†</sup>Top 10 GO processes are shown where number of entries exceeds 10.

**Table 3.3 Pathways significantly enriched with differentially methylated genes<sup>†</sup>.**

<b>Network name</b>	<b><i>p</i>-value</b>
<b>IPA</b>	
Cellular Movement, Cell Death and Survival, Cellular Development	10E-130
Cell Cycle, Cellular Development, Cellular Growth and Proliferation	10E-50
Inflammatory Response, Cellular Movement, Immune Cell Trafficking	10E-50
Organismal Development, Tissue Development, Embryonic Development	10E-43
Cell Death and Survival, Cellular Development, Cellular Growth and Proliferation	10E-35
<b>Partek pathway</b>	
Hematopoietic cell lineage	0.0003
Peroxisome	0.0006
Jak-STAT signaling pathway	0.0006
Lysosome	0.003
Taurine and hypotaurine metabolism	0.009
<b>Enrichr KEGG</b>	
Peroxisome	0.024
Lysosome	0.026

<sup>†</sup>*p*-values for each entry are shown (Fisher's exact test). For list of genes in each pathway, see **Appendix G**.



identified in the histone analysis, the Partek Peroxisome pathway was selected for further analysis (**Figure 3.6**).

#### 3.4.4 Combined DNA & Histone Methylation Analysis

To examine genes proximal to either DNA methylation or histone modification changes, a combined gene list of genes with either a DMR or an RDHM in their promoter/gene body was created. There was minimal overlap between lists, and no single gene contained a DMR, H3K4me3 RDHM, and H3K27me3 RDHM (**Figure 3.7**). The direction of each change in ethanol-exposed mice was standardised between the marks by listing genes with changes predicted to increase gene expression as +1 (i.e. loss of DNA methylation, loss of H3K27me3, gain of H3K4me3) and changes predicted to decrease gene expression as -1 (i.e. gain of DNA methylation, gain of H3K27me3, loss of H3K4me3). Conflicting gains/losses were scored as 0 (22 genes total). The DMR/RDHM *p*-value cut off was kept at  $p < 0.001$ . The list comprised 1589 genes.

#### 3.4.5 Combined Gene Ontology and Pathway Analyses

The combined list was submitted to GO and pathway analysis software. GO analysis of the combined list identified some, but not all of the same processes as the DNA methylation or histone modification lists alone. The top affected biological processes were both cell-cell adhesion related (**Table 3.4**), which was also true for the H3K4me3, H3K27me3, and shared histone methylation GO analyses (Chapter 2). The next to top processes were “Regulation of neuron differentiation”—which was not implicated in any of the individual GO analyses—and “Regulation of neuron projection development”—which was only implicated in the DNA methylation GO analysis (**Table 3.4; Table 3.2; Chapter 2**). Also of note was “Nervous system development” which was also implicated in H3K4me3 GO analysis (**Table 3.4; Chapter 2**). “Myeloid cell differentiation” was also implicated; this was the top hit for the DNA methylation GO analysis but was not implicated in the histone analyses (**Table 3.4; Table 3.2**). “CD4-positive, alpha-beta T cell activation” was implicated, but was not in any of the individual lists (**Table 3.4**).



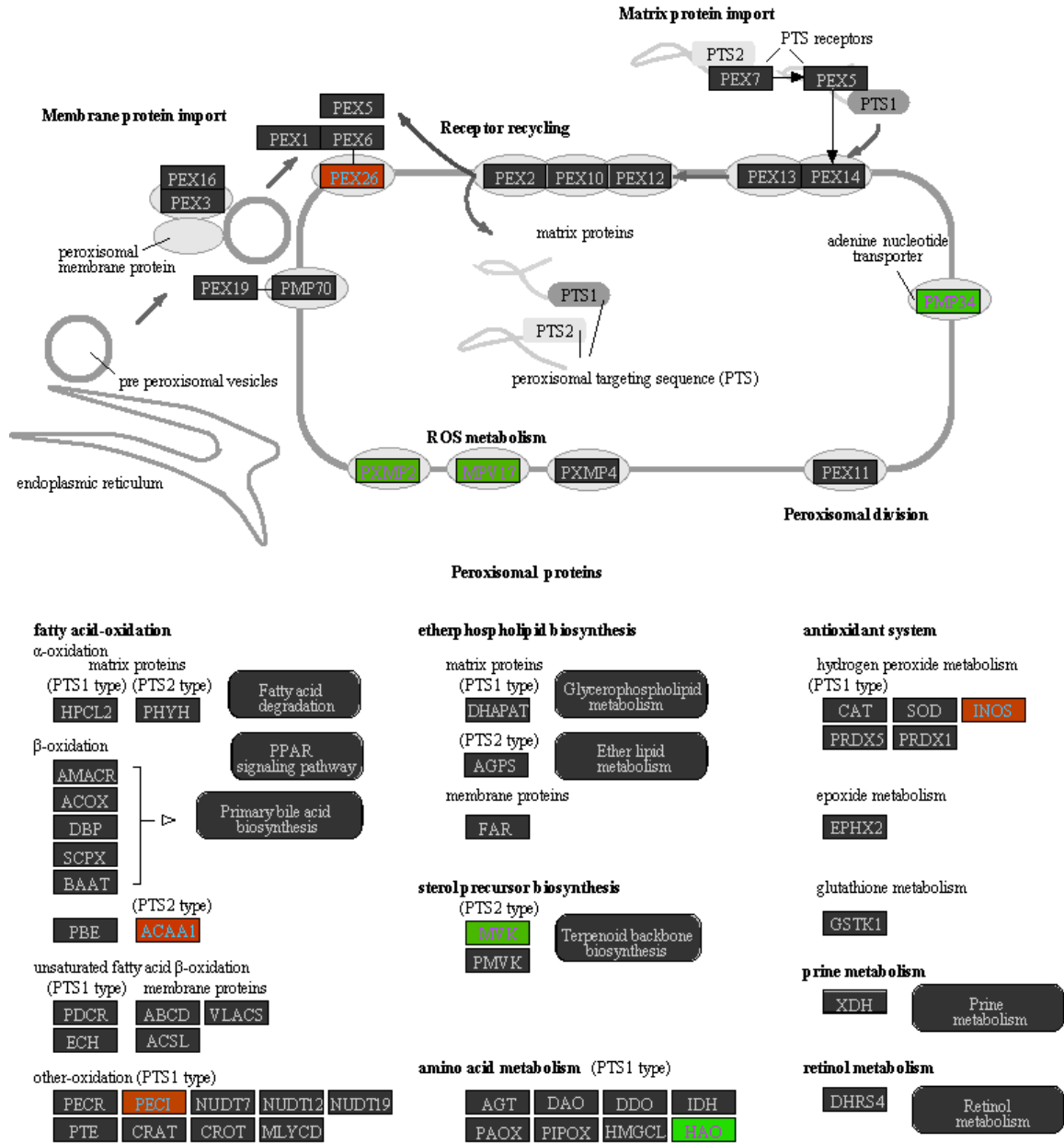


**Figure 3.6 Top Partek pathway for genes proximal to differentially methylated regions (DMRs).**

Pathway is titled “Peroxisome biogenesis”. Proteins whose encoding genes are proximal to an increase in methylation are shown in red, decreases are shown in green.

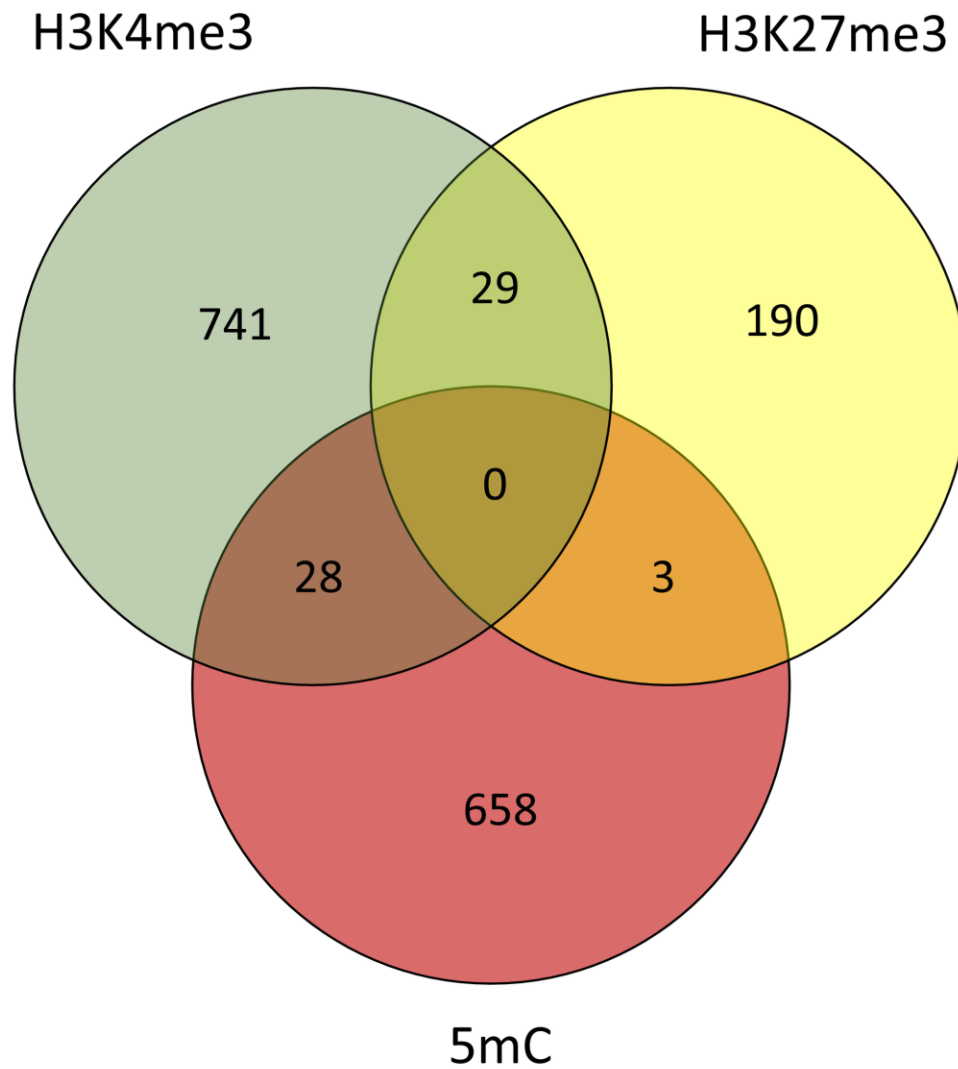


**Figure 3.7 Combined gene list characterization, genes proximal to either a DNA methylation (5mC), H3K4me3, or H3K27me3 change.**

The number of genes proximal to each methylation change are shown in each circle. Genes proximal to multiple changes, regardless of the direction of those changes, are shown in overlapping regions.

**Table 3.4 Gene ontology (GO) analysis of genes proximal to a differential methylated region (DMR) or region of differential histone modification (RDHM)<sup>†</sup>.**

GO term	<i>p</i> -value
<b>GO biological processes</b>	
Cell-cell adhesion via plasma-membrane molecules (GO:0098742)	5.26E-06
Cell-cell adhesion (GO:0098609)	5.81E-06
Regulation of neuron differentiation (GO:0045664)	5.63E-05
Regulation of neuron projection development (GO:0010975)	0.00012
Myeloid cell differentiation (GO:0030099)	0.00034
Regulation of cell projection organization (GO:0031344)	0.00047
Erythrocyte differentiation (GO:0030218)	0.00050
Nervous system development (GO:0007399)	0.00051
CD4-positive, alpha-beta T cell activation (GO:0035710)	0.00062
Mammary gland development (GO:0030879)	0.0011
<b>GO cellular component</b>	
Basement membrane (GO:0005604)	0.0019
Extracellular matrix part (GO:0044420)	0.0026
Transcription factor complex (GO:0005667)	0.0033
Synapse (GO:0045202)	0.005
Extracellular matrix (GO:0031012)	0.0092
Ionotropic glutamate receptor complex (GO:0008328)	0.011
Axon (GO:0030424)	0.012
STAGA complex (GO:0030914)	0.02
Synaptic membrane (GO:0097060)	0.021
Ruffle (GO:0001726)	0.027
<b>GO molecular functions</b>	
Calcium ion binding (GO:0005509)	0.00061
Estrogen receptor binding (GO:0030331)	0.0021
Calmodulin binding (GO:0005516)	0.0047
Growth factor activity (GO:0008083)	0.0058
Integrin binding (GO:0005178)	0.01
Protein tyrosine kinase activity (GO:0004713)	0.011
S100 protein binding (GO:0044548)	0.015
Extracellular matrix structural constituent (GO:0005201)	0.015
Hormone receptor binding (GO:0051427)	0.016
Gamma-catenin binding (GO:0045295)	0.019

<sup>†</sup>Top 10 GO processes are shown for each.

In general, the GO cellular components implicated a mix of structural components and neuronal/synaptic components (**Table 3.4**). The top two components were “Basement membrane” and “Extracellular matrix part”, which was also true for the DNA methylation GO analysis (**Table 3.4; Table 3.2**). “Transcription factor complex”, “Axon”, and synaptic components were implicated and were also present in the H3K4me3 analysis (**Table 3.4; Chapter 2**). “Ionotropic glutamate receptor complex” was implicated and was also present in the H3K4me3 and shared lists (**Table 3.4; Chapter 2**). “STAGA complex” was implicated, but was not in any of the individual analyses (**Table 3.4**). The top molecular function was “Calcium ion binding” which was also true for all three histone lists (**Table 3.4; Chapter 2**). “Estrogen receptor binding” as well as several other receptor binding functions were implicated and also present in the DNA analysis (**Table 3.4; Table 3.2**). The third to top function was “Calmodulin binding” and the fifth was “Integrin binding” neither of which were implicated in any of the other lists (**Table 3.4**).

The combined list was submitted to three pathway analysis software suites (**Table 3.5**). IPA implicated 22 total pathways; the top pathway was “Embryonic Development, Organismal Development, Cellular Development” (**Figure 3.8**). This pathway was not identified in any of the individual analyses. Four of the top six pathways were related to hematological/cardiovascular development and function (**Table 3.5**). Six pathways involved cell-to-cell signaling and interaction. Cell-to-cell signalling pathways were implicated in the histone analyses (Chapter 2). Four pathways involved cell death and survival; this term was also implicated in the DNA methylation analysis (**Table 3.2; Table 3.4**). Four pathways involved nervous system development, which was also identified in the H3K4me3 analysis. Three pathways involving lipid metabolism were implicated. Three lipid metabolism pathways were also implicated in the H3K4me3 analysis (Chapter 2). Partek pathway identified four pathways enriched for genes in the combined DNA methylation and histone modification list (**Table 3.4**). The top affected pathway was “Peroxisome biogenesis” (**Figure 3.9**). The same pathway was implicated in the DNA methylation analysis using Partek as well as the DNA methylation KEGG analysis (**Table 3.3**). The KEGG analysis of the combined list did identify “Peroxisome”

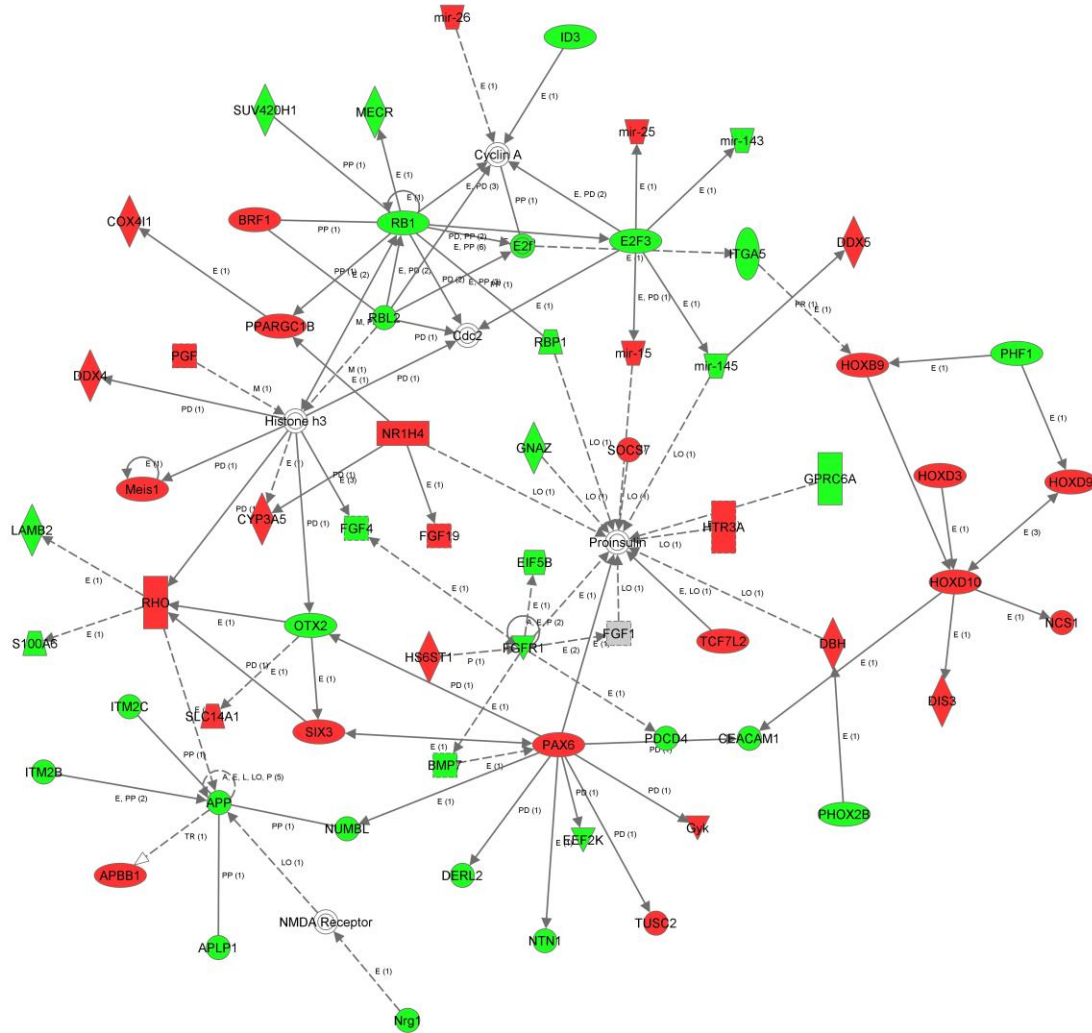
**Table 3.5 Pathways significantly enriched with genes proximal to DNA methylation or histone methylation changes<sup>†</sup>.**

<b>Pathway name</b>	<b><i>p</i>-value</b>
<b>IPA</b>	
Embryonic Development, Organismal Development, Cellular Development	10E-64
Cardiac Hypertrophy, Cardiovascular Disease, Developmental Disorder	10E-56
Humoral Immune Response, Protein Synthesis, Hematological System Development and Function	10E-49
Cellular Development, Cellular Growth and Proliferation, Hematological System Development and Function	10E-41
Skeletal and Muscular Disorders, Developmental Disorder, Hereditary Disorder	10E-30
Hematological System Development and Function, Tissue Morphology, Cell-To-Cell Signaling and Interaction	10E-26
Endocrine System Development and Function, Molecular Transport, Protein Synthesis	10E-24
Cell Death and Survival, Antimicrobial Response, Inflammatory Response	10E-23
Cell-To-Cell Signaling and Interaction, Hematological System Development and Function, Immune Cell Trafficking	10E-21
Embryonic Development, Organismal Development, Cell-To-Cell Signaling and Interaction	10E-20
Cell-To-Cell Signaling and Interaction, Reproductive System Development and Function, Tissue Development	10E-20
Cell Death and Survival, Lipid Metabolism, Small Molecule Biochemistry	10E-20
Cell Cycle, DNA Replication, Recombination, and Repair, Cellular Development	10E-19
Embryonic Development, Organismal Development, Cell Morphology	10E-19
Cell Death and Survival, Cancer, Cellular Development	10E-19
Cell-To-Cell Signaling and Interaction, Nervous System Development and Function, Behavior	10E-18
Lipid Metabolism, Small Molecule Biochemistry, Molecular Transport	10E-18
Cell Morphology, Cell Death and Survival, Nervous System Development and Function	10E-16
Cell-To-Cell Signaling and Interaction, Nervous System Development and Function, Cellular Development	10E-16
Lipid Metabolism, Small Molecule Biochemistry, Vitamin and Mineral Metabolism	10E-15
Tissue Morphology, Embryonic Development, Organismal Development	10E-15
Nervous System Development and Function, Cellular Development, Tissue Morphology	10E-14
<b>Partek Pathway</b>	
Peroxisome	0.008
Hematopoietic cell lineage	0.01
Notch signalling pathway	0.032

ABC transporters	0.036
<b>Enrichr KEGG</b>	
Notch signaling pathway	0.040
Bladder cancer	0.048

†*p*-values for each entry are shown (Fishers exact test). For a list of genes in each pathway, see **Appendix H**.

Network 1 : comined list 0.001 - 2014-07-18 11:30 AM : comined list 0.001 : comined list 0.001 - 2014-07-18 11:30 AM



© 2000-2014 QIAGEN. All rights reserved.

**Figure 3.8 Top affected Ingenuity Pathway Analysis (IPA) pathway for genes proximal to either a DNA methylation or histone methylation change.**

Pathway is titled “Embryonic Development, Organismal Development, Cellular Development” (IPA score 64). Red indicates proteins whose encoding genes are proximal to a DMR or RDHM which is associated with increased gene expression, green indicates those predicted to decrease gene expression. For full legend of symbols used, see **Appendix B**.

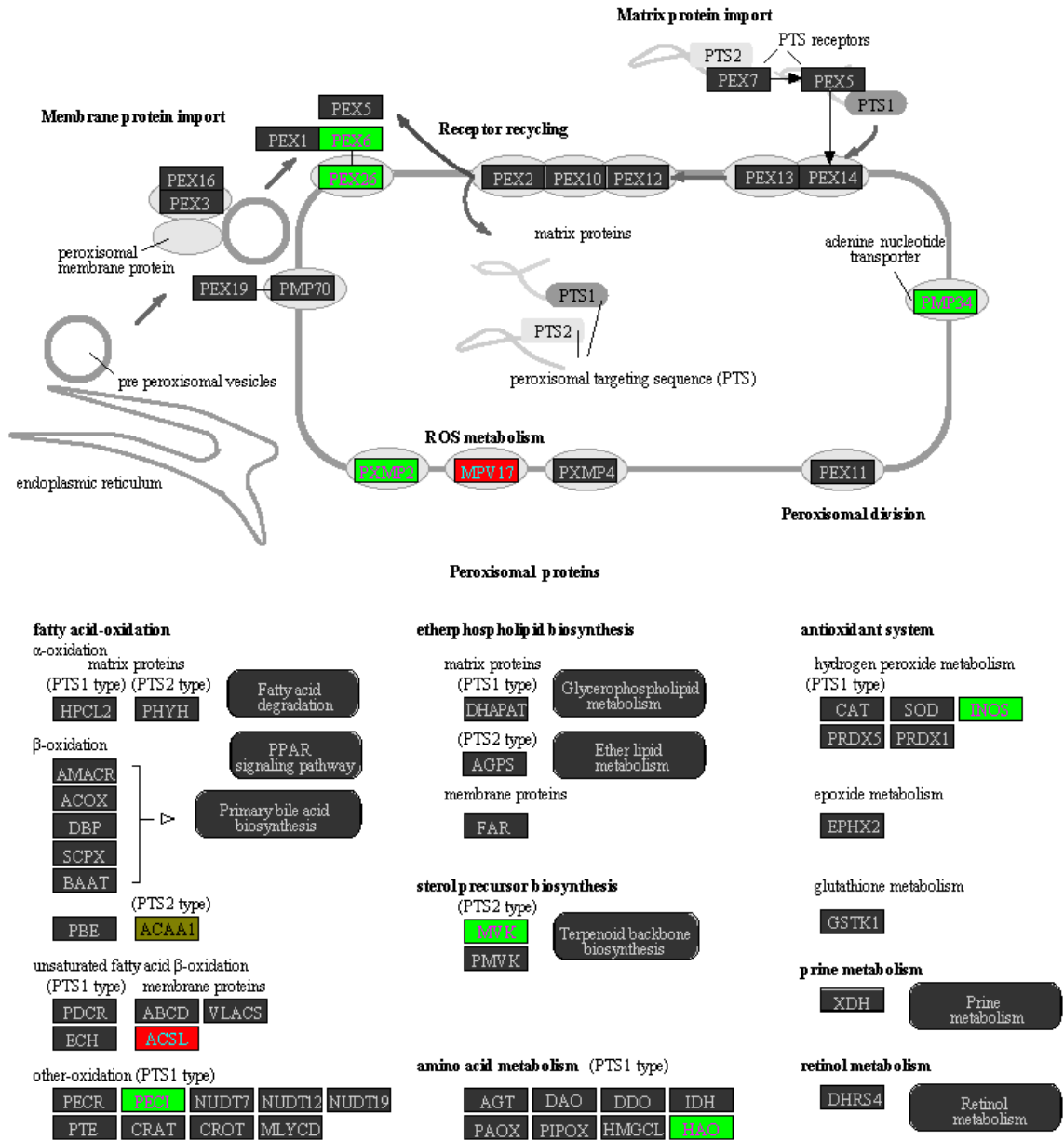


**Figure 3.9 Top Partek pathway for genes proximal to either a DNA methylation or histone methylation change.**

Pathway is titled “Peroxisome biogenesis”. Red indicates proteins whose encoding genes are proximal to a DMR or RDHM which is associated with increased gene expression, green indicates those predicted to decrease gene expression.



as well, however; it a  $p$ -value of 0.070, and as this did not meet the cut-off it was not shown. “Notch signalling pathway” was also implicated in both the Partek and KEGG analyses of the combined list (**Table 3.5**). “Hematopoietic cell lineage” was the second Partek pathway, which was also identified in the DNA methylation analysis (**Table 3.3; Table 3.5**). Given the implication of peroxisomes in both analyses, oxidative damage to hippocampal DNA was assessed. No difference in the DNA oxidative damage marker 8-hydroxy-2'-deoxyguanosine (8-OHdG) was found (**Figure 3.10**).

#### 3.4.5.1 DNA Methylation Confirmations

To confirm differential methylation of cytosines in the identified DMRs, sodium bisulfite pyrosequencing was performed. Five DMRs were selected for confirmation (**Table 3.6**). Two genes were selected which also showed differential expression on the microarray: *Tcf7l2* and *Mafg*. Three genes were selected from the “Peroxisome biogenesis” Partek pathway: *Acaa1*, *Pex6*, and *Pxmp2*. Primers were designed to target as many CpG cytosines in each DMR as possible (**Table 3.6**). There were three DMRs proximal to *Mafg*, the DMR selected for analysis was upstream of the TSS and had a reciprocal change in methylation relative to gene expression. One cytosine was confirmed to have a decrease in methylation in the region proximal to *Acaa1* (**Figure 3.11**). This cytosine was located just outside of the DMR in intron 2 (**Figure 3.12**). There was also a nominally significant change in the *Pex6* DMR (**Figure 3.11**).

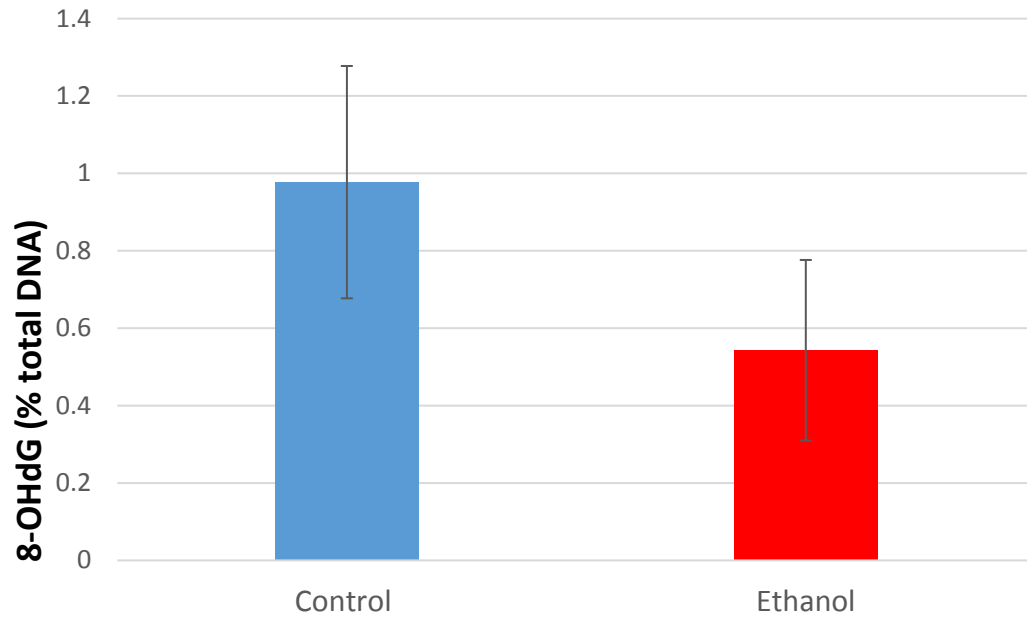


**Figure 3.10 Quantification of oxidative damage to DNA in ethanol-exposed vs. control mice.**

Absolute 8-OHdG levels for each sample were normalized to input DNA amount to obtain the 8-OHdG percentage in total DNA. Data are mean  $\pm$  standard error.  $p=0.16$  (Paired Samples t-Test)

**Table 3.6 Percentage methylation of CpG cytosines in gene of interest differentially methylated regions (DMRs) as assessed by bisulfite pyrosequencing<sup>†</sup>.**

Gene	Location	From TSS (bp)	Mixing control R <sup>2</sup>	Ethanol methylation (%)	Ethanol SEM	Control methylation (%)	Control SEM	T-test <i>p</i> -value
<i>Mafg</i>	chr11:120625270	8331	0.90	5.55	0.37	6.12	0.69	0.44
	chr11:120625261	8340	0.95	13.77	0.16	13.68	0.98	0.45
	chr11:120625225	8376	0.95	3.46	0.52	4.23	0.35	0.37
	chr11:120625205	8396	0.93	3.27	0.28	4.30	0.36	0.44
	chr11:120625131	8470	0.95	2.30	0.09	1.41	0.72	0.13
<i>Acaa1</i>	chr9:119342321	1028	0.99	72.18	0.58	71.94	1.75	0.26
	chr9:119342332	1039	0.99	68.07	1.59	68.32	1.74	0.29
	chr9:119342352	1059	1.00	61.70	1.35	64.89	1.25	0.49
	chr9:119342366	1073	1.00	74.24	1.10	75.49	1.10	0.10
	chr9:119342378	1085	0.98	63.52	0.60	64.54	1.58	<b>0.04</b>
<i>Pex6</i>	chr17:46706646	-4817	0.97	94.02	1.52	93.72	0.72	0.22
	chr17:46706661	-4802	0.99	93.74	0.31	95.33	0.90	0.06
	chr17:46706678	-4785	0.96	87.63	0.45	87.28	1.71	0.12
	chr17:46706715	-4748	0.98	98.52	0.93	98.97	0.68	0.17
<i>Pxmp2</i>	chr5:110285970	217	0.97	0.00	0.00	1.37	1.37	0.21
	chr5:110285964	223	0.98	1.71	0.90	4.91	0.42	0.35
	chr5:110285959	228	0.97	0.00	0.00	0.00	0.00	N/A
	chr5:110285948	239	0.90	2.04	1.02	1.40	1.40	0.22
	chr5:110285944	243	0.95	0.00	0.00	0.00	0.00	N/A
	chr5:110285940	247	0.97	0.00	0.00	0.00	0.00	N/A
	chr5:110285908	279	0.96	0.00	0.00	0.00	0.00	N/A
<i>Tcf7l2</i>	chr19:55745017	3208	0.92	46.89	1.26	50.40	0.94	0.40
	chr19:55745023	3214	0.96	38.90	0.54	40.58	1.46	0.17

<sup>†</sup>Genomic location and distance from nearest gene transcriptional start site (TSS) are shown for each CpG cytosine. Mixing control R<sup>2</sup> value is shown for each location. Mean of n=3 samples and standard error of the mean (SEM) are shown for control and ethanol-exposed mice. The *p*-value for a Paired Samples t-Test comparing these two groups is shown for each cytosine.

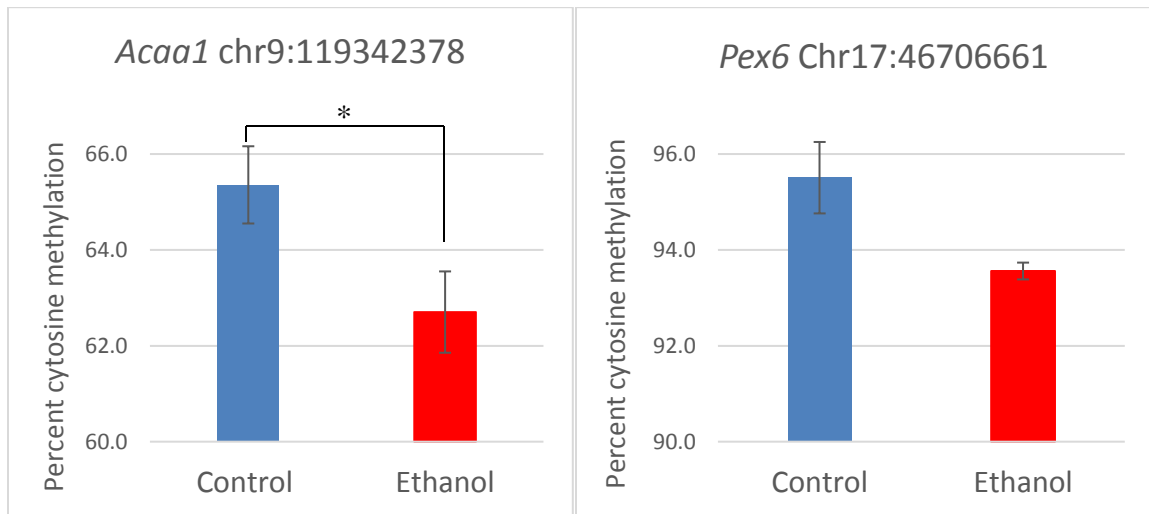


**Figure 3.11 Confirmation of cytosine methylation changes in peroxisome genes.**

Percentage cytosine methylation for each was assessed for n=3 samples per group using pyrosequencing. Data shown are mean  $\pm$  standard error. \* $p < 0.05$ .



**Figure 3.12 Location of differentially methylated CpG position in of *Acaa1* gene.**

Bars denote *Acaa1* exons, lines denote introns, grey bars denote untranslated regions, and black bars denote coding sequence. Yellow bar shows location of DMR from microarray.

Red line shows location of 3.2% decrease in methylation at cytosine in CpG site in ethanol-exposed mice (Paired Samples t-Test). Not pictured an additional DMR 3.7 kb upstream, 1.2 kb in size.

## 3.5 Discussion

There were hundreds of DNA methylation changes identified using MEDIP-chip. Interestingly, the changes were predominantly increases in methylation. This finding became more pronounced as the  $p$ -value cut-off of the DMR was increased and also remained true regardless of the region: gene promoters, CpG islands, and miRNA promoters (**Table 3.1**). The majority of FASD methylation studies have found global hypomethylation after ethanol exposure, consistent with ethanol-impaired cellular methylation processes. The findings presented in this chapter corroborate one of the few studies of similar design, which found hypermethylation in the hippocampus following neonatal ethanol exposure in a rat model of FASD (Otero et al., 2012). The effect of ethanol on the methylome is not simple, with timing, dosage, and tissue/cell type offering dramatically different results. However, the findings may be reproducible with similar experimental designs. This hypermethylation may be explained by ethanol-induced changes in oxidative stress pathways, which also impact methyl donor metabolism (Wallace and Fan, 2010). It may be that this particular ethanol-exposure regime results in specific cellular conditions leading to DNA hypermethylation.

The RMS algorithm, which was not used for analysis, indicated nearly equal increases and decreases in methylation. RMS is simply the AMS normalized to the number of CpG within the region. It is especially useful from comparing regions with different CpG densities (Pelizzola et al., 2008). As such, it was not used in this study, in which only the same regions are compared between treatment groups. The difference between these two algorithms (i.e. hypermethylation in AMS) is likely due to many increases in methylation occurring to relatively few CpGs in CpG dense regions. This is an important consideration of the AMS dataset, as it indicates numerous regions have increased methylation, but not all CpG cytosines in these regions are methylated.

### 3.5.1 Differential Methylation of Growth and Lysosomal Genes

Both the GO and pathway analyses of the DNA methylation data implicated differential methylation at cell growth and development genes. GO analysis implicated myeloid cell differentiation, as well as cell growth and development. Three of the top ten biological processes were related to hormone response (**Table 3.2**). There was also one

lipid and one neuron-related process. In line with the GO analysis, all five IPA pathways related to cell growth and development or cell death. Despite these pathways having similar names, they contain very different genes, with only seven genes occurring in more than one pathway (*Ddx5*, *Polr2a*, *Tmem97*, *Egr2*, *Numbl*, *Thpo*, and *Cdc25c*). *Polr2a* encodes the largest component of the RNA polymerase II complex. *Ddx5* is involved in mRNA splicing. *Egr2*, *Thpo*, and *Cdc25c* are involved in cell cycle and cell growth regulation. *Numbl* is involved in embryonic neurogenesis.

“Peroxisome” and “Lysosome” were implicated by both Partek and KEGG pathway analysis. Though these are both similar organelles in terms of general structure, the genes implicating them were completely different (**Table 3.3**). Lysosomes are organelles which contain hydrolytic enzymes and are responsible for breaking down cellular waste. They are also involved in repair, cell signalling, and metabolism (Settembre et al., 2013). In the developing brain, lysosomal autophagy is believed to be a response to ethanol-induced neurotoxicity and oxidative stress (Chen et al., 2012). Interestingly, peroxisomes, which modulate oxidative stress, were also implicated in pathway analysis. Peroxisomes are discussed in conjunction with the combined methylation results below. *Ap1g2*, *Lamp2*, *Ap1s1*, *Tcirg1*, *Ctsd*, and *Ctsb*

### 3.5.2 Combined Gene Ontology and Pathway Analysis

The DNA methylation changes discussed above do not occur in isolation in the mouse hippocampus. The histone modification changes from Chapter 2 are present in the same tissue at the same time. Biologically, DNA methylation and histone modification cooperate and engage in complex cross-talk to regulation the chromatin environment (Cedar and Bergman, 2009). Therefore, a combined list of the genes proximal to either DNA methylation DMRs or histone modification RDHMs was created to give a more complete picture of the impact ethanol. In general, the GO and pathway analyses of the combined methylation genelist found a mix of the processes implicated by the individual histone and DNA methylation analyses. There were instances of emergent hits not present in the top ten processes of any component analysis. These processes indicate a modest enrichment of these genes in each list, that become more significant when the lists are considered cumulatively. Identifying hits such as these was the intended purpose

of analyzing the combined lists. As the individual lists are discussed in their respective chapters, this section will focus on the emergent processes and pathways.

### 3.5.2.1 GO Analysis

The penultimate GO biological process was “Regulation of neuron differentiation” which was not implicated in any of the individual GO analyses. “CD4-positive, alpha-beta T cell activation” was also implicated, but not in any of the individual lists (**Table 3.4**). Differential methylation of genes involved in neuron differentiation has clear relevance to FASD in the brain. The relevance of T cell genes in the brain is less clear, as T cells are normally prohibited from crossing the blood brain barrier; however they can cross under numerous pathological conditions (Takeshita and Ransohoff, 2012). Differential methylation of T-cell genes may also represent a more general epigenomic response to inflammation, which is a key component of FASD etiology (Drew et al., 2015).

In general, the cellular components were a mix of structural components implicated from the DNA methylation gene list and cell-cell communication genes implicated from the histone lists. An exception was “STAGA complex” which was not in any of the individual analyses (**Table 3.4**). The STAGA complex is transcriptional co-activator protein complex responsible for histone acetylation during transcription, DNA repair, and splicing (Martinez et al., 2001). STAGA genes are crucial for neurodevelopment and their depletion is associated with numerous neurodegenerative diseases (Wang and Dent, 2014). The top molecular function was “Calcium ion binding” which was also true for all three histone lists (**Table 3.4; Chapter 2**). “Estrogen receptor binding” as well as several other receptor binding functions were implicated and also present in the DNA analysis (**Table 3.4; Table 3.2**). The third to top GO molecular function was “Calmodulin binding”. Calmodulin is a calcium-binding messenger protein involved in mediating  $\text{Ca}^{2+}$  signaling cascades. Calmodulin is critical for propagating nerve impulses, and may also be involved in ethanol-induced neurotoxicity (Caillard et al., 1999; Flentke et al., 2014). Differential methylation of calmodulin binding proteins may represent an epigenomic response to early ethanol exposure.



### 3.5.2.2 Pathway Analysis

IPA implicated 22 total pathways. The top pathway was “Embryonic Development, Organismal Development, Cellular Development” (**Figure 3.6**). This pathway was not identified in any of the individual analyses. A hub of this network is proinsulin, which is regulated by *Tcf7l2*, which was differentially expressed (Chapter 4). Proinsulin is the precursor of the peptide hormone insulin. Deregulation of insulin signalling and insulin resistance in the CNS are a key feature of FASD (Demebele et al., 2006a; de la Monte and Wands, 2010). Four of the top six pathways were related to hematological/cardiovascular development and function (**Table 3.3**). There were very few cardiovascular pathways implicated in the histone or DNA methylation analyses. “Cellular Development, Cellular Growth and Proliferation, Hematological System Development and Function” was identified in this analysis, and the exact same pathway was identified in previous work by our laboratory in GD18 fetus (Mantha et al., 2014). None of the same genes were identified however. Malformations in the heart and cardiovascular system are a major component of FASD; congenital heart disease is present in 67% of individuals with FAS (Burd et al., 2007). Changes in epigenetic regulation of heart genes may not be functional in the hippocampus, but if they also occurred in the heart they may be involved with FASD-induced heart defects. The implication of these pathways may arise from the presence of blood in the brain samples. In order to flash freeze hippocampal tissue as fast as possible to preserve RNA quality, the mice in this study were not perfused. This means that blood is still present in the vasculature of the hippocampus. Thus, some of the blood epigenome is likely represented in the epigenomic and transcriptomic data.

Only one pathway—“Endocrine System Development and Function, Molecular Transport, Protein Synthesis Six”—was implicated in the H3K27me3 another analysis (Chapter 2). Many pathways had similar terms however. There were cell-to-cell signalling and nervous system development pathways which were also identified in the H3K4me3 analysis (Chapter 2). Cell death and survival pathways were also prevalent in the DNA methylation analysis (**Table 3.3**). Three pathways involving lipid metabolism were implicated. Three lipid metabolism pathways were also implicated in the H3K4me3 analysis (Chapter 2). Interestingly, the top Partek pathway, “Peroxisome biogenesis” was

also related to lipid metabolism (**Figure 3.9**). The same pathway was implicated in the DNA methylation analysis using Partek as well as the DNA methylation KEGG analysis (See below for discussion).

Notch signaling was implicated by both Partek pathway and KEGG analyses (**Table 3.5**). The same genes made up both pathway lists. Notch signaling promotes neurogenesis in both embryonic development and the adult brain (Imayoshi and Kageyama, 2011). Notch proteins are expressed in the adult brain and appear to be involved in learning and memory (Costa et al., 2003). There is also evidence that Notch signaling is dysregulated in some early developmental models of FASD (Sarmah et al., 2016). Changes in epigenetic marks at Notch signaling genes could represent a maintained “footprint” of ethanol exposure (see Chapter 5).

### 3.5.3 Peroxisome Biogenesis Pathway

The top network from the Partek DNA methylation (**Figure 3.6**) and combined methylation analysis (**Figure 3.9**) was “Peroxisome biogenesis”. Peroxisomes are membrane bound organelles found in all eukaryotic cells. Their main functions are the  $\beta$ -oxidation of very-long-chain fatty acids (VLCFAs) and synthesis of ether lipids such as plasmalogens (Trompier et al., 2014). The  $\beta$ -oxidation genes *Acaa1a* (Acetyl-CoA Acyltransferase 1A) and *Peci* were proximal to hypermethylated DMRs. *Acaa1a* also had increased H3K4me3 levels. Importantly, peroxisomes are key to the redox balance of the cell; both generating and scavenging free radicals (Trompier et al., 2014). The ROS-generating Nitric Oxide Synthase, *Nos2*, gene was proximal to a hypermethylated DMR in this study. NOS2 is also involved in neurotransmission (Vincent, 2010). Peroxisome production in response to oxidative stress is regulated by the *Pex* genes, which assemble peroxisome structure and guide matrix proteins inside the organelle. The *Pex26* and *Pex6* genes were proximal to hypermethylated DMRs in this study. PEX26 is a peroxisome biogenesis factor that anchors Pex1 and Pex6 to the peroxisomal membrane, and is likely required for protein import (Tamura et al., 2014). Five genes (*Acs14*, *Acs16*, *Agt*, *Mpv17*, and *Mpv17l2*) had only histone changes, being implicated in the combined analysis but not the DNA methylation analysis (**Table 3.4**).

Due to the potential for oxidative damage to hippocampal cells, levels of 8-hydroxy-2'-deoxyguanosine (8-OHdG) were assessed in the genomic DNA. 8-OHdG is an excellent biomarker of oxidative DNA damage, as it is directly caused by free radicals. Further, it has high potential for detrimental effects include G-to-T transversions, and inappropriate binding of DNA methylation proteins such as MBD (Valavandis et al., 2009). There was no change in 8-OHdG in the mice used for the MeDIP analysis (**Figure 3.10**). 8-OHdG is repaired by DNA repair enzymes, and thus may not have persisted to PND 70 if it were induced (Valavandis et al., 2009). Other oxidative damage such as lipid peroxidation is not repaired, and has been observed in long-term FASD models (Petkov et al., 1992). Thus, examination 8-OHdG much earlier or other macromolecules at PND 70 may have identified changes in this experiment.

Oxidative stress is a well characterized component of FASD etiology. Ethanol acts directly on mitochondria to produce superoxide, hydroxide, and nitric oxide radicals (Wu and Cederbaum, 2003). Metabolism of ethanol by cytochrome CYP2E1 produces oxidized products and ultimately hydroxide radical generation (Mansouri et al., 2001). Catalase also produces acetaldehyde from alcohol in the brain, further increasing the formation of ROS (Shaw, 1989). Oxidative damage can lead to blood-brain barrier impairment, inflammation, and increased apoptosis (Haorah et al., 2008). Interestingly, these are also key features of FASD etiology. Indeed, oxidative damage is observed in many rodent models of FASD, including lipid peroxidation, protein oxidation, and DNA damage (Brocardo et al., 2011). Lipid peroxidation is not often present in young animals, but accumulates over time into adulthood (Dembele et al., 2006b). In a *Drosophila* model of developmental ethanol exposure, changes in expression of antioxidant genes contributed to oxidative stress in adult flies (Logan-Garbisch et al., 2014). Further, this increased oxidative stress was a primary cause of developmental delay associated with ethanol exposure (Logan-Garbisch et al., 2014).

Peroxisomes are being explored as a target for FASD therapies. A class of drugs known as PPAR (Peroxisome proliferator-activated receptor) agonists were initially developed to treat other disorders. PPARs are nuclear receptors that act as transcription factors when activated by ligand binding. PPAR $\alpha$  is important for lipid metabolism in the liver; when activated by fatty acid ligands it transcribes hundreds of target genes. PPAR $\gamma$

is activated by prostaglandins and regulates fatty acid storage and glucose metabolism. The PPAR $\gamma$  agonist pioglitazone was developed to treat diabetes (Bajaj et al., 2007). Several researchers later noted that pioglitazone reduced inflammation, including inhibition of microglia activation and cytokine production in the brain (Bernardo et al., 2000; Petrova et al., 1999). Kane et al. (2011) found that co-administration of pioglitazone with ethanol prevented cultured granule cells and microglia from the toxic effects of ethanol (Kane et al., 2011). A subsequent *in vivo* study found that co-administration of pioglitazone and ethanol from PND4-9 prevented ethanol-induced increases in cytokines interleukin-1 $\beta$  and tumor necrosis factors in the hippocampus (Drew et al., 2015). These studies suggest that upregulation of peroxisome (and other) gene expression may prevent inflammatory responses associated the brain's response to FASD-induced oxidative stress.

### 3.5.4 Pyrosequencing Confirmations

CpG cytosines in five DMRs were investigated using pyrosequencing. A 3.2% decrease in the methylation of one CpG in the *Acaal* regulatory region was confirmed (**Figure 3.11**). As stated above, this gene is critical for the peroxisomal  $\beta$ -oxidation. No other statistically significant changes were identified, though one nominally significant ( $p=0.057$ ) decrease in methylation occurred at one cytosine in the *Pex6* DMR (**Figure 3.11**). PEX6 is a membrane-associated protein which is necessary for import of peroxisome proteins. Mutations in both *Acaal* and *Pex6* cause peroxisome biogenesis disorders in (Trompier et al., 2014). One possible reason for not confirming more methylation changes by pyrosequencing was the use of anti-methylcytosine antibody for the MeDIP-chip. This would allow any differences in cytosine methylation, not just CpG cytosines, to be identified by MeDIP analysis. Due to the limitations of bisulfite pyrosequencing assay design, only CpG cytosines could be assessed. Non-CpG methylation is highly abundant in the brain, representing 25% of all cytosine methylation in hippocampal dentate granule neurons (Guo et al., 2014). It is possible that the DMRs implicated by MeDIP-chip included many CpH cytosines methylation changes, which would not be assayed by pyrosequencing.

### 3.5.5 Conclusion

This chapter describes genes and pathways affected by DNA methylation changes in the hippocampus in response to early ethanol exposure. These changes provide insight into the long-term effects of PAE on the epigenome. These genes and pathways were distinct from those affected by histone methylation changes. Analysis of the DNA methylation data with the histone data identified novel processes not found in any of the individual analyses. Cardiovascular pathways and notch signalling emerged as affected processes in the combined analysis. These processes are important to FASD etiology and their differential methylation in the hippocampus may be relevant. Peroxisome biogenesis was implicated in the DNA methylation analysis, and was the top affected pathway in the combined methylation analyses. Peroxisomes are key regulators of oxidative stress and lipid metabolism; upregulating their biogenesis is already being explored as a therapy for FASD.

#### **Footnote**

A modified version of this chapter has been published (Chater-Diehl et al., 2016).

### 3.6 References

- Among, D., and Women, P. (2010). Fetal Alcohol Spectrum Disorders By the Numbers. *J. Dev. Behav. Pediatr. samhsa.org*, 2–3.
- Audergon, P.N.C.B., Catania, S., Kagansky, A., Tong, P., Shukla, M., Pidoux, A.L., and Allshire, R.C. (2015). Epigenetics. Restricted epigenetic inheritance of H3K9 methylation. *Science* 348, 132–135.
- Baccarelli, A., and Bollati, V. (2009). Epigenetics and environmental chemicals. *Curr. Opin. Pediatr.* 21, 243–251.
- Bajaj, M., Suraamornkul, S., Hardies, L.J., Glass, L., Musi, N., and DeFronzo, R.A. (2007). Effects of peroxisome proliferator-activated receptor (PPAR)- $\alpha$  and PPAR- $\gamma$  agonists on glucose and lipid metabolism in patients with type 2 diabetes mellitus. *Diabetologia* 50, 1723–1731.
- Bartolomei, M.S., and Tilghman, S.M. (1997). Genomic imprinting in mammals. *Annu. Rev. Genet.* 31, 493–525.
- Bernardo, A., Levi, G., and Minghetti, L. (2000). Role of the peroxisome proliferator-activated receptor-gamma (PPAR-gamma) and its natural ligand 15-deoxy-Delta12, 14-prostaglandin J2 in the regulation of microglial functions. *Eur. J. Neurosci.* 12, 2215–2223.
- Bird, A.P. (1980). DNA methylation and the frequency of CpG in animal DNA. *Nucleic Acids Res.* 8, 1499–1504.
- Bird, A., Taggart, M., Frommer, M., Miller, O.J., and Macleod, D. (1985). A fraction of the mouse genome that is derived from islands of nonmethylated, CpG-rich DNA. *Cell* 40, 91–99.
- Branco, M.R., Ficz, G., and Reik, W. (2011). Uncovering the role of 5-hydroxymethylcytosine in the epigenome. *Nat. Rev.* 13, 7–13.
- Brocardo, P.S., Gil-Mohapel, J., and Christie, B.R. (2011). The role of oxidative stress in fetal alcohol spectrum disorders. *Brain Res. Rev.* 67, 209–225.
- Butcher, L.M., and Beck, S. (2010). AutoMeDIP-seq: a high-throughput, whole genome, DNA methylation assay. *Methods* 52, 223–231.
- Butler, M.G. (2009). Genomic imprinting disorders in humans: a mini-review. *J. Assist. Reprod. Genet.* 26, 477–486.
- Caillard, O., Ben-Ari, Y., and Gaiarsa, J.L. (1999). Long-term potentiation of GABAergic synaptic transmission in neonatal rat hippocampus. *J. Physiol.* 518, 109–119.

- Cedar, H., and Bergman, Y. (2009). Linking DNA methylation and histone modification: patterns and paradigms. *Nat. Rev.* 10, 295–304.
- Chen, G., Ke, Z., Xu, M., Liao, M., Wang, X., Qi, Y., Zhang, T., Frank, J.A., Bower, K.A., Shi, X., et al. (2012). Autophagy is a protective response to ethanol neurotoxicity. *Autophagy* 8, 1577–1589.
- Chen, Y., Ozturk, N.C., and Zhou, F.C. (2013). DNA methylation program in developing hippocampus and its alteration by alcohol. *PLoS One* 8, e60503.
- Compere, S.J., and Palmiter, R.D. (1981). DNA methylation controls the inducibility of the mouse metallothionein-I gene lymphoid cells. *Cell* 25, 233–240.
- Costa, R.M., Honjo, T., and Silva, A.J. (2003). Learning and memory deficits in Notch mutant mice. *Curr. Biol.* 13, 1348–1354.
- Coulondre, C., Miller, J.H., Farabaugh, P.J., and Gilbert, W. (1978). Molecular basis of base substitution hotspots in *Escherichia coli*. *Nature* 274, 775–780.
- Deaton, A.M., and Bird, A. (2011). CpG islands and the regulation of transcription. *Genes Dev.* 25, 1010–1022.
- Dembele, K., Yao, X.-H., Chen, L., and Nyomba, B.L.G. (2006a). Intrauterine ethanol exposure results in hypothalamic oxidative stress and neuroendocrine alterations in adult rat offspring. *Am. J. Physiol. Regul. Integr. Comp. Physiol.* 291, R796–802.
- Dembele, K., Yao, X.-H., Chen, L., and Nyomba, B.L.G. (2006b). Intrauterine ethanol exposure results in hypothalamic oxidative stress and neuroendocrine alterations in adult rat offspring. *Am. J. Physiol. Regul. Integr. Comp. Physiol.* 291, R796–802.
- Drew, P.D., Johnson, J.W., Douglas, J.C., Phelan, K.D., and Kane, C.J.M. (2015). Pioglitazone blocks ethanol induction of microglial activation and immune responses in the hippocampus, cerebellum, and cerebral cortex in a mouse model of fetal alcohol spectrum disorders. *Alcohol. Clin. Exp. Res.* 39, 445–454.
- Feng, J., Chang, H., Li, E., and Fan, G. (2005). Dynamic expression of de novo DNA methyltransferases Dnmt3a and Dnmt3b in the central nervous system. *J. Neurosci. Res.* 79, 734–746.
- Flentke, G.R., Klingler, R.H., Tanguay, R.L., Carvan, M.J., and Smith, S.M. (2014). An Evolutionarily Conserved Mechanism of Calcium-Dependent Neurotoxicity in a Zebrafish Model of Fetal Alcohol Spectrum Disorders. *Alcohol. Clin. Exp. Res.* 38, 1255–1265.
- Garro, A.J., McBeth, D.L., Lima, V., and Lieber, C.S. (1991). Ethanol consumption inhibits fetal DNA methylation in mice: implications for the fetal alcohol

- syndrome. *Alcohol. Clin. Exp. Res.* *15*, 395–398.
- Geiman, T.M., and Muegge, K. (2009). DNA methylation in early development. *Mol. Reprod. Dev.* *77*, n/a-n/a.
- Gil-Mohapel, J., Boehme, F., Kainer, L., and Christie, B.R. (2010). Hippocampal cell loss and neurogenesis after fetal alcohol exposure: Insights from different rodent models. *Brain Res. Rev.* *64*, 283–303.
- Gloyn, A.L., Braun, M., and Rorsman, P. (2009). Type 2 diabetes susceptibility gene TCF7L2 and its role in beta-cell function. *Diabetes* *58*, 800–802.
- Goto, K., Numata, M., Komura, J.I., Ono, T., Bestor, T.H., and Kondo, H. (1994). Expression of DNA methyltransferase gene in mature and immature neurons as well as proliferating cells in mice. *Differentiation.* *56*, 39–44.
- Govorko, D., Bekdash, R.A., Zhang, C., and Sarkar, D.K. (2012). Male germline transmits fetal alcohol adverse effect on hypothalamic proopiomelanocortin gene across generations. *Biol. Psychiatry* *72*, 378–388.
- Gu, H., Smith, Z.D., Bock, C., Boyle, P., Gnirke, A., and Meissner, A. (2011). Preparation of reduced representation bisulfite sequencing libraries for genome-scale DNA methylation profiling. *Nat. Protoc.* *6*, 468–481.
- Guenther, M.G., Levine, S.S., Boyer, L.A., Jaenisch, R., and Young, R.A. (2007). A Chromatin Landmark and Transcription Initiation at Most Promoters in Human Cells. *Cell* *130*, 77–88.
- Guo, J.U., Su, Y., Shin, J.H., Shin, J., Li, H., Xie, B., Zhong, C., Hu, S., Le, T., Fan, G., et al. (2014). Distribution, recognition and regulation of non-CpG methylation in the adult mammalian brain. *Nat. Neurosci.* *17*, 215–222.
- Guttman, M., Amit, I., Garber, M., French, C., Lin, M.F., Feldser, D., Huarte, M., Zuk, O., Carey, B.W., Cassady, J.P., et al. (2009). Chromatin signature reveals over a thousand highly conserved large non-coding RNAs in mammals. *Nature* *458*, 223–227.
- Hamid, A., and Kaur, J. (2007). Decreased Expression of Transporters Reduces Folate Uptake across Renal Absorptive Surfaces in Experimental Alcoholism. *J. Membr. Biol.* *220*, 69–77.
- Han, H., Cortez, C.C., Yang, X., Nichols, P.W., Jones, P.A., and Liang, G. (2011). DNA methylation directly silences genes with non-CpG island promoters and establishes a nucleosome occupied promoter. *Hum. Mol. Genet.* *20*, 4299–4310.
- Haorah, J., Schall, K., Ramirez, S.H., and Persidsky, Y. (2008). Activation of protein tyrosine kinases and matrix metalloproteinases causes blood-brain barrier injury: Novel mechanism for neurodegeneration associated with alcohol abuse. *Glia* *56*,



78–88.

- Haycock, P.C., and Ramsay, M. (2009). Exposure of mouse embryos to ethanol during preimplantation development: effect on DNA methylation in the h19 imprinting control region. *Biol. Reprod.* *81*, 618–627.
- Holliday, R., and Pugh, J.E. (1975). DNA modification mechanisms and gene activity during development. *Science* *187*, 226–232.
- Hotchkiss, R.D. (1948). The quantitative separation of purines, pyrimidines, and nucleosides by paper chromatography. *J. Biol. Chem.* *175*, 315–332.
- Ikonomidou, C., Bittigau, P., Ishimaru, M.J., Wozniak, D.F., Koch, C., Genz, K., Price, M.T., Stefovská, V., Horster, F., Tenkova, T., et al. (2000). Ethanol-induced apoptotic neurodegeneration and fetal alcohol syndrome. *Science* *287*, 1056–1060.
- Illingworth, R.S., Gruenewald-Schneider, U., Webb, S., Kerr, A.R.W., James, K.D., Turner, D.J., Smith, C., Harrison, D.J., Andrews, R., and Bird, A.P. (2010). Orphan CpG Islands Identify Numerous Conserved Promoters in the Mammalian Genome. *PLoS Genet.* *6*, e1001134.
- Imayoshi, I., and Kageyama, R. (2011). The Role of Notch Signaling in Adult Neurogenesis. *Mol. Neurobiol.* *44*, 7–12.
- Ishida, M., and Moore, G.E. (2013). The role of imprinted genes in humans. *Mol. Aspects Med.* *34*, 826–840.
- Ito, S., Shen, L., Dai, Q., Wu, S.C., Collins, L.B., Swenberg, J.A., He, C., and Zhang, Y. (2011). Tet proteins can convert 5-methylcytosine to 5-formylcytosine and 5-carboxylcytosine. *Science* *333*, 1300–1303.
- Jacinto, F. V., Ballestar, E., and Esteller, M. (2008). Methyl-DNA immunoprecipitation (MeDIP): hunting down the DNA methylome. *Biotechniques* *44*, 35, 37, 39 passim.
- Jones, P.A. (2012). Functions of DNA methylation: islands, start sites, gene bodies and beyond. *Nat. Rev. Genet.* *13*, 484–492.
- Kane, C.J.M., Phelan, K.D., Han, L., Smith, R.R., Xie, J., Douglas, J.C., and Drew, P.D. (2011). Protection of neurons and microglia against ethanol in a mouse model of fetal alcohol spectrum disorders by peroxisome proliferator-activated receptor- $\gamma$  agonists. *Brain. Behav. Immun.* *25 Suppl 1*, S137-45.
- Kenyon, S.H., Nicolaou, A., and Gibbons, W.A. (1998). The effect of ethanol and its metabolites upon methionine synthase activity in vitro. *Alcohol* *15*, 305–309.
- Khare, T., Pai, S., Koncevicius, K., Pal, M., Kriukiene, E., Liutkeviciute, Z., Irimia, M.,

- Jia, P., Ptak, C., Xia, M., et al. (2012). 5-hmC in the brain is abundant in synaptic genes and shows differences at the exon-intron boundary. *Nat. Struct. Mol. Biol.* *19*, 1037–1043.
- Kohli, R.M., and Zhang, Y. (2013). TET enzymes, TDG and the dynamics of DNA demethylation. *Nature* *502*, 472–479.
- de la Monte, S.M., and Wands, J.R. (2010). Role of central nervous system insulin resistance in fetal alcohol spectrum disorders. *J. Popul. Ther. Clin. Pharmacol.* *17*, e390-404.
- Laufer, B.I., Mantha, K., Kleiber, M.L., Diehl, E.J., Addison, S.M., and Singh, S.M. (2013). Long-lasting alterations to DNA methylation and ncRNAs could underlie the effects of fetal alcohol exposure in mice. *Dis. Model. Mech.* *6*, 977–992.
- Laufer, B.I., Kapalanga, J., Castellani, C.A., Diehl, E.J., Yan, L., and Singh, S.M. (2015). Associative DNA methylation changes in children with prenatal alcohol exposure. *Epigenomics* 1–16.
- Li, Y., and Tollefsbol, T.O. (2011). DNA methylation detection: bisulfite genomic sequencing analysis. *Methods Mol. Biol.* *791*, 11–21.
- Lim, A.M., Candiloro, I.L., Wong, N., Collins, M., Do, H., Takano, E.A., Angel, C., Young, R.J., Corry, J., Wiesenfeld, D., et al. (2014). Quantitative methodology is critical for assessing DNA methylation and impacts on correlation with patient outcome. *Clin. Epigenetics* *6*, 22.
- Liu, Y., Balaraman, Y., Wang, G., Nephew, K.P., and Zhou, F.C. (2009). Alcohol exposure alters DNA methylation profiles in mouse embryos at early neurulation. *Epigenetics* *4*, 500–511.
- Logan-Garbisch, T., Bortolazzo, A., Luu, P., Ford, A., Do, D., Khodabakhshi, P., and French, R.L. (2014). Developmental ethanol exposure leads to dysregulation of lipid metabolism and oxidative stress in *Drosophila*. *G3 (Bethesda)*. *5*, 49–59.
- Lu, F., Liu, Y., Jiang, L., Yamaguchi, S., and Zhang, Y. (2014). Role of Tet proteins in enhancer activity and telomere elongation. *Genes Dev.* *28*, 2103–2119.
- Lu, H., Liu, X., Deng, Y., and Qing, H. (2013). DNA methylation, a hand behind neurodegenerative diseases. *Front. Aging Neurosci.* *5*, 85.
- Lubin, F.D., Roth, T.L., and Sweatt, J.D. (2008). Epigenetic Regulation of *bdnf* Gene Transcription in the Consolidation of Fear Memory. *J. Neurosci.* *28*, 10576–10586.
- Lyssenko, V., Lupi, R., Marchetti, P., Del Guerra, S., Orho-Melander, M., Almgren, P., Sjögren, M., Ling, C., Eriksson, K.-F., Lethagen, A.-L., et al. (2007). Mechanisms by which common variants in the *TCF7L2* gene increase risk of type 2 diabetes. *J.*

Clin. Invest. *117*, 2155–2163.

- Macleod, D., Ali, R.R., and Bird, A. (1998). An alternative promoter in the mouse major histocompatibility complex class II I-Abeta gene: implications for the origin of CpG islands. *Mol. Cell. Biol.* *18*, 4433–4443.
- Mansouri, A., Demeilliers, C., Amsellem, S., Pessayre, D., and Fromenty, B. (2001). Acute ethanol administration oxidatively damages and depletes mitochondrial dna in mouse liver, brain, heart, and skeletal muscles: protective effects of antioxidants. *J. Pharmacol. Exp. Ther.* *298*, 737–743.
- Mantha, K., Laufer, B.I., and Singh, S.M. (2014). Molecular changes during neurodevelopment following second-trimester binge ethanol exposure in a mouse model of fetal alcohol spectrum disorder: from immediate effects to long-term adaptation. *Dev. Neurosci.* *36*, 29–43.
- Martinez, E., Palhan, V.B., Tjernberg, A., Lymar, E.S., Gamper, A.M., Kundu, T.K., Chait, B.T., and Roeder, R.G. (2001). Human STAGA Complex Is a Chromatin-Acetylating Transcription Coactivator That Interacts with Pre-mRNA Splicing and DNA Damage-Binding Factors In Vivo. *Mol. Cell. Biol.* *21*, 6782–6795.
- Medvedeva, Y.A., Khamis, A.M., Kulakovskiy, I. V, Ba-Alawi, W., Bhuyan, M.S.I., Kawaji, H., Lassmann, T., Harbers, M., Forrest, A.R.R., Bajic, V.B., et al. (2014). Effects of cytosine methylation on transcription factor binding sites. *BMC Genomics* *15*, 119.
- Messerschmidt, D.M., Knowles, B.B., and Solter, D. (2014). DNA methylation dynamics during epigenetic reprogramming in the germline and preimplantation embryos. *Genes Dev.* *28*, 812–828.
- Miller, C.A., and Sweatt, J.D. (2007). Covalent Modification of DNA Regulates Memory Formation. *Neuron* *53*, 857–869.
- Miller, C.A., Gavin, C.F., White, J.A., Parrish, R.R., Honasoge, A., Yancey, C.R., Rivera, I.M., Rubio, M.D., Rumbaugh, G., and Sweatt, J.D. (2010). Cortical DNA methylation maintains remote memory. *Nat. Neurosci.* *13*, 664–666.
- Moore, T., and Haig, D. (1991). Genomic imprinting in mammalian development: a parental tug-of-war. *Trends Genet.* *7*, 45–49.
- Muñoz, P., Estay, C., Díaz, P., Elgueta, C., Ardiles, Á.O., Lizana, P.A., Ardiles, O., Ivarro, and Lizana, P.A. (2016). Inhibition of DNA Methylation Impairs Synaptic Plasticity during an Early Time Window in Rats. *Neural Plast.* *2016*, 1–13.
- Nair, S.S., Coolen, M.W., Stirzaker, C., Song, J.Z., Statham, A.L., Strbenac, D., Robinson, M.D., and Clark, S.J. (2011). Comparison of methyl-DNA immunoprecipitation (MeDIP) and methyl-CpG binding domain (MBD) protein capture for genome-wide DNA methylation analysis reveal CpG sequence

- coverage bias. *Epigenetics* 6, 34–44.
- Okamoto, I., and Heard, E. (2009). Lessons from comparative analysis of X-chromosome inactivation in mammals. *Chromosom. Res.* 17, 659–669.
- Okano, M., Xie, S., and Li, E. (1998). Cloning and characterization of a family of novel mammalian DNA (cytosine-5) methyltransferases. *Nat. Genet.* 19, 219–220.
- Okano, M., Bell, D.W., Haber, D.A., and Li, E. (1999). DNA methyltransferases Dnmt3a and Dnmt3b are essential for de novo methylation and mammalian development. *Cell* 99, 247–257.
- Otero, N.K., Thomas, J.D., Saski, C.A., Xia, X., and Kelly, S.J. (2012). Choline supplementation and DNA methylation in the hippocampus and prefrontal cortex of rats exposed to alcohol during development. *Alcohol. Clin. Exp. Res.* 36, 1701–1709.
- Pelizzola, M., Koga, Y., Urban, A.E., Krauthammer, M., Weissman, S., Halaban, R., and Molinaro, A.M. (2008). MEDME: an experimental and analytical methodology for the estimation of DNA methylation levels based on microarray derived MeDIP-enrichment. *Genome Res.* 18, 1652–1659.
- Petkov, V. V., Stoianovski, D., Petkov, V.D., and Vyglenova, I. (1992). Lipid peroxidation changes in the brain in fetal alcohol syndrome. *Biull. Eksp. Biol. Med.* 113, 500–502.
- Petrova, T. V., Akama, K.T., and Van Eldik, L.J. (1999). Cyclopentenone prostaglandins suppress activation of microglia: down-regulation of inducible nitric-oxide synthase by 15-deoxy-Delta12,14-prostaglandin J2. *Proc. Natl. Acad. Sci. U. S. A.* 96, 4668–4673.
- Portales-Casamar, E., Lussier, A.A., Jones, M.J., MacIsaac, J.L., Edgar, R.D., Mah, S.M., Barhdadi, A., Provost, S., Lemieux-Perreault, L.-P., Cynader, M.S., et al. (2016). DNA methylation signature of human fetal alcohol spectrum disorder. *Epigenetics Chromatin* 9, 25.
- Ratnam, S., Mertineit, C., Ding, F., Howell, C.Y., Clarke, H.J., Bestor, T.H., Chaillet, J.R., and Trasler, J.M. (2002). Dynamics of Dnmt1 Methyltransferase Expression and Intracellular Localization during Oogenesis and Preimplantation Development. *Dev. Biol.* 245, 304–314.
- Robertson, K.D., and Wolffe, A.P. (2000). DNA methylation in health and disease. *Nat. Rev.* 1, 11–19.
- Robinson, M.D., Stirzaker, C., Statham, A.L., Coolen, M.W., Song, J.Z., Nair, S.S., Strbenac, D., Speed, T.P., and Clark, S.J. (2010). Evaluation of affinity-based genome-wide DNA methylation data: effects of CpG density, amplification bias, and copy number variation. *Genome Res.* 20, 1719–1729.

- Sarmah, S., Muralidharan, P., Marrs, J.A., May, P., Baete, A., Russo, J., Elliott, A., Blankenship, J., Kalberg, W., May, P., et al. (2016). Embryonic Ethanol Exposure Dysregulates BMP and Notch Signaling, Leading to Persistent Atrio-Ventricular Valve Defects in Zebrafish. *PLoS One* *11*, e0161205.
- Saxonov, S., Berg, P., and Brutlag, D.L. (2006). A genome-wide analysis of CpG dinucleotides in the human genome distinguishes two distinct classes of promoters. *Proc. Natl. Acad. Sci. U. S. A.* *103*, 1412–1417.
- Schultz, D.C., Ayyanathan, K., Negorev, D., Maul, G.G., and Rauscher, F.J. (2002). SETDB1: a novel KAP-1-associated histone H3, lysine 9-specific methyltransferase that contributes to HP1-mediated silencing of euchromatic genes by KRAB zinc-finger proteins. *Genes Dev.* *16*, 919–932.
- Scott, R.J., and Spielman, M. (2006). Genomic imprinting in plants and mammals: how life history constrains convergence. *Cytogenet. Genome Res.* *113*, 53–67.
- Seisenberger, S., Andrews, S., Krueger, F., Arand, J., Walter, J., Santos, F., Popp, C., Thienpont, B., Dean, W., and Reik, W. (2012). The dynamics of genome-wide DNA methylation reprogramming in mouse primordial germ cells. *Mol. Cell* *48*, 849–862.
- Seitz, H.K., and Stickel, F. (2007). Molecular mechanisms of alcohol-mediated carcinogenesis. *Nat. Rev. Cancer* *7*, 599–612.
- Settembre, C., Fraldi, A., Medina, D.L., and Ballabio, A. (2013). Signals from the lysosome: a control centre for cellular clearance and energy metabolism. *Nat. Rev. Mol. Cell Biol.* *14*, 283–296.
- Shaw, S. (1989). Lipid peroxidation, iron mobilization and radical generation induced by alcohol. *Free Radic. Biol. Med.* *7*, 541–547.
- Shukla, S.D., Velazquez, J., French, S.W., Lu, S.C., Ticku, M.K., and Zakhari, S. (2008). Emerging role of epigenetics in the actions of alcohol. *Alcohol. Clin. Exp. Res.* *32*, 1525–1534.
- Smith, Z.D., and Meissner, A. (2013). DNA methylation: roles in mammalian development. *Nat. Rev.* *14*, 204–220.
- Spijker, S. (2011). Dissection of Rodent Brain Regions. *Neuromethods* *57*, 13–26.
- Spruijt, C.G., and Vermeulen, M. (2014). DNA methylation: old dog, new tricks? *Nat. Struct. Mol. Biol.* *21*, 949–954.
- Takamoto, I., Kubota, N., Nakaya, K., Kumagai, K., Hashimoto, S., Kubota, T., Inoue, M., Kajiwara, E., Katsuyama, H., Obata, A., et al. (2014). TCF7L2 in mouse pancreatic beta cells plays a crucial role in glucose homeostasis by regulating beta cell mass. *Diabetologia* *57*, 542–553.

- Takeshita, Y., and Ransohoff, R.M. (2012). Inflammatory cell trafficking across the blood-brain barrier: chemokine regulation and in vitro models. *Immunol. Rev.* 248, 228–239.
- Tamura, S., Matsumoto, N., Takeba, R., and Fujiki, Y. (2014). AAA peroxins and their recruiter Pex26p modulate the interactions of peroxins involved in peroxisomal protein import. *J. Biol. Chem.* 289, 24336–24346.
- Tanaka, H., Suzuki, N., and Arima, M. (1982). Hypoglycemia in the fetal alcohol syndrome in rat. *Brain Dev.* 4, 97–103.
- Thomson, J.P., Skene, P.J., Selfridge, J., Clouaire, T., Guy, J., Webb, S., Kerr, A.R.W., Deaton, A., Andrews, R., James, K.D., et al. (2010). CpG islands influence chromatin structure via the CpG-binding protein Cfp1. *Nature* 464, 1082–1086.
- Tognini, P., Napoli, D., and Pizzorusso, T. (2015). Dynamic DNA methylation in the brain: a new epigenetic mark for experience-dependent plasticity. *Front. Cell. Neurosci.* 9, 331.
- Trompier, D., Vejux, A., Zarrouk, A., Gondcaille, C., Geillon, F., Nury, T., Savary, S., and Lizard, G. (2014). Brain peroxisomes. *Biochimie* 98, 102–110.
- Valavandis, A., Vlachogianni, T., and Fiotakis, C. (2009). 8-hydroxy-2'-deoxyguanosine (8-OHdG): A Critical Biomarker of Oxidative Stress and Carcinogenesis. *J. Environ. Sci. Heal. Part C* 27, 120–139.
- Vincent, S.R. (2010). Nitric oxide neurons and neurotransmission. *Prog. Neurobiol.* 90, 246–255.
- Wallace, D.C., and Fan, W. (2010). Energetics, epigenetics, mitochondrial genetics. *Mitochondrion* 10, 12–31.
- Wang, L., and Dent, S.Y.R. (2014). Functions of SAGA in development and disease. *Epigenomics* 6, 329–339.
- Wu, D., and Cederbaum, A.I. (2003). Alcohol, oxidative stress, and free radical damage. *Alcohol Res. Health* 27, 277–284.
- Zovkic, I.B., Guzman-Karlsson, M.C., and Sweatt, J.D. (2013). Epigenetic regulation of memory formation and maintenance. *Learn. Mem.* 20, 61–74.

## Chapter 4.

# Effects of Neonatal Ethanol Exposure on the Hippocampal Transcriptome

### 4.1 Overview

Gene expression changes are thought to be an important part of FASD etiology. PAE induces apoptosis, and numerous other changes at the cellular level; they are hypothesized to be involved in altered expression of important genes in response to ethanol. Further, small regulatory RNAs such as microRNAs (miRNAs) are believed to regulate the expression many genes in response to ethanol. Pervious work has investigated ethanol-responsive genes in various models of FASD. Prior to this thesis, no study has investigated long-term gene expression changes in the hippocampus in response to PAE. In this chapter, 59 genes and 60 miRNAs were found to be differentially expressed in 70-day-old mouse hippocampus after neonatal ethanol exposure. Gene ontology and pathway analysis found that the genes are enriched for several functions including oxidative stress-response, biosynthetic, and olfaction. Six genes from the top pathway “Free Radical Scavenging, Gene Expression, Dermatological Diseases and Conditions” were confirmed using droplet digital PCR. Several miRNAs identified have FASD-relevant regulatory functions, and many were implicated in pervious work. Gene expression data were also compared with the epigenetic methylation data from Chapters 2 and 3. *Tcf7l2* was the only differentially expressed gene to have changes in H3K4me3, H3K27me3, and DNA methylation. *Tcf7l2* may thus be a strong candidate gene for FASD given its role in oxidative stress amelioration, and the implication of peroxisome genes in the methylation analysis.

### 4.2 Introduction

Assessment of the transcriptome allows for identification of genes which are responsive to a given condition. Eukaryotic protein-coding genes are transcribed from genomic DNA by RNA polymerase II (RNAPII) (Lee and Young, 2000). Transcription is regulated by numerous transcription factors and enhancer proteins that bind specifically to target genes (Lee and Young, 2000). The timing of these events coordinates expression

of target genes to necessary developmental and regulatory timepoints. Dysregulation of gene expression is associated with altered cellular function, and many disease conditions (Emilsson et al., 2008). Beyond single genes, alteration of transcriptome-wide expression patterns are observed in response to a variety of exposures and environmental factors including ethanol (Jaluria et al., 2007). Such studies assess these changes involving the whole transcriptome using microarrays.

Microarrays have become a common tool to assess the expression of a large subset of genes in one experiment. Developed in the 1990's, microarrays provide enormous scale, allowing the entire transcriptome to be assessed simultaneously (Hoheisel, 2006). Microarrays permit hypothesis-free experimental design. The researcher does not need to have any preconceived knowledge of the experimental system or prior candidate genes in mind. Another main advantage of microarray analyses is the emergence of patterns in gene expression profiles (Khatri et al., 2012). The dysregulation of several genes in the same pathway may represent a meaningful biological change. Pathway analysis tools provide further insight into the biological impact of these groups of gene expression changes.

It is often assumed that changes in mRNA expression translate into changes in protein abundance, and thereby affect cellular processes. However, data show only partial correlation between gene and protein expression levels. In mice, a study found a coefficient of determination of  $R^2=0.41$  between mRNA and protein expression levels for over 5000 genes, indicating only a moderate correlation between the two (Schwanhäusser et al., 2011). Many factors between mRNA and protein expression may account for this discrepancy. For instance, mRNAs are far less stable than proteins. Further, mRNAs are translated at a rate of approximately 2 per hour, whereas dozens of copies of the corresponding protein are produced (Schwanhäusser et al., 2011; Vogel and Marcotte, 2012). Such factors also vary greatly between genes. Regardless of their applicability to protein levels, mRNA studies do make definitive statements on the available mRNA pool, and remain a popular tool in molecular biology.



### 4.2.1 Non-Protein-Coding RNAs

MicroRNAs (miRNAs) are short (~26 base pair), non-protein coding RNA molecules that can regulate mRNAs. Like mRNAs, miRNAs are transcribed by RNAPII and have several similarities in their promoter motifs (Zhou et al., 2007). They are transcribed in stem-loop structures termed primary miRNAs (pri-miRNAs). These pri-miRNAs can be found in protein-coding gene 3'UTRs, and can also contain up to six miRNA hairpin precursors (Lee et al., 2004). These are spliced out, and exported from the nucleus. In the cytoplasm, the RNA-induced silencing complex (RISC) processes the double-stranded hairpin precursor into a single-stranded mature miRNA (Rana, 2007). The mature miRNA can then regulate complementary mRNA by two methods: targeting the mRNA for degradation or preventing translation (Rana, 2007). Perfect pairing of the miRNA and mRNA target promotes degradation of the mRNA via endonucleolytic cleavage, whereas a mismatch promotes translational blockage mediated by the Argonaute family of proteins (Gu and Kay, 2010; Valencia-Sanchez et al., 2006). The latter is more common in mammalian cells. A single miRNA can target hundreds of mRNAs, and a single mRNA can be targeted by dozens of miRNAs. There are approximately 2200 miRNA genes in the mammalian genome, and about one third of the human genome is estimated to be regulated by miRNAs (Urbich et al., 2008).

MiRNAs are important regulators of numerous development- and disease-relevant processes. MiRNAs are a key regulator of cellular differentiation due to their ability to influence expression of many genes simultaneously. Specific miRNA profiles have been observed in numerous cancers (Naeini and Ardekani, 2009). Targeting miRNAs has been suggested as a promising therapeutic strategy in cancer treatment (Cheng et al., 2014). MiRNAs are also important in neurological development and disease. Mammalian brains have a higher expression level of miRNAs than most other tissues (Babak et al., 2004). Several miRNAs have key regulatory roles during neurodevelopment, with alteration in their expression causing abnormal brain growth (Sun and Shi, 2015). They are also involved in complex brain functions such as learning and memory. Expression levels of specific miRNAs regulating signalling pathways during long-term potentiation (Wang et al., 2012). Many neurological diseases impact neuroplasticity, and many do so via

alteration in miRNA expression. Drug addiction, schizophrenia, and autism have well characterized associations with miRNA expression changes (Wang et al., 2012).

#### 4.2.2 Gene Expression Changes in FASD are Gene-Specific

Gene expression changes have been studied in several FASD models. Gene expression changes are part of the mechanisms by which ethanol induces neuronal apoptosis (Ikonomidou, 2000). Exposure of embryos to ethanol early in gestation results in dysregulation of cell proliferation, differentiation, and apoptosis related genes (Hard et al., 2005). Ethanol can also cause changes in immune response and inflammation that are present at the transcript level. PAE mice with induced inflammation show distinct expression profiles in the hippocampus, failing to activate genes and regulators involved in the immune response (Lussier et al., 2015). Gene expression changes may also underlie morphological abnormalities in FASD. Cell growth, apoptosis, and histone variant genes were differentially expressed in a study of neural tube deficits following ethanol exposure to embryos in culture (Zhou et al., 2011). Further, expression profiles were specific to a neural tube phenotype, with closed and open tubes associated with neurotrophic/growth factor and histone variant genes respectively (Zhou et al., 2011).

In addition to expression profiles, there have also been studies characterizing the causal relationship between gene expression change and FASD phenotypes. A study found downregulation of sonic hedgehog (*Shh*) in embryonic neural crest cells associated with ethanol exposure in fetal chicks. Sonic hedgehog is responsible for cranio-facial development, with mutations causing severe facial abnormalities (Nanni et al., 1999). Addition of the SHH protein to ethanol-exposed chicks ablated cranio-facial deformities (Ahlgren et al., 2002). In another study, exposure of *Xenopus* embryos to ethanol resulted in malformation of the eye with associated changes in eye development genes (Peng et al., 2004). Reduction of oxidative stress via upregulation of catalase and of cytosolic and mitochondrial peroxiredoxin prevented the gene expression changes and malformations (Peng et al., 2004). In a study using mouse whole-embryo culture, many developmental morphology parameters (including hindbrain, midbrain, forebrain, and optic systems) were reduced in size by ethanol exposure. Treatment with capsaicin ameliorated most of

these morphogenic changes, likely via the increased antioxidant mRNA expression levels (Kim et al., 2008).

MiRNA expression changes have also been associated with FASD. As in other neurological disorders, miRNAs differentially expressed in FASD disproportionately affect neurological development and function. Suppression of specific miRNAs in fetal neural stem cells (NSCs) and neural progenitor cells (NPCs) accounted for their resistance to apoptosis (Sathyan et al., 2007). Other studies have found miRNAs associated with cranial abnormalities (Sathyan et al., 2007). From these studies, it is clear that gene and miRNA expression changes can underlie the phenotypic effects of PAE.

### 4.2.3 Gene Expression Changes in FASD are Pathway- and Network-Specific

Pathway and network analysis are key tools for understanding how groups of affected genes may interact to affect a phenotype. Gene lists generated from microarray and sequencing experiments provide candidate genes for the phenotype. However, these lists do not provide mechanistic insight into the underlying biology. Reducing the gene list to smaller sets based on pathways reduces complexity. These pathways often provide more explanatory power than a single differentially expressed gene list (Khatri et al., 2012). Many of these tools use over representation analysis (also known as enrichment analysis). Hundreds of biological pathways are assessed for the percentage of their component genes that are differentially expressed in the researcher experiment (Khatri et al., 2012). Using a Fisher's exact test, the software determines the statistical significance of the overlap with each pathway. Partek pathway uses the well annotated list of Kyoto Encyclopedia of Genes and Genomes (KEGG) pathways. Ingenuity pathway analysis (IPA) uses a proprietary network database based on curated literature searches. Gene ontology analysis uses the same principle to assess enrichment of gene functions.

### 4.2.4 Previous Results from the Singh Laboratory in FASD Models

Previously, the Singh laboratory characterized gene expression changes in several FASD models. We have sought to identify genes responsive to PAE across various exposure regimes, developmental endpoints, and after mitigating or exacerbating factors.

Using the continuous preference drinking (CPD) model, significant gene networks were cellular and tissue development, free radical scavenging, lipid metabolism, and nervous system development in PND 70 mouse brain (Kleiber et al., 2012). This study identified relatively few (less than 20) differentially expressed genes with greater than a 1.2 fold change ( $p < 0.05$ ). In another study in this model, we assessed miRNA expression changes in addition to gene expression changes. There was an enrichment of miRNAs with roles in neuronal development and function, as well as an enrichment (20%) of miRNAs which targeted imprinted regions (Laufer et al., 2013).

In the trimester one model of exposure, PND 60 mice showed dysregulation of genes involved in apoptosis, cell-cell signalling, and neurological disease (Mantha et al., 2013). In the trimester two exposure model, short- (GD 16) and long-term (PND 70) gene expression changes in the whole-brain were assessed (Mantha et al., 2013). These genes were enriched for apoptosis, free-radical scavenging, lipid metabolism, and neurological functions (Mantha et al., 2014). There were also 20 miRNAs differentially expressed in the PND 70 mice.

In the trimester three PND 4,7 injection model, short (PND 7) and long (PND 60) gene expression changes in the whole-brain have been assessed. The short term mice showed dysregulation of apoptosis, lipid metabolism, and neurogenesis genes (Kleiber et al., 2014a). In adult mice, genes involved in glutamate signalling, neurological diseases, and cell-cell signalling were differentially expressed (Mantha et al., 2013). There were also 33 differentially expressed miRNAs at PND 60. Together, these previous whole-brain studies have consistently implicated free radical scavenging, lipid metabolism, and brain development and function genes as well as several miRNAs.

#### 4.2.5 Gene Expression Changes in the Hippocampus

The previous work from our laboratory used mouse whole-brain for gene expression microarray analysis. Gene expression patterns differ within the brain; approximately 50% of expressed genes are differently expressed between brain regions in mice and humans (Strand et al., 2007). Pooling all brain regions together will lose this heterogeneity. Changes in specific brain regions may also be washed out by expression in other regions. Furthermore, individual brain regions are associated with specific FASD-

relevant behaviours, while the whole-brain is not associated with any single behaviour. For these reasons, this thesis examined a specific brain region, the hippocampus. The hippocampus is particularly vulnerable to the pro-apoptotic effects of ethanol (Ikonomidou, 2000). It is involved in the formation of new memories and visual/spatial memory (Cho et al., 1999; Morris et al., 1982; Squire, 2009). Mice exposed to ethanol on PND 7 also show spatial learning and memory impairment, similar to mice with hippocampal lesions (Cho et al., 1999; Mantha et al., 2013). Children with FAS show similar spatial deficits (Hamilton et al., 2003; Uecker and Nadel, 1996, 1998). Changes in gene expression are associated with learning impairment in response to PAE (Subbanna and Basavarajappa, 2014). In this chapter, gene and miRNA expression changes in the hippocampus of PND 70 mice exposed to ethanol on PND 4 & 7 are assessed.

## Objectives

1. To assess expression of all mouse protein coding genes and miRNAs in PND 70 mouse hippocampus exposed to ethanol on postnatal days 4 and 7.
2. To identify the ontology and pathway enrichment of differentially expressed genes.
3. To confirm specific changes with qPCR/ddPCR.

## 4.3 Materials and Methods

### 4.3.1 Mouse Care

For the full mouse care protocol, see Chapter 2 Materials and Methods. In brief, all protocols were approved by the Animal Use Subcommittee (AUS) at the University of Western Ontario, London, Ontario, Canada. The day of birth was termed PND zero. Sex and weight-matched littermate pups were divided into two groups: ethanol-treated and saline-injected control mice. Pups were given two subcutaneous dorsal injections on both PND 4 and PND 7. Ethanol-treated mice were injected with 2.5 g/kg of ethanol in 0.15 M NaCl (Ikonomidou et al., 2000). Control mice were injected with 0.15 M saline only. Male mice were used for all subsequent analyses. The mice used in this chapter included the same mice used for the DNA methylation analysis in Chapter 3 (n=9 control and n=9 ethanol-exposed mice; see **Table 2.1**). Mice were sacrificed on PND 70 via carbon dioxide asphyxiation. The hippocampus was dissected out (Spijker, 2011), snap-frozen in liquid nitrogen, and stored at -80°C for no longer than 30 days until formaldehyde fixation.

### 4.3.2 DNA/RNA Isolation

DNA and RNA were isolated with AllPrep DNA/RNA Mini Kit (Qiagen, Valencia, CA, USA) according to the manufacturer's protocol. This kit allows DNA and RNA to be isolated from the same hippocampal sample. DNA and RNA were stored at -20°C and -80°C respectively.

### 4.3.3 Gene and miRNA Expression Microarray

Nine ethanol-exposed and nine control hippocampus samples were used for expression analysis. RNA quality was assessed using the Agilent 2100 Bioanalyzer (Agilent Technologies Inc., Palo Alto, CA) and the RNA 6000 Nano kit (Caliper Life Sciences, Mountain View, CA). RNA from three non-littermate males was then pooled for microarray analysis on three separate arrays per treatment group.

All sample labeling and GeneChip processing was performed at the London Regional Genomics Centre (Robarts Research Institute, London, Ontario, Canada;

<http://www.lrgc.ca>). RNA quality was assessed using the Agilent 2100 Bioanalyzer (Agilent Technologies Inc., Palo Alto, CA) and the RNA 6000 Nano kit (Caliper Life Sciences, Mountain View, CA). Single-stranded complimentary DNA (sscDNA) was prepared from 200 ng of total RNA as per the Ambion WT Expression Kit for Affymetrix GeneChip Whole Transcript WT Expression Arrays ([http://www.ambion.com/techlib/prot/fm\\_4411973.pdf](http://www.ambion.com/techlib/prot/fm_4411973.pdf), Applied Biosystems, Carlsbad, CA) and the Affymetrix GeneChip WT Terminal Labeling kit and Hybridization User Manual ([http://media.affymetrix.com/support/downloads/manuals/wt\\_term\\_label\\_ambion\\_user\\_manual.pdf](http://media.affymetrix.com/support/downloads/manuals/wt_term_label_ambion_user_manual.pdf), Affymetrix, Santa Clara, CA).

Total RNA was first converted to cDNA, followed by *in vitro* transcription to make cRNA. 5.5 µg of single stranded cDNA was synthesized, end labeled and hybridized, for 16 hours at 45°C, to Mouse Gene 1.0 ST arrays (Affymetrix, Santa Clara, CA). One microgram of total RNA was labeled using the Flash Tag Biotin HSR kit from Genisphere ([http://www.genisphere.com/array\\_detection\\_flashtag\\_biotin.html](http://www.genisphere.com/array_detection_flashtag_biotin.html)). Samples were then hybridized to Affymetrix miRNA 2.0 arrays for 16 hours at 48°C. All washing steps were performed by a GeneChip Fluidics Station 450 and GeneChips were scanned with the GeneChip Scanner 3000 7G (Affymetrix, Santa Clara, CA) using Command Console v1.1.

Probe level (.CEL file) data was generated using Affymetrix Command Console v1.1. Probes were summarized at the miRNA and gene level using RMA (Irizarry et al., 2003). Partek was used to determine ANOVA *p*-values and fold changes for genes and miRNAs. Species annotations were added and used to filter miRNAs. Partek Pathway and Ingenuity pathway analysis (IPA) were used to determine and visualize significantly enriched pathways (using a Fisher's exact test). Gene list was also uploaded to Enrichr (Chen et al., 2013) for Gene Ontology (GO) analysis. .CEL files and log2 normalized files were uploaded to GEO. An FDR *q*-value < 0.05 was used to determine multiple testing error; no transcripts survived this threshold.

#### 4.3.4 Gene-Specific Confirmations

Purified RNA was converted to cDNA using the High-Capacity cDNA Reverse Transcription Kit (Thermo-Fisher). cDNA was diluted 10-fold and stored at -20°C until

use. Individual genes were investigated with TaqMan<sup>®</sup> assays (Applied Biosystems), assays IDs: *Vipr2*: Mm01238618\_g1; *Synpo2*: Mm03809162\_m1; *Tcf7l2*: Mm00501505\_m1; *Casp3*: Mm01195085\_m1, *Krt8*: Mm04209403\_g1; *L3mbtl4*: Mm00623914\_m1, *Stac*: Mm00450338\_m1, *Mafg*: Mm00521961\_g1, *Tmem79*: Mm00470361\_m1, *Defb4*: Mm00731768\_m1. For all assays, TATA binding protein (TBP) was used as a reference gene: Mm01277042\_m1. Individual (i.e. not pooled) ethanol-exposed (n=7) and control (n=7) samples from the gene expression microarray were used for these analyses. Four samples from the microarray experiment (E17.1, C17.2, E19.7, C19.8) could not be included as they had insufficient RNA remaining for cDNA synthesis.

#### 4.3.4.1 Real-Time PCR

For each assay, the gene of interest and *Tbp* reference gene were run in multiplex using FAM and VIC labeling respectively. Reactions were prepared using TaqMan<sup>®</sup> Gene Expression Master Mix (Applied Biosystems). Each sample was run in three technical replicates. The probe/primer pairs for each gene of interest were multiplexed with TBP primer/probe; 10  $\mu$ l reactions were used. Gene expression levels were quantified using the comparative delta  $C_t$ , or delta delta  $C_t$  ( $\Delta\Delta C_t$ ) method, where  $C_t$  refers to critical threshold when the amplification signal rises above background levels.  $\Delta\Delta C_t$ , relative quantity, and fold change were calculated by the StepOne software. DataAssist software (Applied Biosystems) was used for statistical analysis, in which average  $\Delta\Delta C_t$  values for each technical replicate were averaged (after removing any outliers), and treatment groups were compared using a Paired Samples t-Test with littermates paired.

#### 4.3.4.2 Droplet Digital PCR

For each assay, the gene of interest and TBP reference gene were run in multiplex using FAM and VIC labeling respectively. Reactions were prepared using ddPCR<sup>™</sup> Supermix for Probes (BioRad), cDNA, and probes according to the manufacturer's protocol. Droplets were generated from the reactions using Droplet Generation Oil for Probes (BioRad) on the QX100 Droplet Generator (BioRad) according to the



manufacturer's protocol. Droplets were cycled on the C1000 Touch Thermal Cycler (BioRad) for 40 cycles, 60°C annealing temperature, 2°C/sec ramp speed. Droplets were read using the QX100 Droplet Reader (BioRad). Data were analyzed in QuantaSoft software (BioRad). All samples had between 17000-20000 droplets indicating high-quality. The concentration of each RNA species and ratio of gene of interest/reference gene concentration were calculated using QuantaSoft for each sample. Each DNA sample was run in three technical replicates, the average ratio across technical replicates for each sample was calculated manually. Each cDNA sample's average ratio was used to compare ethanol-exposed to control samples using a paired sample Paired Samples t-Test with littermates paired. Averages were normalized to 1.00 relative expression level for control group.

## 4.4 Results

### 4.4.1 Differentially Expressed Genes

To describe which transcripts were significantly differentially expressed in the PND 70 mouse hippocampus following PND 4,7 ethanol exposure, a fold-change cut-off of  $>1.2$  or  $<-1.2$  as well as an ANOVA  $p$ -value  $<0.05$  were used to determine statistical significance. These cut-offs are relatively standard in PAE research in the Singh laboratory and others; they are intended to be permissive enough to capture the subtle effects of ethanol without excessive false positives. There were 317 transcripts meeting these criteria, which were visualized using a heat map (**Figure 4.1**). The distance tree shows that the control and ethanol-exposed groups cluster together. The relative expression level for each transcript was quite consistent across the three biological replicates, indicating a consistent effect of ethanol on the abundance of each (**Figure 4.1**). Of these differentially expressed transcripts, there were 59 annotated genes differentially expressed at a fold cut off  $>1.2$  and  $p < 0.05$  (**Table 4.1**). Two thirds of these were upregulated, and one third down-regulated in response to ethanol. The largest increase in expression was 1.5 fold and the largest decrease was -1.39 fold.

### 4.4.2 Ontology of Differentially Expressed Genes

Known and predicted interactions between proteins encoded by differentially expressed genes were assessed using GeneMania. The resulting network illustrates that there were relatively few known functional relationships between these genes. The most common relationships were co-expression or co-localization (**Figure 4.2**). Gene ontology (GO) analysis was performed to categorize differentially expressed genes, and assess their biological impact. The list of 59 differentially expressed genes (fold cut-off  $>1.5$ ,  $p < 0.05$ ) was used for GO analysis using Enrichr (Chen et al., 2013). The top affected biological processes include various biosynthetic processes such as dicarboxylic acid, kynurenine, and tryptophan metabolism (**Table 4.2**). “Intrinsic apoptotic signaling pathway in response to oxidative stress” was also implicated, which is particularly relevant to FASD. The top affected cellular components include various structural components such as Z-disc, contractile fiber, and plasma membrane (**Table 4.2**). The top

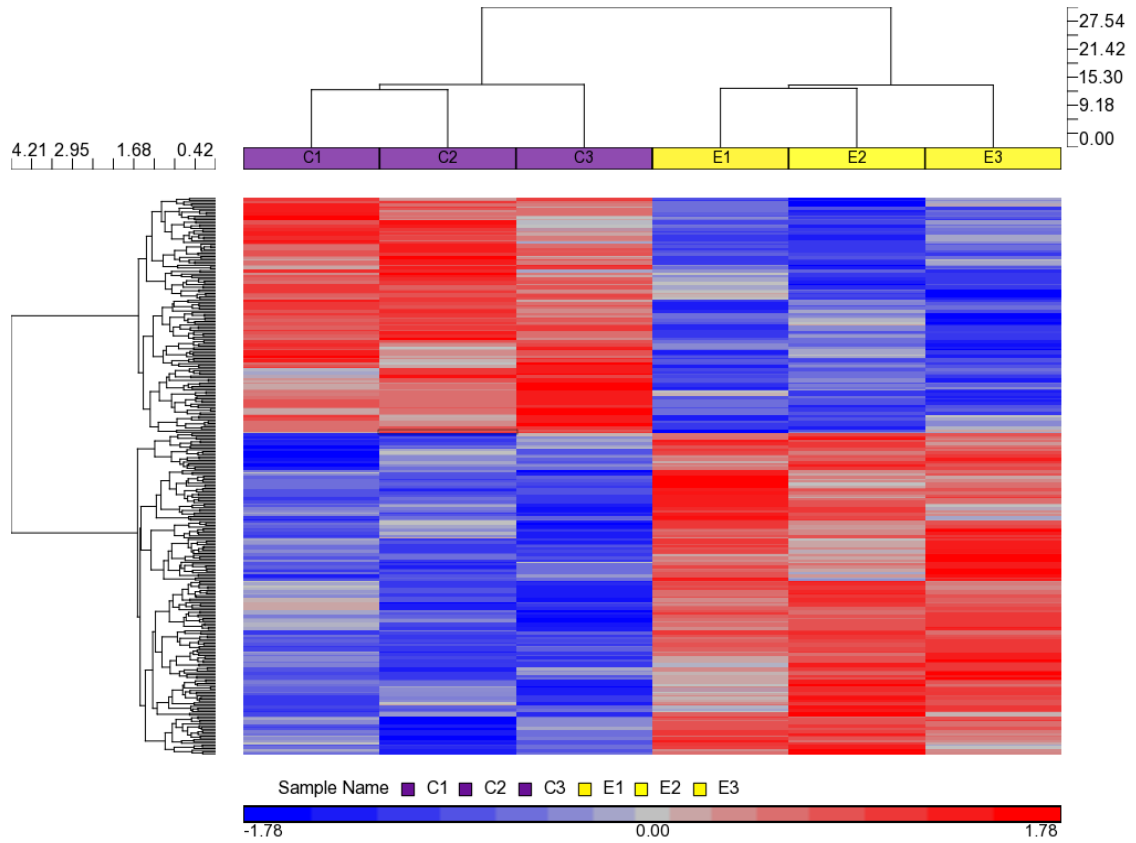


**Figure 4.1 Hierarchical clustering of expression patterns from individual microarrays.**

Differentially expressed transcripts with fold changes  $>1.2$  and  $p < 0.05$  are shown.

Distance trees show similarities in expression patterns among genes and among experimental groups. Consistency of expression changes across biological replicates is evident for each gene by the consistency of the fold (colour) change.

**Table 4.1 Differentially expressed genes in response to neonatal ethanol exposure in the adult mouse hippocampus<sup>†</sup>.**

<b>Gene Symbol</b>	<b><i>p</i>-value</b>	<b>Fold</b>
<i>Tcf7l2</i>	0.032	1.50
<i>Synpo2</i>	0.047	1.43
<i>Vipr2</i>	0.043	1.42
<i>Cypt2</i>	0.012	1.40
<i>Defb5</i>	0.002	1.39
<i>Serpinb1b</i>	0.027	1.35
<i>Gm8994</i>	0.021	1.32
<i>Gm7168</i>	0.016	1.31
<i>Olfr119</i>	0.007	1.30
<i>Vmn2r15</i>	0.049	1.29
<i>Cfhr2</i>	0.023	1.29
<i>LOC10003842</i>	0.025	1.28
<i>Nup210l</i>	0.037	1.27
<i>Kmo</i>	0.024	1.27
<i>Tmprss11a</i>	0.049	1.26
<i>BC094916</i>	0.036	1.26
<i>Krt8</i>	0.013	1.25
<i>Olfr539</i>	0.035	1.25
<i>Slitrk6</i>	0.023	1.24
<i>Cd209f</i>	0.031	1.24
<i>Krt39</i>	0.008	1.23
<i>Olfr121</i>	0.026	1.23
<i>Gm11362</i>	0.041	1.23
<i>Hcn4</i>	0.048	1.23
<i>Olfr1018</i>	0.022	1.23
<i>Cdnf</i>	0.044	1.23
<i>Casp3</i>	0.021	1.23
<i>4933416I08Rik</i>	0.049	1.22
<i>Vmn2r109</i>	0.022	1.22
<i>Stac</i>	0.029	1.22
<i>Vmn1r5</i>	0.042	1.21
<i>Dnm3os</i>	0.050	1.21
<i>Olfr648</i>	0.003	1.21
<i>Olfr1131</i>	0.026	1.21
<i>4930524N10Ri</i>	0.006	1.21
<i>Gm4801</i>	0.011	1.21
<i>Mrgprh</i>	0.007	1.21
<i>Gm11437</i>	0.026	1.20
<i>Apol7a</i>	0.010	1.20

<i>C330022B21Ri</i>	0.020	-1.20
<i>1600015I10Rik</i>	0.005	-1.20
<i>Gm4776</i>	0.024	-1.20
<i>Olf455</i>	0.011	-1.20
<i>Olf979</i>	0.007	-1.21
<i>Mafg</i>	0.036	-1.21
<i>Olf2</i>	0.022	-1.21
<i>Gm16551</i>	0.006	-1.22
<i>4930401B11Ri</i>	0.047	-1.22
<i>L3mbtl4</i>	0.040	-1.22
<i>D4Wsu53e</i>	0.005	-1.22
<i>Olf281</i>	0.013	-1.24
<i>D730002M21R</i>	0.045	-1.25
<i>BC055004</i>	0.039	-1.25
<i>Hdx</i>	0.015	-1.25
<i>Olf1350</i>	0.002	-1.26
<i>Crygb</i>	0.011	-1.27
<i>Tmem79</i>	0.027	-1.29
<i>Zfa</i>	0.023	-1.31
<i>Dnahc7a</i>	0.023	-1.39

†n=3 ethanol-exposed and n=3 control microarrays. *p*-values determined using a one-way ANOVA, fold change in expression vs. control group determined using Partek RMA algorithm. Genes presented passed a fold cut off >1.2 and *p*<0.05.

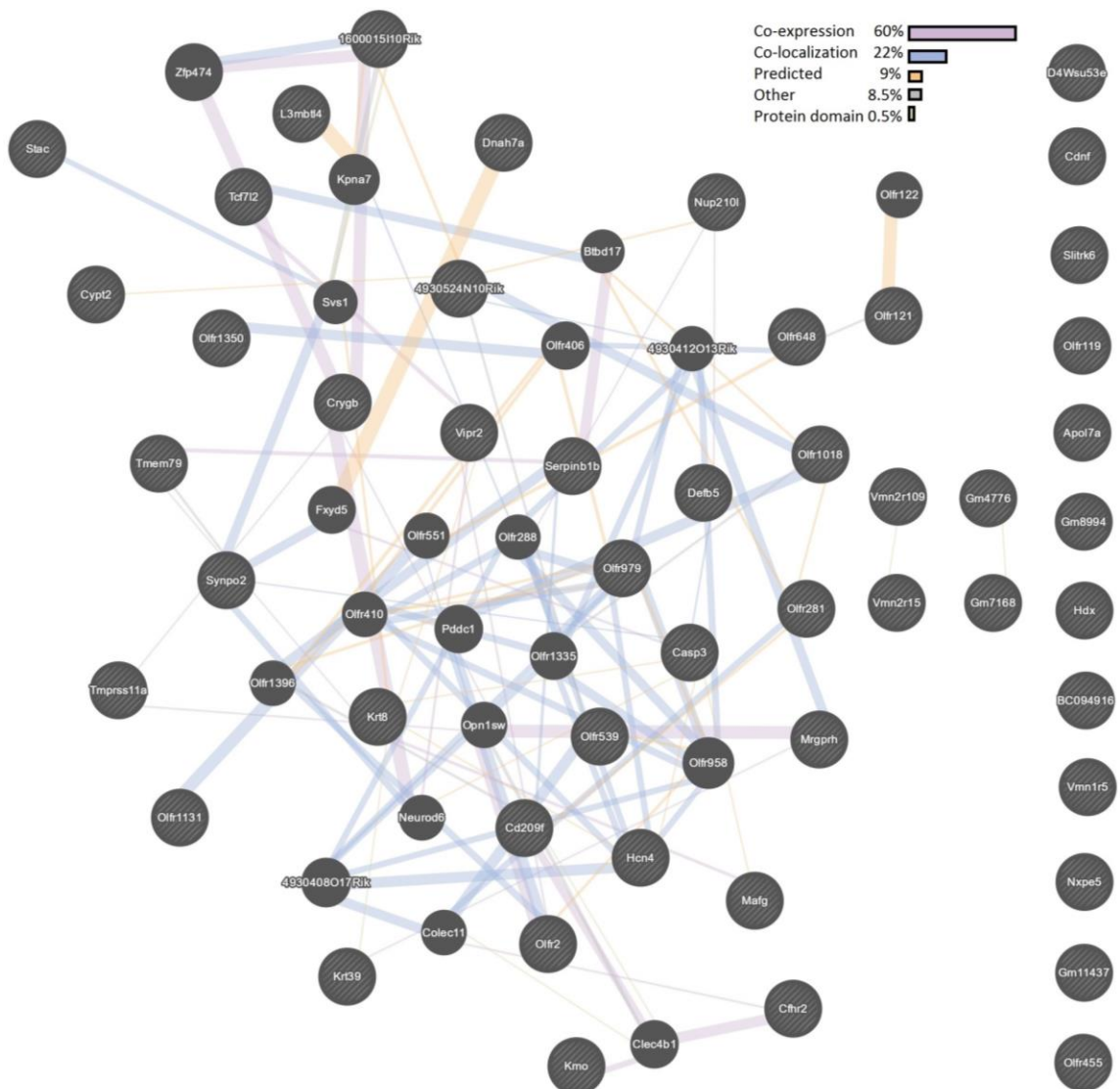


**Figure 4.2 Interaction network of published interactions between differentially expressed genes.**

Gene node increases with increased connections, line width decreases with number of connections from its node. *Co-expression* indicates expression levels are similar across conditions in a published gene expression study. *Co-localization* indicates genes expressed in the same tissue, or proteins found in the same cellular location. *Predicted* indicates a predicated functional relationship between genes, often protein interactions, based on data from other organisms. Examples of *Other* include phenotype correlations from Ensembl or disease information from OMIM. *Protein domain* indicates the same protein domain in each gene.

**Table 4.2 Gene ontology (GO) analysis of differentially expressed genes<sup>†</sup>.**

<b>GO term</b>	<b>p-value</b>
<b>GO biological processes</b>	
Dicarboxylic acid biosynthetic process (GO:0043650)	0.010
Kynurenine metabolic process (GO:0070189)	0.010
Genitalia morphogenesis (GO:0035112)	0.011
Positive regulation of triglyceride biosynthetic process (GO:0010867)	0.011
Positive regulation of glycoprotein biosynthetic process (GO:0010560)	0.012
Positive regulation of gluconeogenesis (GO:0045722)	0.013
Response to auditory stimulus (GO:0010996)	0.013
Tryptophan metabolic process (GO:0006568)	0.013
Positive regulation of protein export from nucleus (GO:0046827)	0.013
Intrinsic apoptotic signaling pathway in response to oxidative stress (GO:0008631)	0.017
<b>GO cellular component</b>	
Z disc (GO:0030018)	0.004
Contractile fiber part (GO:0044449)	0.015
Dystrophin-associated glycoprotein complex (GO:0016010)	0.020
Intermediate filament (GO:0005882)	0.021
Costamere (GO:0043034)	0.025
Integral component of plasma membrane (GO:0005887)	0.028
Intrinsic component of plasma membrane (GO:0031226)	0.038
<b>GO molecular function</b>	
Intracellular cAMP activated cation channel activity (GO:0005222)	0.008
Muscle alpha-actinin binding (GO:0051371)	0.009
armadillo repeat domain binding (GO:0070016)	0.009
Cyclic nucleotide-gated ion channel activity (GO:0043855)	0.010
Intracellular cyclic nucleotide activated cation channel activity (GO:0005221)	0.010
Gamma-catenin binding (GO:0045295)	0.011
Cyclin-dependent protein serine/threonine kinase inhibitor activity (GO:0004861)	0.011
Oxidoreductase activity, acting on NAD(P)H, oxygen as acceptor (GO:0050664)	0.014
14-3-3 protein binding (GO:0071889)	0.016
Structural constituent of eye lens (GO:0005212)	0.018

<sup>†</sup>Top 10 GO processes are shown where number of entries exceeds 20.

affected cellular components included various nucleotide-gated ion channels, as well as structural components and oxidoreductase activity (**Table 4.2**).

#### 4.4.3 Pathways Affected by Differentially Expressed Genes.

The list of differentially expressed genes was also submitted to three separate pathway suites: Ingenuity Pathway Analysis (IPA), Partek Pathway, and Enrichr (**Table 4.3**). The genes *Casp3* and *Tcf7l2* are responsible for implicating many of the genes in these pathways; one or both are present in >90% of the identified pathways. *Casp3* encodes Caspase-3 which is involved in apoptosis, *Tcf7l2* encodes a transcription factor involved in Wnt signalling (D'Amelio et al., 2012). These two genes were also responsible for implicating pathways related to cancer and development across each software platform (**Table 4.3**). The top IPA pathway was “Free radical scavenging, gene expression, dermatological diseases and conditions” which also contained *Tcf7l2* and *Casp3* (**Figure 4.3**). The top Partek pathway was “Olfactory transduction”, implicated by 10 olfactory receptor genes (**Table 4.3**).

#### 4.4.4 Gene-Specific Confirmations

Five differentially expressed genes from the top IPA pathway (**Figure 4.3**) were selected for confirmation via real-time polymerase chain reaction (qPCR). *Casp3*, *Mafg*, *Stac*, *Tcf7l2*, and *Vipr2* qPCR confirmations were attempted (**Table 4.4**). Though *Vipr2* and *Tcf7l2* approached statistical significance, none of these genes were confirmed to be differentially expressed in ethanol-exposed mice. Since several genes approached significance, droplet digital PCR (ddPCR) was employed for each gene using the same cDNA samples. *Casp3*, *Tcf7l2*, and *Vipr2* were confirmed using ddPCR (**Table 4.4; Figure 4.4**). *Mafg* and *Stac* were non-significant (**Table 4.4; Figure 4.4**). Given this success, ddPCR was employed for four more genes, two from the top IPA pathway (*Tmem79* and *Krt8*), one with a targeting miRNA (*L3mbl4*), and one with relevance to brain function (*Synpo2*). *Synpo2* and *L3mbl4* were confirmed, while *Tmem79* and *Krt8* were not (**Table 4.4**).



**Table 4.3 Pathways significantly enriched with differentially expressed genes.**

<b>Pathway name</b>	<b>Affected genes</b>	<b>p-value</b>
<b>IPA network/pathway</b>		
Free Radical Scavenging, Gene Expression, Dermatological Diseases and Conditions	<i>Apol7a, Defb4, Dnah7, Hdx, Ifi204, Kmo, Krt8, Mafg Tcf7l2, Tmem79, Stac, Vipr2</i>	10E-31
Cellular Development, Developmental Disorder, Hereditary Disorder	<i>Casp3, Tcf7l2</i>	0.001
Molecular Transport, RNA Trafficking, Cell Death and Survival	<i>Casp3, Kmo</i>	0.001
Cell Cycle, Nervous System Development and Function, Cell Signaling	<i>Casp3, Tcf7l2</i>	0.001
Cardiovascular System Development and Function, Skeletal and Muscular System Development and Function, Cell-To-Cell Signaling and Interaction	<i>Casp3, Hcn4</i>	0.01
<b>Partek pathway</b>		
Olfactory Transduction	<i>Olfr2, Olfr121, Olfr281, Olfr455, Olfr539, Olfr648, Olfr979, Olfr1018, Olfr1131, Olfr1350</i>	0.001
Colorectal Cancer	<i>Casp3, Tcf7l2</i>	0.012
Amoebiasis	<i>Casp3, Serpinb1b</i>	0.03
<b>Enrichr KEGG</b>		
Colorectal cancer	<i>Casp3, Tcf7l2</i>	0.0012
cAMP signaling pathway	<i>Hcn44, Vipr2</i>	0.011
Thyroid cancer	<i>Tcf7l2</i>	0.025
Tryptophan metabolism	<i>Kmo</i>	0.034
Pathways in cancer	<i>Casp3, Tcf7l2</i>	0.041
Amyotrophic lateral sclerosis (ALS)	<i>Casp3</i>	0.043
Endometrial cancer	<i>Tcf7l2</i>	0.044
Legionellosis	<i>Casp3</i>	0.047
Basal cell carcinoma	<i>Tcf7l2</i>	0.047

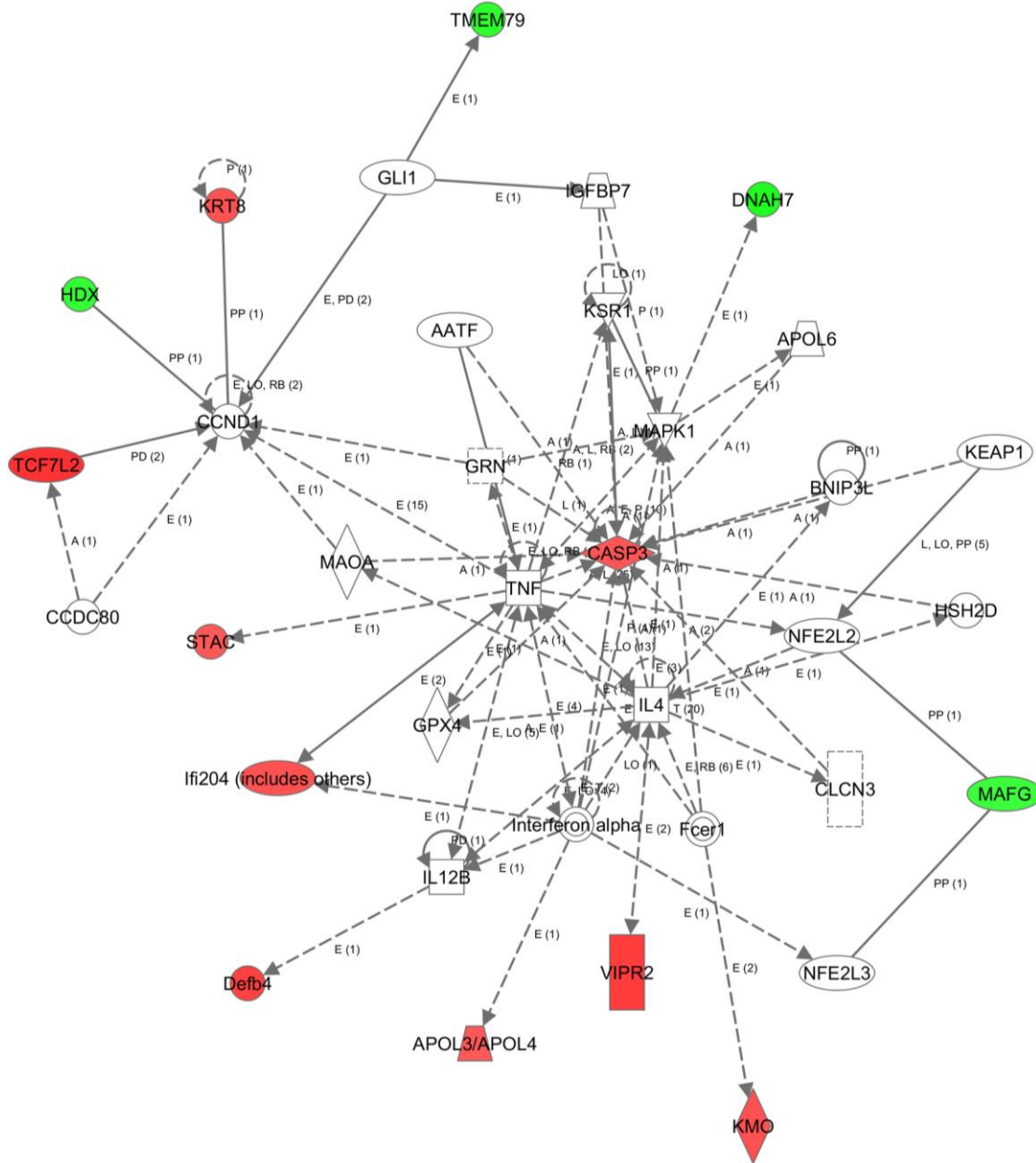


**Figure 4.3 Top IPA network for gene expression changes “Free Radical Scavenging, Gene expression, Dermatological Diseases and Conditions”.**

Red nodes represent proteins whose transcripts were increased in ethanol-exposed mice vs. controls, green nodes represent those that were decreased in ethanol exposed mice. Score determined in IPA was 31 (right-tailed Fisher’s Exact Test). For legend, see **Appendix B).**

**Table 4.4 mRNA abundance from real-time PCR (qPCR) compared to droplet digital PCR (ddPCR)<sup>†</sup>.**

<b>Gene</b>	<b>Microarray</b>		<b>qPCR</b>		<b>ddPCR</b>	
	<i>Fold change</i>	<i>p-value</i>	<i>Fold change</i>	<i>p-value</i>	<i>Fold change</i>	<i>p-value</i>
<i>Casp3</i>	1.23	0.021	-1.07	0.20	2.52	0.040
<i>Mafg</i>	-1.21	0.036	1.08	0.17	1.03	0.30
<i>Stac</i>	1.22	0.029	-1.04	0.43	-1.15	0.18
<i>Tcf7l2</i>	1.50	0.032	1.99	0.08	2.18	0.045
<i>Vipr2</i>	1.42	0.043	3.94	0.07	2.80	0.023

<sup>†</sup>Data presented are fold change in ethanol-exposed vs. control groups. Microarray fold change and *p*-values were determined in Partek. qPCR and ddPCR data are presented as the mean of n=7 biological replicates per group, *p*-values determined by Paired Samples t-Test. Shaded cells denote a *p*-value<0.05.

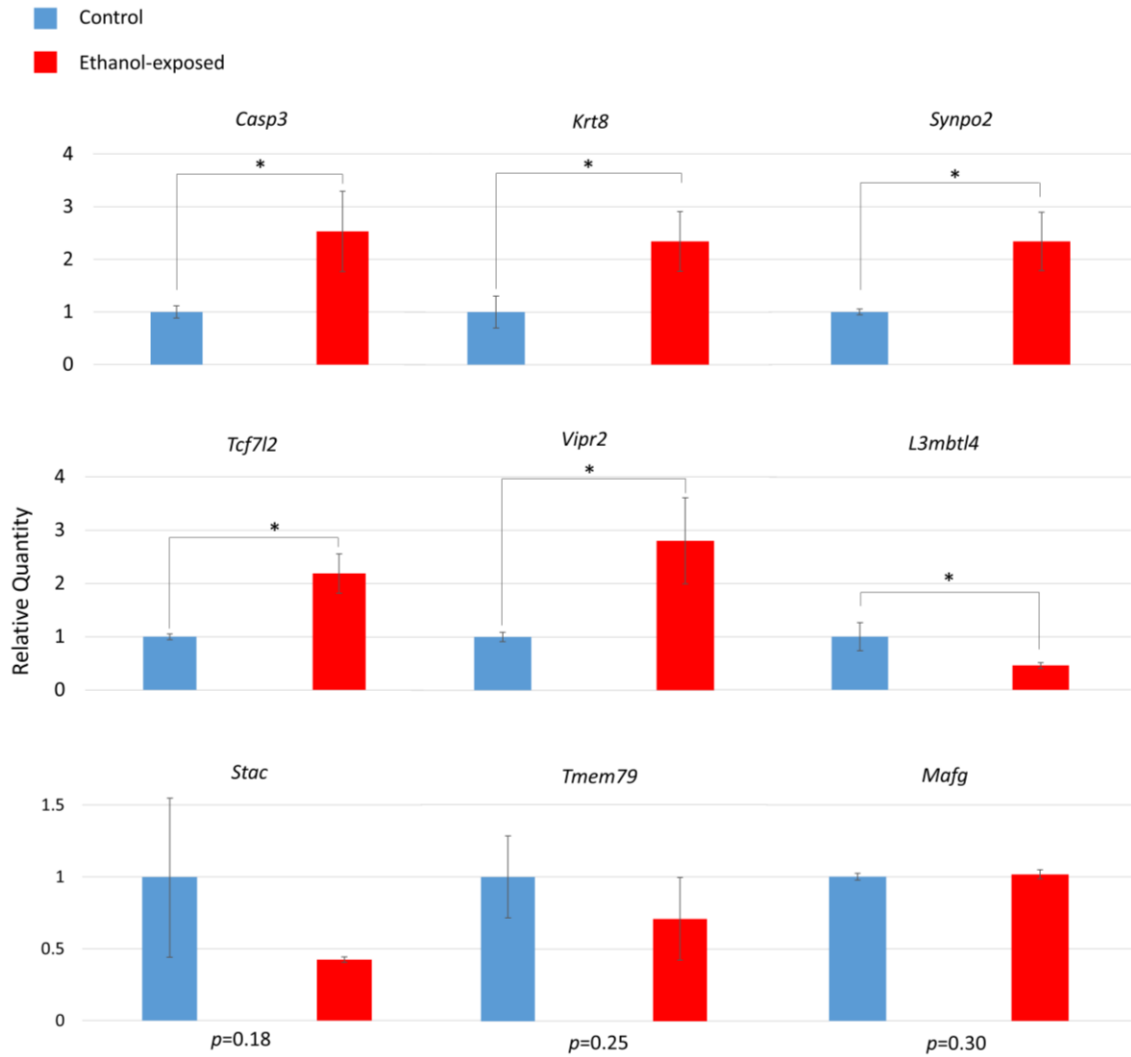


**Figure 4.4 Droplet digital PCR (ddPCR) confirmations of differential gene expression.**

n=14, 7 ethanol-exposed and 7 control mice. Data are presented as relative quantity normalized to control expression level, mean  $\pm$  standard error. \* $p < 0.05$  (Paired Samples t-Test). Not shown is *Defb4* which was undetected in the samples.

The expression patterns of the six confirmed genes in the PND 70 mouse hippocampus were assessed using data from the Allen Brain Atlas (Sunkin et al., 2013). *Casp3* showed high expression in dentate granule neurons and hippocampal pyramidal neurons. The other five genes did not show discernable expression patterns in the hippocampus.

#### 4.4.5 Differentially Expressed MicroRNAs

In addition to the mRNA expression microarray, a microRNA (miRNA) expression microarray was also performed. It identified 60 differentially expressed miRNAs at  $p < 0.05$ , fold cut-off  $> 1.2$  (**Table 4.5**). Most (89%) were increased in expression in ethanol-exposed mice. There were greater fold-change magnitude values compared to mRNAs; ranging from 2.59 to -2.01 fold. Next, interactions between miRNAs and mRNAs were assessed. Using IPA Target Filer™ analysis, miRNAs predicted to target differentially expressed genes were identified (**Table 4.6**). Four genes (*Hcn4*, *Mafg*, *L3mbtl4*, and *Tmem79*) targeted by five miRNAs were identified with reciprocal changes in fold-change. (**Table 4.6**). Other interactions where a miRNA and a predicted target mRNA had the same direction of change were identified; however, they were shown due to unlikely functional relevance.

#### 4.4.6 Epigenetic Changes at Differentially Expressed Genes

The differentially expressed genes from Chapter 2 were compared with the differentially methylated genes from the DNA and histone methylation lists. There was very little overlap between the lists using the genes generated for pathway analysis (i.e.  $p < 0.001$  for the DNA and histone methylation lists; **Figure 4.5**). Only one gene overlapped between the H3K4me3 RDHM list and gene expression list which is significantly less overlap than expected by chance ( $X^2 = 55.6$ ,  $p < 0.00001$ ). The gene was *Tcf7l2* which encodes a transcription factor involving in Wnt signaling. It was part of the top IPA pathway identified in the gene expression analysis and was confirmed with ddPCR. It is also the top differentially expressed gene in terms of fold-change magnitude. In order to identify more potentially biologically relevant relationships between gene expression and epigenetic changes, the expression and methylation datasets were also

**Table 4.5 MicroRNAs and pre-microRNAs identified as differentially expressed from microarray analysis<sup>†</sup>.**

<b>Probe Set ID</b>	<b><i>p</i>-value</b>	<b>Fold change</b>
<i>miR-1935</i>	0.0315	2.59
<i>miR-1946a</i>	0.0160	2.36
<i>miR-184</i>	0.0185	2.35
<i>miR-1306</i>	0.0496	2.28
<i>miR-207</i>	0.0294	2.19
<i>miR-130b</i>	0.0180	2.19
<i>miR-1983</i>	0.0284	2.16
<i>miR-669n</i>	0.0327	2.10
<i>miR-1946b</i>	0.0174	2.07
<i>miR-200c</i>	0.0221	1.95
<i>miR-26a-1</i>	0.0127	1.80
<i>miR-695</i>	0.0146	1.75
<i>miR-188-5p</i>	0.0487	1.70
<i>miR-1894-3p</i>	0.0343	1.67
<i>mir-302b</i>	0.0174	1.65
<i>miR-125b</i>	0.0281	1.64
<i>miR-425</i>	0.0034	1.63
<i>miR-105_st</i>	0.0177	1.60
<i>miR-678_st</i>	0.0264	1.57
<i>miR-671-5p</i>	0.0133	1.52
<i>miR-505</i>	0.0127	1.48
<i>miR-452</i>	0.0058	1.48
<i>miR-511</i>	0.0002	1.46
<i>miR-1937</i>	0.0036	1.43
<i>miR-1962</i>	0.0026	1.43
<i>miR-106b</i>	0.0489	1.43
<i>miR-2136</i>	0.0265	1.41
<i>miR-484</i>	0.0468	1.39
<i>miR-18a</i>	0.0283	1.39
<i>miR-105</i>	0.0069	1.39
<i>miR-490</i>	0.0368	1.38
<i>miR-214</i>	0.0477	1.37
<i>miR-2135-4</i>	0.0241	1.37
<i>miR-466b-1</i>	0.0238	1.35
<i>miR-295</i>	0.0481	1.32
<i>miR-698</i>	0.0403	1.30
<i>miR-377</i>	0.0185	1.29
<i>miR-29b-1</i>	0.0292	1.28

<i>miR-540</i>	0.0455	1.28
<i>miR-700</i>	0.0258	1.26
<i>miR-505</i>	0.0226	1.25
<i>miR-187</i>	0.0366	1.24
<i>miR-704</i>	0.0043	1.24
<i>miR-709</i>	0.0463	1.23
<i>miR-297a-6</i>	0.0428	1.23
<i>miR-3473</i>	0.0157	1.22
<i>miR-1944</i>	0.0319	1.22
<i>miR-466g</i>	0.0300	1.22
<i>miR-450b-3p</i>	0.0165	1.21
<i>miR-876</i>	0.0463	1.20
<i>miR-449c</i>	0.0136	1.20
<i>miR-214</i>	0.0305	-1.21
<i>miR-1956</i>	0.0298	-1.23
<i>miR-882</i>	0.0335	-1.25
<i>miR-290-3p</i>	0.0372	-1.30
<i>miR-1945</i>	0.0125	-1.39
<i>miR-297c</i>	0.0149	-1.95
<i>miR-669</i>	0.0065	-2.01

†n=3 ethanol-exposed and n=3 control microarrays. *p*-values determined using a one-way ANOVA, fold change in expression vs. control group determined using Partek RMA algorithm. Transcripts presented passed a fold cut off >1.2 and *p*<0.05.

**Table 4.6 MicroRNA expression changes with corresponding reciprocal changes in expression of predicted target genes<sup>†</sup>.**

<b>Gene Symbol</b>	<b><i>p</i>-value</b>	<b>Fold change</b>	<b>miRNA ID</b>	<b><i>p</i>-value</b>	<b>Fold change</b>	<b>Confidence</b>
<i>Hcn4</i>	0.048	1.23	<i>miR-185-5p</i>	0.026	-1.26	High
<i>Mafg</i>	0.036	-1.21	<i>miR-130a-3p</i>	0.018	2.19	High
			<i>miR-200b-3p</i>	0.022	1.95	High
<i>L3mbtl4</i>	0.040	-1.22	<i>miR-377-3p</i>	0.019	1.29	High
<i>Tmem79</i>	0.027	-1.29	<i>miR-34a-5p</i>	0.046	1.20	Moderate

<sup>†</sup>Fold changes and *p*-values determined in Partek using the RMA algorithm.

Relationships were identified using IPA Target Scan™. Fold change and *p*-values from microarrays presented. miRNA targets predicted by Ingenuity Target Scan™, only reciprocal changes in miRNA abundance vs. target mRNA abundance shown. Confidence is an output of IPA target scan and refers the likelihood of the predicted miRNA-mRNA interaction occurring *in vivo*.



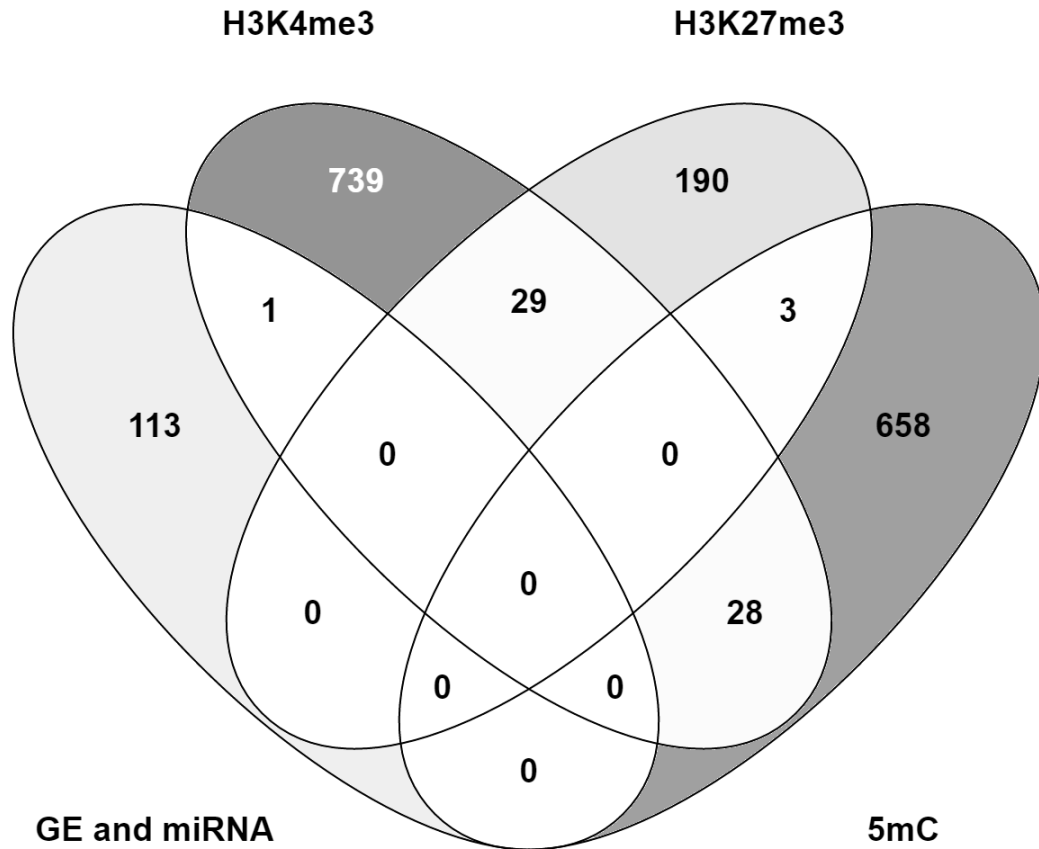


**Figure 4.5 Distribution of implicated genes shared between experiments at  $p < 0.001$ .** Darker shading indicates more genes present at that intersection. Gene expression (GE) and miRNA list generated using  $p < 0.05$ , fold-cut off  $> 1.2$ ; H3K4me3 and H3K27me3 lists generated using MAT score cut-off  $p < 0.001$ ; DNA methylation (5mC) list generated using AMS cut-off  $p < 0.001$ .

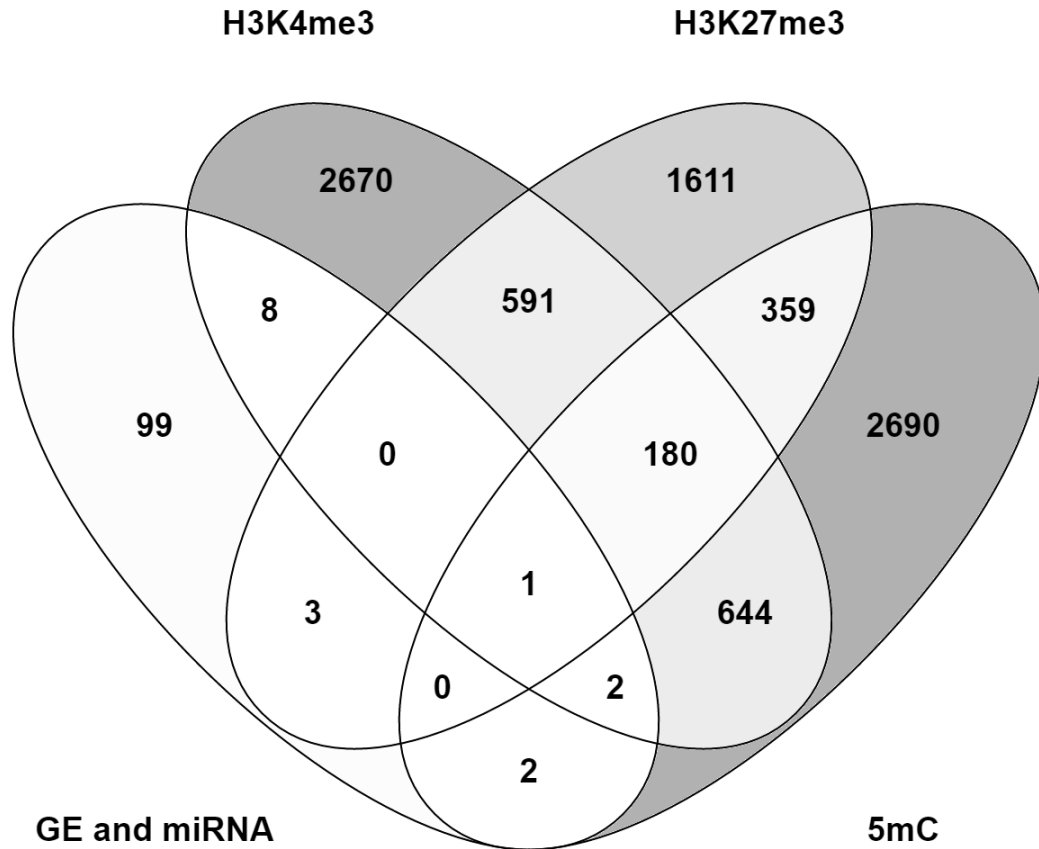


**Figure 4.6 Distribution of implicated genes shared between experiments at  $p < 0.01$ .** Darker shading indicates more genes present at that intersection. Gene expression (GE) and miRNA list generated using  $p < 0.05$ , fold-cut off  $> 1.2$ ; H3K4me3 and H3K27me3 lists generated using MAT score cut-off  $p < 0.01$ ; DNA methylation (5mC) list generated using AMS cut-off  $p < 0.01$ .

**Table 4.7 Differentially expressed genes proximal to a change in DNA methylation or histone methylation<sup>†</sup>.**

Gene expression			5mC DMR		H3K4me3 RDHM		H3K27me3 RDHM	
Gene Symbol	<i>p</i> -value	Fold change	AMS score	<i>p</i> -value	MAT score	<i>p</i> -value	MAT score	<i>p</i> -value
<i>Tcf7l2</i>	0.032	1.50	9.87	0.007	-3.12	0.004	1.86	0.003
					-4.38	0.0009		
<i>Synpo2</i>	0.047	1.43	11.82	0.004	3.10	0.009		
<i>Vipr2</i>	0.043	1.42	10.32	0.002				
<i>Gm8994</i>	0.021	1.32			3.14	0.008		
<i>Olfr119</i>	0.007	1.30			-2.93	0.008		
<i>Vmn2r15</i>	0.049	1.29					1.44	0.004
<i>Cfhr2</i>	0.023	1.29			3.09	0.009		
<i>Krt8</i>	0.013	1.25			3.12	0.008		
<i>Slitrk6</i>	0.023	1.24			3.24	0.006		
<i>Krt39</i>	0.008	1.23			3.05	0.009		
<i>Hcn4</i>	0.048	1.23			-2.95	0.007		
<i>Vmn2r109</i>	0.022	1.22					1.14	0.008
<i>Dnm3os</i>	0.050	1.21					1.16	0.007
<i>Gm4776</i>	0.024	-1.20			-2.91	0.008		
<i>Mafg</i>	0.036	-1.21	9.39	0.009				
			-12.67	0.005				
			13.42	0.001				

<sup>†</sup>Differentially 5-methylcytosine (5mC) methylated regions (DMRs) and regions of differentially histone modification (RDHMs) in gene promoters are also shown (cut-off  $p < 0.01$ ). Positive AMS indicates increased methylation in ethanol exposed mice, while positive MAT score indicates reduced methylation in ethanol exposed mice.

compared with a  $p$ -value $<0.01$  (**Figure 4.6**). There were 16 differentially expressed genes proximal to a change in DNA or histone methylation at this significance level (**Table 4.7**). *Gm8994*, *Olf119*, *Cfhr2*, *Slitrk6*, *Krt39*, *Hcn4*, *Gm4776* and *Olf2* were proximal to H3K4me3 changes only; *Vmn2r15*, *Vmn2r109*, and *Dnm3os* were proximal to H3K27me3 changes only; *Vipr2* and *Mafg* were proximal to DNA methylation changes only; *Synpo2* and *Krt8* were proximal to H3K4me3 and DNA methylation changes; *Tcf7l2* was proximal to H3K4me3, H3K27me3, and DNA methylation changes. Four of these genes (*Krt8*, *Mafg*, *Tcf7l2*, and *Vipr2*) were present in the top IPA pathway (Chapter 2). No differentially expressed miRNAs were proximal to DNA or histone methylation changes. There was significantly more overlap between the gene expression and the H3K4me3 gene lists than expected by chance ( $X^2=31.6$ ,  $p<0.00001$ ) and significantly less overlap than expected by between the gene expression and H3K27me3 lists ( $X^2=48.7$ ,  $p<0.00001$ ) and between the gene expression and DNA methylation lists ( $X^2=42.6$ ,  $p<0.00001$ ).

## 4.5 Discussion

Analysis of the function and interactions of the 59 differentially expressed genes identified in this experiment revealed that diverse cellular processes are affected by neonatal ethanol exposure. Most (60%) of the affected genes are co-expressed and many (22%) are co-localized. None of the gene protein products directly interact, nor transcribe one another.

GO analysis implicated the differentially expressed genes in various biosynthetic processes including dicarboxylic acid, kynurenine, and tryptophan metabolism (**Table 4.2**). The differentially expressed gene *Kmo* (Kynurenine 3-monooxygenase) is responsible for identifying these processes. It encodes an enzyme involved in metabolism of L-tryptophan to the dicarboxylic acid L-3-hydroxykynurenine, part of the synthesis of quinolinic acid. This is part of the cytokine-mediated inflammation response (Dantzer et al., 2011). L-3-hydroxykynurenine is also a source of free radicals, and a neurotoxin; it is an NMDA receptor antagonist, which acts in much the same neurotoxic manner as ethanol during synaptogenesis (Lugo-Huitrón et al., 2013). Its upregulation may indicate a residual inflammatory response after ethanol exposure. Fetal ethanol exposure leads to various neuroimmune changes, including microglia activation and production of pro-inflammatory molecules, leading to altered neuronal survival (Drew and Kane, 2014).

Several other classes of genes were differentially expressed. Upregulation of *Synpo2* (synaptopodin 2) in ethanol-exposed mice was also confirmed (**Figure 4.4**). Synaptopodins are a class of proteins that are highly expressed in telencephalic dendrites. The precise function of synaptopodins is unknown; they found at dendritic spines and post-synaptic densities (Deller et al., 2003; Mundel et al., 1997). *Synpo2* dysregulation may underlie some of their characteristic learning and memory impairment in PND 4,7 ethanol-exposed mice (Kleiber et al., 2014a). Olfactory receptors represent 19% (11/59) of the differentially expressed genes. Olfactory receptors are implicated in several FASD studies, and may be involved in its etiology.

### 4.5.1 Olfactory Receptor Genes

The top Partek Pathway was “Olfactory Transduction” (**Table 4.3**). There were 11 olfactory receptor (*Olf*) genes differentially expressed, five down regulated and 6 upregulated representing 19% of the identified genes (**Figure 4.2**) Olfactory receptors (ORs) are G-protein-coupled receptors that function in the main olfactory epithelium (MOE). They sense external olfactory cues, and through signal transduction pathways, send this information to the brain. ORs are ectopically expressed in the brain and other tissues, but their function remains unclear (Kang and Koo, 2012). The ectopically expressed ORs are evolutionarily constrained between mice, rats and humans, suggesting they serve conserved functions (De la Cruz et al., 2008). Generation of antibodies to study these proteins has been difficult, thus very little is known about their cellular localization (Kang and Koo, 2012). Evidence suggests that they are important for mediating cell-cell communication; in skin, ORs mediate communication between keratinocytes and trigeminal neurons (Sondersorg et al., 2014). During mouse embryogenesis, ORs may act as recognition molecules providing a complex addressing system facilitating cell-cell recognition, migration, and tissue assembly during embryogenesis (Dreyer, 1998). ORs may also have a role in repair. In the rat brain, ORs were upregulated in dorsal root ganglia following nerve injury (Gong et al., 2015). Induction of oxidative stress in cultured rat Schwann cells induced upregulation of 14 ORs (Gong et al., 2015). Several human neurodegenerative diseases are also associated with changes in OR expression, including Alzheimer’s disease, Progressive Supranuclear Palsy, Parkinson’s disease, and Creutzfeldt-Jakob disease (Ansoleaga et al., 2013; Garcia-Esparcia et al., 2013). These data suggest that ORs may play an important role in the development of the brain, and its response to external stress.

Dysregulation of *Olf* genes is common in FASD studies. In previous work from our laboratory using the PND 4,7 model, seven *Olf* genes were differentially expressed at P60, though none of the same genes as in this study (Kleiber et al., 2014a). In a study examining the hippocampus of P28 mice exposed to ethanol from G0.5-8.5, 30% (7/23) of differentially expressed genes were olfactory receptors (Marjonen et al., 2015). This study also found reduction in volume of olfactory bulb and hippocampus. Another study examining the effect of ethanol on whole-embryo culture found changes in DNA

methylation of several olfactory receptor genes (Liu et al., 2009). Interestingly, impaired olfaction is an outcome of fetal ethanol exposure (Muralidharan et al., 2013).

Dysregulation of *Olfir* genes in the brain in response to ethanol may represent a conserved response. If ORs facilitate cell-cell communication in the brain, their dysregulation may be related to the known detrimental effect of ethanol on synaptic pruning/development (Olney et al., 2002). Further, if ORs indeed have a role in response to stresses, their dysregulation may be a result of ethanol-induced effects such as oxidative stress (Brocardo et al., 2011).

#### 4.5.2 Implication of Free Radical Scavenging Pathway

Ingenuity pathway analysis (IPA) identified the top affected gene expression network as “Free Radical Scavenging, Gene Expression, Dermatological Diseases and Conditions” (**Figure 4.3**). This gene network is responsible for coordinating the transcriptional free radical scavenging response. NFE2L2 homodimers and NFE2L2/MAFG heterodimers control the expression of genes with antioxidant response elements (ARE) in their promoters (Nguyen et al., 2009). Such genes are involved in response to inflammation resulting from elevated free radical levels. Other proteins in this network have roles in oxidative stress such as GPX, KEAP1, and apolipoproteins. This network also includes many apoptosis-related proteins including BNIP3L, AATF, and HSD2D as well as proteins important in the brain such as MAOA, CLCN3. Dysregulation of this pathway could impact these critical processes, all of which are relevant to FASD etiology.

Microarray analysis identified 13 genes which were differentially regulated in this top IPA network. Four of these changes were confirmed by ddPCR: *Casp3*, *Krt8*, *Tcf7l2* and *Vipr2* (**Figure 4.4**); *Casp3* (Caspase-3) is a hub of this network. Caspase-3 has a key role in the execution phase of cellular apoptosis, and is inducible by oxidative stress (Ueda et al., 1998). It is involved in many response pathways and processes, and is responsible for implicating many of the pathways in this analysis (**Table 4.3**). Its activation by ethanol is part of the apoptotic cascade that happens in the fetal brain during development (Goodlett et al., 2005). TCF7L2 regulates insulin secretion, acting as a transcription factor in the Wnt pathway. Wnt signaling is key in brain development and

synaptogenesis as well as adult functions such as synaptic modeling and neuronal maintenance (Oliva et al., 2013). It is a key developmental regulator, and as such is responsible for implicating many of the pathways in this analysis (**Table 4.3**). VIPR2 is a G-protein coupled receptor for a small neuropeptide, pituitary adenylate cyclase activating polypeptide (PACAP). PACAP acts as a hypothalamic hormone, a neurotransmitter and a neurotrophic factor (Shioda, 2000). *Vipr2* showed methylation differences in a study of children with ADHD (Wilmot et al., 2015). Downregulation of *L3mbtl4* which is a putative polycomb group protein was also confirmed. These proteins maintain repressive chromatin states by modification of histone modifications.

Other genes in this network have been implicated in FASD-relevant processes. *Defb5* is a defensin, a family of proteins involved in inflammatory response and antimicrobial defense which are produced by microglia and astrocytes (Hao et al., 2001). Our laboratory found *Defb15*, *Defb30* upregulated in PND 70 mice given continuous access to ethanol during pregnancy (Kleiber et al., 2012). A model of gestational ethanol exposure also affected defensin expression (Muralidharan et al., 2013). Upregulation of defensins may indicate stressors, such as oxidative stress occurring in hippocampus. Again, KMO is involved in inflammatory response. The role of keratins in the brain is unclear; however, several keratin genes and keratin-associated protein (KRTAP) have been implicated in FASD models. *Krtap* was downregulated in previous work from our laboratory (Chater-Diehl et al., 2016) and in P28 mice exposed to ethanol during GD 0.5-8.5, (Marjonen et al., 2015). The abundance of another keratin protein (KRT72) was reduced in whole-mouse-embryo culture in ethanol (Mason et al., 2012).

The implication of this pathway, and other evidence presented suggests an altered free-radical-scavenging response in the hippocampus. Oxidative stress is a well characterized component of FASD etiology. Ethanol acts directly on mitochondria to produce superoxide, hydroxide, and nitric oxide radicals (Wu and Cederbaum, 2003). Metabolism of ethanol by CYP2E1 produces oxidized products and ultimately hydroxide radical generation (Mansouri et al., 2001). Catalase also produces acetaldehyde from alcohol in the brain, further increasing the formation of ROS (Shaw, 1989). Oxidative damage can lead to blood-brain barrier impairment, inflammation, and increased apoptosis (Haorah et al., 2008). Interestingly, these are also key features of FASD



etiology. Indeed, oxidative damage is observed in many rodent models of FASD, including lipid peroxidation, protein oxidation, and DNA damage (Brocardo et al., 2011). Lipid peroxidation is not often present in young animals, but accumulates over time into adulthood (Dembele et al., 2006). In a *Drosophila* model of developmental ethanol exposure, changes in expression of antioxidant genes contributed to oxidative stress in adult flies (Logan-Garbisch et al., 2014). Further, this increased oxidative stress was a primary cause of developmental delay associated with ethanol exposure (Logan-Garbisch et al., 2014). Oxidative damage to DNA, protein, membranes, and other cellular components is a key cause of ethanol-induced damage and cell-death in the brain (Guerri, 1998).

Alteration of oxidative stress gene expression has also been reported in FASD models. Oxidative stress response genes such as *c-Fos* have been reported to be differentially expressed in response to ethanol (Incerti et al., 2010; Poggi et al., 2003). Fetal ethanol exposure reduces the expression of antioxidant enzymes in the brain (Drever et al., 2012). The direct role of oxidative stress in FASD phenotypes has been supported by the amelioration of phenotypes with antioxidant treatment (Patten et al., 2013; Wu and Cederbaum, 2003)

#### 4.5.3 Low Expression Levels of Differentially Expressed Genes

Expression localization data from the Allen Brain Atlas revealed that only one of the six differentially expressed genes (*Casp3*) was expressed at high levels in dentate granule neurons and hippocampal pyramidal neurons. Caspase-3 is a crucial protein in many neuronal processes. The other five genes show non-neuron-specific expression patterns, or are expressed at too low a level to be detected. Each of these genes was upregulated in response to ethanol. The upregulation of a gene normally expressed at very low levels could have a substantial impact on the hippocampus.

The low levels of expression, and relatively low fold-changes of these genes made them very difficult to confirm with qPCR. Droplet digital PCR proved to be better able to quantify these changes (**Figure 4.4**). The relative expression in each of the confirmed genes did not differ from the qPCR data; however, the variation was reduced, resulting in significant differences in expression.

All of the genes in this study have a relatively low expression fold change, the maximum magnitude being 1.5 fold. A low fold change does not necessarily imply irrelevance to phenotype. A small 1.2 fold increase in the expression of many genes in a pathway can potentially have a greater impact than a 20 fold change in a single gene (Barabási and Oltvai, 2004; Subramanian et al., 2005). The previous studies from our laboratory also found low (less than 2 fold) changes in expression in response to PAE (Kleiber et al., 2014b; Laufer et al., 2013). Examining a specific brain region did not change this fold change pattern, suggesting that ethanol exerts subtle effects on gene expression across the brain. Similarly, the number of differentially expressed genes was similar to our previous work.

#### 4.5.4 Notable Changes in MicroRNA Expression

There were 60 pre- and mature miRNAs differentially expressed in PND 70 hippocampus after ethanol exposure. Five of these were identified in our laboratory previously: *miR-184* and *miR-466b* were identified in P60 mice exposure to ethanol during late (G14,16) gestation while *miR-184*, *miR-704*, *miR-297a*, and *miR-669* were identified in PND 7 mice exposed to PND 4,7 ethanol injections (Mantha et al., 2014). There were no miRNAs in common with the CPD model. Though the functions of many of the differentially expressed miRNAs remain unknown, several are involved in brain development and other FASD-relevant processes. *MiR-207* and *mir449c* are involved in embryonic neurogenesis (Choi et al., 2008; Maiorano and Mallamaci, 2009). *Mir-200c* and *miR-130b* are involved in neural progenitor cell proliferation (Gong et al., 2013; Peng et al., 2012). *MiR-214* and *miR-207* are involved in promoting apoptosis (Liao et al., 2010; Tan et al., 2014). *MiR-130b* is involved in regulation of peroxisomes (Pan et al., 2015). Two are also involved in inflammatory response in the brain; *miR-125b* promotes microglia activation (Parisi et al., 2016) and *miR-200c* promotes astrocyte activation (Mor et al., 2011).

Using IPA Target Scan™, five of the differentially expressed miRNAs were found to have differentially expressed predicted miRNA targets (**Table 4.6**). Confirmation of differential expression of *Mafg*, *L3mbtl4*, and *Tmem79* was attempted, only downregulation of *L3mbtl4* was confirmed (**Figure 4.4**). *L3mbtl4* encodes a tumour

suppressor protein has been shown to be mutated often in breast cancers (Addou-Klouche et al., 2010). Interestingly, its targeting miRNA, *miR-377* also functions as a tumour suppressor renal cell carcinoma by targeting *Ets1* (Wang et al., 2015). Tumor suppressors have complex and unclear roles in the nervous system; however, their downregulation can trigger apoptosis and abnormal neurodevelopmental trajectories (Baker and McKinnon, 2004). Altered regulation of *L3mbtl4* and its targeting miRNA *miR-377* may be associated with apoptosis present in the PND 4,7 model. Alternatively, they may be a “footprint” of earlier ethanol exposure remaining into adulthood. *Tmem97* encodes a membrane protein involved in regulating cellular cholesterol levels. It was differentially methylated in the DNA methylation analysis, and was present in several top IPA pathways (Chapter 3). Due to its relevance to lipid metabolism, and downregulation of a putative targeting miRNA, confirmation of *Tmem97* upregulation was attempted using ddPCR; it was not confirmed however.

#### 4.5.5 Few Co-occurring Gene Expression and Methylation Changes

Identification of genes across experiments was one of the primary goals of this project during its conception. Genes which are differentially expressed and differentially methylated are better candidates for participating in FASD etiology. Such genes would be implicated by multiple independent elements. Further, differential methylation of these genes would provide an explanation for their differential expression. There were 16 differentially expressed genes that had changes in at least one methylation. Four of these (*Krt8*, *Mafg*, *Tcf7l2*, and *Vipr2*) were present in the top IPA pathway and were assessed using ddPCR. *Krt8*, *Tcf7l2*, and *Vipr2* were confirmed using this technique. *Synpo2* was also confirmed with ddPCR. *Synpo2* and *Krt8* were proximal to H3K4me3 and DNA methylation changes (**Table 4.7**).

There were very few differentially expressed genes that had changes in any methylation. A chi-squared analysis was performed to determine if there was more or less overlap between each of the three methylation gene lists and the gene expression gene list than expected by chance. Interestingly, there was more overlap than expected between the H3K4me3 gene list and the gene expression list ( $X^2=31.6$ ,  $p<0.00001$ ); significantly fewer between the H3K27me3 list gene and the gene expression list ( $X^2=48.7$ ,

$p < 0.00001$ ) and a significantly fewer between the DNA methylation gene list and the gene expression list ( $X^2 = 42.6$ ,  $p < 0.00001$ ). This suggests that the differentially expressed genes are enriched for H3K4me3 changes, and depleted for H3K27me3 and DNA methylation changes. H3K4me3 may be more relevant to the gene expression changes observed here. In Chapter 5, the possible origin and implications of methylation changes without corresponding gene expression changes are discussed.

#### 4.5.6 *Tcf7l2* as an FASD Candidate Gene

*Tcf7l2* is notable since it was the only differentially expressed gene proximal to an epigenetic methylation change with  $p < 0.001$  (**Figure 4.5**) and the only differentially expressed gene proximal to all three assessed epigenetic methylation changes with  $p < 0.01$  (**Figure 4.6**). The proximal H3K4me3 and H3K27me3 RDHMs and 5mC DMR were in the predicted direction with respect to increased gene expression (**Table 4.7**). The agreement between these changes suggest *Tcf7l2* they may play a functional role in its upregulation. It is also the top differentially expressed gene in terms of fold-change magnitude (1.5 fold). Together, these findings make it the single most compelling candidate gene in this thesis.

*Tcf7l2* encodes a transcription factor involved in Wnt signaling. Extracellular Wnt signalling proteins bind to frizzled receptors, triggering axin to bind to the  $\beta$ -catenin destruction complex, inhibiting and promoting  $\beta$ -catenin accumulation.  $\beta$ -catenin enters the nucleus and binds to TCF7L2 which can then bind to target genes promoting their expression (Araoka et al., 2010). In the liver, these target genes are involved in insulin secretion. In the brain, *Tcf7l2* and Wnt signalling are necessary for oligodendrocyte differentiation. TCF7L2 promotes the regulation of key oligodendrocyte-specific genes during their development. It also regulates neuronal lipids, promoting myelination and cholesterol biosynthesis gene transcription (Zhao et al., 2016). *Tcf7l2* is expressed in oligodendrocytes of the hippocampus during mouse fetal development (Weaver et al., 2012). TCF7L2 is also negatively responsive to oxidative stress; oxidative stress signaling diverts  $\beta$ -catenin depleting active TCF7L2 (Gloyn et al., 2009). These interactions implicate TCF7L2 in the top IPA pathway, and its relation to lipid metabolism overlap with peroxisome genes.

Polymorphisms in this gene are the strongest genetic risk factors for type 2 diabetes (Gloyn et al., 2009). Specific polymorphisms are associated with impaired insulin secretion, glucose production, and glucose tolerance (Lyssenko et al., 2007). The mechanisms by which these variants influence glucose homeostasis and diabetes are believed to be through the gene's role in adipogenesis, myogenesis, glucose and pancreatic islet development (Takamoto et al., 2014). The link between hypoglycemia and FASD is not clear, though some studies have found increased incidence in FASD individuals (Tanaka et al., 1982). *Tcf7l2* has not been previously implicated in FASD prior to this study. The status of this gene in the top gene expression and methylation pathways, its overlap with epigenetic changes, indicate that it should be considered as a candidate gene in FASD and investigated further. Given its role in myelination during development, its alteration may underlie ethanol-induced synaptic changes in the hippocampus, contributing to learning and memory impairment.

#### 4.5.7 Conclusion

This chapter describes gene and miRNA expression changes in the adult hippocampus in response to neonatal ethanol exposure. The affected genes were enriched for olfactory receptors and oxidative stress response genes. Delineating the possible role of these genes in FASD etiology is challenging. Exposure of mice to ethanol on PND 4 & 7 results in widespread apoptotic cell death. The surviving cells adapt and alter their developmental trajectories. It is the gene expression changes in these cells that are detected in this study. These gene expression changes may represent adaptations/alterations in the surviving cells, or they may simply reflect the differential cell population created by early apoptotic cell death (Kleiber et al., 2014b). The changes in gene expression identified here provide insight into the state of the hippocampal transcriptome long after ethanol exposure. The conditions responsible for establishing these changes (early ethanol exposure) are well understood. It is unknown what cellular and gene expression changes occur between ethanol exposure and the transcriptional timepoint observed here. Other studies can provide insight into these changes, but given the heterogeneity of ethanol response, it is difficult to make inferences about specific genes between studies. *Tcf7l2* emerged as a strong candidate gene, being upregulated,

present in the top IPA pathway, proximal to DNA, H3K4me3, and H3K27me3 changes. *Tcf7l2* is critical in the regulation of glucose homeostasis, and may be involved in metabolic changes in the brain following PAE. Beyond this gene, few examples of differential gene expression cooccurring with epigenetic methylation changes were found. In the final chapter the possible mechanistic hypotheses and future experiments necessary to test them will be explored.

**Footnote**

A modified version of this chapter has been published (Chater-Diehl et al., 2016).

## 4.6 References

- Addou-Klouche, L., Adélaïde, J., Finetti, P., Cervera, N., Ferrari, A., Bekhouche, I., Sircoulomb, F., Sotiriou, C., Viens, P., Moulessehoul, S., et al. (2010). Loss, mutation and deregulation of L3MBTL4 in breast cancers. *Mol. Cancer* *9*, 213.
- Ahlgren, S.C., Thakur, V., and Bronner-Fraser, M. (2002). Sonic hedgehog rescues cranial neural crest from cell death induced by ethanol exposure. *Proc. Natl. Acad. Sci. U. S. A.* *99*, 10476–10481.
- Ansoleaga, B., Garcia-Esparcia, P., Llorens, F., Moreno, J., Aso, E., and Ferrer, I. (2013). Dysregulation of brain olfactory and taste receptors in AD, PSP and CJD, and AD-related model. *Neuroscience* *248*, 369–382.
- Araoka, T., Abe, H., Tominaga, T., Mima, A., Matsubara, T., Murakami, T., Kishi, S., Nagai, K., and Doi, T. (2010). Transcription factor 7-like 2 (TCF7L2) regulates activin receptor-like kinase 1 (ALK1)/Smad1 pathway for development of diabetic nephropathy. *Mol. Cells* *30*, 209–218.
- Babak, T., Zhang, W., Morris, Q., Blencowe, B.J., and Hughes, T.R. (2004). Probing microRNAs with microarrays: Tissue specificity and functional inference. *RNA* *10*, 1813–1819.
- Baker, S.J., and McKinnon, P.J. (2004). Tumour-suppressor function in the nervous system. *Nat. Rev. Cancer* *4*, 184–196.
- Barabási, A.-L., and Oltvai, Z.N. (2004). Network biology: understanding the cell's functional organization. *Nat. Rev. Genet.* *5*, 101–113.
- Brocardo, P.S., Gil-Mohapel, J., and Christie, B.R. (2011). The role of oxidative stress in fetal alcohol spectrum disorders. *Brain Res. Rev.* *67*, 209–225.
- Chater-Diehl, E.J., Laufer, B.I., Castellani, C.A., Alberry, B.L., and Singh, S.M. (2016). Alteration of Gene Expression, DNA Methylation, and Histone Methylation in Free Radical Scavenging Networks in Adult Mouse Hippocampus following Fetal Alcohol Exposure. *PLoS One* *11*, e0154836.
- Chen, E.Y., Tan, C.M., Kou, Y., Duan, Q., Wang, Z., Meirelles, G. V, Clark, N.R., and Ma'ayan, A. (2013). Enrichr: interactive and collaborative HTML5 gene list enrichment analysis tool. *BMC Bioinformatics* *14*, 128.
- Cheng, C.J., Bahal, R., Babar, I.A., Pincus, Z., Barrera, F., Liu, C., Svoronos, A., Braddock, D.T., Glazer, P.M., Engelman, D.M., et al. (2014). MicroRNA silencing for cancer therapy targeted to the tumour microenvironment. *Nature* *518*, 107–110.
- Cho, Y.H., Friedman, E., and Silva, A.J. (1999). Ibotenate lesions of the hippocampus impair spatial learning but not contextual fear conditioning in mice. *Behav. Brain*

Res. 98, 77–87.

- Choi, P.S., Zakhary, L., Choi, W.-Y., Caron, S., Alvarez-Saavedra, E., Miska, E.A., McManus, M., Harfe, B., Giraldez, A.J., Horvitz, R.H., et al. (2008). Members of the miRNA-200 Family Regulate Olfactory Neurogenesis. *Neuron* 57, 41–55.
- D'Amelio, M., Sheng, M., and Cecconi, F. (2012). Caspase-3 in the central nervous system: beyond apoptosis. *Trends Neurosci.* 35, 700–709.
- Dantzer, R., O'Connor, J.C., Lawson, M.A., and Kelley, K.W. (2011). Inflammation-associated depression: From serotonin to kynurenine. *Psychoneuroendocrinology* 36, 426–436.
- Deller, T., Korte, M., Chabanis, S., Drakew, A., Schwegler, H., Stefani, G.G., Zuniga, A., Schwarz, K., Bonhoeffer, T., Zeller, R., et al. (2003). Synaptopodin-deficient mice lack a spine apparatus and show deficits in synaptic plasticity. *Proc. Natl. Acad. Sci. U. S. A.* 100, 10494–10499.
- Dembele, K., Yao, X.-H., Chen, L., and Nyomba, B.L.G. (2006). Intrauterine ethanol exposure results in hypothalamic oxidative stress and neuroendocrine alterations in adult rat offspring. *Am. J. Physiol. Regul. Integr. Comp. Physiol.* 291, R796-802.
- Drever, N., Yin, H., Kechichian, T., Costantine, M., Longo, M., Saade, G.R., and Bytautiene, E. (2012). The expression of antioxidant enzymes in a mouse model of fetal alcohol syndrome. *Am. J. Obstet. Gynecol.* 206, 358.e19-22.
- Drew, P.D., and Kane, C.J.M. (2014). Fetal Alcohol Spectrum Disorders and Neuroimmune Changes. *Int. Rev. Neurobiol.* 118, 41.
- Dreyer, W.J. (1998). The area code hypothesis revisited: olfactory receptors and other related transmembrane receptors may function as the last digits in a cell surface code for assembling embryos. *Proc. Natl. Acad. Sci. U. S. A.* 95, 9072–9077.
- Emilsson, V., Thorleifsson, G., Zhang, B., Leonardson, A.S., Zink, F., Zhu, J., Carlson, S., Helgason, A., Walters, G.B., Gunnarsdottir, S., et al. (2008). Genetics of gene expression and its effect on disease. *Nature* 452, 423–428.
- Garcia-Esparcia, P., Schlüter, A., Carmona, M., Moreno, J., Ansoleaga, B., Torrejón-Escribano, B., Gustincich, S., Pujol, A., and Ferrer, I. (2013). Functional Genomics Reveals Dysregulation of Cortical Olfactory Receptors in Parkinson Disease: Novel Putative Chemoreceptors in the Human Brain. *J. Neuropathol. Exp. Neurol.* 72, 524–539.
- Gloyn, A.L., Braun, M., and Rorsman, P. (2009). Type 2 diabetes susceptibility gene TCF7L2 and its role in beta-cell function. *Diabetes* 58, 800–802.



- Gong, L., Chen, Q., Gu, X., and Li, S. (2015). Expression and identification of olfactory receptors in sciatic nerve and dorsal root ganglia of rats. *Neurosci. Lett.* *600*, 171–175.
- Gong, X., Zhang, K., Wang, Y., Wang, J., Cui, Y., Li, S., and Luo, Y. (2013). MicroRNA-130b targets *Fmr1* and regulates embryonic neural progenitor cell proliferation and differentiation. *Biochem. Biophys. Res. Commun.* *439*, 493–500.
- Goodlett, C.R., Horn, K.H., and Zhou, F.C. (2005). Alcohol teratogenesis: mechanisms of damage and strategies for intervention. *Exp. Biol. Med. (Maywood)*. *230*, 394–406.
- Gu, S., and Kay, M.A. (2010). How do miRNAs mediate translational repression? *Silence* *1*, 11.
- Guerri, C. (1998). Neuroanatomical and neurophysiological mechanisms involved in central nervous system dysfunctions induced by prenatal alcohol exposure. *Alcohol. Clin. Exp. Res.* *22*, 304–312.
- Hamilton, D.A., Kodituwakku, P., Sutherland, R.J., and Savage, D.D. (2003). Children with Fetal Alcohol Syndrome are impaired at place learning but not cued-navigation in a virtual Morris water task. *Behav. Brain Res.* *143*, 85–94.
- Hao, H.N., Zhao, J., Lotoczky, G., Grever, W.E., and Lyman, W.D. (2001). Induction of human beta-defensin-2 expression in human astrocytes by lipopolysaccharide and cytokines. *J. Neurochem.* *77*, 1027–1035.
- Haorah, J., Schall, K., Ramirez, S.H., and Persidsky, Y. (2008). Activation of protein tyrosine kinases and matrix metalloproteinases causes blood-brain barrier injury: Novel mechanism for neurodegeneration associated with alcohol abuse. *Glia* *56*, 78–88.
- Hard, M.L., Abdolell, M., Robinson, B.H., and Koren, G. (2005). Gene-expression analysis after alcohol exposure in the developing mouse. *J. Lab. Clin. Med.* *145*, 47–54.
- Hoheisel, J.D. (2006). Microarray technology: beyond transcript profiling and genotype analysis. *Nat. Rev. Microbiol.* *7*, 200–210.
- Ikonomidou, C. (2000). Ethanol-Induced Apoptotic Neurodegeneration and Fetal Alcohol Syndrome. *Science (80-. )*. *287*, 1056–1060.
- Incerti, M., Vink, J., Roberson, R., Abebe, D., and Spong, C. (2010). Treatment with Neuropeptides Attenuates *c-fos* Expression in a Mouse Model of Fetal Alcohol Syndrome. *Am. J. Perinatol.* *27*, 743–748.
- Irizarry, R.A., Bolstad, B.M., Collin, F., Cope, L.M., Hobbs, B., and Speed, T.P. (2003).

- Summaries of Affymetrix GeneChip probe level data. *Nucleic Acids Res.* *31*, e15.
- Jaluria, P., Konstantopoulos, K., Betenbaugh, M., and Shiloach, J. (2007). A perspective on microarrays: current applications, pitfalls, and potential uses. *Microb. Cell Fact.* *6*, 4.
- Kang, N., and Koo, J. (2012). Olfactory receptors in non-chemosensory tissues. *BMB Rep.* *45*, 612–622.
- Khatri, P., Sirota, M., Butte, A.J., Glazko, G., Emmert-Streib, F., Green, M., Karp, P., Goeman, J., Buhlmann, P., Khatri, P., et al. (2012). Ten Years of Pathway Analysis: Current Approaches and Outstanding Challenges. *PLoS Comput. Biol.* *8*, e1002375.
- Kim, M.-R., Lee, K.-N., Yon, J.-M., Lee, S.-R., Jin, Y., Baek, I.-J., Lee, B.J., Yun, Y.W., and Nam, S.-Y. (2008). Capsaicin prevents ethanol-induced teratogenicity in cultured mouse whole embryos. *Reprod. Toxicol.* *26*, 292–297.
- Kleiber, M.L., Laufer, B.I., Wright, E., Diehl, E.J., and Singh, S.M. (2012). Long-term alterations to the brain transcriptome in a maternal voluntary consumption model of fetal alcohol spectrum disorders. *Brain Res.* *1458*, 18–33.
- Kleiber, M.L., Laufer, B.I., Stringer, R.L., and Singh, S.M. (2014a). Third trimester-equivalent ethanol exposure is characterized by an acute cellular stress response and an ontogenetic disruption of genes critical for synaptic establishment and function in mice. *Dev. Neurosci.* *36*, 499–519.
- Kleiber, M.L., Diehl, E.J., Laufer, B.I., Mantha, K., Chokroborty-Hoque, A., Alberry, B., and Singh, S.M. (2014b). Long-term genomic and epigenomic dysregulation as a consequence of prenatal alcohol exposure: a model for fetal alcohol spectrum disorders. *Front. Genet.* *5*, 161.
- De la Cruz, O., Blekhman, R., Zhang, X., Nicolae, D., Firestein, S., and Gilad, Y. (2008). A Signature of Evolutionary Constraint on a Subset of Ectopically Expressed Olfactory Receptor Genes. *Mol. Biol. Evol.* *26*, 491–494.
- Laufer, B.I., Mantha, K., Kleiber, M.L., Diehl, E.J., Addison, S.M., and Singh, S.M. (2013). Long-lasting alterations to DNA methylation and ncRNAs could underlie the effects of fetal alcohol exposure in mice. *Dis. Model. Mech.* *6*, 977–992.
- Lee, T.I., and Young, R.A. (2000). Transcription of Eukaryotic Protein-Coding Genes. *Annu. Rev. Genet.* *34*, 77–137.
- Lee, Y., Kim, M., Han, J., Yeom, K.-H., Lee, S., Baek, S.H., Kim, V.N., Ambros, V., Bartel, B., Bartel, D., et al. (2004). MicroRNA genes are transcribed by RNA polymerase II. *EMBO J.* *23*, 4051–4060.
- Liao, Y., Du, X., and Lonnerdal, B. (2010). miR-214 Regulates Lactoferrin Expression

- and Pro-Apoptotic Function in Mammary Epithelial Cells. *J. Nutr.* *140*, 1552–1556.
- Liu, Y., Balaraman, Y., Wang, G., Nephew, K.P., and Zhou, F.C. (2009). Alcohol exposure alters DNA methylation profiles in mouse embryos at early neurulation. *Epigenetics* *4*, 500–511.
- Logan-Garbisch, T., Bortolazzo, A., Luu, P., Ford, A., Do, D., Khodabakhshi, P., and French, R.L. (2014). Developmental ethanol exposure leads to dysregulation of lipid metabolism and oxidative stress in *Drosophila*. *G3 (Bethesda)*. *5*, 49–59.
- Lugo-Huitrón, R., Ugalde Muñiz, P., Pineda, B., Pedraza-Chaverri, J., Ríos, C., and Pérez-de la Cruz, V. (2013). Quinolinic Acid: An Endogenous Neurotoxin with Multiple Targets. *Oxid. Med. Cell. Longev.* *2013*, 1–14.
- Lussier, A.A., Stepien, K.A., Neumann, S.M., Pavlidis, P., Kobor, M.S., and Weinberg, J. (2015). Prenatal alcohol exposure alters steady-state and activated gene expression in the adult rat brain. *Alcohol. Clin. Exp. Res.* *39*, 251–261.
- Maiorano, N., and Mallamaci, A. (2009). Promotion of embryonic cortico-cerebral neurogenesis by miR-124. *Neural Dev.* *4*, 40.
- Mansouri, A., Demeilliers, C., Amsellem, S., Pessayre, D., and Fromenty, B. (2001). Acute ethanol administration oxidatively damages and depletes mitochondrial dna in mouse liver, brain, heart, and skeletal muscles: protective effects of antioxidants. *J. Pharmacol. Exp. Ther.* *298*, 737–743.
- Mantha, K., Kleiber, M., and Singh, S. (2013). Neurodevelopmental Timing of Ethanol Exposure May Contribute to Observed Heterogeneity of Behavioral Deficits in a Mouse Model of Fetal Alcohol Spectrum Disorder (FASD). *Behav. Brain Sci.* *3*, 85–99.
- Mantha, K., Laufer, B.I., and Singh, S.M. (2014). Molecular changes during neurodevelopment following second-trimester binge ethanol exposure in a mouse model of fetal alcohol spectrum disorder: from immediate effects to long-term adaptation. *Dev. Neurosci.* *36*, 29–43.
- Marjonen, H., Sierra, A., Nyman, A., Rogojin, V., Gröhn, O., Linden, A.-M., Hautaniemi, S., and Kaminen-Ahola, N. (2015). Early maternal alcohol consumption alters hippocampal DNA methylation, gene expression and volume in a mouse model. *PLoS One* *10*, e0124931.
- Mason, S., Anthony, B., Lai, X., Ringham, H.N., Wang, M., Witzmann, F.A., You, J.-S., and Zhou, F.C. (2012). Ethanol Exposure Alters Protein Expression in a Mouse Model of Fetal Alcohol Spectrum Disorders. *Int. J. Proteomics* *2012*, 1–10.
- Mor, E., Cabilly, Y., Goldshmit, Y., Zalts, H., Modai, S., Edry, L., Elroy-Stein, O., and Shomron, N. (2011). Species-specific microRNA roles elucidated following

- astrocyte activation. *Nucleic Acids Res.* 39, 3710–3723.
- Morris, R.G., Garrud, P., Rawlins, J.N., and O’Keefe, J. (1982). Place navigation impaired in rats with hippocampal lesions. *Nature* 297, 681–683.
- Mundel, P., Heid, H.W., Mundel, T.M., Krüger, M., Reiser, J., and Kriz, W. (1997). Synaptopodin: an actin-associated protein in telencephalic dendrites and renal podocytes. *J. Cell Biol.* 139, 193–204.
- Muralidharan, P., Sarmah, S., Zhou, F.C., and Marrs, J.A. (2013). Fetal Alcohol Spectrum Disorder (FASD) Associated Neural Defects: Complex Mechanisms and Potential Therapeutic Targets. *Brain Sci.* 3, 964–991.
- Naeini, M.M., and Ardekani, A.M. (2009). Noncoding RNAs and Cancer. *Avicenna J. Med. Biotechnol.* 1, 55–70.
- Nanni, L., Ming, J.E., Bocian, M., Steinhaus, K., Bianchi, D.W., Die-Smulders, C., Giannotti, A., Imaizumi, K., Jones, K.L., Campo, M.D., et al. (1999). The mutational spectrum of the sonic hedgehog gene in holoprosencephaly: SHH mutations cause a significant proportion of autosomal dominant holoprosencephaly. *Hum. Mol. Genet.* 8, 2479–2488.
- Nguyen, T., Nioi, P., and Pickett, C.B. (2009). The Nrf2-antioxidant response element signaling pathway and its activation by oxidative stress. *J. Biol. Chem.* 284, 13291–13295.
- Oliva, C.A., Vargas, J.Y., and Inestrosa, N.C. (2013). Wnts in adult brain: from synaptic plasticity to cognitive deficiencies. *Front. Cell. Neurosci.* 7, 224.
- Olney, J.W., Tenkova, T., Dikranian, K., Qin, Y.Q., Labruyere, J., and Ikonomidou, C. (2002). Ethanol-induced apoptotic neurodegeneration in the developing C57BL/6 mouse brain. *Brain Res. Brain Res.* 133, 115–126.
- Pan, S., Yang, X., Jia, Y., Li, Y., Chen, R., Wang, M., Cai, D., and Zhao, R. (2015). Intravenous injection of microvesicle-delivery miR-130b alleviates high-fat diet-induced obesity in C57BL/6 mice through translational repression of PPAR- $\gamma$ . *J. Biomed. Sci.* 22, 86.
- Parisi, C., Napoli, G., Amadio, S., Spalloni, A., Apolloni, S., Longone, P., and Volonté, C. (2016). MicroRNA-125b regulates microglia activation and motor neuron death in ALS. *Cell Death Differ.* 23, 531–541.
- Patten, A.R., Brocardo, P.S., and Christie, B.R. (2013). Omega-3 supplementation can restore glutathione levels and prevent oxidative damage caused by prenatal ethanol exposure. *J. Nutr. Biochem.* 24, 760–769.
- Peng, C., Li, N., Ng, Y.-K., Zhang, J., Meier, F., Theis, F.J., Merckenschlager, M., Chen, W., Würst, W., and Prakash, N. (2012). A Unilateral Negative Feedback Loop

Between miR-200 microRNAs and Sox2/E2F3 Controls Neural Progenitor Cell-Cycle Exit and Differentiation. *J. Neurosci.* 32, 13292–13308.

- Peng, Y., Yang, P.-H., Guo, Y., Ng, S.S.M., Liu, J., Fung, P.C.W., Tay, D., Ge, J., He, M.-L., Kung, H.-F., et al. (2004). Catalase and peroxiredoxin 5 protect *Xenopus* embryos against alcohol-induced ocular anomalies. *Invest. Ophthalmol. Vis. Sci.* 45, 23–29.
- Poggi, S.H., Goodwin, K.M., Hill, J.M., Brenneman, D.E., Tendi, E., Schinelli, S., and Spong, C.Y. (2003). Differential expression of c-fos in a mouse model of fetal alcohol syndrome. *Am. J. Obstet. Gynecol.* 189, 786–789.
- Rana, T.M. (2007). Illuminating the silence: understanding the structure and function of small RNAs. *Nat. Rev. Mol. Cell Biol.* 8, 23–36.
- Sathyan, P., Golden, H.B., and Miranda, R.C. (2007). Competing Interactions between Micro-RNAs Determine Neural Progenitor Survival and Proliferation after Ethanol Exposure: Evidence from an Ex Vivo Model of the Fetal Cerebral Cortical Neuroepithelium. *J. Neurosci.* 27, 8546–8557.
- Schwanhäusser, B., Busse, D., Li, N., Dittmar, G., Schuchhardt, J., Wolf, J., Chen, W., and Selbach, M. (2011). Global quantification of mammalian gene expression control. *Nature* 473, 337–342.
- Shaw, S. (1989). Lipid peroxidation, iron mobilization and radical generation induced by alcohol. *Free Radic. Biol. Med.* 7, 541–547.
- Shioda, S. (2000). Pituitary adenylate cyclase-activating polypeptide (PACAP) and its receptors in the brain. *Kaibogaku Zasshi.* 75, 487–507.
- Sondersorg, A.C., Busse, D., Kyereme, J., Rothermel, M., Neufang, G., Gisselmann, G., Hatt, H., and Conrad, H. (2014). Chemosensory Information Processing between Keratinocytes and Trigeminal Neurons. *J. Biol. Chem.* 289, 17529–17540.
- Spijker, S. (2011). *Neuroproteomics.* 57, 13–26.
- Squire, L.R. (2009). The legacy of patient H.M. for neuroscience. *Neuron* 61, 6–9.
- Strand, A.D., Aragaki, A.K., Baquet, Z.C., Hodges, A., Cunningham, P., Holmans, P., Jones, K.R., Jones, L., Kooperberg, C., and Olson, J.M. (2007). Conservation of Regional Gene Expression in Mouse and Human Brain. *PLoS Genet.* 3, e59.
- Subbanna, S., and Basavarajappa, B.S. (2014). Pre-administration of G9a/GLP inhibitor during synaptogenesis prevents postnatal ethanol-induced LTP deficits and neurobehavioral abnormalities in adult mice. *Exp. Neurol.* 261, 34–43.
- Subramanian, A., Tamayo, P., Mootha, V.K., Mukherjee, S., Ebert, B.L., Gillette, M.A., Paulovich, A., Pomeroy, S.L., Golub, T.R., Lander, E.S., et al. (2005). Gene set

- enrichment analysis: a knowledge-based approach for interpreting genome-wide expression profiles. *Proc. Natl. Acad. Sci. U. S. A.* *102*, 15545–15550.
- Sun, E., and Shi, Y. (2015). MicroRNAs: Small molecules with big roles in neurodevelopment and diseases. *Exp. Neurol.* *268*, 46–53.
- Sunkin, S.M., Ng, L., Lau, C., Dolbeare, T., Gilbert, T.L., Thompson, C.L., Hawrylycz, M., and Dang, C. (2013). Allen Brain Atlas: an integrated spatio-temporal portal for exploring the central nervous system. *Nucleic Acids Res.* *41*, D996–D1008.
- Tan, P., Du, S., Ren, C., Yao, Q., Zheng, R., Li, R., and Yuan, Y. (2014). MicroRNA-207 enhances radiation-induced apoptosis by directly targeting akt3 in cochlea hair cells. *Cell Death Dis.* *5*, e1433.
- Uecker, A., and Nadel, L. (1996). Spatial locations gone awry: object and spatial memory deficits in children with fetal alcohol syndrome. *Neuropsychologia* *34*, 209–223.
- Uecker, A., and Nadel, L. (1998). Spatial But Not Object Memory Impairments in Children with Fetal Alcohol Syndrome. *Am. J. Ment. Retard.* *103*, 12.
- Ueda, S., Nakamura, H., Masutani, H., Sasada, T., Yonehara, S., Takabayashi, A., Yamaoka, Y., and Yodoi, J. (1998). Redox regulation of caspase-3(-like) protease activity: regulatory roles of thioredoxin and cytochrome c. *J. Immunol.* *161*, 6689–6695.
- Urbich, C., Kuehbacher, A., and Dimmeler, S. (2008). Role of microRNAs in vascular diseases, inflammation, and angiogenesis. *Cardiovasc. Res.* *79*, 581–588.
- Valencia-Sanchez, M.A., Liu, J.D., Hannon, G.J., and Parker, R. (2006). Control of translation and mRNA degradation by miRNAs and siRNAs. *Genes Dev.* *20*, 515–524.
- Vogel, C., and Marcotte, E.M. (2012). Insights into the regulation of protein abundance from proteomic and transcriptomic analyses. *Nat. Rev. Genet.* *13*, 227.
- Wang, R., Ma, Y., Yu, D., Zhao, J., and Ma, P. (2015). miR-377 functions as a tumor suppressor in human clear cell renal cell carcinoma by targeting ETS1. *Biomed. Pharmacother.* *70*, 64–71.
- Wang, W., Kwon, E.J., and Tsai, L.-H. (2012). MicroRNAs in learning, memory, and neurological diseases. *Learn. Mem.* *19*, 359–368.
- Weaver, C., Turner, N., and Hall, J. (2012). Review of the neuroanatomic landscape implicated in glucose sensing and regulation of nutrient signaling: Immunophenotypic localization of diabetes gene Tcf7l2 in the developing murine brain. *J. Chem. Neuroanat.* *45*, 1–17.
- Wilmot, B., Fry, R., Smeester, L., Musser, E.D., Mill, J., and Nigg, J.T. (2015).

Methylomic analysis of salivary DNA in childhood ADHD identifies altered DNA methylation in VIPR2. *J. Child Psychol. Psychiatry*.

- Wozniak, D.F., Hartman, R.E., Boyle, M.P., Vogt, S.K., Brooks, A.R., Tenkova, T., Young, C.L., Olney, J.W., and Muglia, L.J. (2004). Apoptotic neuro degeneration induced by ethanol in neonatal mice is associated with profound learning/memory deficits in juveniles followed by progressive functional recovery in adults RID C-5767-2008. *Neurobiol. Dis.* *17*, 403–414.
- Wu, D., and Cederbaum, A.I. (2003). Alcohol, oxidative stress, and free radical damage. *Alcohol Res. Health* *27*, 277–284.
- Zhou, F.C., Zhao, Q., Liu, Y., Goodlett, C.R., Liang, T., McClintick, J.N., Edenberg, H.J., Li, L., Jones, K., Smith, D., et al. (2011). Alteration of gene expression by alcohol exposure at early neurulation. *BMC Genomics* *12*, 124.
- Zhao, C., Deng, Y., Liu, L., Yu, K., Zhang, L., Wang, H., He, X., Wang, J., Lu, C., Wu, L.N., et al. (2016). Dual regulatory switch through interactions of Tcf712/Tcf4 with stage-specific partners propels oligodendroglial maturation. *Nat. Commun.* *7*, 10883.
- Zhou, X., Ruan, J., Wang, G., and Zhang, W. (2007). Characterization and identification of microRNA core promoters in four model species. *PLoS Comput. Biol.* *3*, e37.

## Chapter 5. Discussion

### 5.1 Overview

The research presented in this thesis describes changes in histone modification (Chapter 2), DNA methylation (Chapter 3), and gene expression (Chapter 4) in hippocampus of adult mice exposed to ethanol during development. The results show that different but related genes show changes in epigenetic marks and expression. These include changes in apoptotic, synaptic, and oxidative stress genes. In this chapter, the results from Chapters 2 to 4 are synthesized, revealing important trends. Free radical scavenging pathways were implicated in each analysis, particularly the gene expression and combined methylation analyses. The meaning and possible origins of these changes are explored, generating hypotheses for additional work. Additional caveats and considerations for future work are considered.

### 5.2 Implications for Biological Processes

A common approach in genetics is to study a perturbation of a system to better understand its function. Ethanol exposure during synaptogenesis alters hippocampal developmental trajectory by removing cells via apoptosis (Ikonomidou, 2000), impairing neurogenesis (Bonthuis and West, 1991; Gil-Mohapel et al., 2010) reducing both synaptic efficacy (Bellinger et al., 1999), and dendritic spine density (Abel et al., 1983). Such alterations provide insight into neurodevelopmental trajectories, and identify sensitive timepoints. The results of this thesis support a role for molecular changes in these processes. GO and pathway analysis from each chapter implicated differential expression/methylation of synaptic and apoptotic genes. Differential expression of the synaptic gene *Synpo2*, and the apoptosis regulator *Casp3* highlights the alteration of neurodevelopmental genes. Similarly, ethanol can be considered an epigenetic disruptor, and its effects viewed as a challenge to the epigenome during development (Fowler et al., 2012). The results of this thesis show that epigenetic disruption using ethanol results in changes in histone and DNA methylation in adulthood. Examining earlier timepoints in



mice would further the understanding of establishment and maintenance of such epigenetic changes after environmental perturbation (see section 5.6 below).

### 5.3 Free Radical Scavenging Pathway

The histone modification, DNA methylation, and gene expression analyses identified free radical scavenging pathways. The top IPA gene expression pathway was related to the gene expression response to increased free radicals. Peroxisome biogenesis was the top Partek pathway for the combined methylation analysis and the penultimate pathway for DNA methylation. Many lipid-related pathways were implicated across analyses also, further implicating peroxisomes. Few individual ROS genes were identified by multiple experiments. Nevertheless, the implication of differentially regulated free-radical scavenging pathways suggests an altered free-radical scavenging response lasting into adulthood. This thesis reports a novel interface of free-radical scavenging and epigenetic mechanisms, two key processes in FASD etiology.

There are three main possibilities for the origin of these expression and epigenetic changes (**Figure 5.1**). First, these changes were established as a direct response to ethanol during exposure and are maintained to adulthood. Second, these changes were indirectly caused by ethanol as a compensation or amelioration response to ethanol-induced oxidative stress. Third, these changes presented later in life in response to long-term accumulation of oxidative damage. The second explanation is most likely, or perhaps a combination of the three. As discussed, ethanol is known to induce ROS as one of its primary effects on the brain. The genes involved in the response to this stress include those differentially methylated/expressed in this thesis. Cells may have altered the epigenetic regulation of these genes to cope with oxidative stress and its effects. The hypothesis that these changes are established early should be tested with future experiments to distinguish between these possible explanations.

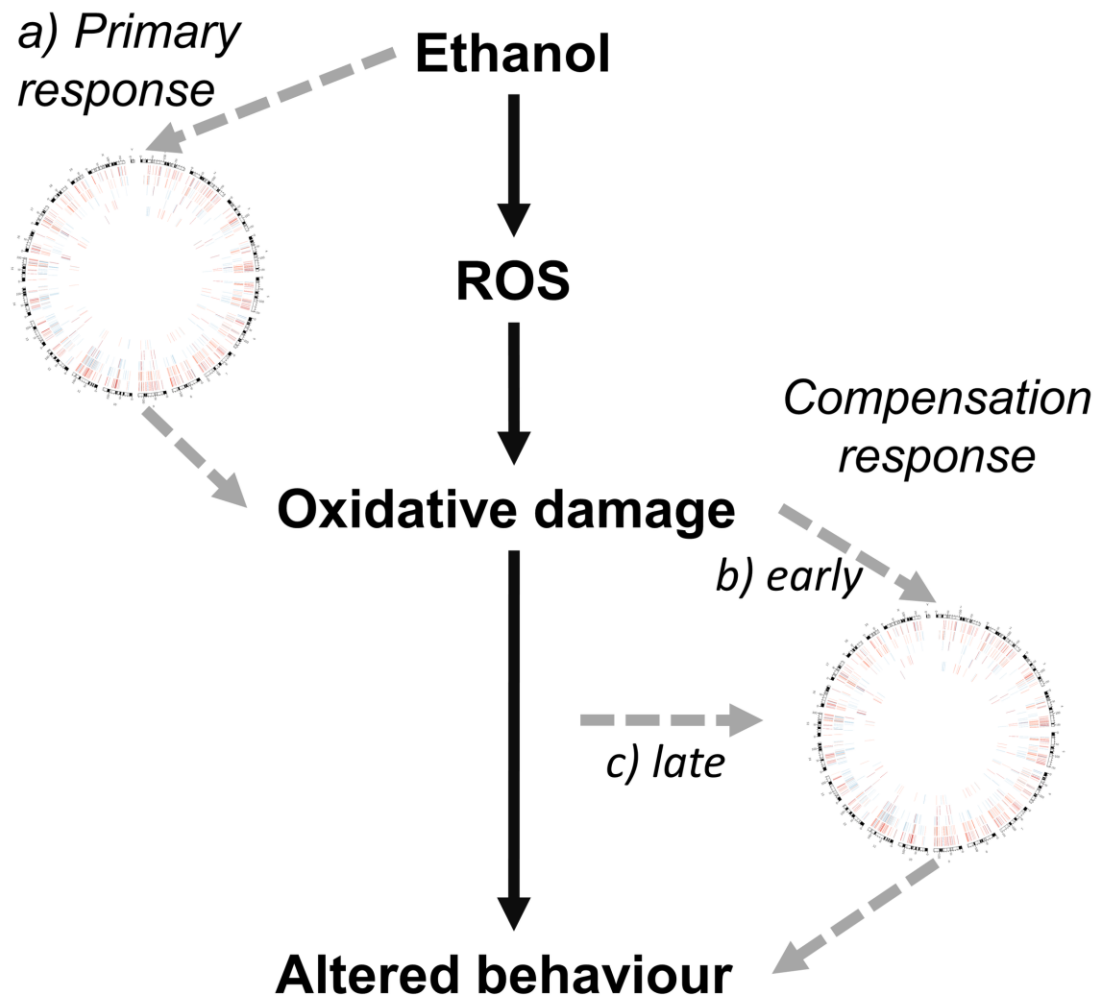


**Figure 5.1 Potential origins of observed epigenetic and gene expression hippocampal profile in response to neonatal ethanol exposure.**

It is well established that in the brain, ethanol leads to increased ROS, leading to oxidative damage, which contributes to altered behaviour (i.e. FASD phenotypes). The epigenetic and gene expression changes identified here (represented by a Circos plot of all the changes identified) may have arisen from: a) the direct action of ethanol during the exposure period, which may then act to perpetuate ethanol-induced oxidative damage; b) an early response to ethanol-induced oxidative cellular damage, acting to ameliorate or compensate for this damage; c) a later response to accumulating oxidative damage over the early life of the mouse, prior to 70 days of age.

## 5.4 Diagnostic and Therapeutic Potential

Biomarkers can serve several roles; an ideal biomarker should be part of the causal pathway of the disease. It should also be well understood, and not related to any unknown factors that are also related to the exposure. If this is the case, it can reduce the validity of the relation between biomarker and disease (Mayeux, 2004). There are two main types of biomarkers: biomarkers of exposure which are used to make predictions, and biomarkers of disease which are used for diagnosis (Mayeux, 2004). Biomarkers of disease in FASD are very challenging since so little is known about its etiology. One can imagine a mark that correlates with the severity of neurodevelopmental challenges, but unless a mechanism is understood, its validity would be suspect. In theory, histone modifications and DNA methylation should have good utility as biomarkers of fetal alcohol exposure. Certain marks at certain genes may indicate how much fetal alcohol exposure has occurred. Importantly, this quantity can be inferred from patient reports and gauged against the molecular changes. These types of markers would be independent of the behavioural outcome however, which is known to vary greatly even with the same exposure.

The data from this thesis implicate *Tcf7l2* as a candidate gene for FASD. *Tcf7l2* showed differential expression, histone methylation, and DNA methylation. *Tcf7l2* encodes a transcription factor in the Wnt signaling pathway. It controls oligodendrocyte differentiation during development, lipid metabolism gene expression, and is the gene most associated with type II diabetes (Oliva et al., 2013). Disruption of myelination via altered *Tcf7l2* expression has the potential to affect synaptic function in the hippocampus and underlie FASD-related learning and memory impairment. Further investigation of this gene may lead to understanding of FASD etiology, and may serve as a diagnostic target.

Changes in H3K4me3 and H4K27me3 occurred at numerous *Pcdh* genes. *Pcdh* genes encode protocadherins, cell-cell signaling molecules involved in synaptogenesis via providing individual neuron identity (Thu et al., 2014). Altered epigenetic regulation of these genes by ethanol could account for some of the abnormalities in synaptic structure in FASD (Sadriani et al., 2012). Recent work from our laboratory and others has implicated differential DNA methylation of *Pcdh* genes in children with FASD (Laufer et

al., 2015; Portales-Casamar et al., 2016). Differential histone methylation at these genes may contribute to an epigenetic signature that will better differentiate affected from unaffected individuals. Employing multiple components makes biomarkers more discerning (Mayeux, 2004).

The implication of oxidative stress pathways, but few single genes does not provide many diagnostic targets. It does however raise the possibility of therapeutics targeting these pathways. Peroxisomes are already the target of therapeutic research in neurological disorders and FASD. Use of peroxisome proliferator-activated receptor (PPAR) agonists is being explored as a possible treatment for FASD (Drew et al., 2015; Kane et al., 2011). Upregulation of peroxisome biogenesis is shown in these studies to prevent many of the detrimental effects of ethanol. Finding therapeutic interventions that work after ethanol exposure is challenging, but important as it is far more relevant to clinical applications. Altered epigenetic methylation of peroxisome genes in this thesis underscores their importance in FASD etiology.

## 5.5 Limitations and Caveats

Each of the technologies used in this thesis have inherent strengths and weaknesses. The use of a promoter microarray focused the study on these regions exclusively, which was more economical and allowed for simplified bioinformatic analysis. However, by examining only promoters, changes in other relevant regions such as enhancers could not be examined. In addition, the DNA capture methods used have inherent biases. For example, MeDIP used in the DNA methylation experiment is most sensitive in regions with low CpG density (Nair et al., 2011). Use of a different technique such as MBD-capture or bisulfite sequencing would likely identify completely different DMRs. ChIP is currently the only viable option to study histone modification changes. The histone modification experiment was inherently limited by characterizing only two modifications out of the 100 or more present in mammalian chromatin. The specific histone modifications assessed in this thesis were chosen for their presence in promoters and known close association with gene expression levels. Nevertheless, it is possible that other more salient changes to other modifications occurred in this model. The results of this thesis are also affected by the intrinsic limitations of mice as a model. Though

mice permit studies not feasible in humans, they are also imperfect models of human disease. In mouse models of FASD specifically, more ethanol per unit body mass must be administered to reach similar BAC levels to humans, since mice metabolize ethanol much faster (Patten et al., 2014). In order to target the third trimester equivalent, ethanol must be injected directly into neonates, bypassing maternal metabolism and the placenta. In terms of the molecular changes identified, mice and humans have similar but distinct genomes, transcriptomes, brain architecture etc. Variation at each of these levels may limit the applicability of specific findings to human FASD. For example, the CpG identified as differentially methylated in Chapter 3 is not present in the human genome. Finally, the experiments of this thesis use a relatively low sample size. Minimal biological replicates were used to reduce microarray costs and allow for multiple epigenetic marks to be assessed. Low sample size may have limited the power of these studies, preventing the possible identification of meaning genes. An increased number of microarrays in each experiment would increase statistical power and potentially identify more/different genes.

## 5.6 Considerations for Future Experiments

The changes in gene expression and epigenetics identified in this thesis represent a component of a much larger field. Expansion of these results to other models and techniques can test their importance in FASD. Several trade-offs were made in this research. Further, questions were generated which could not be addressed in this thesis. As such, there are several improvements and extensions of this research to address for the future. They are as follows:

1. **Additional endpoints in younger mice.** The hypothesis that changes in oxidative stress gene modification and expression can be tested. The hippocampus of younger mice should be assessed for changes in similar free radical pathways, ideally at multiple timepoints from PND 7 to PND 70. This would test whether changes persist from early initiation, or accumulate over time.
2. **Investigation of candidate genes in other models:** Before the candidate genes identified in this thesis (*Tcf7l2*, *Pcdh*) can be explored in a clinical setting, they must be further verified in human studies and animal models. For instance, the

functional significance of *Tcf7l2* should be assessed by determining if protein expression level change in response to ethanol. Functional characterization, such as developmental knock-out studies, would also strengthen the implication of these genes in FASD etiology.

3. **Cell type heterogeneity.** The DNA, RNA, and chromatin samples used in this thesis were extracted from the whole hippocampus. All of the analysis presented represents a mix of the cell types of the region. Bioinformatics techniques to address this heterogeneity, or repetition using cell-type specific techniques may provide further precision and specificity.
4. **Histone modification techniques.** While two histone modifications were assessed from the same chromatin sample, determining modification patterns on individual nucleosomes was not possible. Emerging histone analysis techniques allow characterization of all modifications to each nucleosome (Shema et al., 2016).
5. **Limitations to oxidative damage assays.** Only DNA was available to assess oxidative damage in the experimental mice. As such, more informative and long-lasting markers such as lipid, DNA, and protein peroxidation were not assessed. Use of these assays in the future in this model may validate the oxidative gene expression changes identified here.

## 5.7 Conclusions

A number of conclusions are evident from the results of this thesis. The gene expression, histone modification and DNA methylation analyses provide insight when analyzed separately and together. They show that:

1. Neonatal ethanol exposure results in long-term changes to gene expression, histone modification, and DNA methylation in the mouse hippocampus.
2. In the gene expression experiment, expression of free radical scavenging and olfactory genes were altered.
3. Numerous epigenetic changes occurred across the entire genome; however, changes were enriched a specific gene types.
  - a. H3H4me3 & H3K27me3 changes occurred at:

- i. Protocadherins and other synaptic genes &
    - ii. Imprinted genes
  - b. DNA methylation changes occurred at:
    - i. Peroxisome biogenesis genes.
- 4. The combined analysis of each dataset revealed further enrichment of free-radical scavenging processes.

The results of this thesis provide a compressive dataset on the epigenomic impact of early ethanol exposure. The data provide insight into the actions of ethanol at the molecular level in the hippocampus. The implication of processes observed in other FASD models suggests that similar mechanisms are at work. Failure to identify any one gene consistently supports the heterogeneity the response to ethanol exposure. Oxidative stress pathways are a key component of FASD etiology, and may be a target for therapeutic interventions. Since the epigenome is mutable and regulates many cellular processes it may be an ideal target for such interventions. The results presented also provide insight into basic biologically principles. Chromatin provides both dynamic transcriptional control, and maintenance of long-term repression. Environmental perturbation during brain development was associated with long-lasting changes to chromatin modifications. The fact that a single event during development can have lasting molecular consequences underscores the importance of the environment in shaping human health.

## 5.8 References

- Abel, E.L., Jacobson, S., and Sherwin, B.T. (1983). In utero alcohol exposure: functional and structural brain damage. *Neurobehav. Toxicol. Teratol.* 5, 363–366.
- Bellinger, F.P., Bedi, K.S., Wilson, P., and Wilce, P.A. (1999). Ethanol exposure during the third trimester equivalent results in long-lasting decreased synaptic efficacy but not plasticity in the CA1 region of the rat hippocampus. *Synapse* 31, 51–58.
- Bonthius, D.J., and West, J.R. (1991). Permanent Neuronal Deficits in Rats Exposed to Alcohol during the Brain Growth Spurt. *Teratology* 44, 147–163.
- Drew, P.D., Johnson, J.W., Douglas, J.C., Phelan, K.D., and Kane, C.J.M. (2015). Pioglitazone blocks ethanol induction of microglial activation and immune responses in the hippocampus, cerebellum, and cerebral cortex in a mouse model of fetal alcohol spectrum disorders. *Alcohol. Clin. Exp. Res.* 39, 445–454.
- Fowler, A.K., Hewetson, A., Agrawal, R.G., Dagda, M., Dagda, R., Moaddel, R., Balbo, S., Sanghvi, M., Chen, Y., Hogue, R.J., et al. (2012). Alcohol-induced one-carbon metabolism impairment promotes dysfunction of DNA base excision repair in adult brain. *J. Biol. Chem.* 287, 43533–43542.
- Gil-Mohapel, J., Boehme, F., Kainer, L., and Christie, B.R. (2010). Hippocampal cell loss and neurogenesis after fetal alcohol exposure: Insights from different rodent models. *Brain Res. Rev.* 64, 283–303.
- Ikonomidou, C. (2000). Ethanol-Induced Apoptotic Neurodegeneration and Fetal Alcohol Syndrome. *Science* (80-. ). 287, 1056–1060.
- Kane, C.J., Phelan, K.D., Han, L., Smith, R.R., Xie, J., Douglas, J.C., and Drew, P.D. (2011). Protection of neurons and microglia against ethanol in a mouse model of fetal alcohol spectrum disorders by peroxisome proliferator-activated receptor-gamma agonists. *Brain. Behav. Immun.* 25 *Suppl 1*, S137-45.
- Laufer, B.I., Kapalanga, J., Castellani, C.A., Diehl, E.J., Yan, L., and Singh, S.M. (2015). Associative DNA methylation changes in children with prenatal alcohol exposure. *Epigenomics* 1–16.
- Mayeux, R. (2004). Biomarkers: potential uses and limitations. *NeuroRx* 1, 182–188.
- Nair, S.S., Coolen, M.W., Stirzaker, C., Song, J.Z., Statham, A.L., Strbenac, D., Robinson, M.D., and Clark, S.J. (2011). Comparison of methyl-DNA immunoprecipitation (MeDIP) and methyl-CpG binding domain (MBD) protein.
- Oliva, C.A., Vargas, J.Y., and Inestrosa, N.C. (2013). Wnts in adult brain: from synaptic plasticity to cognitive deficiencies. *Front. Cell. Neurosci.* 7, 224.



- Patten, A.R., Fontaine, C.J., and Christie, B.R. (2014). A comparison of the different animal models of fetal alcohol spectrum disorders and their use in studying complex behaviors. *Front. Pediatr.* 2, 93.
- Portales-Casamar, E., Lussier, A.A., Jones, M.J., MacIsaac, J.L., Edgar, R.D., Mah, S.M., Barhdadi, A., Provost, S., Lemieux-Perreault, L.-P., Cynader, M.S., et al. (2016). DNA methylation signature of human fetal alcohol spectrum disorder. *Epigenetics Chromatin* 9, 25.
- Sadrian, B., Subbanna, S., Wilson, D.A., Basavarajappa, B.S., and Saito, M. (2012). Lithium prevents long-term neural and behavioral pathology induced by early alcohol exposure. *Neuroscience* 206, 122–135.
- Shema, E., Jones, D., Shores, N., Donohue, L., Ram, O., Bernstein, B.E., Rivera, C.M., Ren, B., Bannister, A.J., Kouzarides, T., et al. (2016). Single-molecule decoding of combinatorially modified nucleosomes. *Science* 352, 717–721.
- Thu, C.A., Chen, W. V, Rubinstein, R., Chevee, M., Wolcott, H.N., Felsovalyi, K.O., Tapia, J.C., Shapiro, L., Honig, B., and Maniatis, T. (2014). Single-Cell Identity Generated by Combinatorial Homophilic Interactions between alpha, beta, and gamma Protocadherins. *Cell* 158, 1045–1059.

# Appendices

2007-059-10::6:

**AUP Number:** 2007-059-10

**AUP Title:** Genetic Regulatory Mechanisms: Genes Determining Ethanol Preference in Mice

**Yearly Renewal Date:** 11/01/2013

**The YEARLY RENEWAL to Animal Use Protocol (AUP) 2007-059-10 has been approved, and will be approved for one year following the above review date.**

1. This AUP number must be indicated when ordering animals for this project.
2. Animals for other projects may not be ordered under this AUP number.
3. Purchases of animals other than through this system must be cleared through the ACVS office. Health certificates will be required.

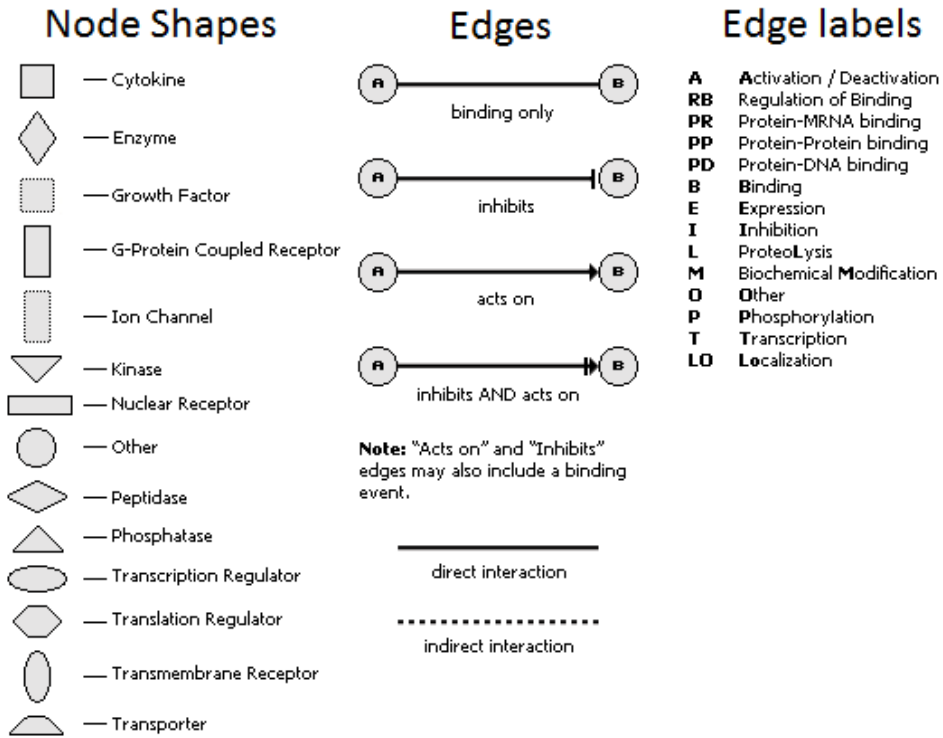
**REQUIREMENTS/COMMENTS**

Please ensure that individual(s) performing procedures on live animals, as described in this protocol, are familiar with the contents of this document.

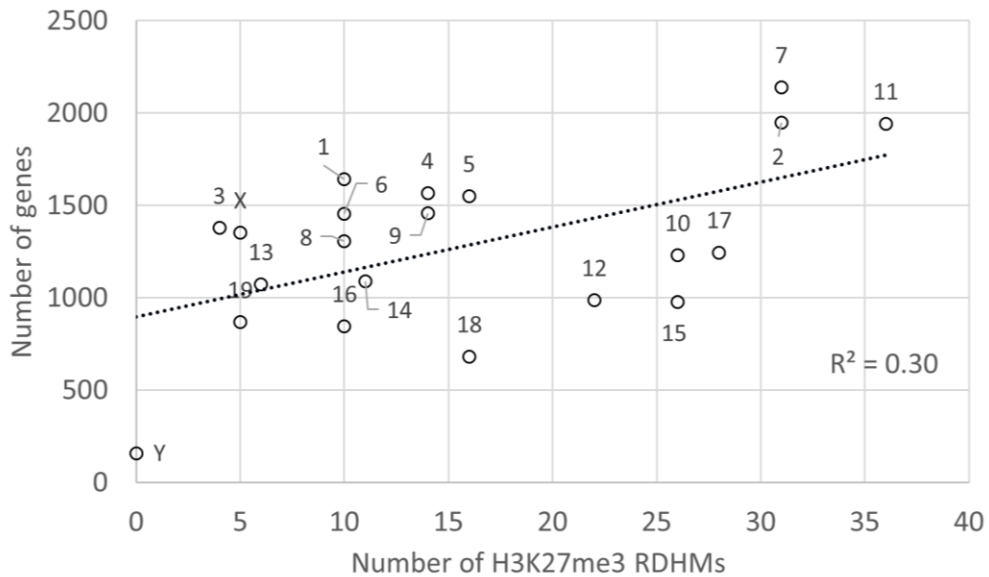
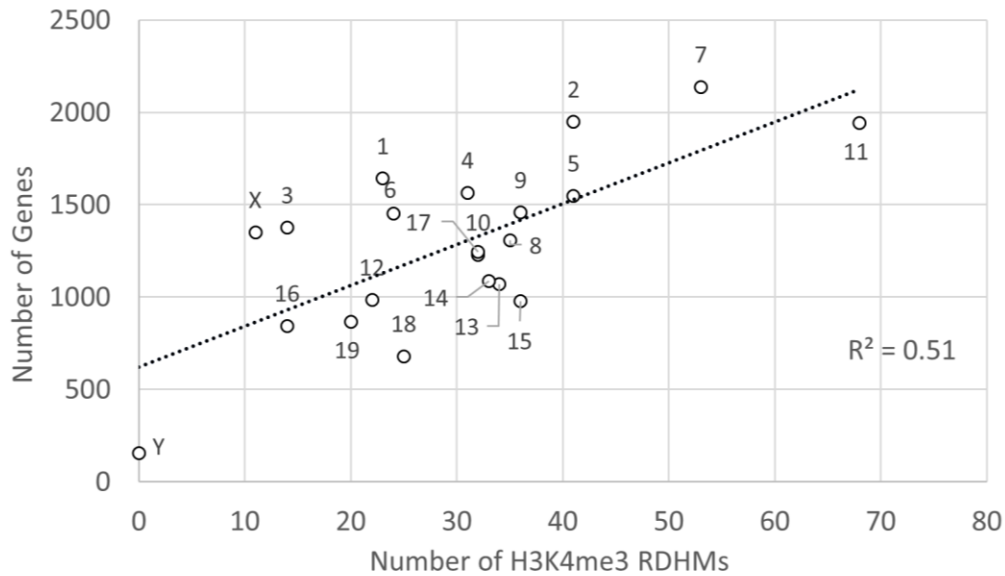
The holder of this Animal Use Protocol is responsible to ensure that all associated safety components (biosafety, radiation safety, general laboratory safety) comply with institutional safety standards and have received all necessary approvals. Please consult directly with your institutional safety officers.

Submitted by: Kinchlea, Will D  
on behalf of the Animal Use Subcommittee

## **Appendix A Animal ethical approval.**



**Appendix B Ingenuity Pathway Analysis (IPA) legend.**



**Appendix C Linear relationship between number of genes and number of regions of differential histone medication (RDHMs) per chromosome.**

Numbers indicate the chromosome associated with each data point.  $R^2$  value calculated in Microsoft Excel.

**Appendix D Affected genes in pathways identified from each software suite in proximity to H3K4me3 changes<sup>†</sup>.**

<b>Pathway name</b>	<b>Genes in pathway and list</b>	<b>p-value</b>
<b>IPA network/pathway</b>		
Carbohydrate Metabolism, Molecular Transport, Small Molecule Biochemistry	<i>Sfrp1, Akt2, Hoxa7, Six3, Tusc2, Socs7, Tspan8, Ctsl, Ddx4, Meis1, Cox4i1, Agt, Mmp2, Brf1, Actn3, Dbh, Pax6, Sox18, Rho, Lipe, Ddit3, Nck2, Tcf7l2, Ralgds, Trpv6, Gyk, Fgf1, Slfn4, Ptpn, Ptpnj, Emx2, Rb1, Arntl, Gprc6a, Iigp1, Flt4, Phox2b, Eef2k, Grk6, Tmem119, Cyp24a1, Pdc4, Prl3d2, Col6a2, Fgfr1, Lamb2</i>	10E-63
Hematological System Development and Function, Tissue Morphology, Cell Death and Survival	<i>Ptpre, Vamp2, Bst2, Ntrk1, Cd27, Thpo, Flii, Jak3, Tln1, Nedd4, Rnf31, Rbck1, Ebf1, Cyp3a16, Col15a1, Rnasel, Myd88, Sh3bp2, Gata3, Arrb1, Sigirr, Ptpn5, Notch4, Drd5, Snap23, Scfd1, Mapk8ip1, Sct, Smpd3, Mir22, Efs, Fas</i>	10E-49
Humoral Immune Response, Protein Synthesis, Cellular Function and Maintenance	<i>Tbc1d17, Rbp3, Tef, Gng4, Crip1, Chill, Pbx2, Pcp4, Cryba1, Nlrp4f, Rad21, Ncs1, Zp1, Muc1, Eci1, Polk, Tia1, Cenpp, Slain1, Senp7, Rnps1, Tra2a, Crybb3, Id3, Snn, Ifi30</i>	10E-31
Endocrine System Disorders, Gastrointestinal Disease, Immunological Disease	<i>Pou3f3, Pip5k1c, Psd2, Tapbpl, Ecsit, Acat3, H2-DMA, Rhcg, Gas7, Gja5, Lpin2, Acsl6, Parp14, Abca8b, Fcgr1, H2-Eb1, Ctsw, Dock5, Mst1, Trex1, Prpf8, Psme2, Capn5, Arhgef10, Spdef, Homer2, Gpr146</i>	10E-25
Endocrine System Development and Function, Lipid Metabolism, Small Molecule Biochemistry	<i>Hoxd3, Hsd17b3, Gdf10, Abcc4, Rps29, Rgs16, Glra1, Ttyh1, Ankrd6, Ndufa7, Ccdc74a, Ogfr, Tll7, Dnmt3a, Col4a3bp, Krtdap, Atp6v1f, Sptb, Cox6c, Rps10, Rps15, Mat2a, Ncoa7, Fgf18, Smarcc1, Taf10, Spen</i>	10E-24
Cellular Development, Cellular Growth and Proliferation, Cancer	<i>Gprasp1, Pcdha2, Mid1, Arpc4, Pcdha3, Pcdha4, Pcdha10, Ryr1, Bai1, Kctd20, Odf3b, Gpr123, Ap1m1, Jph1, Jakmip1, Mir138-2, Cfc1, Lpar3, Nuak2, Inf2, Sema4c, Asic1, Stip1, Cnot6l, Mrgpra3, Faim2, Foxm1, Ltbp4, Serpina5, Akap1</i>	10E-24
Cell Morphology, Connective Tissue Development and Function, Cellular Development	<i>Ptbp1, Eno1, Naip1, Hes5, Creb3, Syn1, Tnk2, Noxa1, Slc14a1, Crip2, Urod, Cnn2, Gtf3c2, Bcr, Fsd11, Mlh1, Ptp4a3, Ptk7, Mzb1, Pcca, Scpep1, Dhrr7, Rbm3, Shisa5, Hdlbp, Rgs12, Idh3g, Slc38a9</i>	10E-23

Energy Production, Lipid Metabolism, Small Molecule Biochemistry	<i>Ndufa8, Chtf18, Akt1s1, Csnk2b, Rasl10b, I100001G20Rik, Akr1c21, Slc4a4, Tmem176a, Tmem176b, Omp, Arpp21, Scd4, C1qtnf5, Gpr17, Recql4, Tc2n, Rai1, Slc16a1, Macrodl, Slco2b1, Trrap, Cacng3, Hap1, Ube2v1</i>	10E-22
Endocrine System Development and Function, Carbohydrate Metabolism, Molecular Transport	<i>Insrr, Mras, Itpr3, Amn, Aars, Irak, Ibp1, Trpm5, Pycr1, Hgfac, Cbx4, Sertad1, Tmod1, Oog1, Slc38a4, Fgf15, Dmtn, Ssbp2, Ank1, Erollb, Fbxl17, Fermt3, Ctbp2, Rph3al</i>	10E-20
Cellular Growth and Proliferation, Cell Morphology, Cellular Assembly and Organization	<i>Rassf1, Vmn2r85, Gm11937, Ndst1, Agtpbp1, Mcf2l, Acaa1a, Hhatl, Nlrp6, Myadml2, Serpina12, Mtus1, Gprin1, Krtap19-3, Mbp, Cmip, Paqr7, Zfp106, Pcyox1, Neu2, Cyp2s1, Cirbp, Pde4c, Gne, Vars, Ip6k2</i>	10E-20
Embryonic Development, Organismal Development, Gene Expression	<i>Plekhf1, Chrd, G530011006Rik, Gcm2, Vmn1r44, Serpinf2, Mical2, Shank2, Lrrfip1, Prrxl1, Isl2, Tsta3, Mmp15, Grik5, Slc22a22, Sv2b, Cit, Rnase2a, Zfp521, Aut2, Lbx1, Pax9, Osr2, Btrc</i>	10E-18
Cellular Movement, Immune Cell Trafficking, Hematological System Development and Function	<i>Pde2a, Rnf19a, Hmnr, Rtcbl, Tst, Serpinb9e, Rbfox1, Dsc3, Kctd10, Rab19, Alyref, Neu1, Slc35d3, Lims2, Snph, Nkx2-3, Cdhr5, H13, Hnrnpk, Eif1</i>	10E-17
Lipid Metabolism, Molecular Transport, Small Molecule Biochemistry	<i>Grik3, Matn1, Cmtm6, Mir7-1, St6galnac4, Krt31, Apbb1, Gfap, Rbpjl, H2-Ke6, Matn4, Mknk2, Erv3, Acsl4, Nr2e3, Olfm1, Prl7d1, Pnoc, Rsl1d1, Chrna9, Pdlim4, Ncor1</i>	10E-14
<b>IPA canonical</b>		
Regulation of cellular mechanics by calpain protease	<i>Ptk2, Capn5, Rb1, Mras, Ln1, Capn9</i>	0.0039
Fatty acid $\beta$ -oxidation	<i>Acaa1, Acsl6, Acsl4, Eci1, Hsd17b8</i>	0.0044
Amyotrophic lateral sclerosis signaling	<i>Capn5, Naip, Grik5, Gdnf, Grik3, Capn9, Rnf19a, Ssr4</i>	0.0088
Bladder cancer signaling	<i>Rb1, Fgf18, Mmp15, Mras, Mmp2, Rassf1, Fgf1, Fgf19</i>	0.013
Thyroid cancer signaling	<i>Gdnf, Ntrk1, Mras, Rxrb, Tcf7l2</i>	0.014
Giloma invasiveness signaling	<i>Ptk2, Timp1, Hmnr, Mras, Mmp2, Timp2</i>	0.016
Non-small cell lung cancer signalling	<i>Rb1, Akt2, Itpr3, Mras, Rxrb, Rassf1</i>	0.029
Sphingomyelin metabolism	<i>Smpd4, Smpd3</i>	0.032
Estrogen biosynthesis	<i>Hsd17b3, Cyp3a5, Hsd17b8, Cyp2s1</i>	0.035

Spliceosomal cycle	<i>U2af2</i>	0.038
FGF signaling	<i>Akt2, Fgf18, Fgfr1, Creb3, Map2k3, Fgf1, Fgf19</i>	0.040
TREM1 signaling	<i>Sigirr, Nod2, Akt2, Nlrp6, Myd88</i>	0.045
FAK signaling	<i>Ptk2, Capn5, Akt2, Hmnr, Mras, Tln1, Capn9</i>	0.048
<b>Partek Pathway</b>		
Pathways in cancer	<i>Akt2, Amn, Bcr, Ctbp2, Fas, Fgf1, Fgf15, Fgf18, Fgfr1, Flt3, Lamb2, Mlh1, Mmp2, Ntrk1, Ptk2, Ralgds, Rassf1, Rb1, Rxb, Tcf712</i>	0.034
Fatty acid metabolism	<i>Acaa1a, Acsl4, Acsl6, Fas, Scd4</i>	0.035
Sphingolipid metabolism	<i>Cers1, Neu1, Neu2, Smpd3, Smpd4</i>	0.040
<b>Enrichr KEGG</b>		
MAPK Signaling pathway	<i>Fas, Map2k3, Ntrk1, Fgf1, Cacng3, Ecsit, Mknk2, Fgf18, Ddit3, Arrb1, Fgfr1, Mras, Ptpn5, Akt2, Mapk8ip1</i>	0.041
Sphingolipid metabolism	<i>Neu1, Neu2, Smpd3, Smpd4</i>	0.046

†*p*-values provided for each pathway are shown (right-tailed Fishers exact test).

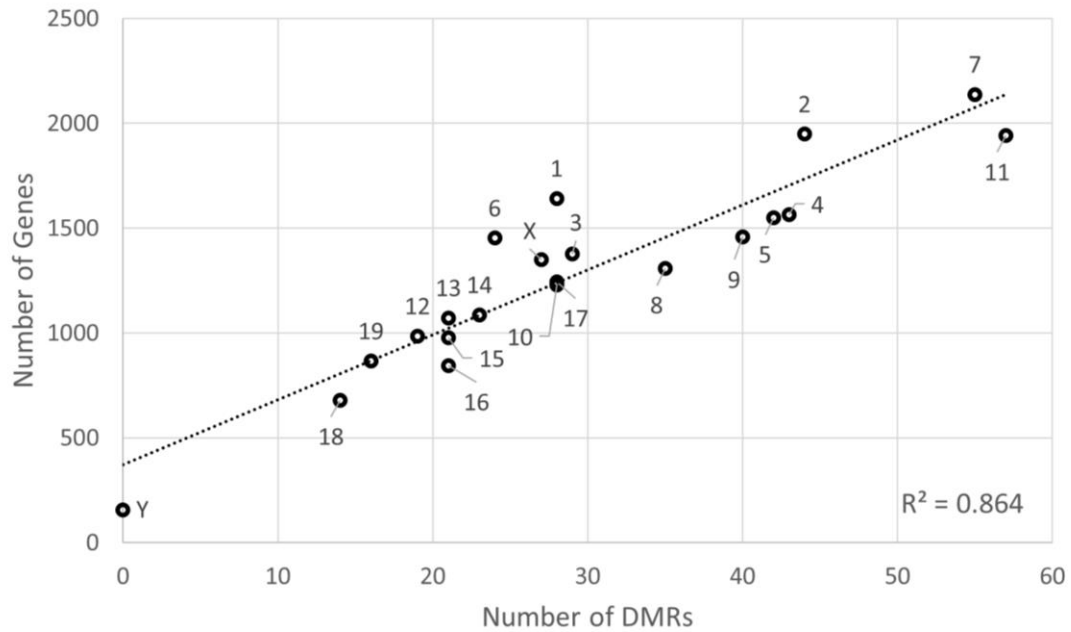
**Appendix E Genes bearing both H3K4me3 and H3K27me3 changes<sup>†</sup>.**

Gene name	H3K4-me3 MAT score	H3K4me3 <i>p</i> -value	Distance from TSS	H3K27- me3 MAT score	H3K27- me3 <i>p</i> - value	Distance from TSS	Reciprocal
<i>E030025P04Rik</i>	4.33	0.000375	-2489	3.14	0.000375	-2489	
<i>Elfn2</i>	-5.24	0.0000936	41237	1.90	0.00246	5169	R
<i>Fbrsl1</i>	-4.35	0.000281	-2406	1.12	0.00815	23673	R
				3.21	0.000375	8911	
<i>Fbxl16</i>	-4.56	0.0000936	6620	12.76	0.000753	6620	R
<i>Flii</i>	6.23	0.0000936	-577	4.42	0.000187	577	
<i>Gareml</i>	5.05	0.0000936	-2491	3.06	0.000385	-2491	
<i>Grik3</i>	-5.15	0.0000936	4162	-13.08	0.000667	4162	
<i>H2-DMa</i>	-4.08	0.0002809	13252	-14.26	0.000475	13252	
<i>Hoxa7</i>	-6.18	0.0000936	-2823	-19.74	0.0000936	-2823	
<i>Mief2</i>	6.22	0.0000936	-579	4.42	0.000187	-579	
<i>Mir5100</i>	6.22	0.0000936	-844	4.42	0.000187	-844	
<i>Myadml2</i>	0.998	0.0002809	1056	-13.03	0.000655	1056	R
<i>Ndor1</i>	-6.04	0.0000936	4744	-12.76	0.000749	4744	
<i>Pcdha4-g</i>	-4.11	0.0002809	486398	-12.45	0.001311	540697	
				-14.11	0.000468	781334	
				-10.87	0.003558	722971	
				1.07	0.00899	365221	R
				2.02	0.001966	400019	R
				-11.29	0.002528	-3178	
<i>Pcdhga1</i>	-11.16	0.0000936	72130	-14.11	0.000468	72130	
	-8.17	0.0000936	13767	-10.87	0.003558	13767	
<i>Pcdhga2</i>	-11.16	0.0000936	64970	-14.11	0.000468	64970	
	-8.17	0.0000936	6607	-10.87	0.003558	6607	
<i>Pcdhga3</i>	-11.1605	0.0000936	59740	-14.11	0.000468	59740	
	-8.17	0.0000936	1377	-10.87	0.003558	1377	
<i>Pcdhga4</i>	-11.16	0.0000936	48675	-14.11	0.000468	48675	
<i>Pcdhga5</i>	-11.16	0.0000936	39574	-14.11	0.000468	39574	
<i>Pcdhga6</i>	-11.16	0.0000936	26846	-14.11	0.000468	26846	
<i>Pcdhga7</i>	-11.16	0.0000936	19241	-14.11	0.000468	19241	
<i>Pcdhga8</i>	-11.16	0.0000936	8369	-14.11	0.000468	8369	
<i>Pcdhga9</i>	-11.16	0.0000936	-2841	-14.11	0.000468	-2841	
<i>Pcdhgb1</i>	-11.16	0.0000936	53617	-14.11	0.000468	53617	
<i>Pcdhgb2</i>	-11.16	0.0000936	44216	-14.11	0.000468	44216	
<i>Pcdhgb4</i>	-11.16	0.0000936	13521	-14.11	0.000468	13521	
<i>Pcdhgb5</i>	-11.16	0.0000936	2921	-14.11	0.000468	2921	



<i>Pebp4</i>	4.30	0.0003747	-2474	4.13	0.000187	-2474	
<i>Pycr1</i>	-4.16	0.0002809	-3591	-13.03	0.000655	-3591	
<i>Rai1</i>	4.28	0.0003745	-2491	1.14	0.007491	10315	
				3.51	0.000375	76874	
<i>Rassf1</i>	-5.00	0.0000936	3765	-13.01	0.000655	3765	
<i>Tmem203</i>	-6.04	0.0000936	-4768	-12.76	0.000749	-4768	
<i>Tusc2</i>	-5.00	0.0000936	-4887	-13.01	0.000655	-4887	

<sup>†</sup>The degree of enrichment (MAT score) and *p*-value for each RDHM is shown for each gene (two-way ANOVA). The distance from the region of differential histone methylation (RDHM) to the transcriptional start site (TSS) of the gene in base pairs is also shown. Negative distance indicates that the RDHM is upstream of the TSS. The reciprocal column is marked if the two methylations have a reciprocal relationship, i.e. one is increased and the other decreased indicating the same predicted effect on gene expression.



**Appendix F Linear relationship between number of genes and number of differentially methylated regions (DMRs) per chromosome.**

Numbers indicate the chromosome associated with each data point.  $R^2$  value calculated in Microsoft Excel.

**Appendix G Affected genes in pathways significantly enriched with genes proximal to differentially methylated regions (DMRs).**

Network name	Affected genes	p-value
<b>IPA</b>		
Cellular Movement, Cell Death and Survival, Cellular Development	<i>Acadvl, Adcyap1, Bai1, Banp, Bmp7, Camk2n1, Cc2d1a, Ccl17, Cd151, Cd1d, Cd38, Cd3e, Cd70, Cdc25c, Cdh15, Cenpa, Csf1r, Csk, Ctsb, Ctsh, Cyld, Cyp11b2, Cyp27b1, Ddx5, Dhx58, Dll4, Dusp4, E2f3, Egr2, Fat1, Fbln2, Fgf1, Flna, Gas2l1, Gata1, Gins2, Gjb1, Golt1b, Grn, Hdac11, Hgs, Hipk2, Hist1h2ab, Hspa1a/hspa1b, Id2, Il13, Il13ra2, Il17rd, Il21r, Itga5, Kat2a, Lsp1, Mcl1, Mir-135, Mir-143, Mir-146, Mir-26, Myd88, Ndfip2, Neurog3, Nos2, Nppc, Ntn1, Numbl, P2ry2, Pcdha5, Pgf, Plcd1, Pole, Polr2a, Ptger4, Rbl2, Rbp1, Recql, Relb, S100a6, S100a9, Sirpa, Slc9a8, Snupn, Socs2, Spn, Stra6, Tac1, Tacc2, Tardbp, Tff1, Thbs4, Thpo, Timp3, Tnfsf4, Tnk2, Tp73, Trak1, Trib3, Trps1, Tshz3, Uba7, Ung, Vdr, Vegfa, Vkorc11l, Wnk2</i>	10E-130
Cell Cycle, Cellular Development, Cellular Growth and Proliferation	<i>Antxr1, Atp5b, Bcl2l12, Bclaf1, Bik, Capn3, Ccdc33, Cchr1, Cdc25c, Ctsd, Cul4a, Cxxc1, Ddx5, Egr2, Eif4a2, Elf4, Foxl2, Foxp4, Fzd4, Gemin5, Gpa33, Hist4h4, Hopx, Ifitm2, Kctd13, Lnx2, Lpin1, Lsm2, Mettl1, Mir-135, Mir-150, Mir-188, Mir-26, Mir-324, Mir-338, Mir-486, Naca, Nav2, Ndufb5, Ndufs8, Nos1, Npas1, Numbl, Pax6, Pla2r1, Poldip2, Ptpu, Rap2b, Rbm3, Sf3a1, Slc39a3, Snapc1, Tagln2, Tall, Thpo, Tmem97, Unc45a</i>	10E-50
Inflammatory Response, Cellular Movement, Immune Cell Trafficking	<i>Acaal, Acss2, Ambp, Aoah, Ap1g2, Aplp1, Bcan, C9orf9, Carhsp1, Cd151, Cd177, Clasp1, Clstn1, Colq, Csnk2a2, Ctsb, Derl2, Dgkz, Dlec1, Dlg4, Efnb3, Epha2, Esrrg, Fam53c, Fat1, Fgf1, Fgf4, Fmn2, Gcc1, Hs6st1, Htr6, Igfbp2, Il17rd, Iscu, Itga5, Itm2c, Kcnip1, Kcnj12, Lamc1, Mir-146, Mir-196, Nos2, Nrn1, Pdlim4, Prmt2, Ptger4, Rab21, Scamp3, Slc1a2, Smtn, Ssh3, Tac1, Timp3, Tnni3, Tspan4, Usp2, Vamp4,</i>	10E-50
Organismal Development, Tissue Development,	<i>Actc1, Arf5, At1l, At12, Cct6a, Cdo1, Ceacam1, Chac1, Cnn2, Ddx5, Dlgap5, Dll1, Dpep1, Eif3i, Enpp4, Exosc6, Gtf2h1, Hsd17b2, Igf2bp2, Il11ra, Impa2, Iqgap2, Krt80, Lamp2, Lef1, Lrch4,</i>	10E-43

Embryonic Development	<i>Lypd6b, Mecr, Mrap, Msl3, Nfx1, Nipal2, Nmb, Nop2, Nup50, Onecut1, Otx2, Oxt, Pik3ap1, Pir, Polr1d, Polr2a, Polr2h, Ptch2, Samm50, Sema3f, Tmem17, Tmem64, Tmem97, Trpv4, Tspan17, Umodl1,</i>	
Cell Death and Survival, Cellular Development, Cellular Growth and Proliferation	<i>Aatk, Abcb10, Agrn, Arl16, Bre, Clqtnf4, C4orf19, Cdc25c, Chpf, Dapk2, Dmrt3, Dpp7, Ebna1bp2, Emilin2, Fam167a, Fgf1, Fhdcl, Galnt6, Gata5, Glp2r, Il20rb, L3mbtl3, Lad1, Mfi2, Mis12, Mybbp1a, Myd88, Nfatc3, Nr1d2, Nr1h4, Nudt11, Pgam1, Rab17, Rhbdl2, Rpp25, Scn1b, Scx, Sema5b, Sema7a, Sos2, Stx12, Sytl2, Tjap1, Tmcc3, Tnfrsf21, Trib3,</i>	10E-35
<b>Partek pathway</b>		
Hematopoietic cell lineage	<i>Cd1d1, Cd3e, Cd38, Csf1r, Gm2002, Gm13305, Il11ra1, Il11ra2, Itga5, Thpo</i>	0.0003
Peroxisome	<i>Acaa1a, Hao2, Mpv17l, Mvk, Nos2, Peci, Pex26, Pxmp2, Slc25a17</i>	0.0006
Jak-STAT signaling pathway	<i>Gm2002, Gm13305, Il11ra1, Il11ra2, Il12rb1, Il13, Il13ra2, Il20rb, Il21r, Socs2, Sos2</i>	0.0006
Lysosome	<i>Abcb9, Ap1g2, Ap1s1, Arsg, Ctsb, Ctsd, Ctsh, Lamp2, Tcirgl</i>	0.003
Taurine and hypotaurine metabolism	<i>Cdo1, Ggt6</i>	0.009
<b>Enrichr KEGG</b>		
Peroxisome	<i>Slc25a17, Mvk, Nos2, Pxmp, Mpv17l, Hao2, Pex26</i>	0.024
Lysosome	<i>Ap1g2, Lamp2, Ap1s1, Ctsh, Arsg, Abcb, Tcirgl, Ctsd, Ctsb</i>	0.026

**Appendix H Affected genes in pathways significantly enriched with genes proximal to differentially methylated regions (DMRs) or regions of differential histone modification (RDHMs).**

Pathway name	Genes in list	p-value
<b>IPA</b>		
Embryonic Development, Organismal Development, Cellular Development	<i>Apbb1, Aplp1, App, Bmp7, Brf1, Ceacam1, Cox4I1, Dbh, Ddx4, Ddx5, Derl2, Dis3, E2F3, Eef2K, Eif5B, Fgf1, Fgf4, Fgfr1, Gnaz, Gprc6A, Gyk, Hoxb9, Hoxd3, Hoxd9, Hoxd10, Hs6St1, Htr3A, Id3, Itga5, Itm2B, Itm2C, Lamb2, Mecer, Meis1, Ncs1, Nr1H4, Nrg1, Ntn1, Numbl, Otx2, Pax6, Pcd4, Pgf, Phf1, Phox2B, Ppargc1B, Rb1, Rbl2, Rbp1, Rho, S100A6, Six3, Slc14A1, Socs7, Suv420H1, Tcf7L2, Tusc2</i>	10E-64
Cardiac Hypertrophy, Cardiovascular Disease, Developmental Disorder	<i>Acss2, Actc1, Adcyap1, Antxr1, Cc2D1A, Cd53, Cd5L, Cdo1, Cxxc1, Cyp24A1, Cyp27B1, Dleu2, Flt3, Flt4, Foxl2, Gdnf, Hoxa7, Igf1, Inhba, Jph4, Lh, Lingol, Mb, Nos1, Nos2, Nrgn, Polr2A, Ptger4, Ptpre, Ptprij, Ptpri, Ralgds, Relb, Retnlb, Serpinh1, Sfrp1, Sfxn1, Slc39A14, Slc8A1, Socs2, Syn1, Tkt, Tmem119, Tnk2, Tnni3, Trpv6, Tspan2, Tspan17, Ttyh1, Vdr, Zbtb20</i>	10E-56
Humoral Immune Response, Protein Synthesis, Hematological System Development and Function	<i>Abcc4, Abcg2, Arhgef10, Bcl3, Bik, Bst2, Cabin1, Ccl17, Cd27, Cd38, Cd70, Dhx58, Dll4, Dnmt3A, Drd5, Ebf1, Efs, Gas7, Gata3, Glra1, Grn, Ifit3, Il25, Il13Ra2, Il20Rb, Il21R, Jak3, Lef1, Mafk, Mapk8Ip1, Mat2A, Myd88, Nod2, Notch4, Ntrk1, Pou3F1, Rxrb, Smarcc1, Tardbp, Tcirg1, Tmem97, Tnfrsf21, Trex1, Uba7, Ung</i>	10E-49
Cellular Development, Cellular Growth and Proliferation, Hematological System Development and Function	<i>Adcy7, Ager, Asap1, Cd3E, Csf1R, Csk, Cyld, Dgkz, Dmtn, Dok3, Dusp4, Egr2, Epha2, Esrrg, Fas, Flii, Il13, Lamc1, Lamp2, Lpin1, Map2K3, Mcf2L, Mcl1, Mif, Pik3Ap1, Plec, Prmt2, Ptk2, Rbck1, Rnf31, Scfd1, Sh2B2, Sh3Bp2, Sigirr, Sirpa, Smpd3, Snap23, Stra6, Thpo, Tnfsf4, Vegfa</i>	10E-41
Skeletal and Muscular Disorders, Developmental Disorder, Hereditary Disorder	<i>Abca7, Acot11, Actc1, Actn3, Ankrd6, Arntl, Atp1B2, Bhmt, Capn3, Cd151, Cd177, Fat1, Flna, Igf2Bp2, Impa2, Inf2, Kcnk3, Ldb3, Lipe, Lpar3, Lrch1, Ncoa7, Nphs1, Nr1D2, P2Ry2, Pnpla2, Rgs19, Slc35D3, Sox18, Srpk3, Tmem40, Tst, Tsta3</i>	10E-30

Hematological System Development and Function, Tissue Morphology, Cell-To-Cell Signaling and Interaction	<i>Acs16, Arsg, Ccl17, Cip1, Cryba1, Crybb3, Dusp4, Ebna1Bp2, Gtf2H4, Homer2, Il12Rb1, Kat2A, Lad1, Map2K3, Mst1, Mvk, Ndfip2, Nedd4, Nrn1, Pbx2, Pla2R1, Polr1D, Rasa2, Rgs16, Rnps1, Skal, Slain1, Socs2, Tia1, Usp2, Vdr, Zfhx3</i>	10E-26
Endocrine System Development and Function, Molecular Transport, Protein Synthesis	<i>Aatk, Ank1, Atp5B, Cbx4, Ctsd, Ero1Lb, Fbxl17, Fem1B, Foxp4, Gpr17, Hipk2, Hsd17B3, Igf1, Insrr, Ip6K1, Itpr3, Kctd10, Lims2, Lpin1, Mfi2, Mrap, Mrpl47, Mybbp1A, Ntrk1, Pnpla2, Rbm39, Rnasel, Rph3A1, Sertad1, Socs2, Sptb, St6, Galnac4, Taf10, Timp2</i>	10E-24
Cell Death and Survival, Antimicrobial Response, Inflammatory Response	<i>Agl, Bcr, Cc2D1A, Ccl17, Cd70, Cd300E, Ceacam1, Clstn1, Dhx58, Dll1, Dock5, Dsc3, Ebf1, Glp2R, Hes5, Ifi47, Ifit3, Iigp1, Irak1Bp1, Lrrfip1, 42801, Mettl1, Mzb1, Parp14, Sigirr, Slc39A14, Sox1, Spn</i>	10E-23
Cell-To-Cell Signaling and Interaction, Hematological System Development and Function, Immune Cell Trafficking	<i>Ap1S1, Apol6, Bcan, C1Qtnf5, Calb2, Capn5, Dpp7, Egr2, Emx2, Fermt3, Gata3, Gdnf, Gins2, Gja5, Gpr146, Hapln2, Il12Rb1, Kenk9, Mras, Nfatc3, Nr1H4, Orail, Pam16, Pip5K1C, Pou3F3, Prpf8, Psd2, Rhcg, Socs2, Tac1, Tapbpl, Tc2N, Tcirg1</i>	10E-21
Embryonic Development, Organismal Development, Cell-To-Cell Signaling and Interaction	<i>Arpp21, Atp2B3, Cacng3, Casz1, Cdadcl, Cnot6L, Dapk2, Dhrrs7, Dll1, Eif1, Epha2, Fam32A, Flna, Fmn2, Fzd4, Fzr1, Gdf10, Hes5, Hmnr, Hnrnpk, Macf1, Macrodl, Mapk8Ip1, Mesp1, Myo1F, Neu1, Nup50, Pde2A, S100A9, Scn1B, Snn, Spen, Tff1</i>	10E-20
Cell-To-Cell Signaling and Interaction, Reproductive System Development and Function, Tissue Development	<i>Abcb10, Acs14, Adam3, Appl2, Ccl6, Chrna9, Clasp1, Cmtm6, Cyth3, E330034G19Rik, Erv3, Fscn3, Hoxc10, Krt31, Lpin1, Lpin2, Map2K3, Mbnl3, Mtus1, Muc1, Neu2, Nlrp4F, Pcyox1, Pde4C, Rbp3, Rsl1D1, Tia1, Tmem64, Tpst2, Tspan4, Usp2, Wee2, Zpl</i>	10E-20
Cell Death and Survival, Lipid Metabolism, Small Molecule Biochemistry	<i>Acadvl, Als2Cr12, Ap1b1, Asb2, Cenpp, Chtf18, Csf1r, Ctsd, Epha2, Faim2, Gng4, Gpr160, Inhba, Mlh1, Ndst1, Omp, Plscr3, Pole, Ppargc1b, Rai1, Rasl10b, Recql4, Rhof, Scd4, Senp7, Stip1, Tac1, Timp3, Tmem176a, Tmem176b, Ublcpl</i>	10E-20

Cell Cycle, DNA Replication, Recombination, and Repair, Cellular Development	<i>Arl6ip6, Asic1, Banp, Bclaf1, Camk2n1, Colq, Cyp2s1, Dhx40, Dnal4, Emilin2, Eno1, Fscb, Ip6k2, Ldlrad3, Matn1, Matn4, Naf1, Nr2e3, Olfm1, Pcdha2, Pcdha3, Pdlim4, Pgam1, Ptp4A3, Qrich1, Sema3F, Serpina12, Slc16a1, Smtn, Snrk, Trrap</i>	10E-19
Embryonic Development, Organismal Development, Cell Morphology	<i>Ap1m1, Auts2, Ccdc74a, Cenpa, Col4a3bp, Cst12, Disp2, Dmrt3, Dmrta2, Dmrtc1b, Dnm1, Dock9, Emb, Fgfr1, Foxm1, Fsd11, Gata1, Gzmc, Hsd17b2, Id2, Ifitm2, Inhba, Klr1, Krtdap, Mical2, Nav2, Ogfr, Ptbp1, Ptk7, Rab19, Sult1e1, Sv2b, Sytl2, Tbx4</i>	10E-19
Cell Death and Survival, Cancer, Cellular Development	<i>Anapc4, Astn2, Atp5k, Carhsp1, Cd38, Cnn2, Creb3, Crip2, Dpep1, Elf4, Fbln2, Gtf2h1, Gtf3c2, Hdlbp, Idh3G, Ifi30, Lsp1, Mlh1, Mpv17l, Noxa1, Pcca, Prdx4, Ptp4a3, Ptpu, Rap2b, Rbm3, Rgs12, Scpep1, Stip1, Tacc2, Tinagl1, Urod</i>	10E-19
Cell-To-Cell Signaling and Interaction, Nervous System Development and Function, Behavior	<i>Adam11, Arpc4, Atp5B, Bai1, Bcl3, Bhmt, Cant1, Cirbp, Cit, Cmip, Ctsw, Dlg4, Dusp4, Emilin1, Gemin5, Gne, Gpr123, Grik5, Iqsec2, Nuak2, Pcdha4, Sema4c, Sf3a1, Shank2, Sik1, Slc1a2, Slc4a4, Spdef, Stx1b, Svs2, Tbc1d17, Vamp2</i>	10E-18
Lipid Metabolism, Small Molecule Biochemistry, Molecular Transport	<i>1100001G20Rik, Acadvl, Apoc1, B3gnt6, Ctsd, Eci1, Fgf18, Lbx1, Matk, Mir705, Ncor1, Nthl1, Paqr7, Prl7dg1, Rbpjl, Rnf19a, Sardh, Sfxn4, Socs2, Sycp3, Tef, Tmem159</i>	10E-18
Cell Morphology, Cell Death and Survival, Nervous System Development and Function	<i>Agtpbp1, Aoah, Atp6v1f, Cct6a, Chrd, Cox6c, Evc, Fyttl1, Gfap, Hhatl, Hoxb3, Htr6, Jph1, Mbp, Ndufa7, Ndufa8, Ndufb5, Ndufs8, Psme2, Rassf1, Rgs16, Rpl10a, Rps10, Rps15, Rps29, Ryr1, Sct, Tln1, Tnpo3, Tll7, Vars</i>	10E-16
Cell-To-Cell Signaling and Interaction, Nervous System Development and Function, Cellular Development	<i>Aars, Agap1, Agrn, Akap1, Ccdc109b, Cdhr5, Ebf2, Gprasp1, Gprin1, Ifitm5, Jakmip1, Mfap4, Mid1, Odf3b, Otx2, Pde1b, Polk, Pycr1, Rab17, Rad21, Rbfox1, Retnlb, Sephs1, Shisa5, Ssbp2, Thbs4, Tra2a</i>	10E-16
Lipid Metabolism, Small Molecule Biochemistry, Vitamin and Mineral Metabolism	<i>Aspa, B3gnt3, Bcl6b, Cd151, Fhl5, Hgfac, Hgs, Krtap19-3, Muc4, Myadml2, Neurog3, Nlrp6, Npas1, Nptx2, Nr1h4, Oaz1, Onecut1, Pxmp2, Slc38a4, Slco2b1, Spic, Tagln2, Tmprss4, Trpm5, Trps1, Ube2v1</i>	10E-15
Tissue Morphology, Embryonic	<i>Akt1s1, Arrb1, Bmp7, Btrc, Cdh15, Csnk1a1, Csnk2a2, Csnk2b, Ctbp2, Ctnnd2, Ctsh, Ecsit,</i>	10E-15

Development, Organismal Development	<i>Ggt6, Glis2, Iqgap2, Kctd20, Lef1, Mmp15, Naca, Nkx2-3, Nppc, Ptch2, Rab18, Scnn1b, Slc26a11, Smad1, Timp3, Tmem17</i>	
Nervous System Development and Function, Cellular Development, Tissue Morphology	<i>Amn, Dnajc6, G530011006Rik, Gcm2, Grik3, Hao2, Inpp5j, Isl2, Kcnip1, Lhx5, Mctp2, Pcp4, Plekhf1, Pnoc, Prrxl1, Rbm47, Sall3, Scarf1, Slc22a6, Slc22a22, Slc47a1</i>	10E-14
<b>Partek Pathway</b>		
Peroxisome	<i>Acaa1a, Acsl4, Acsl6, Agt, Hao2, Mpv17, Mpv17l, Mpv17l2, Mvk, Nos2, Peci, Pex26, Pxmp2, Slc25a17</i>	0.008
Hematopoietic cell lineage	<i>Cd1d1, Cd3e, Cd38, Csf1r, Fcgr1, Flt3, Gm2002, Gm13305, H2-Eb1, Il11ra1, Il11ra2, Itga5, Thpo</i>	0.01
Notch signalling pathway	<i>Ctbp2, Dll1, Dll4, Hes5, Kat2a, Notch4, Numbl, Rbpjl</i>	0.032
ABC transporters	<i>Abca6, Abca7, Abca8b, Abcb9, Abcb10, Abcc4, Abcc10, Abcg2</i>	0.036
<b>Enrichr KEGG</b>		
Notch signaling pathway	<i>Rbpjl, Dll4, Kat2A, Numbl, Ctbp2, Notch4, Dll1, Hes5</i>	0.040
Bladder cancer	<i>Rb1, Rassf1, Dapk2, Mmp2, E2F3, Vegfa, Tymp</i>	0.048



**Appendix I Journal copyright approval.****ELSEVIER LICENSE  
TERMS AND CONDITIONS**

This Agreement between Eric Chater ("You") and Elsevier ("Elsevier") consists of your license details and the terms and conditions provided by Elsevier and Copyright Clearance Center.

License Number	4044721442406
License date	
Licensed Content Publisher	Elsevier
Licensed Content Publication	Alcohol
Licensed Content Title	Changes to histone modifications following prenatal alcohol exposure: An emerging picture
Licensed Content Author	Eric J. Chater-Diehl, Benjamin I. Laufer, Shiva M. Singh
Licensed Content Date	Available online 4 February 2017
Licensed Content Volume	n/a
Licensed Content Issue	n/a
Licensed Content Pages	1
Type of Use	reuse in a thesis/dissertation
Intended publisher of new work	other
Portion	excerpt
Number of excerpts	3
Format	both print and electronic
Are you the author of this Elsevier article?	Yes
Will you be translating?	No
Order reference number	
Title of your thesis/dissertation	Hippocampal epigenetic changes in a mouse model of Fetal Alcohol Spectrum Disorders
Expected completion date	Apr 2017
Estimated size (number of pages)	200
Elsevier VAT number	GB 494 6272 12

## ELSEVIER LICENSE TERMS AND CONDITIONS

This Agreement between Eric Chater ("You") and Elsevier ("Elsevier") consists of your license details and the terms and conditions provided by Elsevier and Copyright Clearance Center.

License Number	4044281125091
License date	
Licensed Content Publisher	Elsevier
Licensed Content Publication	Alcohol
Licensed Content Title	Changes to histone modifications following prenatal alcohol exposure: An emerging picture
Licensed Content Author	Eric J. Chater-Diehl, Benjamin I. Laufer, Shiva M. Singh
Licensed Content Date	Available online 4 February 2017
Licensed Content Volume	n/a
Licensed Content Issue	n/a
Licensed Content Pages	2
Type of Use	reuse in a thesis/dissertation
Portion	figures/tables/illustrations
Number of figures/tables/illustrations	2
Format	both print and electronic
Are you the author of this Elsevier article?	Yes
Will you be translating?	No
Order reference number	
Original figure numbers	figures 1 and 2
Title of your thesis/dissertation	Hippocampal epigenetic changes in a mouse model of Fetal Alcohol Spectrum Disorders
Expected completion date	Apr 2017
Estimated size (number of pages)	200
Elsevier VAT number	GB 494 6272 12

## Curriculum Vitae

Eric J. Chater-Diehl  
 Biological & Geological Sciences Building,  
 Western University, London, Ontario, Canada N6A 5B7

### Present Position

*PhD candidate:* Department of Biology, Western University,

- Supervisor: Dr. Shiva M. Singh
- Thesis: Hippocampal epigenetic changes in response to early ethanol exposure
- Comprehensive examinations completed with distinction

### Academic Training

PhD in Biology	Molecular genetics stream; Western University, London, Ontario, Canada	2017
B.Sc. in Biology	Honors Specialization in Genetics, Western University, honors thesis completed in 4 <sup>th</sup> year	2011

### Awards and Scholarships

NSERC Alexander Graham Bell Scholarship (CGS D), \$105,000	2013-2016
Travel Award, Department of Biology	2015
Ontario Graduate Scholarship (OGS), \$15,000	2012-2013
National Institute on Alcohol Abuse and Alcoholism Travel Award, \$2,000	2012
NSERC Alexander Graham Bell Scholarship (CGS M), \$35,000	2011-2012
Ontario Graduate Scholarship (OGS), \$15,000 (declined)	2011-2012
Continuing Admission Scholarship, Western University, \$40,000	2007-2011
Gold Medal - Honors Specialization in Genetics program	2011
NSERC Undergraduate Student Research Award (USRA), \$5,400	2009

### Teaching Experience

Biology 3592: Human Genetics. <i>Teaching Assistant</i> , Western University	2015-present
Biology 4582: Investigative Techniques in Genetics. <i>Teaching Assistant</i> , Western University	2011-2015

### Professional Service

Biology graduate research forum Abstract committee chair	2016
Society of Graduate Students Bursaries and Subsidies Committee Chair	2014-present
Society of Graduate Students Bursary Committee member	2013-2014
Society of Biology Graduate Students executive committee	2011-2013

**Employment Experience**

Epigenie Research blog

2013-present

*Digital marking specialist & Technical writer***Invited Lectures***Highlights of the American Society of Human Genetics (ASHG) annual meeting.*

McMaster Genetics Education Rounds. November 12, 2015. MUMC McMaster University.

Research lecture: *Long term epigenetic changes in a mouse model of FASD.* Biology 4582 – Investigative techniques in Genetics. November 19, 2015. Western University.*Peroxisomes and human disease.* Biology 3316A – Advanced Cell Biology. November 26, 2015. Western University.*Peroxisomes and human disease.* Biology 3316A – Advanced Cell Biology. November 16, 2014. Western University.**Graduate Courses**

Biology 9563A – Mutation	95%	2014
Biology 9563B – Epigenetics	96%	2013
Biology 9315B – Biology of Aging	88%	2012
Biology 9563A – Genetic Variation	98%	2011

**Thesis Supervision**

Dustin Sokolowski September 2016 – April 2017. Fourth year honors thesis student.

Thesis entitled: *Integration of multiple genomic datasets from adolescent mouse hippocampus exposed to ethanol as neonates.*

Eric Kirk. September 2014 – April 2015. Fourth year honors thesis student. Thesis

entitled: *Neuromuscular responses of tendon stiffness determined by COL5A1 (rs12722) single nucleotide polymorphisms.* Published in *Experimental Physiology* (2016).Brienne Robinson. September 2013 – April 2014. Third year Scholar's Electives thesis student. Thesis entitled: *Conformation of gene expression changes in a mouse model of Fetal Alcohol Spectrum Disorders.*Randa Stringer. September 2012 – April 2014. Fourth year honors thesis student. Thesis entitled: *Gene expression and DNA methylation changes in a mouse model of Fetal Alcohol Spectrum Disorders.***Thesis Adviser**

Vindu Joshi. September 2016 – April 2017. Fourth year honors thesis student, Dr. Shawn

Li. Thesis entitled: *Functional role of mutations in tyrosine kinases in tumorigenesis.***Media Coverage***Study confirms dangers of fetal alcohol exposure.* Western News, November 20, 2014.*A single drink can have a lifetime of consequences.* Biomed Central, August 30, 2013.*In Fetal Alcohol Study, IPA Finds the Signal in the Noise.* Qiagen, Ingenuity, July, 2013.

*Study explores fetal alcohol impact at molecular level.* Western News, July 18, 2013.

### **Professional Organizations**

American Society of Human Genetics (ASHG) member

International Society of Psychiatric Genetics (ISPG) member

### **Publications**

13. **Chater-Diehl, E.J.**, Laufer, B.I., and Singh, S.M. (2017). Changes to histone modifications following prenatal alcohol exposure: An emerging picture. *Alcohol*.
12. Laufer, B.I., **Chater-Diehl, E.J.**, Kapalanga, J., and Singh, S.M. (2016). Long-term alterations to DNA methylation as a biomarker of prenatal alcohol exposure: From mouse models to human children with fetal alcohol spectrum disorders. *Alcohol*.
11. Kirk, E.A., Moore, C.W., **Chater-Diehl, E.J.**, Singh, S.M., and Rice, C.L. (2016). Human COL5A1 polymorphisms and quadriceps muscle-tendon mechanical stiffness in vivo. *Experimental Physiology*.
10. **Chater-Diehl, E.J.**, Laufer, B.I., Castellani, C.A., Alberry, B. L., and Singh, S.M. (2016). Alteration of free radical scavenging gene expression, DNA methylation, and histone modification in adult mouse hippocampus following fetal alcohol exposure. *PLoS ONE*.
9. Laufer, B.I., Kapalanga, J., Castellani, C.A., **Diehl, E.J.**, Liying Yan, L. and Singh, S.M. (2015). Associative DNA methylation changes in children with prenatal alcohol exposure. *Future Medicine*. 7(8): 1259-1274.
8. Castellani, C.A., Laufer, B.I., Melka, M.G., **Diehl, E.J.**, O'Reilly, R.L., Singh, S.M. (2015). DNA methylation differences in monozygotic twin pairs discordant for schizophrenia identifies psychosis related genes and networks. *BMC Med Genomics*. 8(17).
7. Castellani, C.A.\*, Melka, M.G.\*, **Diehl, E.J.**, Laufer, B.I., O'Reilly, R.L., Singh, S.M. (2015). DNA Methylation in Psychosis: Insights into Aetiology and Treatment. *Epigenomics* 7(1): 67-74. \*Equal Contribution.
6. Kleiber, M.L., **Diehl, E.J.**, Laufer, B.I., Mantha, K., Chokroborty Hoque, A., Alberry, B. and Singh, S.M. (2014). Long-term genomic and epigenomic dysregulation as a consequence of prenatal alcohol exposure: a model for fetal alcohol spectrum disorders. *Front. Genet*. 5.
5. Laufer, B.I., **Diehl, E.J.** and Singh, S.M. (2013). Neurodevelopmental epigenetic etiologies: insights from studies on mouse models of fetal alcohol spectrum disorders. *Epigenomics* 5(5): 1-4.

4. Laufer, B.I., Mantha, K., Kleiber, M.L. **Diehl, E.J.** Addison, S.M.F. and Singh, S.M. (2013). Long lasting alterations to DNA methylation and ncRNAs may underlie the effects of fetal alcohol exposure. *Dis. Model. Mech.*, 4:977-91.
3. Kleiber, M., Laufer, B.I., Wright, E., **Diehl, E.J.**, and Singh, S. (2012). Long-term alterations to the brain transcriptome in a maternal voluntary consumption model of fetal alcohol spectrum disorders. *Brain Res.* 1458:18-33.
2. Symons, M.N., Weng, J., **Diehl, E.J.**, Heo, E., Kleiber, M.L., and Singh, S.M. (2010) Delineation of the role nicotinic acetylcholine receptor genes in alcohol preference in mice. *Behav. Genet.*, 40:660-71.
1. Anderson-Schmidt H., Beltcheva O., Brandon M.D., Byrne E.M., **Diehl E.J.**, Duncan L., Gonzalez S.D., Hannon E., Kantojärvi K., Karagiannidis I., Kos M.Z., Kotyuk E., Laufer B.I., Mantha K., McGregor N.W., Meier S., Nieratschker V., Spiers H., Squassina A., Thakur G.A., Tiwari Y., Viswanath B., Way M.J., Wong C.C., O'Shea A., Delisi L.E. (2013). Selected rapporteur summaries from the XX world congress of psychiatric genetics, Hamburg, Germany, October 14-18, 2013. *Am J Med Genet B Neuropsychiatr Genet.* 162(2):96-121.

### Presentations

11. **Chater-Diehl, E.J.\***, Laufer, BI, and Singh, S. Hippocampal DNA methylation changes affect oxidative stress genes in fetal alcohol-exposed adolescent mice. American Society of Human Genetics (ASHG) meeting. Vancouver, British Columbia, Canada. October 18-22, 2016. International. *Poster Presentation.*
10. **Chater-Diehl, E.J.\***, Laufer, BI, Castellani, CA, and Singh, S. Oxidative stress pathways implicated in comprehensive epigenetic and transcriptomic assessment of hippocampus in a model of Fetal Alcohol Spectrum Disorder. World Congress of Psychiatric Genetics (WCPG). Toronto, Ontario, Canada. October 16-20, 2015. International. *Oral Presentation.* Nominee: Best trainee talk.
9. **Chater-Diehl, E.J.\***, Laufer, BI, Castellani, CA, Alberry, BL, and Singh, S. Oxidative stress pathways implicated in comprehensive epigenetic and transcriptomic assessment of adult hippocampus from fetal ethanol-exposed mice. American Society of Human Genetics (ASHG) meeting. Baltimore, Maryland, USA. October 6-10, 2015. International. *Poster Presentation.*
8. **Chater-Diehl, E.J.\***, Laufer, BI, Castellani, CA, Alberry, BL, Chokroborty-Hoque, A, Kapalanga, J, and Singh, S. Epigenetic footprints in FASD etiology, insights from human and mouse models. Fetal Alcohol Canadian Expertise (FACE) meeting. Ottawa, Ontario, Canada. September 17 2015. National. *Oral/Poster Presentations.*
7. **Diehl, E.J.\***, Laufer, B., Castellani, C.A. and Singh, S. Oxidative stress pathways implicated in comprehensive epigenetic and transcriptomic assessment of hippocampus of FASD-like mice. Keystone Symposia: Neuroepigenetics. Santa Fe, New Mexico, USA. Feb 22-26 2015. International. *Poster Presentation.*

6. **Diehl, E.J.\***, Laufer, B.I., and Singh, S. Comprehensive Assessment of Epigenetic and Gene Expression Changes in the Hippocampus of Fetal Ethanol-Exposed Mice. 2014. Biology Graduate Research Forum. London, Ontario, Canada. October 3, 2014. Institutional. *Oral Presentation*. Winner: best short talk.
5. **Diehl, E.J.\***, Laufer, B.I., Robinson, B., and Singh, S. Comprehensive Assessment of Epigenetic and Gene Expression Changes in the Hippocampus of Fetal Ethanol-Exposed Mice. Epigenetics Eh! Canada, London, Ontario, Canada. June 24-27, 2014. International. *Poster Presentation*.
4. **Diehl, E.J.\***, Laufer, B.I., Janus, K., Kleiber, M.L., and Singh, S.M. Alterations in hippocampal gene expression and epigenetic methylation in a mouse model of Fetal Alcohol Spectrum Disorder: Towards understanding cognitive deficits. World Congress of Psychiatric Genetics, Hamburg, Germany. October 14-18, 2012. International. *Poster Presentation*.
3. Laufer, B.I.\*, Mantha, K., Kleiber, M.L., **Diehl, E.J.**, Addison, S.M.F., and Singh, S.M. Alterations in genomically imprinted miRNA and snoRNA clusters in a mouse model of Fetal Alcohol Spectrum Disorders (FASD). Mouse Molecular Genetics. 4 October, 2012, Pacific Grove, California, USA. International. *Oral Presentation*.
2. Laufer, B.I.\*, Mantha, K., Kleiber, M.L., **Diehl, E.J.**, Addison, S.M.F., and Singh, S.M. Alterations in genomically imprinted miRNA and snoRNA clusters in a mouse model of Fetal Alcohol Spectrum Disorders (FASD). American Society of Human Genetics (ASHG). 9 November, 2012, San Francisco, California, USA. International. *Oral Presentation*.
1. Laufer, B.I.\*, **Diehl, E.J.\***, Kleiber, M., Janus, K., Wright, E., and Singh, S. Disruption of Imprinted Regions in a Mouse Model of Fetal Alcohol Spectrum Disorders (FASD). 2011 Congress of Human Genetics, Montreal, Canada. October 11-15, 2011. International. *Poster Presentation*.